Filtering algorithms and avionics systems for unmanned aerial vehicles

Erwan Salaün

ED n°431 : ICMS

T H E S E

pour obtenir le grade de

DOCTEUR DE L'ECOLE NATIONALE SUPERIEURE DES MINES DE PARIS

Spécialité "Mathématiques et Automatique"

présentée et soutenue publiquement par
Erwan SALAÜN

le 13 janvier 2009

ALGORITHMES DE FILTRAGE ET SYSTEMES AVIONIQUES POUR VEHICULES AERIENS AUTONOMES

Directeur de thèse : Philippe MARTIN

Jury

M. Tarek HAMEL	Président
M. Eric FERON	Rapporteur
M. Robert MAHONY	Rapporteur
Mme Cécile DURIEU	Examinateur
M. Pascal MORIN	Examinateur
M. Philippe MARTIN	Examinateur

Erwan SALAÜN

FILTERING ALGORITHMS AND AVIONICS SYSTEMS FOR UNMANNED AERIAL VEHICLES

Erwan SALAÜN
Mines ParisTech, Centre Automatique et Systèmes, 60, Bd. Saint-Michel, 75272 Paris Cedex 06, France.
E-mail : erwan.salaun@mines-paristech.fr

Key words and phrases. — Unmanned aerial vehicles, low-cost embedded avionics systems, data fusion, navigation solutions, attitude and heading reference system, nonlinear observers, invariance, symmetry, extended Kalman filter, quadrotor, rotor drag.

Mots clés. — Véhicules aériens autonomes, systèmes avioniques embarqués bas-coûts, fusion de données, solutions de navigation, système de référence d'attitude et de cap, observateurs non-linéaires, invariance, symétrie, filtre de Kalman étendu, quadrotor, traînée de rotor.

July 8, 2010

FILTERING ALGORITHMS AND AVIONICS SYSTEMS FOR UNMANNED AERIAL VEHICLES

Erwan SALAÜN

***Résumé* (Algorithmes de filtrage et systèmes avioniques pour véhicules aériens autonomes)**

L'essor récent des mini-véhicules aériens autonomes (ou mini-drones) est intrasèquement lié au développement des différentes composantes des systèmes avioniques embarqués (capteurs, calculateurs et liaison de données), à la fois au niveau de leur coût, de leur poids, de leurs dimensions et de leurs performances. Ces engins volants doivent en effet répondre à un cahier des charges spécifique très exigeant: être capable d'accomplir des missions de surveillance ou de poursuite de manière autonome, tout en étant léger ($<$2kg), de petite envergure ($<$1m) et assez "bon marché". L'avionique embarquée, dite "bas-coûts", doit elle-même satisfaire ces contraintes: elle ne peut contenir que des systèmes aux performances médiocres (e.g. mesures des capteurs fortement biaisées ou bruitées, calculateur peu puissant), qui doivent alors être compensés par des algorithmes de fusion de données et de contrôle "intelligement" pensés et implémentés.

Le travail présenté dans ce mémoire concerne le développement théorique et la validation expérimentale d'algorithmes de fusion de données originaux pour mini-drones, dépassant les limitations des estimateurs communément utilisés. En effet, les observateurs usuels (e.g. le Filtre de Kalman Etendu ou les filtres particulaires) possèdent plusieurs inconvénients: leur convergence, même au premier ordre, est difficile à prouver, leur comportement local est souvent mal appréhendé et leur réglage est délicat (de nombreux coefficients sont à régler). Ils sont de plus gourmand en calculs (nombreuses opérations matricielles), ce qui les empêchent d'être implémentés sur des calculateurs bon marché et donc peu puissants. Ce mémoire présente des solutions alternatives à ces filtres, remédiant aux défauts précédents et pouvant être implémentés aisément et efficacement dans une avionique bas-coûts.

Nous proposons tout d'abord des observateurs invariants "génériques", préservant les symétries naturelles du système physique. Ces observateurs fusionnent les mesures de capteurs bon marché usuels (tels qu'inertiels, magnétomètres, GPS ou baromètre) afin d'estimer avec précision l'état de l'appareil (angles d'attitude et de cap, vitesse et position). Ils possèdent un large domaine de convergence; ils sont également faciles à régler et très économiques en temps de calcul. Ils ne supposent pas de modèle connu de l'engin (hormis les lois cinématiques habituelles) et peuvent donc être adaptés à toute plateforme mobile.

Puis nous développons des observateurs "spécifiques", adaptés au type de véhicule aérien considéré, en l'occurence un mini-quadrotor. Nous décrivons tout d'abord son modèle physique, tenant compte explicitement de la traînée de rotor. Ce modèle nous permet alors de contruire des observateurs estimant la vitesse du quadrotor à partir de mesures uniquement inertielles, menant à un contrôle en vitesse de l'appareil. Cette approche est validée par des vols stabilisés autonomes.

Enfin, nous présentons en détails l'intégration du système avionique bas-coûts utilisé, composé de capteurs "bruts" et d'un microcontrôleur sur lequel sont implémentés les observateurs précédents. Nous validons ces algorithmes en comparant leurs estimations avec ceux fournit par un produit commercial coûteux, mettant ainsi en évidence leur excellent rapport "qualité/prix".

REMERCIEMENTS

Je remercie Tarek Hamel, président du jury, Eric Feron et Robert Mahony, rapporteurs, Cécile Durieu et Pascal Morin, examinateurs de ma thèse.

Je tiens également à remercier toute l'équipe du centre, en particulier Nicolas Petit et Pierre Rouchon, pour leurs conseils et l'intérêt qu'ils ont porté à mon travail.

J'ai une grande pensée pour mes compagnons de route qui m'ont aidé par bien des manières: Laure et Jonathan pour s'être brûlés avec moi au fer à souder; Caroline et Christophe pour avoir partagé ma passion de l'ATmega128; Pierre-Jean et Johann pour m'avoir aidé à construire notre quadricoptère; Silvère pour m'avoir initié au monde de l'invariance.

Merci à mes proches, en particulier à Marine, qui ont su m'épauler pendant toutes ces années et me faire vivre tant de bons moments qui m'ont permis de me ressourcer.

Je souhaite enfin remercier Philippe Martin qui a été beaucoup plus qu'un simple directeur de thèse. Merci d'avoir toujours été à mes côtés: de la gestion des interruptions du microcontrôleur au lemme de Barbalat, en passant par le choix et l'achat de connecteurs en tous genres. Je vais regretter nos (longues) pauses cafés, les finitions d'articles à 4h du matin et les vols du quadri dans le jardin des Mines.

CONTENTS

CHAPTER 1

PROBLEM POSITION

Dans ce chapitre introductif nous présentons la problématique des algorithmes de filtrage pour mini-drones, mettant en perspective certains travaux menés dans ce domaine, ainsi que les différents types de capteurs et systèmes de navigation commerciaux utilisés. Nous faisons également un rappel de la théorie des observateurs invariants, élément essentiel à la construction des estimateurs "génériques" développés par la suite.

1.1. Roles of the embedded avionics system

The mini-Unmanned Aerial Vehicles (or mini-UAVs) have been subject to an exponential growth for the past 15 years, created to satisfy first military and then civilian needs. There is a wide variety of mini-UAV shapes and configurations, but they all share several common characteristics:

- they are small ($<$1m), light ($<$2kg) and low-cost
- they can be autonomous and accomplish many tasks (hovering, following waypoints,...) by themselves
- they can be remotely controlled by a non-specialist pilot giving high-level orders (e.g. go forward, go left, take off)
- they should be able to fly in many different environments: indoor/outdoor, in presence of wind, obstacles,...

In order to meet these very demanding requirements, an embedded avionics system is used: it is composed of a computational board that is interfaced with the sensors, the actuators, and the communication devices. This system must accomplish two main tasks:

- *filter role*: it must estimate the state of the flying system, i.e. its orientation, its velocity, and its position,
- *controller role*: it must send the proper commands to the actuators as a function of the reference (provided by the pilot for instance) and the vehicle state estimated by the filtering algorithm.

Both roles (filter and controller) are crucial for the safety of the mini-UAV and the success of its mission, and both raise theoretical and experimental deep questions. Nevertheless, linear control laws are often sufficient if an accurate estimate of the vehicle state is provided by the filtering algorithm, and especially for near-hovering flights and non-aggressive maneuvers. Therefore, the study we present in this thesis focuses on the filtering task of the embedded avionics system. Many expressions exist for the name of the algorithm dedicated to this task, depending on the scientific community that uses it: filtering algorithm, observer or estimator. We consider here that they are all equivalent.

1.2. Challenges of the filtering algorithms

1.2.1. Two different strategies. — The role of the observer is to give an estimate of the vehicle state that is "good" enough (accurate, with a high update rate and a low latency) for the "user", which is almost always the control algorithm in the case of mini-UAVs. To get this estimate, the various measurements provided by the sensors are "merged" with some filtering algorithm. This filter can be based on two different strategies

- *generic observer*: this kind of filter uses the general kinematic laws applied to the moving body. Therefore it can be used for any platform, whatever the structure of the mini-UAV is (even for a bigger UAV or a car for instance), since no study of the mechanical and aerodynamical forces and torques applied to the system is required. This filter allows then a gain of time (and money).
- *specific observer*: this kind of filter uses a physical model of the vehicle (written from the dynamics laws), so it may have a better performance than the generic observer. However it needs more time to be built: the model needs to be identified and the algorithm needs to be implemented and tuned for each kind of UAV.

The *generic observer*, often called "Attitude and Heading Reference System" (AHRS) or "aided Attitude and Heading Reference System" (aided AHRS) as we will detail it later, has been the subject of numerous studies (see for instance the references in the survey [**26**] and the recent works [**52, 71**] for the AHRS, the recent results in [**5, 50, 24, 38, 86**] for the aided AHRS). This kind of filtering algorithm is also used in commercial devices

that can be mounted on any UAV (i.e. the MIDG II from Microbotics, the MTi from Xsens, the 3DM-GX1 from Microstrain or the GuideStar from Athena). On the contrary, few works developed *specific observers* since much more effort in the system modeling is required (see for instance [**87, 88**]).

1.2.2. The challenges to face. — The filtering algorithm for mini-UAV must meet the following requirements

- *large domain of convergence*: the domain of convergence should be as large as possible. At least, the local convergence around the most common trajectories followed by the mini-UAV (and then not only around the stationary point, e.g. an hovering flight) is highly desired
- *sensible local behavior*: once the estimations have converged to their true value (e.g. after a bad initialization), we can consider only the local behavior of the filter. Therefore it is important for the local behavior to be coherent with some physical considerations
- *easy to tune*: from a practical viewpoint, it is a great advantage if there are only a few number of coefficients to dial, and if this tuning is easy to do.

Due to the very demanding requirements in terms of weight, dimensions and price, the whole avionics system can only contain low-cost systems. Then the filtering algorithm must also face two challenges specific to the mini-UAV application:

- *use of low-cost sensors*: the observer must cope with the imperfections of the embedded low-cost sensors, especially the intrinsic time-varying biases in some measurements and the possible influence of the "environment" on the measurements (e.g. presence of buildings or parasite magnetic field from the motors) must be taken into account
- *use of low-cost computational board*: the filtering algorithm must be implemented on a low-cost microcontroller, with a limited computational power.

The usual filtering techniques commonly applied on larger UAVs (and on ground vehicles), such as Extended Kalman Filter ([**8, 29**]), Sigma-point Kalman filtering ([**24, 82**]), particle filtering ([**21**]), unscented filtering ([**25**]), adaptative filtering ([**22, 37, 75**]) or genetic algorithm ([**70**]), give great results when they are properly tuned. Nevertheless, they do not really match with the preceding requirements. Especially it is difficult to prove the convergence of the filters (even at the first order) and it is not easy to tune the numerous parameters (e.g. the coefficients of the covariance matrices). Furthermore, these filters require too much computation to be implemented on low-cost microcontrollers.

In order to bypass these limitations, many nonlinear filtering algorithms have been developed, for AHRS (see [**35, 52, 55, 67, 81, 26, 53, 54, 73**]) as well as for aided AHRS (see [**84, 86, 3, 85**]). Another approach has been recently proposed, introducing nonlinear filters preserving by construction the natural symmetries of the considered system. Therefore they are often called "invariant" or "symmetry-preserving" observers. A theoretical investigation of such filters is presented in [**11, 12, 13, 46, 47, 48**], including the definition of invariance properties and a systematic method to construct the invariant filters. A brief recall of the main results is given in section 1.4. The majority of the observers we develop in this thesis is based on this approach.

1.3. Sensors and commercial navigation systems

The filtering algorithms we present in this thesis handle with measurements from the most usual low-cost sensors embedded on a mini-UAV. We present here their characteristics (price (in €), weight (in g), dimensions (in mm), update rate (in Hz)), as well as an "inertial class" inertial measurement unit (IMU) Sigma 30 from Sagem and the two commercial devices used to validate the estimations given by our algorithms (the MIDG II from Microbotics and the 3DM-GX1 from Microstrain). For clarity, we divide the sensors into two groups: the sensors that give measurements in the Body-fixed frame and those that give measurements in the Earth-fixed frame.

1.3.1. Sensors providing Body-fixed measurements. — The following strapdown sensors provide measurements with respect to the body-fixed coordinates. Unlike "inertial class" systems, the low-cost sensors are based on the Micro-Electro-Mechanical Systems (MEMS) technology, allowing them to be very small and light, but less accurate.

- *("inertial class") inertial measurement unit={accelerometers+gyroscopes}*: an IMU contains two kind of sensors: a tri-axial *accelerometer* that measures the specific acceleration vector, i.e. the linear acceleration minus the gravity vector, and a tri-axial *gyroscope* that measures the instantaneous angular velocity vector. An "inertial class" IMU, such as Sigma 30 from Sagem (see Figure 1.1), provides very accurate measurements at a high update rate. Nevertheless, it is very expensive, big and heavy (20kg), then it is not possible to use it on a mini-UAV.
- *(low cost) inertial measurement unit*: our IMU is an ADIS16355 from Analog Devices (see Figure 1.2). It contains low-cost a tri-axial accelerometer and gyroscope. Slowly time-varying biases exist in the measurements.

FIGURE 1.1. "Inertial class" IMU Sigma 30

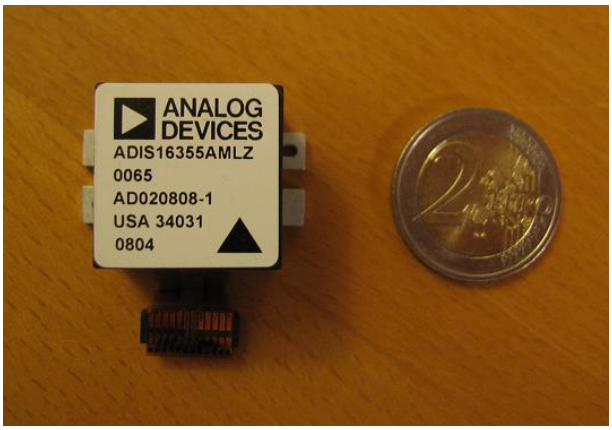

Cost	Weight	Size	Update rate
300	25	23,32,23	100

FIGURE 1.2. Inertial measurement unit ADIS16355

– *(low cost) magnetometers*: our tri-axial magnetometer is a Micromag3 from PNI (see Figure 1.3). It measures the magnetic field, which then may be subject to magnetic disturbances (in urban areas for instance).
– *(low cost) air velocity sensor*: we use the D6FW-04A1 from Omron that measures the air flow (see Figure 1.4).

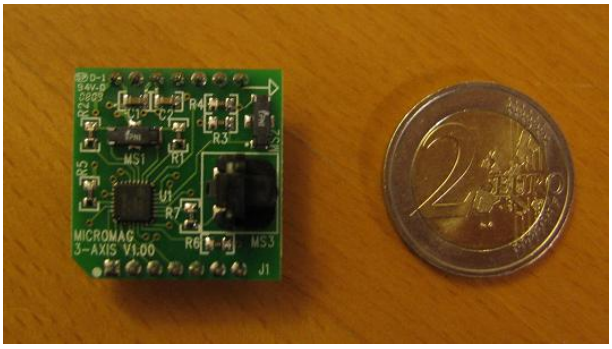

Cost	Weight	Size	Update rate
40	20	25,25,19	50

FIGURE 1.3. Magnetometer Micromag3

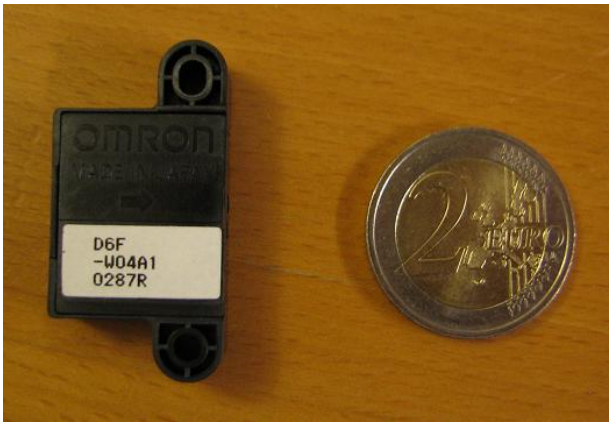

Cost	Weight	Size	Update rate
120	15	30,30,3	50

FIGURE 1.4. Air flow sensor D6FW-04A1

1.3.2. Sensors providing Earth-fixed measurements. — The following strapdown sensors provide measurements with respect to the Earth-fixed coordinates:

– *(low cost) GPS module*: our GPS is an LEA-4T from u-blox (see Figure 1.5). Its navigation solutions give the position and velocity vectors. It provides measurements at a lower update rate than the other sensors, and can be used only outdoors. Its accuracy (and especially the Circular Error Probable in position) depends on the

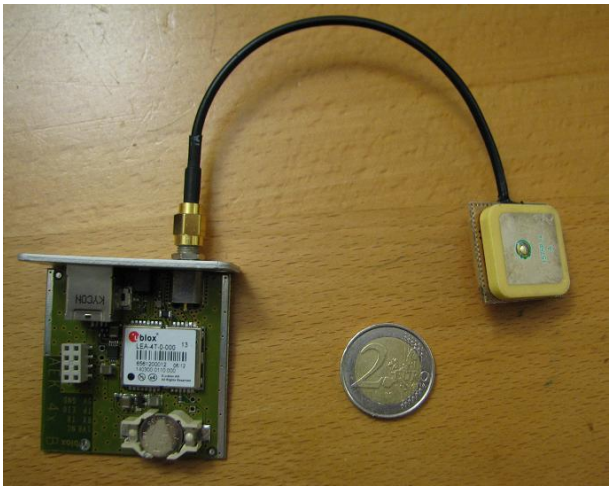

Cost	Weight	Size	Update rate
60	20	17,22,3	4

FIGURE 1.5. GPS module LEA-4T

"environment": building locations around the system, satellite configuration in the sky,... It is important to note that the velocity measurements are much more accurate than the position measurements, since the GPS velocity is obtained from the carrier phase and/or Doppler shift data, and not by differentiating the GPS position.

– *(low cost) barometer*: our barometer is a MS-5534 from Intersema (see Figure 1.6). It measures the pressure and temperature, which are used to calculate the standard altitude.
– *(low cost) sonar*: we use the sonar SRF10 from Devantech (see Figure 1.7). It measures the relative distance to the ground. It is more accurate than the barometer (because independent of the environmental changes such as wind and temperature), but is limited in altitude (<2m). The update rate of the measurements varies as a function of the relative distance to the ground.

1.3.3. Commercial navigation systems. — Commercial devices have already packaged low-cost sensors and filtering algorithms. They provide the raw measurements and the vehicle state estimate, often computed by some EKF (according to the user manuals). Therefore they are very useful for comparison and validation purposes.

Cost	Weight	Size	Update rate
10	10	9,9,2	20

FIGURE 1.6. Barometer MS-5534

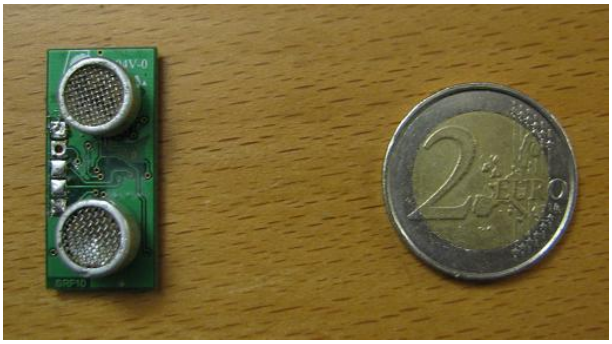

Cost	Weight	Size	Update rate
40	10	32,15,10	40

FIGURE 1.7. Sonar SRF10

– *inertial navigation systems*: this kind of system contains tri-axial accelerometer, gyroscope and magnetometer. We use the 3DM-GX1 from Microstrain (see Figure 1.8).

– *aided inertial navigation systems*: this kind of system contains tri-axial accelerometer, gyroscope and magnetometer, with some additional sensors: GPS, barometer,... We use the MIDG II from Microbotics, which has a GPS antenna (see Figure 1.9).

Cost	Weight	Size	Update rate
1000	40	40,50,20	50

FIGURE 1.8. Inertial navigation system 3DM-GX1

Cost	Weight	Size	Update rate
3500	50	38,40,22	50

FIGURE 1.9. GPS Aided - Inertial navigation system MIDG II

1.4. Symmetry-preserving observers theory

The construction of the generic observers described in Chapters 3 and 4 comes directly from the symmetry-preserving (or invariant) observer theory introduced in [**12**]. We

briefly recall here the main ideas and definitions of this previous work, completed with an additional result (for further details, see [**12**]).

1.4.1. Invariant systems and equivariant outputs. —

Definition. — *Let G be a Lie Group with identity e and Σ an open set (or more generally a manifold). An* action of a transformation group $(\phi_g)_{g\in G}$ *on Σ is a smooth map*

$$(g,\xi)\in G\times\Sigma\mapsto\phi_g(\xi)\in\Sigma$$

such that:

- $\phi_e(\xi)=\xi$ *for all* ξ
- $\phi_{g_2}\circ\phi_{g_1}(\xi)=\phi_{g_2g_1}(\xi)$ *for all* g_1,g_2,ξ.

By construction ϕ_g is a diffeomorphism on Σ for all g. The transformation group is *local* if $\phi_g(\xi)$ is defined only for g in a neighborhood of e. In this case the transformation law $\phi_{g_2}\circ\phi_{g_1}(\xi)=\phi_{g_2g_1}(\xi)$ is defined only when it makes sense. We consider only local transformation groups. "For all g" thus means "for all g around e", and "for all ξ" means "for all ξ in some neighborhood".

Consider now the smooth output system

$$\dot{x}=f(x,u) \tag{1}$$

$$y=h(x,u) \tag{2}$$

where x belongs to an open subset $\mathcal{X}\subset\mathbb{R}^n$, u to an open subset $\mathcal{U}\subset\mathbb{R}^m$ and y to an open subset $\mathcal{Y}\subset\mathbb{R}^p$, $p\leq n$.

We assume the signals $u(t),y(t)$ to be known (y is measured, and u is measured or known as a control input).

Consider also the local group of transformations on $\mathcal{X}\times\mathcal{U}$ defined by $(X,U)=\big(\varphi_g(x),\psi_g(u)\big)$, where φ_g and ψ_g are local diffeomorphisms.

Definition. — *The system $\dot{x}=f(x,u)$ is* G-invariant *if* $f\big(\varphi_g(x),\psi_g(u)\big)=D\varphi_g(x)\cdot f(x,u)$ *for all* g,x,u.

With $(X,U)=\big(\varphi_g(x),\psi_g(u)\big)$, the property also reads $\dot{X}=f(X,U)$, i.e., the system is left unchanged by the transformation.

Definition. — *The output $y=h(x,u)$ is* G-equivariant *if there exists a transformation group $(\rho_g)_{g\in G}$ on $\mathcal{Y}$ such that $h\big(\varphi_g(x),\psi_g(u)\big)=\rho_g\big(h(x,u)\big)$ for all g,x,u.*

With $(X,U)=\big(\varphi_g(x),\psi_g(u)\big)$ and $Y=\varrho_g(y)$, the definition reads $Y=h(X,U)$.

1.4.2. Invariant preobservers. —

***Definition* (Preobserver).** — *The system* $\dot{\hat{x}} = F(\hat{x}, u, y)$ *is a* preobserver *of the system* (1)-(2) *if* $F\big(x, u, h(x)\big) = f(x, u)$ *for all* x, u.

An observer is then a preobserver such that $\hat{x}(t) \to x(t)$ (possibly only locally).

Definition. — *The preobserver* $\dot{\hat{x}} = F(\hat{x}, u, y)$ *is* G-invariant *if* $F\big(\varphi_g(\hat{x}), \psi_g(u), \rho_g(y)\big) = D\varphi_g(\hat{x}) \cdot F(\hat{x}, u, y)$ *for all* $g, \hat{x}, u, y$.

The property also reads $\dot{\hat{X}} = F(\hat{X}, U, Y)$, i.e., the system is left unchanged by the transformation.

The key idea to build an invariant preobserver is to use an invariant output error.

Definition. — *The smooth map* $(\hat{x}, u, y) \mapsto E(\hat{x}, u, y) \in \mathcal{Y}$ *is an* invariant output error *if*

- *the map* $y \mapsto E(\hat{x}, u, y)$ *is invertible for all* $\hat{x}, u$
- $E\big(\hat{x}, u, h(\hat{x}, u)\big) = 0$ *for all* $\hat{x}, u$
- $E\big(\varphi_g(\hat{x}), \psi_g(u), \rho_g(y)\big) = E(\hat{x}, u, y)$ *for all* $\hat{x}, u, y$

The first and second properties mean E is an "output error", i.e. it is zero if and only if $h(\hat{x}, u) = y$; the third property, which also reads $E(\hat{X}, U, Y) = E(\hat{x}, u, y)$, defines invariance.

Similarly, the key idea to study the convergence of an invariant preobserver is to use an invariant state error.

Definition. — *The smooth map* $(\hat{x}, x) \mapsto \eta(\hat{x}, x) \in \mathcal{X}$ *is an* invariant state error *if*

- *it is a diffeomorphism on* $\mathcal{X} \times \mathcal{X}$
- $\eta(x, x) = 0$ *for all* x
- $\eta\big(\varphi_g(\hat{x}), \varphi_g(x)\big) = \eta(\hat{x}, x)$ *for all* $\hat{x}, x$.

We now state the two main results –based on the Cartan moving frame method– in the special case where $g \mapsto \varphi_g(x)$ is a free and transitive action, see [**12**] for the general case. The *moving frame* $x \mapsto \gamma(x)$ is obtained by solving for g the so-called *normalization equation* $\varphi_g(x) = c$ for some arbitrary constant c; in other words $\varphi_{\gamma(x)}(x) = c$. The function ψ_g may also be used in the normalization equation $\big(\varphi_g(x), \psi_g(u)\big) = c$, as illustrated in section 4.3.

Theorem. — *The general form of any invariant preobserver is*

$$F(\hat{x}, u, y) = f(\hat{x}, u) + \sum_{i=1}^{n} \big(L_i(E, I) \cdot E\big) w_i(\hat{x}),$$

where:

- w_i,$i = 1, \ldots, n$, *is the invariant vector field defined by*

$$w_i(\hat{x}) = \big[D\varphi_{\gamma(\hat{x})}(\hat{x})\big]^{-1} \cdot \frac{\partial}{\partial x_i},$$

  with $\frac{\partial}{\partial x_i}$ *the* i^{th} *canonical vector field on* $\mathcal{X}$,
- E *is the invariant error defined by*

$$E(\hat{x}, u, y) = \rho_{\gamma(\hat{x})}\big(h(\hat{x}, u)\big) - \rho_{\gamma(\hat{x})}(y),$$

- I *is the (complete) invariant defined by*

$$I(\hat{x}, u) = \psi_{\gamma(\hat{x})}(u),$$

- L_i, $i = 1, \ldots, n$, *is a* $1 \times p$ *matrix with entries possibly depending on* E *and* I, *and can be freely chosen.*

Theorem. — *The error system reads* $\dot{\eta} = \Upsilon(\eta, I)$ *for some smooth function* Υ, *where* η *is the invariant state error defined by*

$$\eta(\hat{x}, x) = \varphi_{\gamma(x)}(\hat{x}) - \varphi_{\gamma(x)}(x).$$

This result greatly simplifies the convergence analysis of the preobserver, since the error equation is autonomous but for the "free" known invariant I. Indeed for a general nonlinear (not invariant) observer the error equation depends on the trajectory $t \mapsto \big(x(t), u(t)\big)$ of the system, hence is in fact of dimension $2n + m$, whereas the dimension of the invariant state error equation is only $2n + m - dim(G)$. To simplify, we will use from now on the term "observer" instead of "preobserver".

1.5. Thesis outline

The thesis contains three main parts:

- in Chapters 3, 4 and 5, we propose symmetry-preserving generic nonlinear observers for a moving body, and validate them through experimental comparisons with a commercial device. In Chapter 2, we present an discuss the moving body models that we considered to build these observers.

- in Chapter 6, we construct specific observers for a mini-quadrotor based on the rotor drag, and validate them through flight tests
- in Chapter 7, we present the real-time implementation of the preceding observers on a "home-built" low-cost embedded prototype system.

In Chapter 2, we first introduce different models used in the navigation systems and highlight the differences between "true inertial navigation" based on the Schuler effect thanks to very accurate inertial sensors, and the low-cost navigation systems based on a flat Earth assumption. These low-cost navigation systems are called "Attitude and Heading Reference Systems" (AHRS) when they use only inertial sensors (often completed by magnetometers), and they are called "aided Attitude and Heading Reference Systems" (aided AHRS) when they have additional velocity and/or position sensors. Then we construct invariant (or symmetry-preserving) nonlinear observers for AHRS in Chapter 3 (see [**60, 62**]), and for aided AHRS in Chapter 4 (see [**61, 64, 63**]): by preserving the geometrical properties of the system, they bypass the limitations of the usual filtering methods. Especially we study their nice first-order behavior (even in presence of magnetic disturbances), their large convergence domain and their easy tuning. We validate these filters by comparing their estimations with those provided by commercial devices. We also present the Invariant Extended Kalman Filter in Chapter 5 (see [**14**]), which combines the EKF approach and the advantages of the invariant observers. Especially we extend the Multiplicative Extended Kalman Filter (MEKF), commonly used in avionics systems.

In Chapter 6, we first give the physical model of the mini-quadrotor: in this model, we consider especially the rotor drag that comes in addition to the usual thrust and drag torques (see [**59**]). Then we construct a specific observer based on this model, which estimates the velocity of the quadrotor with only inertial sensors measurements. This allows to control the quadrotor velocity thanks to a linear control laws and to achieve a hovering flight with only inertial sensors. We validate this model trough experimental flights, giving by the way new perspectives in the mini-quadrotor modeling and control. Moreover, it gives a new interpretation of the usual approach followed by the previous researches in this area, which assume a small linear acceleration to estimate the attitude angles thanks to the accelerometer. measurementsor which use commercial AHRS.

In Chapter 7, we first implement the generic observers of Chapters 3 and 4 on a cheap 8-bit microcontroller, highlighting their computational efficiency compared to the usual filtering algorithms. Then we detail the hardware and software architecture of the embedded avionics system we developed, which contains low-cost sensors and microcontroller and can be easily mounted on any kind of mini-UAV. We validate the preceding filters on

this prototype system by comparing the estimations given by our generic observers with those provided by commercial devices (see [**66, 65, 61**]).

CHAPTER 2

MODELS FOR NAVIGATION SYSTEMS

Dans ce chapitre, nous présentons les différents modèles génériques, principalement fonctions du type et de la nature des capteurs embarqués, utilisés habituellement dans les systèmes de navigation. Dans la section 2.1, nous rappelons l'effet Schuler, basé sur un modèle de terre ronde, et dont on peut bénéficier lorsque l'on a accès à des capteurs inertiels haut de gamme. Seuls des capteurs bas-coûts sont utilisés sur un mini-drone, nous ne pouvons donc pas béneficier de l'effet Schuler, et le modèle de terre plate décrit dans la section 2.2 est amplement suffisant. Nous présentons alors les modèles utilisés par la suite pour construire les filtres des "Attitude and Heading Reference Systems" (section 2.4) et des "aided Attitude and Heading Reference Systems" (section 2.4). Les propriétés d'invariance des différents modèles sont présentées dans la section 2.5.

2.1. Round Earth model and "true inertial navigation"

2.1.1. Earth and moving rigid body models. — The "true" inertial navigation is mainly based on measurements provided by two "strap-down" high-precision sensors: a tri-axial accelerometer that measures the specific acceleration vector, i.e. the linear

acceleration minus the gravity vector, and a tri-axial gyroscope that measures the angular velocity vector. These measurements are given in the body-fixed frame and are very accurate (small and very time-stable biases, small noise). An accurate model of the Earth is used in the observer algorithm: it is considered as a rotating ellipsoid with a gravity vector depending on the altitude. To illustrate the benefits of this kind of system, and especially the "Schuler effect", we consider for simplicity a 3-dimensional non-rotating round Earth (radius R): indeed the main conclusions depend only on the roundness of the Earth and its gravity vector varying with the altitude. A more detailed study of the Schuler effect can be found in [**28, 23, 31, 6, 76, 30, 19**].

We define the three following frames:
- the body-fixed frame: $\mathcal{R}_b = (\overrightarrow{i_b}, \overrightarrow{j_b}, \overrightarrow{k_b})$
- the local North-East-Down frame: $\mathcal{R}_l = (\overrightarrow{i_l}, \overrightarrow{j_l}, \overrightarrow{k_l})$
- the Earth-fixed frame: $\mathcal{R}_e = (\overrightarrow{i_e}, \overrightarrow{j_e}, \overrightarrow{k_e})$

For a 3×1 vector $\overrightarrow{P}$ we define $\overrightarrow{P}|_i$ as the projection of $\overrightarrow{P}$ on the frame $\mathcal{R}_i$ and the matrix $M_{i/j}$ as the rotation matrix from the frame $\mathcal{R}_j$ to the frame $\mathcal{R}_i$, where $i, j \in \{b, l, e\}$. For instance $\overrightarrow{P}|_b = M_{b/l}\overrightarrow{P}|_l$. We define also the instantaneous angular velocity vector $\overrightarrow{\Omega}_{i/j}$ of the frame $\mathcal{R}_i$ with respect to the frame $\mathcal{R}_j$. For more details in the definition of the different frames we use, see [**28, 23, 79, 69**].

The motion equations of a moving rigid body are

$$\dot{\overrightarrow{V}} = \overrightarrow{g} + \overrightarrow{a} \tag{3}$$

$$\dot{\overrightarrow{X}} = \overrightarrow{V} \tag{4}$$

where:
- $\overrightarrow{V}$ is the velocity vector of the center of mass with respect to the Earth-fixed frame
- $\overrightarrow{g}$ is the gravitational acceleration vector
- $\overrightarrow{a}$ is the specific acceleration vector
- $\overrightarrow{X}$ is the position vector of the center of mass

We define the following projected vectors

$$V = \overrightarrow{V}|_l = (V_N, V_E, V_D)$$
$$v = \overrightarrow{V}|_b$$
$$X_e = \overrightarrow{X}|_e = (x_0, y_0, z_0) \text{ with the altitude } h \text{ defined by } R + h = \sqrt{x_0^2 + y_0^2 + z_0^2}$$
$$A = \overrightarrow{g}|_l = (0, 0, g(h))$$
$$a = \overrightarrow{a}|_b$$
$$\omega_{b/l} = \overrightarrow{\Omega_{b/l}}|_b$$
$$\omega_{b/e} = \overrightarrow{\Omega_{b/e}}|_b$$
$$\Omega_{l/e} = \overrightarrow{\Omega_{l/e}}|_l = (\frac{V_E}{R+h}, \frac{-V_N}{R+h}, \frac{-V_E}{R+h}\tan\lambda) \text{ where } \lambda \text{ is the latitude.}$$

To be coherent with the North-East-Down frame we define $z = -h$. For a vector $P = (P_1, P_2, P_3)$ we define $P^\times$ the skew-symmetric matrix

$$P^\times = \begin{pmatrix} 0 & -P_3 & P_2 \\ P_3 & 0 & -P_1 \\ -P_2 & P_1 & 0 \end{pmatrix}.$$

Let (ϕ, θ, ψ) the usual Euler angles (roll, pitch, yaw). Then the rotation matrix $M_{b/l}$ writes ($c\theta = \cos\theta$ and $s\theta = \sin\theta$)

$$M_{b/l} = \begin{pmatrix} c\theta c\psi & c\theta s\psi & -s\theta \\ s\phi s\theta c\psi - c\phi s\psi & s\phi s\theta s\psi + c\phi c\psi & s\phi c\theta \\ c\phi s\theta c\psi + s\phi s\psi & c\phi s\theta s\psi - s\phi c\psi & c\phi c\theta \end{pmatrix}.$$

The projected motion equations write

$$\dot{M}_{b/l} = M_{b/l}\omega_{b/l}^\times = M_{b/l}(\omega_{b/e}^\times - M_{b/l}\Omega_{l/e}^\times) \tag{5}$$
$$\dot{V} = -\Omega_{l/e} \times V + A + M_{l/b}a \tag{6}$$
$$\dot{z} = V_D. \tag{7}$$

We suppose that the gravity varies with altitude according to the inverse square law:

$$g(z) = \frac{g_0}{(1 - \frac{z}{R})^2}.$$

We use 2 kinds of sensors: a tri-axial gyroscope measures ω_m ($= \omega_{b/e}$ if perfect) and a tri-axial accelerometer measures a_m ($= a$ if perfect). Even if very accurate sensors are

used in "true" inertial navigation, some imperfections still remain in their measurements, and especially biases. With such high-precision sensors, their biases are small and very stable in time. Then we consider that the gyroscope measures $\omega_m = \omega_{b/e} + \omega_b$ and the accelerometer measures $a_m = a + a_b$, where ω_b and a_b are constant biases.

Considering these imperfections in the measurements, the system (5)–(7) becomes

$$\dot{M}_{b/l} = M_{b/l}((\omega_m - \omega_b)^\times - M_{b/l}\Omega_{l/e}^\times) \tag{8}$$

$$\dot{V} = -\Omega_{l/e} \times V + A + M_{l/b}(a_m - a_b) \tag{9}$$

$$\dot{z} = V_D \tag{10}$$

$$\dot{\omega}_b = 0 \tag{11}$$

$$\dot{a}_b = 0. \tag{12}$$

2.1.2. Can we estimate the state?— To estimate the state of the moving rigid body, we must construct an observer based on Equations (8)–(12). The correction terms of the estimator depend on the estimations and the measurements that are considered as outputs of the system.

The 6 measurements provided by the inertial sensors are the inputs of the system (8)–(12). So this system has no output, and then it is not observable. The only way to estimate the state is writing an observer as just a copy of the nonlinear system (8)–(12). Since the observer has no correction terms, we need to figure out the behavior of the estimated state in the presence of errors: does the system diverge or not? It is an analysis of its detectability. We first study the system linearized around the equilibrium point$(\overline{M_{b/l}}, \overline{V}, \overline{z}, \overline{\lambda}, \overline{\omega_b}, \overline{a_b})$

$$\begin{aligned}
\delta\dot{M}_{b/l} &= \delta M_{b/l}((\overline{\omega_m} - \overline{\omega_b})^\times - \overline{M_{b/l}\Omega_{l/e}}^\times) + \overline{M_{b/l}}((\delta\omega_m - \delta\omega_b)^\times - \overline{M_{b/l}}\delta\Omega_{l/e}^\times - \delta M_{b/l}\overline{\Omega_{l/e}}^\times) \\
\delta\dot{V} &= -\overline{\Omega_{l/e}} \times \delta V - \delta\Omega_{l/e} \times \overline{V} + A + \overline{M_{l/b}}(\delta a_m - \delta a_b) + \delta M_{l/b}(\overline{a_m} - \overline{a_b}) \\
\delta\dot{z} &= \delta V_D \\
\delta\dot{\omega}_b &= 0 \\
\delta\dot{a}_b &= 0.
\end{aligned}$$

For simplicity, we consider the "nominal" equilibrium point

$$(\overline{M_{b/l}}, \overline{V}, \overline{z}, \overline{\lambda}, \overline{\omega_b}, \overline{a_b}) = (I_3, 0, \overline{z}, \overline{\lambda}, \overline{\omega_m}, \overline{a_m} + A).$$

The linearized system splits into three decoupled subsystems and one cascaded subsystem:

– the lateral subsystem

$$\begin{aligned}\delta\dot{\phi} &= -\frac{\delta V_E}{R-\overline{z}} - \delta\omega_{b1} + \delta\omega_{m1}\\ \delta\dot{V}_E &= g(\overline{z})\delta\phi - \delta a_{b2} + \delta a_{m2}\\ \delta\dot{\omega}_{b1} &= 0\\ \delta\dot{a}_{b2} &= 0\end{aligned}$$

– the longitudinal subsystem

$$\begin{aligned}\delta\dot{\theta} &= \frac{\delta V_N}{R-\overline{z}} - \delta\omega_{b2} + \delta\omega_{m2}\\ \delta\dot{V}_N &= -g(\overline{z})\delta\theta - \delta a_{b1} + \delta a_{m1}\\ \delta\dot{\omega}_{b2} &= 0\\ \delta\dot{a}_{b1} &= 0\end{aligned}$$

– the vertical subsystem

$$\begin{aligned}\delta\dot{V}_D &= \frac{2g(\overline{z})}{R-\overline{z}}\delta z - \delta a_{b3} + \delta a_{m3}\\ \delta\dot{z} &= \delta V_D\\ \delta\dot{a}_{b3} &= 0\end{aligned}$$

– the heading subsystem (cascaded with the lateral subsystem)

$$\begin{aligned}\delta\dot{\psi} &= \frac{\tan\overline{\lambda}}{R-\overline{z}}\delta V_E - \delta\omega_{b3} + \delta\omega_{m3}\\ \delta\dot{\omega}_{b3} &= 0.\end{aligned}$$

We construct the corresponding linearized observer:

– the lateral subsystem

$$\begin{aligned}\delta\dot{\hat{\phi}} &= -\frac{\delta\hat{V}_E}{R-\overline{z}} - \delta\hat{\omega}_{b1} + \delta\omega_{m1}\\ \delta\dot{\hat{V}}_E &= g(\overline{z})\delta\hat{\phi} - \delta\hat{a}_{b2} + \delta a_{m2}\\ \delta\dot{\hat{\omega}}_{b1} &= 0\\ \delta\dot{\hat{a}}_{b2} &= 0\end{aligned}$$

– the longitudinal subsystem

$$\begin{aligned}
\delta\dot{\hat{\theta}} &= \frac{\delta V_N}{R-\overline{z}} - \delta\hat{\omega}_{b2} + \delta\omega_{m2} \\
\delta\dot{\hat{V}}_N &= -g(\overline{z})\delta\hat{\theta} - \delta\hat{a}_{b1} + \delta a_{m1} \\
\delta\dot{\hat{\omega}}_{b2} &= 0 \\
\delta\dot{\hat{a}}_{b1} &= 0
\end{aligned}$$

– the vertical susbsytem

$$\begin{aligned}
\delta\dot{\hat{V}}_D &= \frac{2g(\overline{z})}{R-\overline{z}}\delta\hat{z} - \delta\hat{a}_{b3} + \delta a_{m3} \\
\delta\dot{\hat{z}} &= \delta\hat{V}_D \\
\delta\dot{\hat{a}}_{b3} &= 0
\end{aligned}$$

– the heading subsystem

$$\begin{aligned}
\delta\dot{\hat{\psi}} &= \frac{\tan\overline{\lambda}}{R-\overline{z}}\delta\hat{V}_E - \delta\hat{\omega}_{b3} + \delta\omega_{m3} \\
\delta\dot{\hat{\omega}}_{b3} &= 0.
\end{aligned}$$

We define the linearized error $\delta x^e = \delta\hat{x} - \delta x$. For instance $\delta\theta^e = \delta\hat{\theta} - \delta\theta$. We find the 4 error subsystems:

– the lateral error subsystem

$$\begin{aligned}
\delta\dot{\phi}^e &= -\frac{\delta V_E^e}{R-\overline{z}} - \delta\omega_{b1}^e \\
\delta\dot{V}_E^e &= g(\overline{z})\delta\phi^e - \delta a_{b2}^e \\
\delta\dot{\omega}_{b1}^e &= 0 \\
\delta\dot{a}_{b2}^e &= 0
\end{aligned}$$

– the longitudinal error subsystem

$$\begin{aligned}
\delta\dot{\theta}^e &= \frac{\delta V_N^e}{R-\overline{z}} - \delta\omega_{b2}^e \\
\delta\dot{V}_N^e &= -g(\overline{z})\delta\theta^e - \delta a_{b1}^e \\
\delta\dot{\omega}_{b2}^e &= 0 \\
\delta\dot{a}_{b1}^e &= 0
\end{aligned}$$

– the vertical error subsystem

$$\begin{aligned}\delta\dot{V}_D^e &= \frac{2g(\overline{z})}{R-\overline{z}}\delta z^e - \delta a_{b3}^e\\ \delta\dot{z}^e &= \delta V_D^e\\ \delta\dot{a}_{b3}^e &= 0\end{aligned}$$

– the heading error subsystem

$$\begin{aligned}\delta\dot{\psi}^e &= \frac{\tan\overline{\lambda}}{R-\overline{z}}\delta V_E^e - \delta\omega_{b3}^e\\ \delta\dot{\omega}_{b3}^e &= 0.\end{aligned}$$

We define $\omega_s = \sqrt{\frac{g(\overline{z})}{R-\overline{z}}}$ and $\tau = \sqrt{\frac{R-\overline{z}}{2g(\overline{z})}}$. Initialization errors in the estimation cannot be avoided in real systems, so we consider for each error $\delta x^e(t=0) = \delta x_0^e$. We find the following expressions of the linearized errors

– the lateral error subsystem

$$\begin{aligned}(13)\quad \delta\phi^e(t) &= \frac{1}{g(\overline{z})}\big(-(\delta V_{E0}^e\omega_s + \frac{g(\overline{z})}{\omega_s}\delta\omega_{b10}^e)\sin(\omega_s t) + (\delta\phi_0^e - \frac{\delta a_{b20}^e}{g(\overline{z})})\cos(\omega_s t) + \delta a_{b20}^e\big)\\ \delta V_E^e(t) &= (\delta V_{E0}^e + \frac{g}{\omega_s^2}\delta\omega_{b10}^e)\cos(\omega_s t) + \frac{g(\overline{z})}{\omega_s}(\delta\phi_0^e - \frac{\delta a_{b20}^e}{g(\overline{z})})\sin(\omega_s t) - \frac{g}{\omega_s^2}\delta\omega_{b10}^e\\ \delta\omega_{b1}^e(t) &= \delta\omega_{b10}^e\\ \delta a_{b2}^e(t) &= \delta a_{b20}^e\end{aligned}$$

– the longitudinal error subsystem

$$\begin{aligned}(14)\quad \delta\theta^e(t) &= -\frac{1}{g(\overline{z})}\big(-(\delta V_{N0}^e\omega_s + \frac{g(\overline{z})}{\omega_s}\delta\omega_{b20}^e)\sin(\omega_s t) + (\delta\theta_0^e - \frac{\delta a_{b10}^e}{g(\overline{z})})\cos(\omega_s t) + \delta a_{b10}^e\big)\\ \delta V_N^e(t) &= (\delta V_{N0}^e + \frac{g(\overline{z})}{\omega_s^2}\delta\omega_{b20}^e)\cos(\omega_s t) + \frac{g(\overline{z})}{\omega_s}(\delta\theta_0^e - \frac{\delta a_{b10}^e}{g(\overline{z})})\sin(\omega_s t) - \frac{g}{\omega_s^2}\delta\omega_{b20}^e\\ \delta\omega_{b2}^e(t) &= \delta\omega_{b20}^e\\ \delta a_{b1}^e(t) &= \delta a_{b10}^e\end{aligned}$$

– the vertical error subsystem

$$\begin{aligned}
\delta V_D^e(t) &= \frac{\delta V_{D0}^e + \tau \delta \dot{V}_{D0}^e}{2} \exp \frac{t}{\tau} + \frac{\delta V_{D0}^e - \tau \delta \dot{V}_{D0}^e}{2} \exp -\frac{t}{\tau} + \delta V_{D0}^e \\
\delta z^e(t) &= \tau \left(\frac{\delta V_{D0}^e + \tau \delta \dot{V}_{D0}^e}{2} \exp \frac{t}{\tau} - \frac{\delta V_{D0}^e - \tau \delta \dot{V}_{D0}^e}{2} \exp -\frac{t}{\tau} \right) + \delta a_{b30}^e \\
\delta a_{b3}^e(t) &= \delta a_{b30}
\end{aligned}$$

– the heading error subsystem

$$\delta \psi^e(t) = \frac{\tan \lambda}{R - \overline{z}} \Big(\frac{1}{\omega_s} (\delta V_{E0}^e + \frac{g}{\omega s} \delta \omega_{b10}^e) \cos(\omega_s t) + \frac{\delta \dot{V}_{E0}^e}{\omega_s^2} (-\cos(\omega_s t) + 1) - \frac{g}{\omega_s^2} \delta \omega_{b10}^e t \Big) + \delta \psi_0^e$$

$$\delta \omega_{b3}^e(t) = \delta \omega_{b30}^e.$$

Even in presence of biases on the accelerometer and gyroscope measurements, the errors in the horizontal subsystems, and especially the velocity estimations errors, are bounded: they oscillate with the "Schuler" pulsation ω_s. On the contrary the heading estimation diverges linearly in time and the altitude estimation exponentially diverges with a time constant τ. So the horizontal subsystems are detectable: non observable but stable. On the contrary the vertical and heading subsystems are not detectable: non observable and unstable (see [**28, 23, 31**] for further details).

2.1.3. Nonlinear observer and error equations. — Since the system has no output, the nonlinear observer is just a copy of the nonlinear system itself:

$$\begin{aligned}
\dot{\hat{M}}_{b/l} &= \hat{M}_{b/l} ((\omega_m - \hat{\omega}_b)^\times - \hat{M}_{b/l} \hat{\Omega}_{l/e}^\times) \\
\dot{\hat{V}} &= -\hat{\Omega}_{l/e} \times \hat{V} + A + \hat{M}_{l/b} (a_m - \hat{a}_b) \\
\dot{\hat{z}} &= -\hat{V}_D \\
\dot{\hat{\omega}}_b &= 0 \\
\dot{\hat{a}}_b &= 0.
\end{aligned}$$

Considering the error state

$$\begin{pmatrix} M_{b/l}^e \\ V^e \\ z^e \\ \omega_b^e \\ a_b^e \end{pmatrix} = \begin{pmatrix} \hat{M}_{b/l} M_{b/l}^{-1} \\ \hat{V} - V \\ \hat{z} - z \\ \hat{\omega}_b - \omega_b \\ \hat{a}_b - a_b \end{pmatrix}$$

the linearized error equations, and thus the conclusions, are the same as in the preceding section. Even if we cannot conclude directly about the behavior of the non linear observer, further analysis would lead to the same conclusion on the detectability -or not- of the estimated variables.

2.1.4. Conclusion. — The first conclusion is that the biases cannot be estimated. It is straightforward since our observer has no correction terms. An accurate initialization is hence necessary when the vehicle is at rest. Once it is done, the sensors high-quality implies that the bias error remains small.

Although the gyroscope and accelerometer biases cannot be estimated, the errors corresponding to the horizontal subsystems are bounded due to the model of a round Earth, so called the "Schuler effect". Indeed the attitude angles and the horizontal velocities errors oscillate with an undamped natural "Schuler" pulsation $\omega_s = \sqrt{\frac{g(\overline{z})}{R-\overline{z}}} = \frac{2\pi}{T_s}$.

On the contrary the heading subsystem diverges linearly in time and the vertical subsystem error exponentially diverges with a time constant $\tau = \sqrt{\frac{R-\overline{z}}{2g(\overline{z})}}$, due to a gravity model dependent of the altitude.

If the system is moving at low altitude ($\overline{z} << R$), we find $T_s \simeq 84$ minutes and $\tau \simeq 14$ minutes.

To illustrate the "Schuler effect", let consider only initialization errors in the gyroscope measurements. Then the roll and pitch errors equations (13)–(14) write

$$\delta\phi^e(t) = -\frac{\delta\omega^e_{b10}}{\omega_s}\sin(\omega_s t) \tag{15}$$

$$\delta\theta^e(t) = \frac{\delta\omega^e_{b20}}{\omega_s}\sin(\omega_s t). \tag{16}$$

The high-precision inertial sensors that are used for "true" inertial navigation systems have a gyro drift rate less than $\omega_b = 0.01°/hour$ and very stable in time. From Equations (15)–(16), the pitch and roll errors oscillate with a very small amplitude of

$$\Delta\phi^e = \Delta\theta^e = 2\frac{\omega_b}{\omega_s} = 0.0045°.$$

On the contrary, if we use low-cost inertial sensors that have a gyroscope bias usually around $\omega_b = 0.3°/s$, the amplitude of the pitch and roll angles errors is

$$\Delta\phi^e = \Delta\theta^e = 2\frac{\omega_b}{\omega_s} = 481°.$$

So we definitely cannot use the Schuler effect with low-cost inertial sensors: the amplitude of the oscillations of the estimations becomes too important too quickly. Then we need correction terms in our observer, and thus additional measurements or assumptions.

2.2. Flat Earth model

Since low-cost sensors are embedded on a mini-UAV, we cannot benefit from the Schuler effect. So a flat Earth model is sufficient, which is equivalent for the Earth radius to tend to infinity ($R \to \infty$) in the model equations (5)–(7). $\mathcal{R}_e$ ($\equiv \mathcal{R}_l$ from now on) defines an inertial frame and the gravity vector $A = ge_3$ is constant (the unit vectors e_1, e_2, e_3 point respectively North, East, Down). Since the frames $\mathcal{R}_l$ and $\mathcal{R}_e$ are the same, we introduce $\omega = \omega_{b/l}$ and $X = \overrightarrow{X}|_l = (x, y, z)$. The system (5)–(7) becomes

$$\dot{M}_{b/l} = M_{b/l}\omega^{\times} \tag{17}$$

$$\dot{V} = A + M_{l/b}a \tag{18}$$

$$\dot{X} = V, \tag{19}$$

and if we consider the same imperfections in the accelerometer and gyroscope measurement as in section 2.1, the system (8)–(12) writes (slightly generalized in position)

$$\dot{M}_{b/l} = M_{b/l}(\omega_m - \omega_b)^{\times} \tag{20}$$

$$\dot{V} = A + M_{l/b}(a_m - a_b) \tag{21}$$

$$\dot{X} = V \tag{22}$$

$$\dot{\omega}_b = 0 \tag{23}$$

$$\dot{a}_b = 0. \tag{24}$$

Alternatively we can write the velocity equation in the body-fixed frame and it leads to the following system:

$$\begin{aligned}
\dot{M}_{b/l} &= M_{b/l}(\omega_m - \omega_b)^{\times} \\
\dot{v} &= v \times (\omega_m - \omega_b) + M_{b/l}A + a_m - a_b \\
\dot{X} &= M_{l/b}v \\
\dot{\omega}_b &= 0 \\
\dot{a}_b &= 0.
\end{aligned}$$

In order to compare the flat Earth model with the round Earth model of section 2.1, we consider only the altitude z and measurements provided by the tri-axial accelerometer and gyroscope. As in the preceding section, the inertial measurements are seen as the input of the system (20)–(24). Since the system (20)–(24) has no output, the corresponding observer will be just a copy of the equations, without correction terms. We therefore analyze the detectability of the linearized system to conclude about the behavior of the estimated variables. The linearized system around the equilibrium point$(\overline{M_{b/l}}, \overline{V}, \overline{z}, \overline{\omega_b}, \overline{a_b})$ write

$$\begin{aligned}
\delta\dot{M}_{b/l} &= \delta M_{b/l}(\overline{\omega_m} - \overline{\omega_b})^\times + \overline{M_{b/l}}(\delta\omega_m - \delta\omega_b)^\times \\
\delta\dot{V} &= A + \overline{M_{l/b}}(\delta a_m - \delta a_b) + \delta M_{l/b}(\overline{a_m} - \overline{a_b}) \\
\delta\dot{z} &= \delta V_D \\
\delta\dot{\omega}_b &= 0 \\
\delta\dot{a}_b &= 0.
\end{aligned}$$

Considering the "nominal" equilibrium point

$$(\overline{M_{b/l}}, \overline{V}, \overline{z}, \overline{\omega_b}, \overline{a_b}) = (I_3, 0, \overline{z}, \overline{\omega_m}, \overline{a_m} + A),$$

the linearized system leads to the four decoupled linearized error systems

– the lateral error subsystem

$$\begin{aligned}
\delta\dot{\phi}^e &= -\delta\omega^e_{b1} \\
\delta\dot{V}^e_E &= g\delta\phi^e - \delta a^e_{b2} \\
\delta\dot{\omega}^e_{b1} &= 0 \\
\delta\dot{a}^e_{b2} &= 0
\end{aligned}$$

– the longitudinal error subsystem

$$\begin{aligned}
\delta\dot{\theta}^e &= -\delta\omega^e_{b2} \\
\delta\dot{V}^e_N &= -g\delta\theta^e - \delta a^e_{b1} \\
\delta\dot{\omega}^e_{b2} &= 0 \\
\delta\dot{a}^e_{b1} &= 0
\end{aligned}$$

– the heading error subsystem

$$\begin{aligned}
\delta\dot{\psi}^e &= -\delta\omega^e_{b3} \\
\delta\dot{\omega}^e_{b3} &= 0
\end{aligned}$$

– the vertical error subsystem

$$\begin{aligned}\delta\dot{V}_D^e &= -\delta a_{b3}^e \\ \delta\dot{z}^e &= \delta V_D^e \\ \delta\dot{a}_{b3}^e &= 0.\end{aligned}$$

Errors in the initialization of the estimated variables cannot be avoided in real systems. If we define as in section 2.1 the linearized error $\delta x^e = \delta\hat{x} - \delta x$, we obtain the four following error subsystems

– the lateral error subsystem

$$\begin{aligned}\delta\phi^e(t) &= -\delta\omega_{b10}^e t + \delta\phi_0^e \\ \delta V_E^e(t) &= -\frac{g}{2}\delta\omega_{b10}^e t^2 - \delta a_{b20}^e t + \delta V_{E0}^e \\ \delta\omega_{b1}^e(t) &= \delta\omega_{b10}^e \\ \delta a_{b2}^e(t) &= \delta a_{b20}^e\end{aligned}$$

– the longitudinal error subsystem

$$\begin{aligned}\delta\theta^e(t) &= -\delta\omega_{b20}^e t + \delta\theta_0^e \\ \delta V_N^e(t) &= \frac{g}{2}\delta\omega_{b20}^e t^2 - \delta a_{b10}^e t + \delta V_{N0}^e \\ \delta\omega_{b2}^e(t) &= \delta\omega_{b20}^e \\ \delta a_{b1}^e(t) &= \delta a_{b10}^e\end{aligned}$$

– the heading error subsystem

$$\begin{aligned}\delta\psi^e(t) &= -\delta\omega_{b30}^e t + \delta\psi_0 \\ \delta\omega_{b3}^e(t) &= \delta\omega_{b30}^e\end{aligned}$$

– the vertical error subsystem

$$\begin{aligned}\delta V_D^e(t) &= -\delta a_{b30} t + \delta V_{D0}^e \\ \delta z^e(t) &= -\frac{\delta a_{b30}}{2} t^2 + \delta V_{D0}^e t + \delta z_0^e \\ \delta a_{b3}^e(t) &= \delta a_{b30}\end{aligned}$$

Conclusion As expected considering a flat Earth model, we lose the Schuler effect benefit since all the estimation errors now diverge. Therefore the observer cannot be just a copy of the dynamic of the system: it needs correction terms. To construct it, it is then necessary to use other sensors or to make other assumptions.

If we do not have measurements from other sensors (giving information of the velocity or position of the vehicle, for instance), the additional assumption we make is that the linear acceleration is small, i.e. $\dot{V} = 0$. Then we can construct an observer that estimates the attitude angles despite sensors biases. To also estimate the yaw angle, a tri-axial magnetometer is usually used as well, leading to an "Attitude and Heading Reference System" (AHRS).

On the contrary, if we have additional measurements (velocity, position, altitude), the "aided Attitude and Heading Reference Systems" (aided AHRS) can estimate the whole sate without making the preceding assumption.

Quaternion representation

To study the AHRS and aided AHRS, we will use the quaternion representation instead of the matrix representation from now on. Indeed it is customary to use quaternions instead of Euler angles (and rotation matrices) since they provide a global parametrization of the body orientation, and are well-suited for calculations and computer simulations. For more details see **[79]**, and section 2.6 for useful formulas used in this paper.

Using the quaternion representation, the system (17)–(19) becomes

$$\dot{q} = \frac{1}{2} q * \omega \tag{25}$$

$$\dot{V} = A + q * a * q^{-1} \tag{26}$$

$$\dot{X} = V, \tag{27}$$

where q is the unit quaternion representing the orientation of the body with respect to the Earth-fixed frame. We can also consider v the projection of the velocity vector in the body-fixed frame, which writes $v = q^{-1} * V * q$. Then the motion equations write

$$\begin{aligned} \dot{q} &= \frac{1}{2} q * \omega \\ \dot{v} &= v \times \omega + q^{-1} * A * q + a \\ \dot{X} &= q * v * q^{-1}. \end{aligned}$$

We now linearize the system (25)–(27) around the equilibrium point $(\overline{q}, \overline{\omega} = 0, \overline{V} = 0, \overline{X})$. Since $\overline{a} = -\overline{q}^1 * A * \overline{q}$, the linearized equation (26) writes

$$\begin{aligned}\delta\dot{V} &= \delta q * (-\overline{q}^{-1} * A * \overline{q}) * \overline{q}^{-1} + \overline{q}^1 * \delta a * \overline{q} + \overline{q} * (-\overline{q}^{-1} * A * \overline{q}) * (-\overline{q}^{-1} * \delta q * \overline{q}^{-1}) \\ &= -(\delta q * \overline{q}^{-1}) * A + A * (\delta q * \overline{q}^{-1}) + \overline{q}^{-1} * \delta a * \overline{q} \\ &= 2A \times (\delta q * \overline{q}^{-1}) + \overline{q} * \delta a * \overline{q}^{-1}.\end{aligned}$$

Then the system (25)–(27) linearized around the equilibrium point $(\overline{q}, \overline{\omega} = 0, \overline{V} = 0, \overline{X})$ writes

$$\begin{aligned}\delta\dot{q} &= \frac{1}{2}\overline{q} * \delta\omega \\ \delta\dot{V} &= 2A \times (\delta q * \overline{q}^{-1}) + \overline{q} * \delta a * \overline{q}^{-1} \\ \delta\dot{X} &= \delta V.\end{aligned}$$

Let us define the following vectors

$$\begin{pmatrix} e_q \\ e_V \\ e_X \\ e_a \\ e_\omega \end{pmatrix} = \begin{pmatrix} \delta q * \overline{q}^{-1} \\ \delta V \\ \delta X \\ \overline{q} * \delta a * \overline{q}^{-1} \\ \overline{q} * \delta\omega * \overline{q}^{-1} \end{pmatrix},$$

where e_q, e_V, e_X are linearized errors and e_a, e_ω are vectors expressed in a new frame. The linearized error equations writes

$$\begin{aligned}\dot{e}_q &= \frac{1}{2} * e_\omega \\ \dot{e}_V &= 2A \times e_q + e_a \\ \dot{e}_X &= e_V.\end{aligned}$$

What is noticeable is that we obtain the same linearized error system whatever the value of $\overline{q}$ is. This notion of "invariance" by rotation will be detailed further.

2.3. Model for AHRS

2.3.1. Measurements and motion equations. — In an Attitude and Heading Reference System, we do not have any velocity or position measurements: we generally use only three triaxial sensors providing nine scalar measurements: a triaxial gyroscope measures ω_m ($= \omega$ if perfect); a triaxial magnetometer measures the magnetic field in the

body-fixed frame $y_B = q^{-1} * B * q$ (if perfect), where $B = B_1 e_1 + B_3 e_3$ is the Earth magnetic field in North-East-Down (NED) coordinates ; a triaxial accelerometer measures a_m ($= a$ if perfect). In an AHRS, we assume that the linear acceleration $\dot{V}$ is small, hence we approximate the specific acceleration vector (see Equation (26)) by $a = -q^{-1} * A * q$. If the accelerometer measurements are perfect $y_A = a_m = -a = q^{-1} * A * q$ (the sign is reversed for convenience).

Then the physical system (25)–(27) becomes

$$\dot{q} = \frac{1}{2} q * \omega, \tag{28}$$

with the output

$$\begin{pmatrix} y_A \\ y_B \end{pmatrix} = \begin{pmatrix} q^{-1} * A * q \\ q^{-1} * B * q \end{pmatrix}. \tag{29}$$

2.3.2. Observability analysis of the measurements imperfections. — The sensors we use are low-cost and therefore they have imperfections. We do a simple first-order observability analysis, i.e. an analysis of the observability of the linearized system, to know how we can model these imperfections. For simplicity, we linearize the system (28)–(29) around $(\overline{q}, \overline{\omega}) = (1, 0)$ (linearizing around any $\overline{q}$ leads to the same conclusion):

$$\delta\dot{q} = \frac{1}{2}\delta\omega,$$

with the output

$$\begin{pmatrix} \delta y_A \\ \delta y_B \end{pmatrix} = \begin{pmatrix} 2A \times \delta q \\ 2B \times \delta q \end{pmatrix} = \begin{pmatrix} -2g\delta q_2 \\ 2g\delta q_1 \\ 0 \\ -2B_3\delta q_2 \\ 2(B_3\delta q_1 - B_1\delta q_3) \\ 2B_1\delta q_2 \end{pmatrix}.$$

There is some freedom when modeling the sensors' imperfections. We see that up to six unknown constants can be estimated. We first consider as usual a constant vector bias ω_b on the gyroscopes measurements. Beside it, it is possible to estimate two imperfections on y_B and one on y_a, or one on y_B and two on y_a. Nevertheless it is impossible to model three imperfections on y_a: in particular if we write $y_a = a_m = -a - a_b$, with a_b a constant

vector bias, only two components of a_b are observable. Indeed considering a_b leads to

$$\delta y_A = \begin{pmatrix} -2g\delta q_2 - \delta a_{b1} \\ 2g\delta q_1 - \delta a_{b2} \\ -\delta a_{b3} \end{pmatrix}.$$

So we can get δq_2, δa_{b3}, δa_{b1} from the equations

$$\begin{aligned} \delta q_2 &= \frac{1}{2B_1}\delta y_{B3} \\ \delta a_{b3} &= -\delta y_{A3} \\ \delta a_{b1} &= -2g\delta q_2 - \delta y_{A1} \end{aligned}$$

but δa_{b2} and δq_3 cannot be recovered since there is only one relationship:

$$\delta a_{b2} = \frac{g}{B_3}(\delta y_{B2} + B_1\delta q_3) - \delta y_{A2}.$$

On the other hand it is also impossible to estimate the three components of the magnetic field B, but only the North and Down components.

2.3.3. Magnetic disturbances considerations. — In an AHRS, it is usually desirable to use the magnetic measurements to estimate the heading only, so that a magnetic disturbance does not affect the estimated attitude, which is more critical than the estimated yaw angle for the mini-UAV safety. Only one imperfection on a_m can be estimated without relying on the possibly disturbed magnetic measurements, so we consider a scaling factor a_s on the accelerometers measurements: $a_m = y_A = a_s q^{-1} * A * q$. We will see the heading decoupling can be achieved by considering $y_C = y_A \times y_B$ and $C = A \times B$, rather than the direct measurement y_B. Notice that $\langle y_A, y_C \rangle = \langle A, C \rangle = 0$, so that we are left with 8 independent measurements; as a consequence only five unknown constants can now be estimated. This is not a drawback and is even beneficial since the observer will then not depend on the latitude-varying B_3. Then $y_C = c_s q^{-1} * C * q$, where $c_s > 0$. So we consider that 3 gyros measure $\omega_m = \omega + \omega_b$, where ω_b is a constant vector bias; 3 accelerometers measure $a_m = y_A = a_s q^{-1} * A * q$, where $a_s > 0$ is a constant scaling factor; 3 magnetometers measure $y_B = b_s q^{-1} * B * q$, where $b_s > 0$ is a constant scaling factor which is transformed into $y_C = c_s q^{-1} * C * q$, where $c_s > 0$ is a constant scaling factor. All the nine measurements are of course also corrupted by noise.

2.3.4. The model in an AHRS. — To design our observer we thus consider the system

$$\dot{q} = \frac{1}{2} q * (\omega_m - \omega_b) \tag{30}$$

$$\dot{\omega}_b = 0 \tag{31}$$

$$\dot{a}_s = 0 \tag{32}$$

$$\dot{c}_s = 0, \tag{33}$$

with the output

$$\begin{pmatrix} y_A \\ y_C \end{pmatrix} = \begin{pmatrix} a_s q^{-1} * A * q \\ c_s q^{-1} * C * q \end{pmatrix}. \tag{34}$$

This system is observable since all the state variables can be recovered from the known quantities ω_m, y_A, y_C and their derivatives: from Equation (34), $a_s = \frac{1}{g} \|y_A\|$ and $c_s = \frac{1}{B_1 g} \|y_C\|$; hence we know the action of q on the two independent vectors A and C, which completely defines q as a function of y_A, y_C, a_s, c_s. Finally Equation (30) yields $\omega_b = \omega_m - 2q^{-1}\dot{q}$.

2.4. Model for aided AHRS

2.4.1. Measurements and motion equations. — In addition to the three triaxial sensors used in an AHRS, for an aided AHRS other sensors give velocity vector (V or v) and may also give the position vector (X). They are usually provided by the navigation solutions y_X and y_V of a GPS engine giving a measure of X and V, or by some air-data system providing a measure of v, y_v. A barometric sensor may also provide a measurement of the altitude $y_h = \langle X, e_3 \rangle$.

We consider the system described by Equations (35)–(37) where the velocity is expressed in the Earth-fixed frame

$$\dot{q} = \frac{1}{2} q * \omega \tag{35}$$

$$\dot{V} = A + q * a * q^{-1} \tag{36}$$

$$\dot{X} = V \tag{37}$$

or the system described by Equations (38)–(40) where the velocity is expressed in the body-fixed frame

$$\dot{q} = \frac{1}{2} q * \omega \tag{38}$$

$$\dot{v} = v \times \omega + q^{-1} * A * q + a \tag{39}$$

$$\dot{X} = q * v * q^{-1}, \tag{40}$$

the input is the inertial sensors' measurement (a and ω) and the output

$$\begin{pmatrix} y_V \\ y_v \\ y_X \\ y_h \\ y_B \end{pmatrix} = \begin{pmatrix} V \\ v \\ X \\ \langle X, e_3 \rangle \\ q^{-1} * B * q \end{pmatrix}. \tag{41}$$

We have some freedom to express the velocity in the Earth-fixed frame of body-fixed frame, since $y_V = V = q^{-1} * v * q$ and $y_v = v = q^{-1} * V * q$.

2.4.2. Imperfections of the measurements. — As in section 2.3, a simple first-order observability analysis reveals that up to thirteen unknown constants can be estimated. There are many ways to model the eight additional imperfections on the measurements. We choose to use only five extra constants to model imperfections: we consider here 3 biases on the gyroscope, one scaling factor on the accelerometer and one bias on the altitude measurement, in order to ensure that the estimated velocity equals the measured velocity (see §4.1.5.2) during level flight. The barometric sensor thus provides a measure of the altitude $y_h = \langle X, e_3 \rangle - h_b$, where h_b is a constant scalar bias. All these measurements are of course also corrupted by noise.

2.4.3. The considered system. — To design our observers, we therefore consider the system

$$\dot{q} = \frac{1}{2} q * (\omega_m - \omega_b) \tag{42}$$

$$\dot{V} = A + \frac{1}{a_s} q * a_m * q^{-1} \tag{43}$$

$$\dot{X} = V \tag{44}$$

$$\dot{\omega}_b = 0 \tag{45}$$

$$\dot{a}_s = 0 \tag{46}$$

$$\dot{h}_b = 0 \tag{47}$$

where ω_m and a_m are seen as known inputs, together with the measured output

$$\begin{pmatrix} y_V \\ y_v \\ y_X \\ y_h \\ y_B \end{pmatrix} = \begin{pmatrix} V \\ v \\ X \\ \langle X, e_3 \rangle - h_b \\ q^{-1} * B * q \end{pmatrix}. \tag{48}$$

This system is observable provided $B \times (q * a_m * q^{-1}) \neq 0$ since all the state variables can be recovered from the known quantities $\omega_m, a_m, y_V, y_X, y_h, y_B$ and their derivatives. Indeed from Equation (43), $a_s = \frac{\|a_m\|}{\|\dot{y}_V - A\|}$ and $\frac{a_m}{\|a_m\|} = q^{-1} * \frac{\dot{y}_V - A}{\|\dot{y}_V - A\|} * q$. We thus know the action of q on the two known vectors B and $\dot{y}_V - A$, which are independent by the above assumption; this completely defines q as a function of $y_B, \dot{y}_B, a_m$. Finally $\omega_b = \omega_m - 2q^{-1}\dot{q}$ is determined from Equation (42) and $h_b = \langle y_X, e_3 \rangle - y_h$ from Equation (48).

2.5. Invariance properties of the flat Earth model

The generic observers we construct in this thesis are based on the invariance properties of the considered system. So we are looking for frame changes that leave the system (35)–(41) unchanged. For simplicity, we consider here only ideal measurements: the imperfections of the sensors will be taken into account in the next chapters. Several transformations will be considered:

– a right rotation: defined by the unit quaternion q_0 and the relationship $q \longrightarrow q * q_0$

– a left rotation: defined by the unit quaternion p_0 and the relationship $q \longrightarrow p_0 * q$

- a translation in the body-fixed frame: defined by the 3×1 vector v_0 and the relationship $v \to v + v_0$
- a translation in the Earth-fixed frame: defined by the 3×1 vector V_0 and the relationship $V \to V + V_0$

We do not first consider the position variable X, since some additional difficulties appear as we will see later. So we consider the systems

$$(49) \qquad \begin{aligned} \dot{q} &= \frac{1}{2} q * \omega \\ \dot{V} &= A + q * a * q^{-1} \end{aligned} \qquad \text{and} \qquad \begin{aligned} \dot{q} &= \frac{1}{2} q * \omega \\ \dot{v} &= v \times \omega + q^{-1} * A * q + a. \end{aligned}$$

A global transformation of the variables (q, V) and (q, v) is a combination of the four preceding transformations. We define the group composition law $\star$ by

$$\begin{pmatrix} p_0 \\ V_0 \end{pmatrix} \star \begin{pmatrix} p_1 \\ V_1 \end{pmatrix} = \begin{pmatrix} p_0 * p_1 \\ V_0 + p_0 * V_1 * p_0^{-1} \end{pmatrix}.$$

A global coordinate change of (q, V) is the transformation group action defined by

$$\begin{aligned} \varphi_{(p_0,q_0,V_0,v_0)}(q, V) = \begin{pmatrix} \tilde{q} \\ \tilde{V} \end{pmatrix} &= \begin{pmatrix} p_0 \\ V_0 \end{pmatrix} \star \begin{pmatrix} q \\ V \end{pmatrix} \star \begin{pmatrix} q_0 \\ v_0 \end{pmatrix} \\ &= \begin{pmatrix} p_0 * q * q_0 \\ V_0 + p_0 * (V + q * v_0 * q^{-1}) p_0^{-1} \end{pmatrix} \end{aligned}$$

where p_0, q_0 are unit quaternions and V_0, v_0 are vectors in $\mathbb{R}^3$. This transformation group consists of the mix of left and right multiplication by $\star$, i.e. the mix of rotations and translations in the Earth-fixed and the body-fixed frames. The associated group law is

$$\begin{pmatrix} p_0 \\ q_0 \\ V_0 \\ v_0 \end{pmatrix} \diamond \begin{pmatrix} p_1 \\ q_1 \\ V_1 \\ v_1 \end{pmatrix} = \begin{pmatrix} p_0 * p_1 \\ q_0 * q_1 \\ V_0 + p_0 * V_1 * p_0^{-1} \\ v_1 + q_1 * v_0 * q_1^{-1} \end{pmatrix}.$$

It is indeed a transformation group since

$$\varphi_{(p_1,q_1,V_1,v_1)} \circ \varphi_{(p_0,q_0,V_0,v_0)} \begin{pmatrix} q \\ V \end{pmatrix} = \varphi_{(p_1,q_1,V_1,v_1) \diamond (p_0,q_0,V_0,v_0)} \begin{pmatrix} q \\ V \end{pmatrix}.$$

In the considered system (49), other vectors must be taken into account in addition to (q, V) in order to have a transformation group action on the complete set of variables.

Indeed, the vectors (ω, a, A) must be changed into

$$\begin{aligned}\tilde{\omega} &= q_0 * \omega * q_0^{-1}\\ \tilde{a} &= q_0^{-1} * (a + \omega \times v_0) * q_0\\ \tilde{A} &= p_0 * A * p_0^{-1}\end{aligned}$$

if we want the system (49) to be invariant by a transformation group action. Therefore, a global coordinate change of (q, ω, V, a, A) is the transformation group action defined by

$$\varphi_{(p_0,q_0,V_0,v_0)}(q,\omega,V,a,A) = \begin{pmatrix}\tilde{q}\\ \tilde{\omega}\\ \tilde{V}\\ \tilde{a}\\ \tilde{A}\end{pmatrix} = \begin{pmatrix} p_0 * q * q_0\\ V_0 + p_0 * (V + q * v_0 * q^{-1}) * p_0^{-1}\\ q_0^{-1} * \omega * q_0\\ q_0^{-1} * (a + \omega \times v_0) * q_0\\ p_0 * A * p_0^{-1}\end{pmatrix}.$$

The system (49) is invariant by this transformation group since

$$\begin{aligned}\dot{\tilde{q}} &= \dot{\overbrace{p_0 * q * q_0}} = p_0 * \dot{q} * q_0 = \frac{1}{2}(p_0 * q * q_0) * (q_0^{-1} * \omega * q_0) = \frac{1}{2}\tilde{q} * \tilde{\omega}\\ \dot{\tilde{V}} &= \dot{\overbrace{V_0 + p_0 * (V + q * v_0 * q^{-1}) * p_0^{-1}}}\\ &= p_0 * \dot{V} * p_0^{-1} + p_0 * \dot{q} * v_0 * q^{-1} * p_0^{-1} - p_0 * q * v_0 * q^{-1} * \dot{q} * q^{-1} * p_0^{-1}\\ &= p_0 * A * p_0^{-1} + p_0 * q * a * q^{-1} * p_0^{-1} + p_0 * q * (\omega \times v_0) * q^{-1} * p_0^{-1}\\ &= p_0 * A * p_0^{-1} + p_0 * q * q_0 * (q_0^{-1} * (a + \omega \times v_0) * q_0) * (p_0 * q * q_0)^{-1}\\ &= \tilde{A} + \tilde{q} * \tilde{a} * \tilde{q}^{-1}.\end{aligned}$$

When we consider imperfections on the measurements, the global transformation group needs to be completed. The choice of the values of the parameters (p_0, q_0, V_0, v_0) depends on the considered output (since the output must also be left unchanged by the transformation group) and on the position X considered or not in the equations (it is impossible then to consider a translation in the body-fixed frame in the transformation group: v_0 would be automatically set to 0). Therefore the value of some parameters will be automatically defined in order to preserve invariance properties:

- in Section 3 (inertial and magnetic measurements): $p_0 = V_0 = v_0 = 0$ and any q_0
- in Section 4.1 (inertial, magnetic and Earth-fixed velocity measurements): $p_0 = v_0 = 0$ and any q_0, V_0
- in Section 4.2 (inertial, magnetic, Earth-fixed velocity and position measurements): $v_0 = V_0 = 0$ and any p_0, q_0

– in Section 4.3 (inertial, magnetic, Earth-fixed and body-fixed velocity measurements): $v_0 = V_0 = 0$ and any p_0, q_0.

2.6. Quaternions

Thanks to their four coordinates, quaternions provide a global parametrization of the orientation of a rigid body (whereas a parametrization with three Euler angles necessarily has singularities). Indeed, to any quaternion q with unit norm is associated a rotation matrix $R_q \in SO(3)$ by

$$q^{-1} * \vec{p} * q = R_q \cdot \vec{p} \quad \text{for all } \vec{p} \in \mathbb{R}^3.$$

A quaternion p can be thought of as a scalar $p_0 \in \mathbb{R}$ together with a vector $\vec{p} \in \mathbb{R}^3$,

$$p = \begin{pmatrix} p_0 \\ \vec{p} \end{pmatrix}.$$

The (non commutative) quaternion product $*$ then reads

$$p * q \triangleq \begin{pmatrix} p_0 q_0 - \vec{p} \cdot \vec{q} \\ p_0 \vec{q} + q_0 \vec{p} + \vec{p} \times \vec{q} \end{pmatrix}.$$

The unit element is $e \triangleq \begin{pmatrix} 1 \\ \vec{0} \end{pmatrix}$, and $(p * q)^{-1} = q^{-1} * p^{-1}$.

Any scalar $p_0 \in \mathbb{R}$ can be seen as the quaternion $\begin{pmatrix} p_0 \\ \vec{0} \end{pmatrix}$, and any vector $\vec{p} \in \mathbb{R}^3$ can be seen as the quaternion $\begin{pmatrix} 0 \\ \vec{p} \end{pmatrix}$. We systematically use these identifications in the thesis, which greatly simplify the notations.

We have the useful formulas

$$p \times q \triangleq \vec{p} \times \vec{q} = \frac{1}{2}(p * q - q * p)$$

$$(\vec{p} \cdot \vec{q})\vec{r} = -\frac{1}{2}(p * q + q * p) * r.$$

If q depends on time, then $\dot{q}^{-1} = -q^{-1} * \dot{q} * q^{-1}$.

Finally, consider the differential equation $\dot{q} = q * u + v * q$ where u, v are vectors $\in \mathbb{R}^3$. Let q^T be defined by $\begin{pmatrix} q_0 \\ -\vec{q} \end{pmatrix}$. Then $q * q^T = \|q\|^2$. Therefore,

$$\dot{\overbrace{q * q^T}} = q * (u + u^T) * q^T + \|q\|^2 (v + v^T) = 0$$

since u, v are vectors. Hence the norm of q is constant.

CHAPTER 3

SYMMETRY-PRESERVING OBSERVERS FOR ATTITUDE AND HEADING REFERENCE SYSTEMS

Dans ce chapitre nous nous intéressons aux observateurs pour les "Attitude and Heading Reference Systems", dans lesquels seuls des capteurs bas-coûts inertiels et magnétiques sont utilisés. Le filtre présenté est un observateur nonlinéaire invariant, qui préserve certaines symétries naturelles et propriétés physiques du système considéré. Le choix des termes de correction permet d'assurer un large domaine de convergence, ainsi qu'un découplage intéressant d'estimations des angles d'attitude et de lacet. Ce dernier sera alors le seul vraiment affecté par une perturbation magnétique tandis que les estimations d'angles d'attitude, plus importantes pour le contrôle d'un mini-drone, restent très bonnes. Il est également facile à régler grâce à un nombre réduit de paramètres à choisir.

3.1. Nonlinear observer

3.1.1. Model of the rigid body. — Attitude and Heading References Systems rely on low-cost inertial and magnetic sensors. Therefore we consider the system (30)–(34)

described in section 2.3 and repeated here for convenience:

$$\dot{q} = \frac{1}{2} q * (\omega_m - \omega_b) \tag{50}$$

$$\dot{\omega}_b = 0 \tag{51}$$

$$\dot{a}_s = 0 \tag{52}$$

$$\dot{c}_s = 0 \tag{53}$$

with the output

$$\begin{pmatrix} y_A \\ y_C \end{pmatrix} = \begin{pmatrix} a_s q^{-1} * A * q \\ c_s q^{-1} * C * q \end{pmatrix}. \tag{54}$$

3.1.2. Invariance of the system equations. — We presented in section 2.5 a global transformation group on the variables (q, ω, V, a, A) depending on the parameters p_0, q_0, v_0, V_0. We adapt this transformation to our system (with no velocity) and therefore we consider only the quaternion transformation. We also extend this transformation to the new state variables. All the measurements are expressed in the body-fixed frame. From a physical and engineering viewpoint, a sensible observer using these measurements should not be affected by the actual choice of body-fixed coordinates, i.e. by a constant rotation in the body-fixed frame. Similarly, a translation of the gyro bias by a vector that is constant in the body-fixed frame and a scaling of the output should not affect the observer. We therefore consider the transformation group generated by constant rotations, translations in the body-fixed frame and scaling (i.e. defined by constant parameters)

$$\varphi_{(q_0,\omega_0,a_0,c_0)} \begin{pmatrix} q \\ \omega_b \\ a_s \\ c_s \end{pmatrix} = \begin{pmatrix} q * q_0 \\ q_0^{-1} * \omega_b * q_0 + \omega_0 \\ a_0 a_s \\ c_0 c_s \end{pmatrix}$$

$$\psi_{(q_0,\omega_0,a_0,c_0)}(\omega_m) = q_0^{-1} * \omega_m * q_0 + \omega_0$$

$$\rho_{(q_0,\omega_0,a_0,c_0)} \begin{pmatrix} y_A \\ y_C \end{pmatrix} = \begin{pmatrix} a_0 q_0^{-1} * y_A * q_0 \\ c_0 q_0^{-1} * y_C * q_0 \end{pmatrix},$$

where q_0 is a unit quaternion, ω_0 a vector in $\mathbb{R}^3$ and $a_0, c_0 > 0$. It is indeed a transformation group since

$$\varphi_{(q_1,\omega_1,a_1,c_1)} \circ \varphi_{(q_0,\omega_0,a_0,c_0)} \begin{pmatrix} q \\ \omega_b \\ a_s \\ c_s \end{pmatrix} = \varphi_{(q_1,\omega_1,a_1,c_1)\diamond(q_0,\omega_0,a_0,c_0)} \begin{pmatrix} q \\ \omega_b \\ a_s \\ c_s \end{pmatrix}$$

$$\psi_{(q_1,\omega_1,a_1,c_1)} \circ \psi_{(q_0,\omega_0,a_0,c_0)}(\omega_m) = \psi_{(q_1,\omega_1,a_1,c_1)\diamond(q_0,\omega_0,a_0,c_0)}(\omega_m)$$

$$\rho_{(q_1,\omega_1,a_1,c_1)} \circ \rho_{(q_0,\omega_0,a_0,c_0)} \begin{pmatrix} y_A \\ y_C \end{pmatrix} = \rho_{(q_1,\omega_1,a_1,c_1)\diamond(q_0,\omega_0,a_0,c_0)} \begin{pmatrix} y_A \\ y_C \end{pmatrix},$$

where the group composition law $\diamond$ is defined by

$$\begin{pmatrix} q_1 \\ \omega_1 \\ a_1 \\ c_1 \end{pmatrix} \diamond \begin{pmatrix} q_0 \\ \omega_0 \\ a_0 \\ c_0 \end{pmatrix} = \begin{pmatrix} q_0 * q_1 \\ q_1^{-1} * \omega_0 * q_1 + \omega_1 \\ a_1 a_0 \\ c_1 c_0 \end{pmatrix}.$$

The system (50)-(53) is of course invariant by the transformation group since

$$\dot{\overbrace{q * q_0}} = \dot{q} * q_0 = \frac{1}{2}(q * q_0) * \left((q_0^{-1} * \omega_m * q_0 + \omega_0) - (q_0^{-1} * \omega_b * q_0 + \omega_0)\right)$$

$$\dot{\overbrace{q_0^{-1} * \omega_b * q_0 + \omega_0}} = q_0^{-1} * \dot{\omega}_b * q_0 = 0$$

$$\dot{\overbrace{a_0 a_s}} = a_0 \dot{a}_s = 0$$

$$\dot{\overbrace{c_0 c_s}} = c_0 \dot{c}_s = 0,$$

whereas the output (54) is equivariant since

$$\begin{pmatrix} (a_0 a_s)(q * q_0)^{-1} * A * (q * q_0) \\ (c_0 c_s)(q * q_0)^{-1} * C * (q * q_0) \end{pmatrix} = \rho_{(q_0,\omega_0,a_0,c_0)} \begin{pmatrix} a_s q^{-1} * A * q \\ c_s q^{-1} * C * q \end{pmatrix}.$$

3.1.3. Construction of the general invariant observer. — We solve the normalization equations for $(q_0, \omega_0, a_0, c_0)$

$$\begin{aligned} q * q_0 &= 1 \\ q_0^{-1} * \omega_b * q_0 + \omega_0 &= 0 \\ a_0 a_s &= 1 \\ c_0 c_s &= 1 \end{aligned}$$

to find the moving frame

$$\gamma(q, \omega_b, a_s, c_s) = \begin{pmatrix} q^{-1} \\ -q * \omega_b * q^{-1} \\ \frac{1}{a_s} \\ \frac{1}{c_s} \end{pmatrix}.$$

We then get the 6-dimensional invariant output error

$$\begin{aligned} \begin{pmatrix} E_A(\hat{q}, \hat{\omega}_b, \hat{a}_s, \hat{c}_s, y_A) \\ E_C(\hat{q}, \hat{\omega}_b, \hat{a}_s, \hat{c}_s, y_C) \end{pmatrix} &= \rho_{\gamma(\hat{q}, \hat{\omega}_b, \hat{a}_s, \hat{c}_s)} \begin{pmatrix} \hat{a}_s \hat{q}^{-1} * A * \hat{q} \\ \hat{c}_s \hat{q}^{-1} * C * \hat{q} \end{pmatrix} - \rho_{\gamma(\hat{q}, \hat{\omega}_b, \hat{a}_s, \hat{c}_s)} \begin{pmatrix} y_A \\ y_C \end{pmatrix} \\ &= \begin{pmatrix} A - \frac{1}{\hat{a}_s} \hat{q} * y_A * \hat{q}^{-1} \\ C - \frac{1}{\hat{c}_s} \hat{q} * y_C * \hat{q}^{-1} \end{pmatrix} \end{aligned} \tag{55}$$

and the 3-dimensional complete invariant

$$I(\hat{q}, \hat{\omega}_b, \hat{a}_s, \hat{c}_s, \omega_m) = \psi_{\gamma(\hat{q}, \hat{\omega}_b, \hat{a}_s, \hat{c}_s)}(\omega_m) = \hat{q} * (\omega_m - \hat{\omega}_b) * \hat{q}^{-1}.$$

It is straightforward to check that E_A, E_C and I are indeed invariant. For instance,

$$\begin{aligned} E_A(\hat{q} * q_0, q_0^{-1} * \hat{\omega}_b * q_0 + \omega_0, a_0 \hat{a}_s, c_0 \hat{c}_s, a_0 q_0^{-1} * y_A * q_0) \\ &= A - \frac{1}{a_0 \hat{a}_s} (\hat{q} * q_0) * (a_0 q_0^{-1} * y_A * q_0) * (\hat{q} * q_0)^{-1} \\ &= A - \frac{1}{\hat{a}_s} \hat{q} * y_A * \hat{q}^{-1} \\ &= E_A(\hat{q}, \hat{\omega}_b, \hat{a}_s, \hat{c}_s, y_A). \end{aligned}$$

To find the invariant vector fields, we solve the 8 vector equations for $w(q, \omega_b, a_s, c_s)$

$$\left[D\varphi_{\gamma(q, \omega_b, a_s, c_s)} \begin{pmatrix} q \\ \omega_b \\ a_s \\ c_s \end{pmatrix} \right] \cdot w(q, \omega_b, a_s, c_s) = \begin{pmatrix} e_i \\ 0 \\ 0 \\ 0 \end{pmatrix}, \begin{pmatrix} 0 \\ e_i \\ 0 \\ 0 \end{pmatrix}, \begin{pmatrix} 0 \\ 0 \\ 1 \\ 0 \end{pmatrix} \text{ or } \begin{pmatrix} 0 \\ 0 \\ 0 \\ 1 \end{pmatrix}, \quad i = 1, 2, 3,$$

where the e_i's are the canonical basis of $\mathbb{R}^3$ (we have identified the tangent space of the unit norm quaternions space to $\mathbb{R}^3$). Since

$$\left[D\varphi_{(q_0, \omega_0, a_0, c_0)} \begin{pmatrix} q \\ \omega_b \\ a_s \\ c_s \end{pmatrix} \right] \cdot \begin{pmatrix} \delta q \\ \delta \omega_b \\ \delta a_s \\ \delta c_s \end{pmatrix} = \begin{pmatrix} \delta q * q_0 \\ q_0^{-1} * \delta \omega_b * q_0 \\ a_0 \delta a_s \\ c_0 \delta c_s \end{pmatrix},$$

this yields the 8 independent invariant vector fields

$$\begin{pmatrix} e_i * q \\ 0 \\ 0 \\ 0 \end{pmatrix}, \begin{pmatrix} 0 \\ q^{-1} * e_i * q \\ 0 \\ 0 \end{pmatrix}, \begin{pmatrix} 0 \\ 0 \\ a_s \\ 0 \end{pmatrix} \text{ and } \begin{pmatrix} 0 \\ 0 \\ 0 \\ c_s \end{pmatrix}, \quad i = 1, 2, 3.$$

It is easy to check that these vector fields are indeed invariant. For instance,

$$\left[D\varphi_{(q_0,\omega_0,a_0,c_0)} \begin{pmatrix} q \\ \omega_b \\ a_s \\ c_s \end{pmatrix} \right] \cdot \begin{pmatrix} e_i * q \\ 0 \\ 0 \\ 0 \end{pmatrix} = \begin{pmatrix} (e_i * q) * q_0 \\ 0 \\ 0 \\ 0 \end{pmatrix} = \begin{pmatrix} e_i * (q * q_0) \\ 0 \\ 0 \\ 0 \end{pmatrix}.$$

The general invariant observer then reads

$$\begin{aligned} \dot{\hat{q}} &= \frac{1}{2}\hat{q} * (\omega_m - \hat{\omega}_b) + \sum_{i=1}^{3} (L_{Ai}E_A + L_{Ci}E_C)e_i * \hat{q} \\ \dot{\hat{\omega}}_b &= \sum_{i=1}^{3} \hat{q}^{-1} * (M_{Ai}E_A + M_{Ci}E_C)e_i * \hat{q} \\ \dot{\hat{a}}_s &= \hat{a}_s(N_A E_A + N_C E_C) \\ \dot{\hat{c}}_s &= \hat{c}_s(O_A E_A + O_C E_C), \end{aligned}$$

where the L_{Ai}, L_{Ci}, M_{Ai}, M_{Ci}'s, N_A, N_C, O_A, O_C are arbitrary 1×3 matrices with entries possibly depending on E_A, E_C, and I. Noticing

$$\sum_{i=1}^{3} (L_{Ai}E_A)e_i = \begin{pmatrix} L_{A1} \\ L_{A2} \\ L_{A3} \end{pmatrix} E_A = L_A E_A,$$

where L_A is the 3×3 matrix whose rows are the L_{Ai}'s, and defining L_B, M_A and M_B in the same way, we can rewrite the observer as

$$\dot{\hat{q}} = \frac{1}{2}\hat{q} * (\omega_m - \hat{\omega}_b) + (L_A E_A + L_C E_C) * \hat{q} \tag{56}$$

$$\dot{\hat{\omega}}_b = \hat{q}^{-1} * (M_A E_A + M_C E_C) * \hat{q} \tag{57}$$

$$\dot{\hat{a}}_s = \hat{a}_s(N_A E_A + N_C E_C) \tag{58}$$

$$\dot{\hat{c}}_s = \hat{c}_s(O_A E_A + O_C E_C). \tag{59}$$

Only 5 of the 6 possible projections are independent since $\langle A, C\rangle = 0$ and $\langle y_A, y_C\rangle = 0$ imply

$$\langle E_A, E_C\rangle = \langle A, E_C\rangle + \langle E_A, C\rangle. \tag{60}$$

So we define the invariant output error E, 5×1 vector,

$$E = \Big(\langle E_A, e_1\rangle, \langle E_A, e_2\rangle, \langle E_A, e_3\rangle, \langle E_C, e_1\rangle, \langle E_C, e_2\rangle\Big)^T \tag{61}$$

made up of the projections of the vectors E_A and E_C.

The general invariant observer thus writes

$$\dot{\hat{q}} = \frac{1}{2}\hat{q} * (\omega_m - \hat{\omega}_b) + (LE) * \hat{q} \tag{62}$$

$$\dot{\hat{\omega}}_b = \hat{q}^{-1} * (ME) * \hat{q} \tag{63}$$

$$\dot{\hat{a}}_s = \hat{a}_s NE \tag{64}$$

$$\dot{\hat{c}}_s = \hat{c}_s OE. \tag{65}$$

L, M are 3×5 matrices and N, O are 1×5 matrices with entries possibly depending on the components of E and on the complete invariant I.

It is easy to check this observer is invariant. Notice also the built-in desirable geometric feature: the norm of $\hat{q}$ is left unchanged by Equation (62), i.e. $\|\hat{q}(t)\| = \|\hat{q}(0)\| = 1$, since LE is a vector of $\mathbb{R}^3$ (see section 2.6).

3.1.4. The invariant error system. — The invariant state error is given by

$$\begin{pmatrix}\eta\\ \beta\\ \alpha\\ \gamma\end{pmatrix} = \varphi_{\gamma(q,\omega_b,a_s,c_s)}\begin{pmatrix}\hat{q}\\ \hat{\omega}_b\\ \hat{a}_s\\ \hat{c}_s\end{pmatrix} - \varphi_{\gamma(q,\omega_b,a_s,c_s)}\begin{pmatrix}q\\ \omega_b\\ a_s\\ c_s\end{pmatrix} = \begin{pmatrix}\hat{q} * q^{-1} - 1\\ q * (\hat{\omega}_b - \omega_b) * q^{-1}\\ \frac{a_s}{\hat{a}_s}\\ \frac{c_s}{\hat{c}_s}\end{pmatrix}.$$

It is in fact more natural –though completely equivalent– to take $\eta = \hat{q} * q^{-1}$ (rather than $\eta = \hat{q} * q^{-1} - 1$), so that $\eta(x, x) = 1$, the unit element of the group of quaternions.

Therefore,

$$\begin{aligned}
\dot{\eta} &= \dot{\hat{q}} * q^{-1} - \hat{q} * (q^{-1} * \dot{q} * q^{-1}) = (LE) * \eta - \frac{1}{2}\eta * \beta \\
\dot{\beta} &= q * (\dot{\hat{\omega}}_b - \dot{\omega}_b) * q^{-1} + \dot{q} * (\hat{\omega}_b - \omega_b) * q^{-1} - q * (\hat{\omega}_b - \omega_b) * q^{-1} * \dot{q} * q^{-1} \\
&= (\eta^{-1} * I * \eta) \times \beta + \eta^{-1} * (ME) * \eta \\
\dot{\alpha} &= -\frac{a_s \dot{\hat{a}}_s}{\hat{a}_s^2} = -\alpha NE \\
\dot{\gamma} &= -\frac{c_s \dot{\hat{c}}_s}{\hat{c}_s^2} = -\gamma OE.
\end{aligned}$$

Since E is obtained from

$$E_A = A - \frac{a_s}{\hat{a}_s}\hat{q} * (q^{-1} * A * q) * \hat{q}^{-1} = A - \alpha\eta * A * \eta^{-1} \tag{66}$$

$$E_C = C - \gamma\eta * C * \eta^{-1} \tag{67}$$

we find as expected that the error system

$$\dot{\eta} = (LE) * \eta - \frac{1}{2}\eta * \beta \tag{68}$$

$$\dot{\beta} = (\eta^{-1} * I * \eta) \times \beta + \eta^{-1} * (ME) * \eta \tag{69}$$

$$\dot{\alpha} = -\alpha NE \tag{70}$$

$$\dot{\gamma} = -\gamma OE \tag{71}$$

depends only on the invariant state error $(\eta, \beta, \alpha, \gamma)$ and the "free" known invariant I, but not on the trajectory of the observed system (50)–(53). This property greatly simplifies the convergence analysis of the observer.

The linearized error system around the no-error equilibrium point $(\overline{\eta}, \overline{\beta}, \overline{\alpha}, \overline{\gamma}) = (1, 0, 1, 1)$ then reads

$$\delta\dot{\eta} = L\delta E - \frac{1}{2}\delta\beta \tag{72}$$

$$\delta\dot{\beta} = I \times \delta\beta + M\delta E \tag{73}$$

$$\delta\dot{\alpha} = -N\delta E \tag{74}$$

$$\delta\dot{\gamma} = -O\delta E, \tag{75}$$

where δE is the 5×1 vector

$$\Big(\langle \delta E_A, e_1\rangle, \langle \delta E_A, e_2\rangle, \langle \delta E_A, e_3\rangle, \langle \delta E_C, e_1\rangle, \langle \delta E_C, e_2\rangle\Big)^T \\ = g\big(-2\delta\eta_2, 2\delta\eta_1, -\delta\alpha, 2B_1\delta\eta_3, -B_1\delta\gamma\big)^T$$

made up from the projections of the vectors

$$\delta E_A = A * \delta\eta - \delta\eta * A - \delta\alpha A = 2A \times \delta\eta - \delta\alpha A$$
$$\delta E_C = 2C \times \delta\eta - \delta\gamma C.$$

3.2. Design of the observer gain matrices

Up to now, we have only investigated the structure of the observer. We now must choose the gain matrices L, M, N, O to meet the following requirements:

- the error must converge to zero, at least locally
- the local error behavior should be easily tunable, if possible with a clear physical interpretation
- the magnetic measurements should not affect the attitude estimate, but only the heading
- the behavior of the filter under acceleration and/or magnetic disturbances should be sensible and understandable.

3.2.1. Local design. — It turns out that the previous requirements can easily be met *locally around every trajectory* by taking

$$L = \frac{1}{2g}\begin{pmatrix} 0 & -l_1 & 0 & 0 & 0 \\ l_2 & 0 & 0 & 0 & 0 \\ 0 & 0 & 0 & -\frac{1}{B_1}l_3 & 0 \end{pmatrix} \qquad M = \frac{1}{2g}\begin{pmatrix} 0 & m_1 & 0 & 0 & 0 \\ -m_2 & 0 & 0 & 0 & 0 \\ 0 & 0 & 0 & \frac{1}{B_1}m_3 & 0 \end{pmatrix} \tag{76}$$

$$N = \frac{1}{g}\begin{pmatrix} 0 & 0 & -n & 0 & 0 \end{pmatrix} \qquad O = \frac{1}{B_1 g}\begin{pmatrix} 0 & 0 & 0 & 0 & -o \end{pmatrix} \tag{77}$$

for any constant $l_1, l_2, l_3, m_1, m_2, m_3, n, o > 0$. This will follow from the very simple form of the linearized error system (72)–(75). We insist that it is not usually obvious to come up with a similar convergence result for an EKF.

Indeed, Equations (72)–(75) now read

$$\delta\dot{\eta} = \mathrm{D_l}\delta\eta - \frac{1}{2}\delta\beta \tag{78}$$

$$\delta\dot{\beta} = \mathrm{D_m}\delta\eta + I \times \delta\beta \tag{79}$$

$$\delta\dot{\alpha} = -n\delta\alpha \tag{80}$$

$$\delta\dot{\gamma} = -o\delta\gamma \tag{81}$$

where

$$\mathrm{D_l} = \begin{pmatrix} -l_1 & 0 & 0 \\ 0 & -l_2 & 0 \\ 0 & 0 & -l_3 \end{pmatrix} \quad \text{and} \quad \mathrm{D_m} = \begin{pmatrix} m_1 & 0 & 0 \\ 0 & m_2 & 0 \\ 0 & 0 & m_3 \end{pmatrix}.$$

When $I = 0$ (i.e. the system is at rest) the system completely decouples into:
– the longitudinal subsystem

$$\begin{pmatrix} \delta\dot{\eta}_1 \\ \delta\dot{\beta}_1 \end{pmatrix} = \begin{pmatrix} -l_1 & -\frac{1}{2} \\ m_1 & 0 \end{pmatrix} \begin{pmatrix} \delta\eta_1 \\ \delta\beta_1 \end{pmatrix}$$

– the lateral subsystem

$$\begin{pmatrix} \delta\dot{\eta}_2 \\ \delta\dot{\beta}_2 \end{pmatrix} = \begin{pmatrix} -l_2 & -\frac{1}{2} \\ m_2 & 0 \end{pmatrix} \begin{pmatrix} \delta\eta_2 \\ \delta\beta_2 \end{pmatrix}$$

– the heading subsystem

$$\begin{pmatrix} \delta\dot{\eta}_3 \\ \delta\dot{\beta}_3 \end{pmatrix} = \begin{pmatrix} -l_3 & -\frac{1}{2} \\ m_3 & 0 \end{pmatrix} \begin{pmatrix} \delta\eta_3 \\ \delta\beta_3 \end{pmatrix}$$

– the scaling subsystem

$$\delta\dot{\alpha} = -n\delta\alpha$$
$$\delta\dot{\gamma} = -o\delta\gamma.$$

When $I \neq 0$ the longitudinal, lateral and heading subsystems are slightly coupled by the biases errors $\delta\beta$.

We now prove the local asymptotically convergence around every trajectory of the observer (62)–(65) with the preceding choice of correction terms, i.e. $(\delta\eta, \delta\beta, \delta\alpha, \delta\gamma) \to (0, 0, 0, 0)$, whatever $(l_1, l_2, l_3, m_1, m_2, m_3, n, o) > 0$.

Theorem 1. — *Consider the physical system* (50)–(53) *with the measurements* (54). *Consider the nonlinear invariant observer defined by*

$$\begin{aligned}\dot{\hat{q}} &= \frac{1}{2}\hat{q} * (\omega_m - \hat{\omega}_b) + (LE) * \hat{q} \\ \dot{\hat{\omega}}_b &= \hat{q}^{-1} * (ME) * \hat{q} \\ \dot{\hat{a}}_s &= \hat{a}_s NE \\ \dot{\hat{c}}_s &= \hat{c}_s OE\end{aligned}$$

with the expression of the output errors given by Equations (55) *and* (61), *and the gain matrices given by Equations* (76)–(77), *and assume* $\omega(t) = \omega_m(t) - \omega_b$ *is bounded, which is physically sensible. Then for any value* $(l_1, l_2, l_3, m_1, m_2, m_3, n, o) > 0$, *the solution* $(\hat{q}(t), \hat{\omega}_b(t), \hat{a}_s(t), \hat{c}_s(t))$ *locally asymptotically converges to* $(q(t), \omega_b, a_s, c_s)$ *around every trajectory.*

Proof 1. — *Proving the asymptotic local convergence of the observer around every trajectory means proving* $(\delta\eta, \delta\beta, \delta\alpha, \delta\gamma) \to (0, 0, 0, 0)$ *whatever* $(l_1, l_2, l_3, m_1, m_2, m_3, n, o) > 0$, *i.e. the convergence of the preceding longitudinal, lateral, heading, and scaling subsystems.*

The scaling subsystem obviously converges. For the other variables we consider the candidate Lyapunov function

$$V = \frac{l_1}{2}\delta\eta_1^2 + \frac{l_2}{2}\delta\eta_2^2 + \frac{l_3}{2}\delta\eta_3^2 + \frac{1}{4}\|\delta\beta\|^2.$$

Differentiating V *and using* $\langle \delta\beta, I \times \delta\beta \rangle = 0$, *we get*

$$\dot{V} = -\left(l_1 m_1 \delta\eta_1^2 + l_2 m_2 \delta\eta_2^2 + l_3 m_3 \delta\eta_3^2\right) \leq 0.$$

Since V *is bounded from below, this implies that* $V(\delta\eta(t), \delta\beta(t))$ *converges when* $t \to \infty$. *Since*

$$\lim_{t\to\infty} \int_0^t \dot{V}(\delta\eta(\tau), \delta\beta(\tau))d\tau = \lim_{t\to\infty} V(\delta\eta(t), \delta\beta(t)) - V(\delta\eta(0), \delta\beta(0)),$$

we conclude $\lim_{t\to\infty} \int_0^t \dot{V}(\delta\eta(\tau), \delta\beta(\tau))d\tau$ *exists and is finite. On the other hand,* $\dot{V} \leq 0$ *also implies*

$$0 \leq V(\delta\eta(t), \delta\beta(t)) \leq V(\delta\eta(0), \delta\beta(0)).$$

Therefore $\delta\eta(t)$ *and* $\delta\beta(t)$ *are bounded. Equation* (78) *implies that* $\delta\dot{\eta}(t)$ *is bounded too, and finally that* $\ddot{V}$ *is bounded. Hence* $\dot{V}$ *is uniformly continuous and by Barbalat's lemma*

$$\dot{V} \to 0 \quad \Rightarrow \quad \delta\eta \to 0.$$

Integrating Equation (78)*, we get*

$$\int_0^t \delta\dot{\eta}(\tau)d\tau = \delta\eta(t) - \delta\eta(0) = \int_0^t (D_l\delta\eta(\tau) - \frac{1}{2}\delta\beta(\tau))d\tau.$$

Since $\delta\eta(t) \to 0$*, it follows*

$$\lim_{t\to\infty} \int_0^t (D_l\delta\eta(\tau) - \frac{1}{2}\delta\beta(\tau))d\tau = -\delta\eta(0).$$

We assumed ω *is bounded, so* I *is bounded too. Since* $\delta\eta(t)$ *and* $\delta\beta(t)$ *are bounded,* $D_l\delta\dot{\eta}(t) - \frac{1}{2}\delta\dot{\beta}(t)$ *is bounded too. Hence* $D_l\delta\eta(t) - \frac{1}{2}\delta\beta(t)$ *is uniformly continuous. Applying Barbalat's lemma once again yields*

$$\lim_{t\to\infty} (D_l\delta\eta(t) - \frac{1}{2}\delta\beta(t)) = 0.$$

Since $\delta\eta \to 0$*, we conclude* $\delta\beta \to 0$*, which ends the proof.*

3.2.2. Global design. — The tuning in the previous section ensures local convergence around *every* trajectory of the system, which is already a very strong property. It is possible to further improve the convergence domain by modifying the correction terms at higher-order. Consider the new vector $y_D := y_C \times y_A = q^{-1} * D * q$, where $D := C \times A = g^2 B_1 e_1$, and the associated invariant error

$$E_D := D - \frac{1}{\hat{a}_s\hat{c}_s}\hat{q} * y_D * \hat{q}^{-1}.$$

Of course E_D carries no new information since by construction $D - E_D = (C - E_C) \times (A - E_A)$. But it is a convenient means to express the observer matrices; a related trick is used in [**67**]. Define now L, M, N, O by

$$\begin{aligned}
LE &:= \frac{l_a}{g^2}A \times E_A + \frac{l_c}{(B_1 g)^2}C \times E_C + \frac{l_d}{(B_1 g^2)^2}D \times E_D \\
ME &:= -\sigma LE \\
NE &:= \frac{n}{l_a + l_d}\left(\frac{l_a\langle E_A, E_A - A\rangle}{g^2} + \frac{l_d\langle E_D, E_D - D\rangle}{(B_1 g^2)^2}\right) \\
OE &:= \frac{o}{l_c + l_d}\left(\frac{l_c\langle E_C, E_C - C\rangle}{(B_1 g)^2} + \frac{l_d\langle E_D, E_D - D\rangle}{(B_1 g^2)^2}\right)
\end{aligned}$$

with $l_a, l_c, l_d, \sigma, n, o > 0$. LE is the same as in Section 3.2.1 up to first order with $(l_1, l_2, l_3) = 2(l_a + l_c, l_a + l_d, l_c + l_d)$; so is ME with $(m_1, m_2, m_3) = 2\sigma(l_a + l_c, l_a + l_d, l_c + l_d)$.

the first order expansion of the new tuning thus gives a special case of (78)-(79). As for (80)-(81), they become coupled since

$$N\delta E = -\frac{n}{g}\begin{pmatrix} 0 & 0 & 1 & 0 & \frac{ld}{(l_a+l_d)B_1} \end{pmatrix}\delta E$$
$$O\delta E = -\frac{o}{g}\begin{pmatrix} 0 & 0 & \frac{ld}{(l_c+l_d)B_1} & 0 & \frac{1}{B_1} \end{pmatrix}\delta E.$$

This choice of matrices provides a Lyapunov function that guarantees a large domain of convergence, while essentially preserving the nice local behavior of the error dynamics, as described in the previous section. Indeed, time differentiating the function

$$W := \|\beta\|^2 + \frac{\sigma l_a}{g^2}\|E_A\|^2 + \frac{\sigma l_c}{(B_1 g)^2}\|E_C\|^2 + \frac{\sigma l_d}{(B_1 g^2)^2}\|E_D\|^2$$

and using $\dot{E}_A = (A - E_A)NE + (A - E_A) \times (2LE - \beta)$ and similar expressions for $\dot{E}_C, \dot{E}_D$ yields

$$\dot{W} = -2(LE)^2 - 2\frac{l_a + l_d}{n}(NE)^2 - 2\frac{l_c + l_d}{o}(OE)^2 \leq 0.$$

Therefore W is a Lyapunov function which globally decreases for all $l_a, l_c, l_d, \sigma, n, o > 0$. Though it ensures a large domain of convergence, it is not clear it is enough for global convergence; see [**52**] for a convergence result in a simpler case (only gyro biases).

Notice the Lyapunov function V used in Section 3.2.1 can be seen as a low-order approximation of W since

$$\frac{m_a}{g^2}\|\delta E_A\|^2 + \frac{m_c}{(B_1 g)^2}\|\delta E_C\|^2 + \frac{m_d}{(B_1 g^2)^2}\|\delta E_D\|^2 + \|\delta\beta\|^2$$
$$= V + m_a\delta\alpha^2 + m_c\delta\gamma^2 + m_d(\delta\alpha + \delta\gamma)^2.$$

The tuning proposed in Section 3.2.1 is very simple and ensures the observer converges locally around every trajectory. This is already a very strong property, but there is no guarantee regarding a larger convergence domain. The tuning proposed in this section is computationally slightly more complicated. It also ensures a nice local behavior, though with less freedom: since there are now only 4 parameters (instead of 6) for (78)-(79), the longitudinal, lateral and heading subsystems may have different settling times but must have the same damping; the scaling subsystem (80)-(81) is now coupled but still has 2 tuning parameters. The guaranteed domain of convergence is much larger. Also notice the observer structure is flexible enough to accommodate yet other tunings.

3.3. Effects of disturbances

Two main disturbances may affect the model. When $\dot{V} \neq 0$, the accelerometers measure in fact $a_s q^{-1} * A^* * q$ where $A^* = -\dot{V} + A$. Magnetic disturbances will also change B into some B^*. For simplicity we consider that A^*, B^* are constant. The measured outputs now become

$$\begin{pmatrix} y_{A^*} \\ y_{C^*} \end{pmatrix} = \begin{pmatrix} a_s q^{-1} * A^* * q \\ c_s q^{-1} * C^* * q \end{pmatrix}.$$

The error system is unchanged but E is now the 5×1 vector

$$E = \Big(\langle E_A, e_1 \rangle, \langle E_A, e_2 \rangle, \langle E_A, e_3 \rangle, \langle E_C, e_1 \rangle, \langle E_C, e_2 \rangle \Big)^T$$

made up of the projections of the vectors

$$E_A = A - \frac{1}{\hat{a}_s} \hat{q} * y_{A^*} * \hat{q}^{-1} \qquad \text{and} \qquad E_C = C - \frac{1}{\hat{c}_s} \hat{q} * y_{C^*} * \hat{q}^{-1}.$$

Let us define the points $(\overline{\eta}, \overline{\beta}, \overline{\alpha}, \overline{\gamma})$ as follows

$$\begin{aligned} \overline{\beta} &= 0 \\ \overline{\eta} * A^* * \overline{\eta}^{-1} &= (0 \ 0 \ \|A^*\|) \\ \overline{\eta} * C^* * \overline{\eta}^{-1} &= (0 \ \|C^*\| \ 0) \\ \overline{\alpha} = \frac{\|A^*\|}{\|A\|} \quad &\text{and} \quad \overline{\gamma} = \frac{\|C^*\|}{\|C\|} \end{aligned}$$

Doing the frame rotation defined by $\overline{\eta}$ we can define the new variables

$$\begin{aligned} \tilde{\eta} &= \eta * \overline{\eta}^{-1} & \tilde{\beta} &= \overline{\eta} * \beta * \overline{\eta}^{-1} \\ \tilde{\alpha} &= \alpha \overline{\alpha} & \tilde{\gamma} &= \gamma \overline{\gamma}. \end{aligned}$$

The error system with these new variables writes

$$\begin{aligned} \dot{\tilde{\eta}} &= -\frac{1}{2} \tilde{\eta} * \tilde{\beta} + (\tilde{L}\tilde{E}) * \tilde{\eta} \\ \dot{\tilde{\beta}} &= (\tilde{\eta}^{-1} * \tilde{I} * \tilde{\eta}) \times \tilde{\beta} + \tilde{\eta}^{-1} * (\tilde{M}\tilde{E}) * \tilde{\eta} \\ \dot{\tilde{\alpha}} &= -\tilde{\alpha} \tilde{N} \tilde{E} \\ \dot{\tilde{\gamma}} &= -\tilde{\gamma} \tilde{O} \tilde{E} \end{aligned}$$

where the new output error $\tilde{E}$ is made up of the projections of the vectors

$$\tilde{E}_A = A - \tilde{\alpha}\tilde{\eta} * A * \tilde{\eta}^{-1} \qquad \text{and} \qquad \tilde{E}_C = C - \tilde{\alpha}\tilde{\eta} * C * \tilde{\eta}^{-1}.$$

So $(\tilde{\eta}, \tilde{\beta}, \tilde{\alpha}, \tilde{\gamma})$ satisfy the same error system as $(\eta, \beta, \alpha, \gamma)$. In the new frame (A^*, C^*) play the same role as (A, C). All the properties of the observer are therefore preserved in the new frame.

An important case is when only the magnetic field is perturbed, where we consider A and $C^* = (C_1^* \; C_2^* \; 0)$ (instead of $C = (0 \; gB_1 \; 0)$). Writing the new equilibrium point $(\overline{\eta}, \overline{\beta}, \overline{\alpha}, \overline{\gamma})$ of the error system explicitly it can be seen that

$$\overline{\phi} = \overline{\theta} = 0 \text{ and } \overline{\psi} = \arctan \frac{C_1^*}{C_2^*}$$
$$\overline{\beta} = \overline{\alpha} = 0 \text{ and } \overline{\gamma} = \frac{\|C^*\|}{\|C\|},$$

where $(\overline{\phi}, \overline{\theta}, \overline{\psi})$ are the Euler angles corresponding to $\overline{\eta}$. In particular only the yaw angle $\overline{\psi}$ and $\overline{\gamma}$ are affected by the magnetic disturbance.

3.4. Experimental validation

We now compare the behavior of our observer with the commercial Microbotics MIDG II system used in Vertical Gyro mode. The following results have been obtained with the observer

$$\dot{\hat{q}} = \frac{1}{2}\hat{q} * (\omega_m - \hat{\omega}_b) + (LE) * \hat{q} + k(1 - \|\hat{q}\|^2)\hat{q} \tag{82}$$
$$\dot{\hat{\omega}}_b = \hat{q}^{-1} * (ME) * \hat{q} \tag{83}$$
$$\dot{\hat{a}}_s = \hat{a}_s NE \tag{84}$$
$$\dot{\hat{c}}_s = \hat{c}_s OE, \tag{85}$$

and the choice of matrices defined by the parameters below. Compared to the observer (62)–(65), the added term $k(1 - \|\hat{q}\|^2)\hat{q}$ is a well-known numerical trick to keep $\|\hat{q}\| = 1$. Notice this term is also invariant.

We feed the observer with the raw measurements from the MIDG II gyroscopes, accelerometers and magnetic sensors. The observer is implemented in Matlab Simulink and its values are compared to the MIDG II results (computed according to the user manual by some Kalman filter). In order to have similar behaviors between MIDG II filter and

the invariant observer, we have chosen

$$\begin{array}{lll} l_a = 6e-2 & l_c = 1e-1 & l_d = 6e-2 \\ m_a = 3.2e-3 & m_c = 5.3e-3 & m_d = 3.2e-3 \\ n = 0.25 & o = 0.5. & \end{array}$$

3.4.1. Comparison with a commercial device (Figure 3.1). — We first want to illustrate the different invariant observer properties mentioned in Section 3.2. Therefore we performed a long-lasting experiment, which can be divided into 3 parts:

- for $t < 240s$ the system is left at rest until the biases reach constant values. Figure 3.1(a) highlights the importance of the correction term in the angle estimation: without correction the estimated roll angle diverges with a slope of $-0.18°/s$ (bottom plot), which is indeed the final value of the estimated bias (middle plot) (Figures 3.1(a) and 3.1(b)).
- for $240s < t < 293s$ we move the system in all directions. The observer and the MDG II give very similar results (Figure 3.1(c)).
- at $t = 385s$ the system is motionless and a magnet is put close to the sensors for 10s. As expected only the estimated yaw angle is affected by the magnetic disturbance (Figure 3.1(d)); the MIDG II exhibits a similar behavior.

3.4.2. Influence of the observer correction terms (Figure 3.2). — We have chosen the correction terms so that the magnetic measurements correct essentially the yaw angle and its corresponding bias, whereas the accelerometers measurements act on the other variables. We highlight this property on the following experiment (Figure 3.2). Once the biases have reached constant values, the system is left at rest during 35 minutes:

- for $t < 600s$ the results are very similar for the observer and the MIDG II.
- at $t = 600s$ the "magnetic correction terms" are switched off, i.e. the gains l_c,l_d,m_c,m_d and o are set to 0. The yaw angle estimated by the observer diverges because the corresponding bias is not perfectly estimated. Indeed, these variables are not observable without the magnetic measurements. The other variables are not affected.
- at $t = 1300s$ the "accelerometers correction terms" are also switched off, i.e. l_a,m_a and n are set to 0. All the estimated angles now diverge.

3.4.3. Acceleration disturbance: $\dot{V} \neq 0$ (Figure 3.3). — The hypothesis $\dot{V} = 0$ may be wrong. In this case the observer does not converge to the true values anymore. Indeed we illustrate this point on Figure 3.3 by comparing the roll angle estimated by

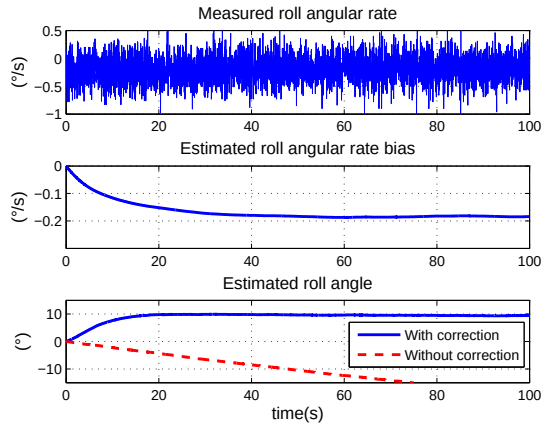

(a) Motionless estimated roll angle

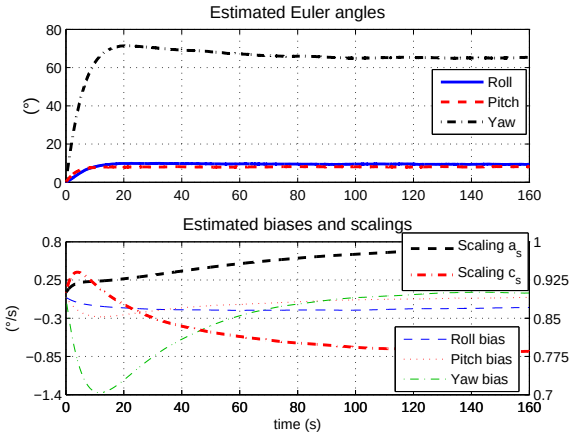

(b) Motionless estimated gyros biases and Euler angles

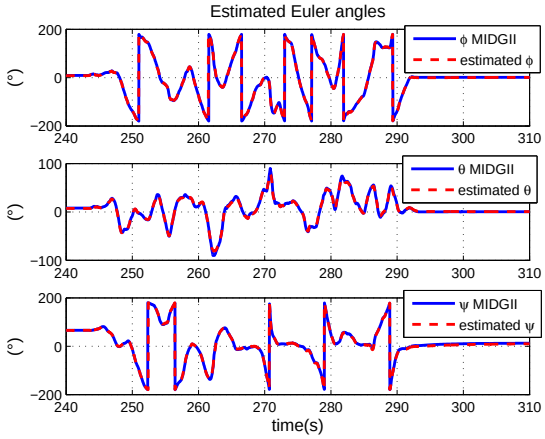

(c) Dynamic estimated Euler angles

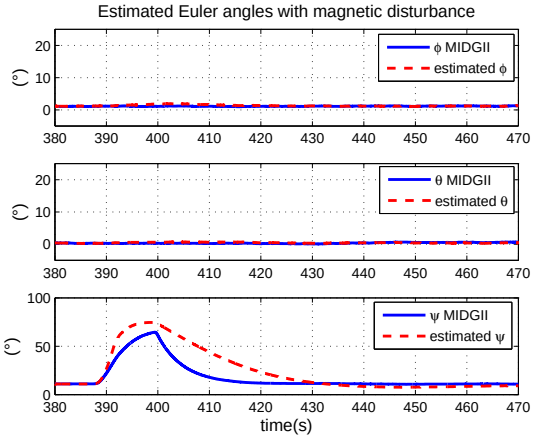

(d) Estimated Euler angles with magnetic disturbances

FIGURE 3.1. Experimental validation using Matlab

our observer and the roll angle estimated by the MIDG II in INS mode (in this mode the attitude and heading estimates are aided by a GPS engine, hence are close to the "true" values).

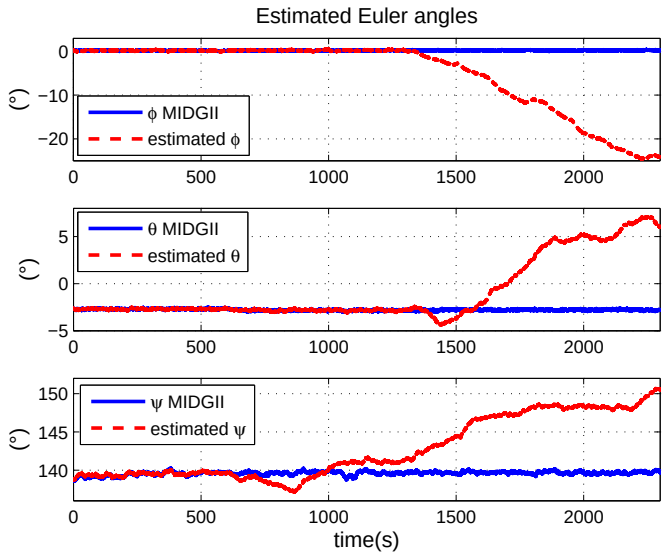

FIGURE 3.2. Influence of correction terms

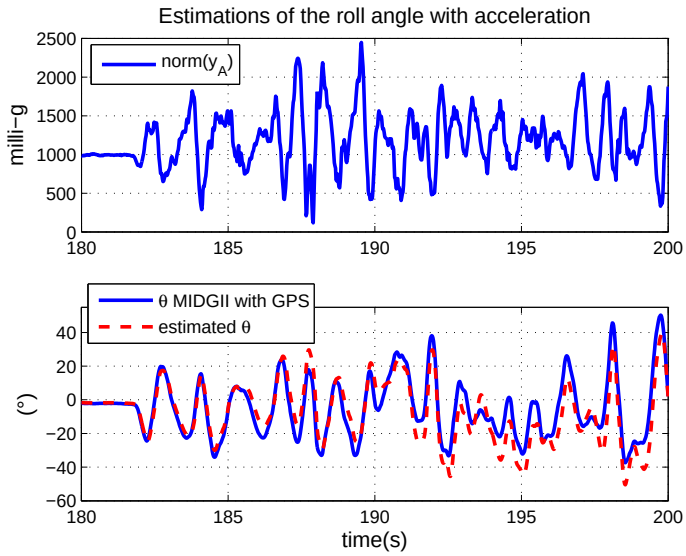

FIGURE 3.3. Estimated roll angle when $\dot{V} \neq 0$

CHAPTER 4

SYMMETRY-PRESERVING OBSERVERS FOR AIDED ATTITUDE AND HEADING REFERENCE SYSTEMS

Dans ce chapitre nous nous intéressons aux observateurs pour les "aided Attitude and Heading Reference Systems", dans lequels des capteurs de vitesse (dans le repère engin ou terre) et éventuellement de position (GPS ou baromètre) sont utilisés en plus des capteurs inertiels et magnétiques. Les filtres présentés sont des observateurs nonlinéaires invariants, préservant les symétries naturelles du système considéré. Le choix des termes de corrections permet d'assurer une convergence locale autour des trajectoires usuelles (non aggressives) des mini-drones. Comme pour les estimateurs présentés dans le Chapitre 3, ces filtres permettent également un découplage intéressant des angles d'attitude et de lacet, afin de limiter les conséquences d'une perturbation magnétique sur le mini-drone, tout en étant facile à régler grâce à un découplage naturelle en sous-systèmes et à un nombre réduit de paramètres à choisir.

4.1. Earth-velocity-aided AHRS

4.1.1. The considered system. — Attitude and Heading References Systems rely on low-cost inertial and magnetic sensors, aided by velocity or/and position sensors. In

this section, we consider only velocity measurements in Earth-fixed coordinates (e.g. from a GPS engine) coming in addition to the accelerometers, gyroscopes and magnetometers measurements. Therefore we consider the following system, coming from Equations (42),(43),(45),(46) described in Section 2.4

$$\dot{q} = \frac{1}{2} q * (\omega_m - \omega_b) \tag{86}$$

$$\dot{V} = A + \frac{1}{a_s} q * a_m * q^{-1} \tag{87}$$

$$\dot{\omega}_b = 0 \tag{88}$$

$$\dot{a}_s = 0, \tag{89}$$

where ω_m and a_m are seen as known inputs, together with the output

$$\begin{pmatrix} y_V \\ y_B \end{pmatrix} = \begin{pmatrix} V \\ q^{-1} * B * q \end{pmatrix}. \tag{90}$$

4.1.2. Invariance of the system equations. — The physical system is obviously unaffected by a constant velocity translation in the Earth-fixed frame and a constant rotation of the body-fixed frame. It is natural to expect a similar behavior from an observer. We therefore consider the following transformation group generated by rotations, translations and scaling

$$\varphi_{(q_0,V_0,\omega_0,a_0)} \begin{pmatrix} q \\ V \\ \omega_b \\ a_s \end{pmatrix} = \begin{pmatrix} q * q_0 \\ V + V_0 \\ q_0^{-1} * \omega_b * q_0 + \omega_0 \\ a_s a_0 \end{pmatrix}$$

$$\psi_{(q_0,V_0,\omega_0,a_0)} \begin{pmatrix} \omega_m \\ a_m \end{pmatrix} = \begin{pmatrix} q_0^{-1} * \omega_m * q_0 + \omega_0 \\ a_0 q_0^{-1} * a_m * q_0 \end{pmatrix}$$

$$\rho_{(q_0,V_0,\omega_0,a_0)} \begin{pmatrix} y_V \\ y_B \end{pmatrix} = \begin{pmatrix} y_V + V_0 \\ q_0^{-1} * y_B * q_0 \end{pmatrix}.$$

There are $3 + 2 * 3 + 1 = 10$ parameters: the unit quaternion q_0, the $\mathbb{R}^3$-vectors V_0, ω_0 and the positive scalar a_0. The group composition law $\diamond$ is given by

$$\begin{pmatrix} q_1 \\ V_1 \\ \omega_1 \\ a_1 \end{pmatrix} \diamond \begin{pmatrix} q_0 \\ V_0 \\ \omega_0 \\ a_0 \end{pmatrix} = \begin{pmatrix} q_0 * q_1 \\ V_0 + V_1 \\ q_1^{-1} * \omega_0 * q_1 + \omega_1 \\ a_0 a_1 \end{pmatrix}.$$

The system (86)–(89) is of course invariant by the transformation group since

$$\dot{\overbrace{q * q_0}} = \dot{q} * q_0 = \frac{1}{2}(q * q_0) * \left((q_0^{-1} * \omega_m * q_0 + \omega_0) - (q_0^{-1} * \omega_b * q_0 + \omega_0)\right)$$

$$\dot{\overbrace{V + V_0}} = \dot{V} = A + \frac{1}{a_s a_0}(q * q_0) * (a_s q_0^{-1} * a_m * q_0) * (q * q_0)^{-1}$$

$$\dot{\overbrace{q_0^{-1} * \omega_b * q_0 + \omega_0}} = q_0^{-1} * \dot{\omega}_b * q_0 = 0$$

$$\dot{\overbrace{a_s a_0}} = \dot{a}_s a_0 = 0,$$

whereas the output (90) is equivariant since

$$\begin{pmatrix} V + V_0 \\ (q * q_0)^{-1} * B * (q * q_0) \end{pmatrix} = \rho_{(q_0, V_0, \omega_0, a_0)} \begin{pmatrix} V \\ q^{-1} * B * q \end{pmatrix}.$$

4.1.3. Construction of the general invariant observer. — We solve for $(q_0, V_0, \omega_0, a_0)$ the normalization equations

$$\begin{aligned} q * q_0 &= 1 \\ V + V_0 &= 0 \end{aligned} \qquad \text{and} \qquad \begin{aligned} q_0^{-1} * \omega_b * q_0 + \omega_0 &= 0 \\ a_s a_0 &= 1 \end{aligned}$$

to find the moving frame

$$\gamma(q, V, \omega_b, a_s) = \begin{pmatrix} q^{-1} \\ -V \\ -q * \omega_b * q^{-1} \\ 1/a_s \end{pmatrix}.$$

We then get the 6-dimensional invariant error

$$\begin{aligned} \begin{pmatrix} E_V \\ E_B \end{pmatrix} &= \rho_{\gamma(\hat{q}, \hat{V}, \hat{\omega}_b, \hat{a}_s)} \begin{pmatrix} \hat{y}_V \\ \hat{y}_B \end{pmatrix} - \rho_{\gamma(\hat{q}, \hat{V}, \hat{\omega}_b, \hat{a}_s)} \begin{pmatrix} y_V \\ y_B \end{pmatrix} \\ &= \begin{pmatrix} \hat{y}_V - y_V \\ B - \hat{q} * q^{-1} * B * q * \hat{q}^{-1} \end{pmatrix} = \begin{pmatrix} \hat{y}_V - y_V \\ B - \hat{q} * y_B * \hat{q}^{-1} \end{pmatrix} \end{aligned} \tag{91}$$

and the 6-dimensional complete invariant

$$\begin{pmatrix} I_\omega \\ I_a \end{pmatrix} = \psi_{\gamma(\hat{q}, \hat{V}, \hat{\omega}_b, \hat{a}_s)} \begin{pmatrix} \omega_m \\ a_m \end{pmatrix} = \begin{pmatrix} \hat{q} * (\omega_m - \hat{\omega}_b) * \hat{q}^{-1} \\ \frac{1}{\hat{a}_s} \hat{q} * a_m * \hat{q}^{-1} \end{pmatrix}.$$

Notice that I_ω,I_a,E_V and E_B are functions of the estimates and the measurements. Hence they are known quantities which can be used in the construction of the observer. It is

straightforward to check they are indeed invariant. For instance,

$$\begin{aligned} E_B(\hat{q} * q_0, \hat{V} + V_0, q_0^{-1} * \hat{\omega}_b * q_0 + \omega_0, \hat{a}_s a_0, q_0^{-1} * y_B * q_0) \\ &= B - (\hat{q} * q_0) * (q_0^{-1} * y_B * q_0) * (\hat{q} * q_0)^{-1} \\ &= B - \hat{q} * y_B * \hat{q}^{-1} \\ &= E_B(\hat{q}, \hat{V}, \hat{\omega}_b, \hat{a}_s, y_B). \end{aligned}$$

To find invariant vector fields, we solve for $w(q, V, \omega_b, a_s)$ the 10 vector equations

$$\left[D\varphi_{\gamma(q,V,\omega_b,a_s)} \begin{pmatrix} q \\ V \\ \omega_b \\ a_s \end{pmatrix} \right] \cdot w(q, V, \omega_b, a_s) = \begin{pmatrix} e_i \\ 0 \\ 0 \\ 0 \end{pmatrix}, \begin{pmatrix} 0 \\ e_i \\ 0 \\ 0 \end{pmatrix}, \begin{pmatrix} 0 \\ 0 \\ e_i \\ 0 \end{pmatrix}, \begin{pmatrix} 0 \\ 0 \\ 0 \\ e_{10} \end{pmatrix}, i = 1, 2, 3,$$

where the e_i's are the canonical basis of $\mathbb{R}^3$ (we have identified the tangent space of the unit norm quaternions space to $\mathbb{R}^3$). Since

$$\left[D\varphi_{(q_0,V_0,\omega_0,a_0)} \begin{pmatrix} q \\ V \\ \omega_b \\ a_s \end{pmatrix} \right] \cdot \begin{pmatrix} \delta q \\ \delta V \\ \delta\omega_b \\ \delta a_s \end{pmatrix} = \begin{pmatrix} \delta q * q_0 \\ \delta V \\ q_0^{-1} * \delta\omega_b * q_0 \\ a_0 \delta a_s \end{pmatrix},$$

this yields the 10 independent invariant vector fields

$$\begin{pmatrix} e_i * q \\ 0 \\ 0 \\ 0 \end{pmatrix}, \begin{pmatrix} 0 \\ e_i \\ 0 \\ 0 \end{pmatrix}, \begin{pmatrix} 0 \\ 0 \\ q^{-1} * e_i * q \\ 0 \end{pmatrix}, \begin{pmatrix} 0 \\ 0 \\ 0 \\ a_s e_{10} \end{pmatrix}, \quad i = 1, 2, 3.$$

These vector fields are invariant. Indeed for instance,

$$\left[D\varphi_{(q_0,V_0,\omega_0,a_0)} \begin{pmatrix} q \\ V \\ \omega_b \\ a_s \end{pmatrix} \right] \cdot \begin{pmatrix} e_i * q \\ 0 \\ 0 \\ 0 \end{pmatrix} = \begin{pmatrix} (e_i * q) * q_0 \\ 0 \\ 0 \\ 0 \end{pmatrix} = \begin{pmatrix} e_i * (q * q_0) \\ 0 \\ 0 \\ 0 \end{pmatrix}.$$

The general invariant observer then reads

$$\begin{aligned}
\dot{\hat{q}} &= \frac{1}{2}\hat{q} * (\omega_m - \hat{\omega}_b) + \sum_{i=1}^{3}(L_{Vi}E_V + L_{Bi}E_B)e_i * \hat{q} \\
\dot{\hat{V}} &= A + \frac{1}{\hat{a}_s}\hat{q} * a_m * \hat{q}^{-1} + \sum_{i=1}^{3}(M_{Vi}E_V + L_{Bi}E_B)e_i \\
\dot{\hat{\omega}}_b &= \sum_{i=1}^{3}\hat{q}^{-1} * (N_{Vi}E_V + N_{Bi}E_B)e_i * \hat{q} \\
\dot{\hat{a}}_s &= \hat{a}_s(O_V E_V + O_B E_B),
\end{aligned}$$

where the L_{Vi}, L_{Bi}, M_{Vi}, M_{Bi}, N_{Vi}, N_{Bi}, O_V, O_B are arbitrary 1×3 matrices with entries possibly depending on E_V, E_B, I_ω and I_a. Noticing

$$\sum_{i=1}^{3}(L_{Vi}E_V)e_i = \begin{pmatrix} L_{V1} \\ L_{V2} \\ L_{V3} \end{pmatrix} E_V = L_V E_V,$$

where L_V is the 3×3 matrix whose rows are the L_{Vi}'s, and defining L_B, M_V, M_B, N_V and N_B in the same way, we can rewrite the observer as

$$\dot{\hat{q}} = \frac{1}{2}\hat{q} * (\omega_m - \hat{\omega}_b) + (L_V E_V + L_B E_B) * \hat{q} \tag{92}$$

$$\dot{\hat{V}} = \frac{1}{\hat{a}_s}\hat{q} * a_m * \hat{q}^{-1} + A + (M_V E_V + M_B E_B) \tag{93}$$

$$\dot{\hat{\omega}}_b = \hat{q}^{-1} * (N_V E_V + N_B E_B) * \hat{q} \tag{94}$$

$$\dot{\hat{a}}_s = \hat{a}_s(O_V E_V + O_B E_B). \tag{95}$$

As a by-product of its geometric structure, the observer automatically has a desirable feature: the norm of $\hat{q}$ is left unchanged by Equations (92), since $L_V E_V + L_B E_B$ is a vector in $\mathbb{R}^3$ (see section 2.6).

4.1.4. The invariant error system. — The invariant state error is given by

$$\begin{pmatrix} \eta \\ \nu \\ \beta \\ \alpha \end{pmatrix} = \varphi_{\gamma(q,V,\omega_b,a_s)} \begin{pmatrix} \hat{q} \\ \hat{V} \\ \hat{\omega}_b \\ \hat{a}_s \end{pmatrix} - \varphi_{\gamma(q,V,\omega_b,a_s)} \begin{pmatrix} q \\ V \\ \omega_b \\ a_s \end{pmatrix} = \begin{pmatrix} \hat{q} * q^{-1} - 1 \\ \hat{V} - V \\ q * (\hat{\omega}_b - \omega_b) * q^{-1} \\ \frac{\hat{a}_s}{a_s} - 1 \end{pmatrix}.$$

As in section 3.1, we consider $\eta = \hat{q} * q^{-1}$ (rather than $\eta = \hat{q} * q^{-1} - 1$), so that $\eta(x, x) = 1$, the unit element of the group of quaternions. In the same way, we take $\alpha = \frac{\hat{a}_s}{a_s}$ to keep α in $\mathbb{R}^+$. Hence,

$$\begin{aligned}
\dot{\eta} &= \dot{\hat{q}} * q^{-1} + \hat{q} * (-q^{-1} * \dot{q} * q^{-1}) = -\frac{1}{2}\eta * \beta + (L_A E_A + L_C E_C) * \eta \\
\dot{\nu} &= \dot{\hat{V}} - \dot{V} = I_a - \alpha\eta^{-1} * I_a * \eta + (M_V E_V + M_B E_B) \\
\dot{\beta} &= \dot{q} * (\hat{\omega}_b - \omega_b) * q^{-1} - q * (\hat{\omega}_b - \omega_b) * q^{-1} * \dot{q} * q^{-1} + q * (\dot{\hat{\omega}}_b - \dot{\omega}_b) * q^{-1} \\
&= (\eta^{-1} * I_\omega * \eta) \times \beta + \eta^{-1} * (N_V E_V + N_B E_B) * \eta \\
\dot{\alpha} &= \frac{\dot{\hat{a}}_s}{a_s} = \alpha(O_V E_V + O_B E_B).
\end{aligned}$$

Since we can write

$$E_V = \nu \qquad \text{and} \qquad E_B = B - \eta * B * \eta^{-1},$$

we find that the error system

$$\dot{\eta} = -\frac{1}{2}\eta * \beta + (L_A E_A + L_C E_C) * \eta \tag{96}$$

$$\nu = I_a - \alpha\eta^{-1} * I_a * \eta + (M_V E_V + M_B E_B) \tag{97}$$

$$\dot{\beta} = (\eta^{-1} * I_\omega * \eta) \times \beta + \eta^{-1} * (N_V E_V + N_B E_B) * \eta \tag{98}$$

$$\dot{\alpha} = \alpha(O_V E_V + O_B E_B) \tag{99}$$

depends only on the invariant state error $(\eta, \nu, \beta, \alpha)$ and the "free" known invariants I_ω and I_a, but not on the trajectory of the observed system (86)–(89).

The linearized error system around $(\overline{\eta}, \overline{\nu}, \overline{\beta}, \overline{\alpha}) = (1, 0, 0, 1)$, i.e. the estimated state equals the actual state, is given by

$$\begin{aligned}
\delta\dot{\eta} &= -\frac{1}{2}\delta\beta + (L_V \delta E_V + L_B \delta E_B) \\
\delta\dot{\nu} &= -2I_a \times \delta\eta - \delta\alpha I_a + (M_V \delta E_V + M_B \delta E_B) \\
\delta\dot{\beta} &= I_\omega \times \delta\beta + (N_V \delta E_V + N_B \delta E_B) \\
\delta\dot{\alpha} &= (O_V \delta E_V + O_B \delta E_B),
\end{aligned}$$

where

$$\begin{aligned}\delta E_V &= \delta\nu \\ \delta E_B &= -\delta\eta * B * \overline{\eta}^{-1} - \overline{\eta} * B * (-\overline{\eta}^{-1} * \delta\eta * \overline{\eta}^{-1}) \\ &= 2(\overline{\eta} * B * \overline{\eta}^{-1}) \times (\delta\eta * \overline{\eta}^{-1}) = 2B \times \delta\eta.\end{aligned}$$

4.1.5. Design of the observer gain matrices. —

4.1.5.1. Choice of the gain matrices. — The linearized error system without correction terms turns out to be decoupled into 4 independent subsystems when I_a is constant and $I_\omega = 0$ (in particular when the aircraft is in level flight). To make sure tuning remains simple, the gain matrices should respect this decoupling. On the other hand, the Earth magnetic field is quite perturbed in urban areas, which are usual areas of operation for a small UAV. We do not want these magnetic disturbances – which unavoidably corrupt the heading estimate – to affect the attitude and velocity estimates too much. The idea is thus to rely on the magnetic measurement y_B as little as possible. Therefore we choose

$$L_V E_V = -l_V I_a \times E_V \qquad L_B E_B = l_B \langle B \times E_B, I_a \rangle I_a \tag{100}$$

$$M_V E_V = -m_V E_V \qquad M_B E_B = 0 \tag{101}$$

$$N_V E_V = n_V I_a \times E_V \qquad N_B E_B = -n_B \langle B \times E_B, I_a \rangle I_a \tag{102}$$

$$O_V E_V = o_V \langle I_a, E_V \rangle \qquad O_B E_B = 0 \tag{103}$$

with $(l_V, l_B, m_V, n_V, n_B, o_V) > 0$.

4.1.5.2. Equilibrium points of the observer equations. — When the observer has converged, the last two equations of the observer write

$$N_V E_V + N_B E_B = 0 \quad \text{and} \quad O_V E_V = 0.$$

With the choice of gain matrices above it leads to

$$\overline{I}_a \times E_V = 0 \quad \text{and} \quad \langle \overline{I}_a, E_V \rangle = 0.$$

So even if the model is wrong, for example if the Earth magnetic field is perturbed, the observer equations ensure $\hat{V} = V$ once it has converged. This important property is satisfied because we considered the scaling on the accelerometers measurements a_s in addition to the usual gyroscopes biases ω_b. A similar conclusion is not possible with the Euler angles even if we consider additional biases: $E_B = 0$ does not ensure that the yaw angle, for example, is correctly estimated.

4.1.5.3. First-order approximation and coordinate change. — Considering the gain matrices described above, the linearized error equations around the equilibrium point $(1, 0, 0, 1)$ write

$$\begin{aligned}
\delta\dot{\eta} &= -\frac{1}{2}\delta\beta - l_V I_a \times \delta E_V + l_B\langle B \times \delta E_B, I_a\rangle I_a \\
\delta\dot{\nu} &= -2I_a \times \delta\eta - \delta\alpha I_a - m_V \delta E_V \\
\delta\dot{\beta} &= I_\omega \times \delta\beta + n_V I_a \times \delta E_V - n_B\langle B \times \delta E_B, I_a\rangle I_a \\
\delta\dot{\alpha} &= o_V\langle I_a, \delta E_V\rangle
\end{aligned}$$

with $\delta E_V = \delta\nu$ and $\delta E_B = 2B \times \delta\eta$.

We change the coordinate so that the estimated specific acceleration vector I_a is vertical. Let η_0 be this frame rotation defined by

$$\eta_0^{-1} * I_a * \eta_0 = -kA, \quad \text{where} \quad k > 0 \tag{104}$$

$$\eta_0^{-1} * B * \eta_0 = \tilde{B} \quad \text{with} \quad \tilde{B} = (\tilde{B}_1\ 0\ \tilde{B}_3). \tag{105}$$

It follows

$$\begin{aligned}
\tilde{\eta} &= \eta_0^{-1} * \eta * \eta_0 \qquad \tilde{\nu} = \eta_0^{-1} * \nu * \eta_0 \\
\tilde{\beta} &= \eta_0^{-1} * \beta * \eta_0.
\end{aligned}$$

The error system then becomes

$$\begin{aligned}
\delta\dot{\tilde{\eta}} &= 2\delta\tilde{\eta} \times (\eta_0^{-1} * \dot{\eta}_0) - \frac{1}{2}\delta\tilde{\beta} + kl_V A \times \delta\tilde{E}_V + k^2 l_B\langle\tilde{B} \times \delta\tilde{E}_B, A\rangle A \\
\delta\dot{\tilde{\nu}} &= 2\delta\tilde{\nu} \times (\eta_0^{-1} * \dot{\eta}_0) + 2kA \times \delta\eta + k\delta\alpha A - m_V \delta\tilde{E}_V \\
\delta\dot{\tilde{\beta}} &= 2\delta\tilde{\beta} \times (\eta_0^{-1} * \dot{\eta}_0) + \tilde{I}_\omega \times \delta\tilde{\beta} - kn_V A \times \delta\tilde{E}_V - k^2 n_B\langle\tilde{B} \times \delta\tilde{E}_B, A\rangle A \\
\delta\dot{\alpha} &= -o_V k\langle A, \delta\tilde{E}_V\rangle
\end{aligned}$$

with $\delta\tilde{E}_V = \delta\tilde{\nu}$ and $\delta\tilde{E}_B = 2\tilde{B} \times \delta\tilde{\eta}$.

We suppose now that the system is moving along a "smooth" trajectory, i.e the magnitudes of $\dot{\eta}_0$, $\dot{I}_a$, and I_ω are negligible. All the terms of the form $\cdot \times (\eta_0^{-1} * \dot{\eta}_0)$ then disappear and k is now constant. The error system splits into three decoupled subsystems and one cascaded subsystem:

– the longitudinal subsystem

$$\begin{pmatrix} \dot{\delta\tilde{\eta}_2} \\ \dot{\delta\tilde{\nu}_1} \\ \dot{\delta\tilde{\beta}_2} \end{pmatrix} = \begin{pmatrix} 0 & kl_V g & -\frac{1}{2} \\ -2kg & -m_V & 0 \\ 0 & -kn_V g & 0 \end{pmatrix} \begin{pmatrix} \delta\tilde{\eta}_2 \\ \delta\tilde{\nu}_1 \\ \delta\tilde{\beta}_2 \end{pmatrix}$$

– the lateral subsystem

$$\begin{pmatrix} \dot{\delta\tilde{\eta}_1} \\ \dot{\delta\tilde{\nu}_2} \\ \dot{\delta\tilde{\beta}_1} \end{pmatrix} = \begin{pmatrix} 0 & -kl_V g & -\frac{1}{2} \\ 2kg & -m_V & 0 \\ 0 & kn_V g & 0 \end{pmatrix} \begin{pmatrix} \delta\tilde{\eta}_1 \\ \delta\tilde{\nu}_2 \\ \delta\tilde{\beta}_1 \end{pmatrix}$$

– the vertical subsystem

$$\begin{pmatrix} \dot{\delta\tilde{\nu}_3} \\ \delta\dot{\alpha} \end{pmatrix} = \begin{pmatrix} -m_V & kg \\ -kgo_V & 0 \end{pmatrix} \begin{pmatrix} \delta\tilde{\nu}_3 \\ \delta\alpha \end{pmatrix}$$

– the heading subsystem

$$\begin{pmatrix} \dot{\delta\tilde{\eta}_3} \\ \dot{\delta\tilde{\beta}_3} \end{pmatrix} = \begin{pmatrix} -2k^2g^2l_B\tilde{B}_1^2 & -\frac{1}{2} \\ 2k^2g^2n_B\tilde{B}_1^2 & 0 \end{pmatrix} \begin{pmatrix} \delta\tilde{\eta}_3 \\ \delta\tilde{\beta}_3 \end{pmatrix} + \begin{pmatrix} 2k^2g^2l_B\tilde{B}_3\tilde{B}_1 \\ -2k^2g^2n_B\tilde{B}_3\tilde{B}_1 \end{pmatrix} \delta\tilde{\eta}_1.$$

Thanks to this decoupled structure, the convergence of each subsystem, and then the local convergence of the invariant observer, is straightforward, and leads to Theorem 2.

Theorem 2. — *Consider the physical system* (86)–(89) *with the measurements* (90). *Consider the nonlinear invariant observer defined by*

$$\begin{aligned} \dot{\hat{q}} &= \frac{1}{2}\hat{q} * (\omega_m - \hat{\omega}_b) + (L_V E_V + L_B E_B) * \hat{q} \\ \dot{\hat{V}} &= \frac{1}{\hat{a}_s}\hat{q} * a_m * \hat{q}^{-1} + A + (M_V E_V) \\ \dot{\hat{\omega}}_b &= \hat{q}^{-1} * (N_V E_V + N_B E_B) * \hat{q} \\ \dot{\hat{a}}_s &= \hat{a}_s(O_V E_V), \end{aligned}$$

with the expression of the output errors given by Equation (91) *and the gain matrices given by Equations* (100)–(103). *Then for any value* $(l_V, l_B, m_V, n_V, n_B, o_V) > 0$, *the solution* $(\hat{q}(t), \hat{V}(t), \hat{\omega}_b(t), \hat{a}_s(t))$ *locally asymptotically converges to* $(q(t), V(t), \omega_b, a_s)$ *around every "smooth" trajectory, i.e when* $\dot{\eta}_0$, $\dot{I}_a$, *and* I_ω *can be neglected (first order terms).*

We insist that it is not usually obvious to come up with a similar convergence result for an EKF. The gains $l_V, l_B, m_V, n_V, n_B, o_V$ are also easy to tune, since the behaviors of each

subsystem are independent. Moreover the lateral, longitudinal and vertical subsystems do not depend on the magnetic measurements, so they are not affected if the magnetic field is perturbed.

4.1.5.4. Influence of magnetic disturbances on static behavior. — We now investigate how the equilibrium point $(1,0,0,1)$ is modified when the magnetic field is (statically) perturbed. We show that only the yaw angle ψ is affected while all the other variables, in particular the attitude angles ϕ, θ, remain unchanged. Here the Euler angles ϕ, θ, ψ correspond to the error quaternion $\tilde{\eta}$ in the new frame described by Equations (104)-(105).

The equilibrium points $(\overline{\tilde{\eta}}, \overline{\tilde{\nu}}, \overline{\tilde{\omega}}, \overline{\tilde{\alpha}})$ are defined by

$$\begin{aligned}
(l_V kA \times \overline{\tilde{\nu}} + l_B \langle \tilde{B} \times \tilde{E}_B, kA \rangle kA) * \overline{\tilde{\eta}} - \frac{1}{2} \overline{\tilde{\eta}} * \overline{\tilde{\beta}} &= 0 \\
-kA + \overline{\alpha} \overline{\tilde{\eta}}^{-1} * kA * \overline{\tilde{\eta}} - m_V \overline{\tilde{\nu}} &= 0 \\
\overline{\tilde{\eta}}^{-1} * (-n_V kA \times \overline{\tilde{\nu}} - n_B \langle \tilde{B} \times \tilde{E}_B, kA \rangle kA) * \overline{\tilde{\eta}} \quad + (\overline{\tilde{\eta}}^{-1} * \overline{\tilde{I}}_\omega * \overline{\tilde{\eta}}) \times \overline{\tilde{\beta}} &= 0 \\
o_V \langle kA, \overline{\tilde{\nu}} \rangle \overline{\alpha} &= 0.
\end{aligned}$$

We ensure $\overline{\tilde{\beta}} = 0$ by choosing $L_V E_V + L_B E_B$ colinear to $N_V E_V + N_B E_B$, that is $\frac{n_V}{l_V} = \frac{n_B}{l_B} \triangleq \sigma$. This implies $\overline{\tilde{\nu}} = 0$, $\overline{\alpha} \overline{\tilde{\eta}} * A * \overline{\tilde{\eta}}^{-1} - A = 0$ and $\langle \tilde{B} \times \tilde{E}_B, kA \rangle = 0$.

Finally $(\overline{\tilde{\eta}}, \overline{\tilde{\nu}}, \overline{\tilde{\beta}}, \overline{\tilde{\alpha}}) = (\overline{\tilde{\eta}}, 0, 0, 1)$; moreover $\overline{\phi} = \overline{\theta} = 0$ and $\overline{\psi}$ is determined by $\langle \tilde{B} \times \tilde{E}_B, kA \rangle = 0$, where the Euler angles $\overline{\phi}, \overline{\theta}, \overline{\psi}$ correspond to the error quaternion $\overline{\tilde{\eta}}$.

4.1.6. Simulation results. — We first use simulations to illustrate the behavior of the invariant observer

$$\begin{aligned}
\dot{\hat{q}} &= \frac{1}{2} \hat{q} * (\omega_m - \hat{\omega}_b) + (L_V E_V + L_B E_B) * \hat{q} + \lambda (1 - \|\hat{q}\|^2) \hat{q} \\
\dot{\hat{V}} &= \frac{1}{\hat{a}_s} \hat{q} * a_m * \hat{q}^{-1} + A + (M_V E_V + M_B E_B) \\
\dot{\hat{\omega}}_b &= \hat{q}^{-1} * (N_V E_V + N_B E_B) * \hat{q} \\
\dot{\hat{a}}_s &= \hat{a}_s (O_V E_V + O_B E_B)
\end{aligned}$$

with the choice of gain matrices described in §4.1.5.1.

We choose here time constants around 10s by taking $l_V = n_V = 4e-2$, $l_B = n_B = 2e-3$, $m_V = 5$, $o_V = 1e-2$ and $\lambda = 1$. The system follows the trajectory defined by

$$a_s = 1.1 \qquad \omega_b = \begin{pmatrix} .01 \\ -.012 \\ .08 \end{pmatrix}$$

$$V = \begin{pmatrix} 3 - 2\cos(.3t) \\ 3 - 2.8\cos(.25t + \pi/4) \\ -1 - 1.7\sin(.3t) \end{pmatrix} \qquad \omega_m = \begin{pmatrix} \sin(.5t) \\ \sin(.3t) \\ -\sin(.5t) \end{pmatrix},$$

in SI units, which is quite representative of a small UAV flight. The states are initialized far from their true values.

At $t = 30s$, the magnetic field is changed from $B = (1\ 0\ 1)^T$ (roughly the value in France) to $B = (1\ 0.4\ 1)^T$.

Though we have no proof of convergence other than local, the domain of attraction seems to be quite large, see Figure 4.1. As expected, only the estimated yaw angle ψ is strongly affected by the magnetic disturbance. Because of the coupling terms $\tilde{I}_w$ and I_a, there is some dynamic influence on the other variables.

4.1.7. Experimental results. — We now compare the behavior of our observer with the commercial INS-GPS device MIDG II from Microbotics Inc. We feed the observer with the raw measurements from the MIDG II gyroscopes, accelerometers and magnetic sensors, and the velocity provided by the navigation solutions of its GPS engine. The estimates of the observer are then compared with the estimates given by the MIDG II (computed according to the user manual by some Kalman filter). We have chosen $l_V = 2.8e-3$, $l_B = 7e-3$, $n_V = 4e-5$, $n_B = 1e-4$, $m_V = 0.9$, $o_V = 9.4e-5$ and $\lambda = 1$.

4.1.7.1. Dynamic behavior (Figure 4.2). — We wait a few minutes until the biases reach constant values, then move the system in all directions. Our observer and the MIDG II give very similar results (Figures 4.2(a) and 4.2(b)).

4.1.7.2. Usefulness of the observer terms (Figure 4.3). — As explained in §4.1.5.1 we have chosen the correction terms so that the magnetic measurements essentially correct the yaw angle and its corresponding bias, whereas the velocity measurements act on the other variables.

We highlight this property as well as the importance of correction terms on the following experiment. Once the biases have reached constant values, the system is left at rest during 50 minutes:

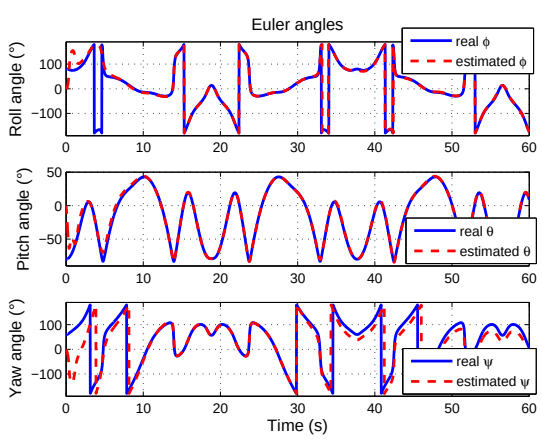

(a) Estimated Euler angles

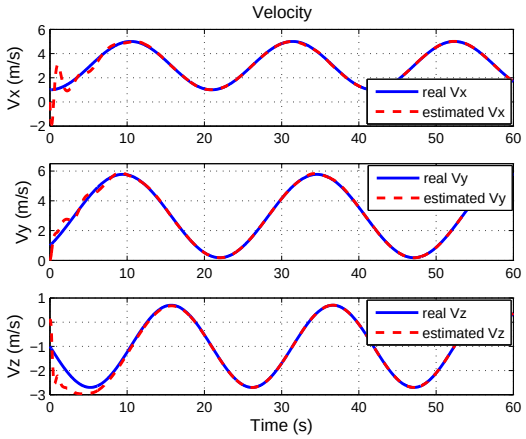

(b) Estimated velocity

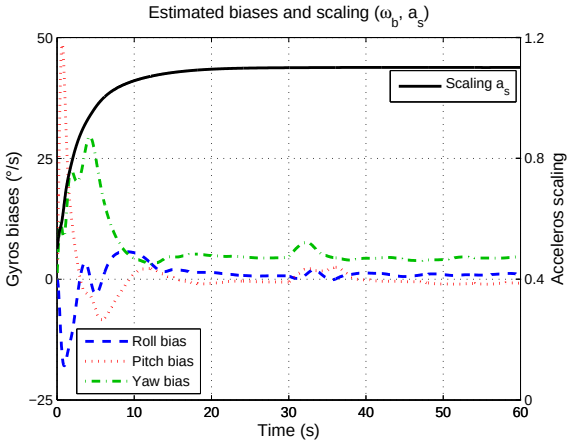

(c) Estimated biases

FIGURE 4.1. Simulation validation using Matlab

- for $t < 700s$ provided by the observer are very similar to those provided by the MIDG II (Figures 4.3(a) and 4.3(b))
- at $t = 700s$ the "magnetic correction terms" are switched off, i.e. the gains l_B and n_B are set to 0. The yaw angle estimated by the observer diverges because the corresponding bias is not perfectly estimated. Indeed, these variables are not observable without the magnetic measurements. The other variables are not affected (Figures 4.3(a) and 4.3(b))

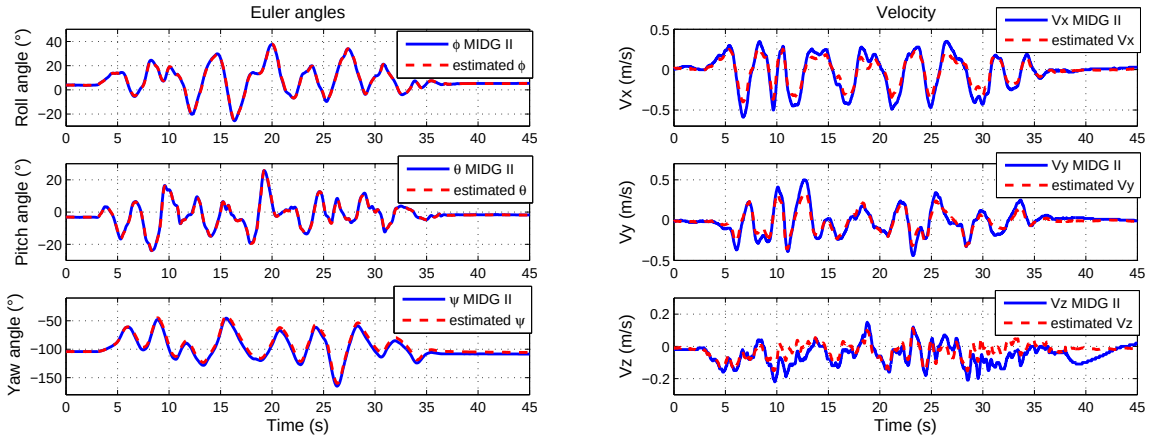

(a) Estimated Euler angles

(b) Estimated velocity

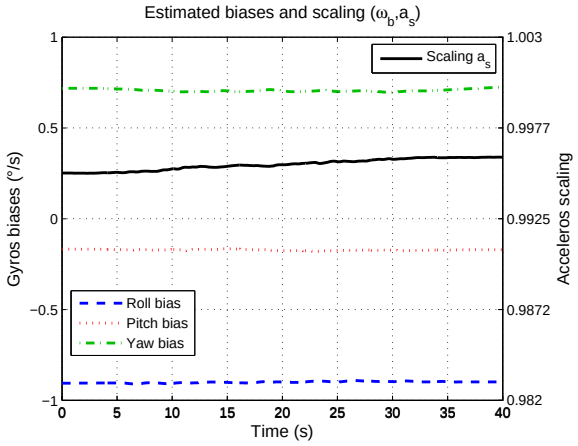

(c) Estimated biases

FIGURE 4.2. Experimental validation using Matlab

– at $t = 1700s$ the "velocity correction terms" are also switched off, i.e. l_V, m_V, n_V and o_V are set to 0. All the estimated angles and velocities now diverge (Figures 4.3(a) and 4.3(b)). Zooming around $t = 1700s$, we see on Figure 4.3(d) that the estimated pitch angle diverges with a slope corresponding to the almost-constant difference between the estimated and actual pitch angular rate biases. This explains why the estimated velocity V_x diverges quadratically in time.

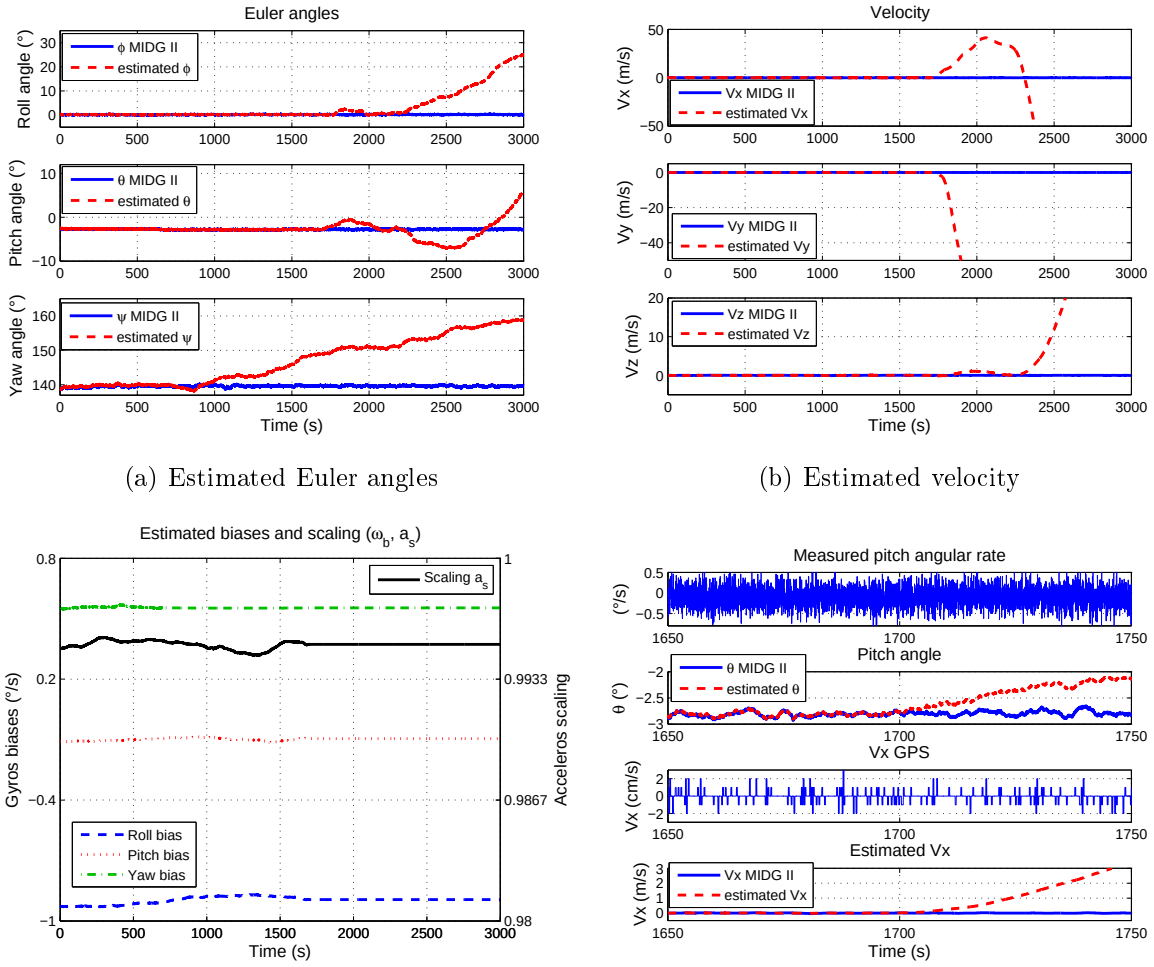

(a) Estimated Euler angles

(b) Estimated velocity

(c) Estimated biases

(d) Zoomed view at t=1700s

FIGURE 4.3. Usefulness of the correction terms (experiment)

4.1.7.3. Influence of magnetic disturbances (Figure 4.4). — Once the biases have reached constant values, the system is left motionless for $60s$. At $t = 13s$ a magnet is put close to the sensors for $10s$. As expected only the estimated yaw angle is affected by the magnetic disturbance (Figures 4.4(a)- 4.4(b)); the MIDG II exhibits a similar behavior.

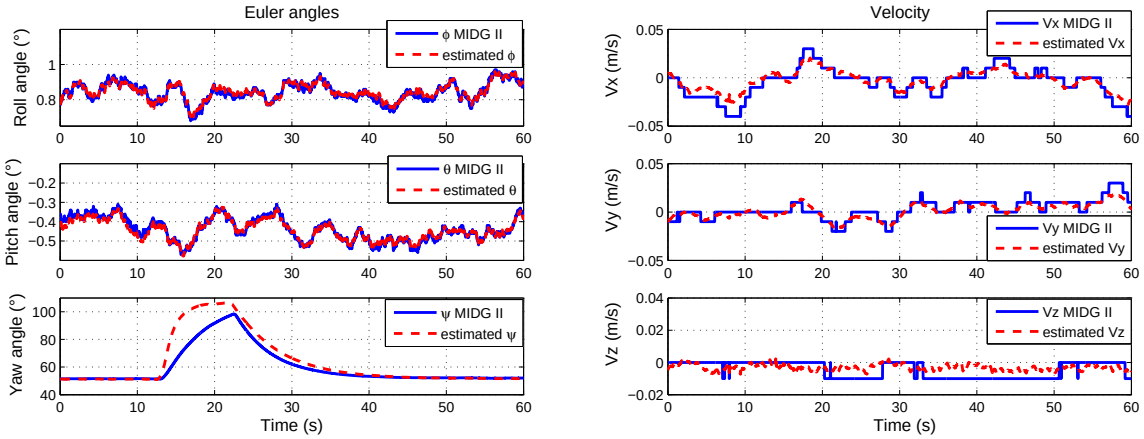

(a) Estimated Euler angles

(b) Estimated velocity

FIGURE 4.4. Influence of magnetic disturbances (experiment)

4.2. Earth-velocity-and-position-aided AHRS

4.2.1. The considered system. — In this section, we add position measurements in Earth-fixed coordinates, provided, for instance, by a GPS engine and a barometer. We therefore consider the following system, described in details in section 2.4

$$\dot{q} = \frac{1}{2} q * (\omega_m - \omega_b) \tag{106}$$

$$\dot{V} = A + \frac{1}{a_s} q * a_m * q^{-1} \tag{107}$$

$$\dot{X} = V \tag{108}$$

$$\dot{\omega}_b = 0 \tag{109}$$

$$\dot{a}_s = 0 \tag{110}$$

$$\dot{h}_b = 0 \tag{111}$$

where ω_m and a_m are seen as known inputs, together with the output

$$\begin{pmatrix} y_V \\ y_X \\ y_h \\ y_B \end{pmatrix} = \begin{pmatrix} V \\ X \\ \langle X, e_3 \rangle - h_b \\ q^{-1} * B * q \end{pmatrix}. \tag{112}$$

4.2.2. Invariance of the system equations. — The considered transformation generated by constant rotations and translations in the earth-fixed and body-fixed frame

$$\varphi_{(p_0,q_0,X_0,\omega_0,a_0,h_0)}\begin{pmatrix} q \\ V \\ X \\ \omega_b \\ a_s \\ h_b \end{pmatrix} = \begin{pmatrix} p_0 * q * q_0 \\ p_0 * V * p_0^{-1} \\ p_0 * (X + X_0) * p_0^{-1} \\ q_0^{-1} * \omega_b * q_0 + \omega_0 \\ a_s a_0 \\ h_b + h_0 \end{pmatrix}$$

$$\psi_{(p_0,q_0,X_0,\omega_0,a_0,h_0)}\begin{pmatrix} \omega_m \\ a_m \\ A \\ B \end{pmatrix} = \begin{pmatrix} q_0^{-1} * \omega_m * q_0 + \omega_0 \\ a_0 q_0^{-1} * a_m * q_0 \\ p_0 * A * p_0^{-1} \\ p_0 * B * p_0^{-1} \end{pmatrix}$$

$$\rho_{(p_0,q_0,X_0,\omega_0,a_0,h_0)}\begin{pmatrix} y_V \\ y_X \\ y_h \\ y_B \end{pmatrix} = \begin{pmatrix} p_0 * y_V * p_0^{-1} \\ p_0 * (y_X + X_0) * p_0^{-1} \\ y_h - h_0 + \langle X_0, e_3 \rangle \\ q_0^{-1} * y_B * q_0 \end{pmatrix}$$

is easily seen to be a transformation group. There are $2*3+2*3+2*1 = 14$ parameters: the two unit quaternion p_0, q_0, the $\mathbb{R}^3$-vectors X_0, ω_0 and the two scalars a_0, h_0. So the transformation group has one fewer dimension than the system (106)–(111). We could add another scaling v_0 for the transformation on V, which would lead only to a kind of gain normalization, and then will not be considered here. The group law $\diamond$ is given by

$$\begin{pmatrix} p_1 \\ q_1 \\ X_1 \\ \omega_1 \\ a_1 \\ h_1 \end{pmatrix} \diamond \begin{pmatrix} p_0 \\ q_0 \\ X_0 \\ \omega_0 \\ a_0 \\ h_0 \end{pmatrix} = \begin{pmatrix} p_1 * p_0 \\ q_0 * q_1 \\ X_0 + p_0^{-1} * X_1 * p_0 \\ q_1^{-1} * \omega_0 * q_1 + \omega_1 \\ a_1 a_0 \\ h_1 + h_0 \end{pmatrix}.$$

The system (106)–(111) is indeed invariant by the transformation group since

$$\begin{aligned}
\overbrace{(p_0 * q * q_0)}^{\cdot} &= p_0 * \dot{q} * q_0 = \frac{1}{2}(p_0 * q * q_0) * \left((q_0^{-1} * \omega_m * q_0 + \omega_0) - (q_0^{-1} * \omega_b * q_0 + \omega_0)\right) \\
\overbrace{p_0 * V * p_0^{-1}}^{\cdot} &= p_0 * \dot{V} * p_0^{-1} \\
&= p_0 * A * p_0^{-1} + \frac{1}{a_s a_0}(p_0 * q * q_0) * (a_s q_0^{-1} * a_m * q_0) * (p_0 * q * q_0)^{-1} \\
\overbrace{(q_0^{-1} * \omega_b * q_0 + \omega_0)}^{\cdot} &= q_0^{-1} * \dot{\omega}_b * q_0 = 0 \\
\overbrace{(a_s a_0)}^{\cdot} &= \dot{a}_s a_0 = 0 \\
\overbrace{(h_b + h_0)}^{\cdot} &= \dot{h}_b = 0,
\end{aligned}$$

whereas the output (112) is equivariant since

$$\begin{pmatrix} p_0 * V * p_0^{-1} \\ p_0 * (X + X_0) * p_0^{-1} \\ \langle p_0 * (X + X_0) * p_0^{-1}, p_0 * e_3 * p_0^{-1} \rangle - (h_b + h_0) \\ (p_0 * q * q_0)^{-1} * (p_0 * B * p_0^{-1}) * (p_0 * q * q_0) \end{pmatrix} = \rho_{(p_0,q_0,X_0,\omega_0,a_0,h_0)} \begin{pmatrix} V \\ X \\ \langle X, e_3 \rangle - h_b \\ q^{-1} * B * q \end{pmatrix}.$$

Velocity measurements y_v in the body-fixed frame can commonly be provided by an air-data system (or a Doppler radar on bigger UAV or aircraft). Since $y_v = q^{-1} * V * q$ this new output is also equivariant:

$$(p_0 * q * q_0)^{-1} * (p_0 * V * p_0^{-1}) * (p_0 * q * q_0) = \rho_{(p_0,q_0,X_0,\omega_0,a_0,h_0)} \left(q^{-1} * V * q\right).$$

Thus the nonlinear observer we construct can be adapted to also use measurements in the body-fixed frame. For simplicity's sake, air data probe measurements will not be considered in this section, but only in Section 4.3.

Notice also that from a physical and engineering viewpoint, it is perfectly sensible for an observer using measurements expressed in the body-fixed frame not to be affected by the actual choice of coordinates, i.e. by a constant rotation in the body-fixed frame. Similarly, a translation of the gyro bias by a vector constant in the body-fixed frame and a translation of the position measurements by a constant vector in the Earth-fixed frame should not affect the observer.

4.2.3. Construction of the general invariant observer. — In this section we detail the steps to construct the general invariant observer, which consists of a generalization of the observer described in Ref. [**10**].

We solve for $(p_0, q_0, X_0, \omega_0, a_0, h_0)$ the normalization equations

$$\begin{aligned} p_0 * q * q_0 &= 1 \\ p_0 * e_i * p_0^{-1} &= \tilde{e}_i \\ p_0 * (X + X_0) * p_0^{-1} &= 0 \\ q_0^{-1} * \omega_b * q_0 + \omega_0 &= 0 \\ a_s a_0 &= 1 \\ h_b + h_0 &= 0 \end{aligned}$$

to find the moving frame $\gamma(q, X, \omega_b, a_s, h_b, e_1, e_2, e_3)$ defined by the equations

$$\begin{aligned} q_0 &= q^{-1} * p_0^{-1} \\ X_0 &= -X \\ \omega_0 &= -p_0 * q * \omega_b * q^{-1} * p_0^{-1} \\ h_0 &= -h_b + \langle X, e_3 \rangle \end{aligned}$$

where p_0 represents the rotation between the two frames (e_1, e_2, e_3) and $(\tilde{e}_1, \tilde{e}_2, \tilde{e}_3)$.

We can then find the 10 scalar invariant errors which correspond to the projections of the output error

$$\rho_{\gamma(\hat{q},\hat{X},\hat{\omega}_b,\hat{a}_s,\hat{h}_b,e_1,e_2,e_3)} \begin{pmatrix} \hat{y}_V \\ \hat{y}_X \\ \hat{y}_B \end{pmatrix} - \rho_{\gamma(\hat{q},\hat{X},\hat{\omega}_b,\hat{a}_s,\hat{h}_b,e_1,e_2,e_3)} \begin{pmatrix} y_V \\ y_X \\ y_B \end{pmatrix}$$

on the new frame $(\tilde{e}_1, \tilde{e}_2, \tilde{e}_3)$ and to the output error related to y_h which is directly invariant. We get

$$\begin{aligned} E_{Vi} &= \langle \hat{y}_V - y_V, e_i \rangle \\ E_{Xi} &= \langle \hat{y}_X - y_X, e_i \rangle \\ E_h &= \langle \hat{X} - X, e_3 \rangle - \hat{h}_b + h_b \\ E_{Bi} &= \langle B - \hat{q} * y_B * \hat{q}^{-1}, e_i \rangle, \end{aligned}$$

where $i = 1, 2, 3$. We detail for instance how to get E_{Vi}:

$$\begin{aligned}\langle \rho_{\gamma(\hat{q},\hat{X},\hat{\omega}_b,\hat{a}_s,\hat{h}_b,e_1,e_2,e_3)}\left(\hat{y}_V\right) - \rho_{\gamma(\hat{q},\hat{X},\hat{\omega}_b,\hat{a}_s,\hat{h}_b,e_1,e_2,e_3)}\left(y_V\right), \tilde{e}_i\rangle &= \langle p_0 * \hat{y}_V * p_0^{-1} - p_0 * y_V * p_0^{-1}, \tilde{e}_i\rangle \\ &= \langle \hat{y}_V - y_V, p_0^{-1} * \tilde{e}_i * p_0\rangle \\ &= \langle \hat{y}_V - y_V, e_i\rangle.\end{aligned}$$

We get also the 9 scalar complete invariants which correspond to the projections of

$$\phi_{\gamma(\hat{q},\hat{X},\hat{\omega}_b,\hat{a}_s,\hat{h}_b,e_1,e_2,e_3)}\left(\hat{V}\right) \quad \text{and} \quad \psi_{\gamma(\hat{q},\hat{X},\hat{\omega}_b,\hat{a}_s,\hat{h}_b,e_1,e_2,e_3)}\begin{pmatrix}\omega_m \\ a_m\end{pmatrix}$$

on the new frame $(\tilde{e}_1, \tilde{e}_2, \tilde{e}_3)$. We find

$$\begin{aligned}I_{\hat{V}i} &= \langle \hat{V}, e_i\rangle \\ I_{\omega i} &= \langle \hat{q} * (\omega_m - \hat{\omega}_b) * \hat{q}^{-1}, e_i\rangle \\ I_{ai} &= \langle \frac{1}{\hat{a}_s}\hat{q} * a_m * \hat{q}^{-1}, e_i\rangle \qquad \text{with} \qquad i = 1, 2, 3.\end{aligned}$$

Notice that $I_{\hat{V}i}$, $I_{\omega i}$, I_{ai}, E_{Vi}, E_{Xi}, E_{Bi}'s and E_h are functions of the estimates and the measurements. Hence they are known quantities which can be used in the construction of the observer. It is straightforward to check they are indeed invariant. For instance,

$$\begin{aligned}E_{Bi}(p_0 * \hat{q} * q_0, p_0 * B * p_0^{-1}, q_0^{-1} * y_B * q_0) &= \langle p_0 * B * p_0^{-1} \\ &\qquad - (p_0 * \hat{q} * q_0) * (q_0^{-1} * y_B * q_0) * (p_0 * \hat{q} * q_0)^{-1}, \tilde{e}_i\rangle \\ &= \langle B - \hat{q} * y_B * \hat{q}^{-1}, e_i\rangle \\ &= E_{Bi}(\hat{q}, B, y_B).\end{aligned}$$

To find invariant vector fields, we solve the 14 vector equations ($i = 1, 2, 3$) in the unknown $w(q, V, X, \omega_b, a_s, h_b)$

$$\left[D\varphi_{\gamma(q,X,\omega_b,a_s,h_b,e_1,e_2,e_3)}\begin{pmatrix}q \\ V \\ X \\ \omega_b \\ a_s \\ h_b\end{pmatrix}\right]\cdot w(q, V, X, \omega_b, a_s, h_b) = \begin{pmatrix}\tilde{e}_i \\ 0 \\ 0 \\ 0 \\ 0 \\ 0\end{pmatrix}, \begin{pmatrix}0 \\ \tilde{e}_i \\ 0 \\ 0 \\ 0 \\ 0\end{pmatrix}, \begin{pmatrix}0 \\ 0 \\ \tilde{e}_i \\ 0 \\ 0 \\ 0\end{pmatrix}, \begin{pmatrix}0 \\ 0 \\ 0 \\ \tilde{e}_i \\ 0 \\ 0\end{pmatrix}, \begin{pmatrix}0 \\ 0 \\ 0 \\ 0 \\ e_{13} \\ 0\end{pmatrix}, \begin{pmatrix}0 \\ 0 \\ 0 \\ 0 \\ 0 \\ e_{14}\end{pmatrix}.$$

Since

$$\left[D\varphi_{(p_0,q_0,X_0,\omega_0,a_0,h_0)} \begin{pmatrix} q \\ V \\ X \\ \omega_b \\ a_s \\ h_b \end{pmatrix} \right] \cdot \begin{pmatrix} \delta q \\ \delta V \\ \delta X \\ \delta \omega_b \\ \delta a_s \\ \delta h_b \end{pmatrix} = \begin{pmatrix} p_0 * \delta q * q_0 \\ p_0 * \delta V * p_0^{-1} \\ p_0 * \delta X * p_0^{-1} \\ q_0^{-1} * \delta \omega_b * q_0 \\ a_0 \delta a_s \\ \delta h_b \end{pmatrix},$$

this yields the 14 independent invariant vector fields

$$\begin{pmatrix} e_i * q \\ 0 \\ 0 \\ 0 \\ 0 \\ 0 \end{pmatrix}, \begin{pmatrix} 0 \\ e_i \\ 0 \\ 0 \\ 0 \\ 0 \end{pmatrix}, \begin{pmatrix} 0 \\ 0 \\ e_i \\ 0 \\ 0 \\ 0 \end{pmatrix}, \begin{pmatrix} 0 \\ 0 \\ 0 \\ q^{-1} * e_i * q \\ 0 \\ 0 \end{pmatrix}, \begin{pmatrix} 0 \\ 0 \\ 0 \\ 0 \\ a_s e_{13} \\ 0 \end{pmatrix}, \begin{pmatrix} 0 \\ 0 \\ 0 \\ 0 \\ 0 \\ e_{14} \end{pmatrix}, \quad i = 1, 2, 3.$$

Indeed for instance the equations $p_0 * \delta q * q_0 = \tilde{e}_i$ gave us

$$\delta q = p_0^{-1} * \tilde{e}_i * q_0^{-1} = (p_0^{-1} * \tilde{e}_i * p_0) * (q_0 * p_0)^{-1} = e_i * q.$$

It is easy to check that these vector fields are indeed invariant.

The general invariant observer then reads

$$\begin{aligned}
\dot{\hat{q}} &= \frac{1}{2}\hat{q} * (\omega_m - \omega_b) + \sum_{i=1}^{3}\Big(\sum_{j=1}^{3}(l_{Vij}E_{Vj} + l_{Xij}E_{Xj} + l_{Bij}E_{Bj}) + l_{hi}E_h\Big)e_i * \hat{q} \\
\dot{\hat{V}} &= A + \frac{1}{\hat{a}_s}\hat{q} * a_m * \hat{q}^{-1} + \sum_{i=1}^{3}\Big(\sum_{j=1}^{3}(m_{Vij}E_{Vj} + m_{Xij}E_{Xj} + m_{Bij}E_{Bj}) + m_{hi}E_h\Big)e_i \\
\dot{\hat{X}} &= \hat{V} + \sum_{i=1}^{3}\Big(\sum_{j=1}^{3}(n_{Vij}E_{Vj} + n_{Xij}E_{Xj} + n_{Bij}E_{Bj}) + n_{hi}E_h\Big)e_i \\
\dot{\hat{\omega}}_b &= \hat{q}^{-1} * \Big(\sum_{i=1}^{3}\Big(\sum_{j=1}^{3}(o_{Vij}E_{Vj} + o_{Xij}E_{Xj} + o_{Bij}E_{Bj}) + o_{hi}E_h\Big)e_i\Big) * \hat{q} \\
\dot{\hat{a}}_s &= \hat{a}_s\Big(\sum_{j=1}^{3}(r_{Vj}E_{Vj} + r_{Xj}E_{Xj} + r_{Bj}E_{Bj}) + r_hE_h\Big) \\
\dot{\hat{b}}_b &= \sum_{j=1}^{3}(s_{Vj}E_{Vj} + s_{Xj}E_{Xj} + s_{Bj}E_{Bj}) + s_hE_h,
\end{aligned}$$

where the l_{Vij}, l_{Xij}, l_{Bij}, l_{hi}, m_{Vij}, m_{Xij}, m_{Bij}, m_{hi}, n_{Vij}, n_{Xij}, n_{Bij}, n_{hi}, o_{Vij}, o_{Xij}, o_{Bij}, o_{hi}, r_{Vj}, r_{Xj}, r_{Bj}, s_{Vj}, s_{Xj}, s_{Bj}'s, r_h and s_h are arbitrary scalars which possibly depend on E_{Vi}, E_{Xi}, E_{Bi}, E_h, $I_{\hat{V}i}$, $I_{\omega i}$ and I_{ai}'s. Noticing

$$\sum_{i=1}^{3}\Big(\sum_{j=1}^{3}(l_{Vij}E_{Vj})\Big)e_i = L_VE_V$$

where $E_V = \hat{V} - V$ and L_V is the 3×3 matrix whose coefficients are the l_{Vij}'s, and defining E_X, E_B, L_X, L_h, L_B, M_V, M_X, M_h, M_B, N_V, N_X, N_h, N_B, O_V, O_X, O_h, O_B, R_V, R_X, R_B, R_h, S_V, S_X, S_h and S_B in the same way, we can rewrite the observer as

$$\dot{\hat{q}} = \frac{1}{2}\hat{q} * (\omega_m - \omega_b) + (L_V E_V + L_X E_X + L_h E_h + L_B E_B) * \hat{q} \tag{113}$$

$$\dot{\hat{V}} = A + \frac{1}{\hat{a}_s}\hat{q} * a_m * \hat{q}^{-1} + (M_V E_V + M_X E_X + M_h E_h + M_B E_B) \tag{114}$$

$$\dot{\hat{X}} = \hat{V} + (N_V E_V + N_X E_X + N_h E_h + N_B E_B) \tag{115}$$

$$\dot{\hat{\omega}}_b = \hat{q}^{-1} * (O_V E_V + O_X E_X + O_h E_h + O_B E_B) * \hat{q} \tag{116}$$

$$\dot{\hat{a}}_s = \hat{a}_s(R_V E_V + R_X E_X + R_h E_h + R_B E_B) \tag{117}$$

$$\dot{\hat{h}}_b = (S_V E_V + S_X E_X + S_h E_h + S_B E_B), \tag{118}$$

where L_V, L_X, L_B, M_V, M_X, M_B, N_V, N_X, N_B, O_V, O_X, O_B are 3×3 matrices, R_V, R_X, R_B, S_V, S_X, S_B are 1×3 matrices, L_h, M_h, N_h, O_h are 3×1 matrices and R_h, S_h are scalars whose coefficients possibly depend on E_V, E_X, E_B, E_h, $I_{\hat{V}}$, I_ω and I_a with the invariant output

$$E_V = \hat{V} - y_V \tag{119}$$

$$E_X = \hat{X} - y_X \tag{120}$$

$$E_B = B - \hat{q} * y_B * \hat{q}^{-1} \tag{121}$$

$$E_h = \langle \hat{X}, e_3 \rangle - \hat{h}_b - y_h \tag{122}$$

and the complete invariant

$$\begin{aligned} I_{\hat{V}} &= \hat{V} \\ I_\omega &= \hat{q} * (\omega_m - \hat{\omega}_b) * \hat{q}^{-1} \\ I_a &= \frac{1}{\hat{a}_s}\hat{q} * a_m * \hat{q}^{-1}. \end{aligned}$$

The observer is indeed invariant by considering the projection of the output errors E_V, E_X and E_B on the frame (e_1, e_2, e_3). As in Section 4.1.3, the norm of $\hat{q}$ is left unchanged by Equation (113).

4.2.3.1. The invariant error system. — The state error is given by

$$\begin{pmatrix}\eta\\ \nu\\ \chi\\ \beta\\ \alpha\\ \lambda\end{pmatrix} = \varphi_{\gamma(q,V,X,\omega_b,a_s,h_b)}\begin{pmatrix}\hat{q}\\ \hat{V}\\ \hat{X}\\ \hat{\omega}_b\\ \hat{a}_s\\ \hat{h}_b\end{pmatrix} - \varphi_{\gamma(q,V,X,\omega_b,a_s,h_b)}\begin{pmatrix}q\\ V\\ X\\ \omega_b\\ a_s\\ h_b\end{pmatrix} = \begin{pmatrix}\hat{q}*q^{-1}-1\\ \hat{V}-V\\ \hat{X}-X\\ q*(\hat{\omega}_b-\omega_b)*q^{-1}\\ \frac{\hat{a}_s}{a_s}-1\\ \hat{h}_b-h_b\end{pmatrix}.$$

As in Section 4.1.4, we take $\eta = \hat{q}*q^{-1}$ and $\alpha = \frac{\hat{a}_s}{a_s}$. As we did in the preceding subsection it can be easily checked that α, λ and the projections of η, ν, χ and β on the frame (e_1, e_2, e_3) are invariant. Hence for $(i,j) = \{1,2,3\}^2$,

$$\begin{aligned}
\langle\dot{\overbrace{\eta e_i \eta^{-1}}}, e_j\rangle &= \langle\dot{\eta}*e_i*\eta^{-1} - \eta*e_i*\eta^{-1}\dot{\eta}\eta^{-1}, e_j\rangle\\
&= 2\langle(-\frac{1}{2}\eta\beta\eta^{-1} + L_V E_V + L_X E_X + L_B E_B + L_h E_h)\times(\eta e_i\eta^{-1}), e_j\rangle\\
\langle\dot{\nu}, e_i\rangle &= \langle I_a - \alpha\eta^{-1}*I_a*\eta + M_V E_V + M_X E_X + M_B E_B + M_h E_h, e_i\rangle\\
\langle\dot{\chi}, e_i\rangle &= \langle\nu + N_V E_V + N_X E_X + N_B E_B + N_h E_h, e_i\rangle\\
\langle\dot{\beta}, e_i\rangle &= \langle(\eta^{-1}I_\omega\eta)\times\beta + \eta^{-1}*(O_V E_V + O_X E_X + O_B E_B + O_h E_h)*\eta, e_i\rangle\\
\dot{\alpha} &= \alpha(R_V E_V + R_X E_X + R_B E_B + R_h E_h)\\
\dot{\lambda} &= S_V E_V + S_X E_X + S_B E_B + S_h E_h.
\end{aligned}$$

Since we can write

$$\begin{aligned}
E_V &= \nu\\
E_X &= \chi\\
E_B &= B - \eta*B*\eta^{-1}\\
E_h &= \langle\chi, e_3\rangle - \lambda,
\end{aligned}$$

we find as expected that the error system

$$\overdot{\eta e_i \eta^{-1}} = 2(-\frac{1}{2}\eta\beta\eta^{-1} + L_V E_V + L_X E_X + L_B E_B + L_h E_h) \times (\eta e_i \eta^{-1}) \tag{123}$$

$$\dot{\nu} = I_a - \alpha\eta^{-1} * I_a * \eta + M_V E_V + M_X E_X + M_B E_B + M_h E_h \tag{124}$$

$$\dot{\chi} = \nu + N_V E_V + N_X E_X + N_B E_B + N_h E_h \tag{125}$$

$$\dot{\beta} = (\eta^{-1} I_\omega \eta) \times \beta + \eta^{-1} * (O_V E_V + O_X E_X + O_B E_B + O_h E_h) * \eta \tag{126}$$

$$\dot{\alpha} = \alpha(R_V E_V + R_X E_X + R_B E_B + R_h E_h) \tag{127}$$

$$\dot{\lambda} = S_V E_V + S_X E_X + S_B E_B + S_h E_h \tag{128}$$

depends only on the invariant state error $(\eta, \nu, \chi, \beta, \alpha, \lambda)$ and the "free" known invariants $I_{\hat{V}}$, I_ω and I_a, but not on the trajectory of the observed system (106)–(111). The error system (123)–(128) is invariant by considering the projection of the equations (123)–(126) on the frame (e_1, e_2, e_3).

The linearized error system around $(\overline{\eta}, \overline{\nu}, \overline{\chi}, \overline{\beta}, \overline{\alpha}, \overline{\lambda}) = (1, 0, 0, 0, 1, 0)$, i.e. the estimated state equals the actual state, is given by

$$\begin{aligned}
\delta\dot{\eta} &= -\frac{1}{2}\delta\beta + (L_V \delta E_V + L_X \delta E_X + L_B \delta E_B + L_h \delta E_h) \\
\delta\dot{\nu} &= -2I_a \times \delta\eta - \delta\alpha I_a + (M_V \delta E_V + M_X \delta E_X + M_B \delta E_B + M_h \delta E_h) \\
\delta\dot{\chi} &= \delta\nu + (N_V \delta E_V + N_X \delta E_X + N_B \delta E_B + N_h \delta E_h) \\
\delta\dot{\beta} &= I_\omega \times \delta\beta + (O_V \delta E_V + O_X \delta E_X + O_B \delta E_B + O_h \delta E_h) \\
\delta\dot{\alpha} &= (R_V \delta E_V + R_X \delta E_X + R_B \delta E_B + R_h \delta E_h) \\
\delta\dot{\lambda} &= (S_V \delta E_V + S_X \delta E_X + S_B \delta E_B + S_h \delta E_h)
\end{aligned}$$

where

$$\delta E_V = \delta\nu$$

$$\delta E_X = \delta\chi$$

$$\delta E_B = -\delta\eta * B * \overline{\eta}^{-1} - \overline{\eta} * B * (-\overline{\eta}^{-1} * \delta\eta * \overline{\eta}^{-1}) = 2(\overline{\eta} * B * \overline{\eta}^{-1}) \times (\delta\eta * \overline{\eta}^{-1}) = 2B \times \delta\eta$$

$$\delta E_h = \langle \delta\chi, e_3 \rangle - \delta\lambda.$$

4.2.4. Design of the observer gain matrices. —

4.2.4.1. Choice of the gain matrices. — The linearized error system without correction terms turns out to be decoupled into 4 independent subsystems (see §4.2.4.3) when I_a is constant and $I_\omega = 0$ (in particular when the aircraft is in level flight). To ensure a

simple tuning, the gain matrices should respect this decoupling. On the other hand, as previously explained, we do not want these magnetic disturbances – which unavoidably corrupt the heading estimation – to affect the attitude, velocity and position estimates too much. The idea is thus to rely on the magnetic measurement y_B as little as possible.

Therefore we choose

$$\begin{array}{llll}
L_V E_V = -l_V I_a \times E_V & L_X E_X = 0 & L_B E_B = l_B \langle B \times E_B, I_a \rangle I_a & L_h E_h = 0 \\
M_V E_V = -m_V E_V & M_X E_X = 0 & M_B E_B = 0 & M_h E_h = -m_h E_h e_3 \\
N_V E_V = 0 & N_X E_X = -n_X E_X & N_B E_B = 0 & N_h E_h = -n_h E_h e_3 \\
O_V E_V = o_V I_a \times E_V & O_X E_X = 0 & O_B E_B = -o_B \langle B \times E_B, I_a \rangle I_a & O_h E_h = 0 \\
R_V E_V = r_V \langle I_a, E_V \rangle & R_X E_X = 0 & R_B E_B = 0 & R_h E_h = -r_h E_h \\
S_V E_V = 0 & S_X E_X = 0 & S_B E_B = 0 & S_h E_h = s_h E_h
\end{array}$$

with $(l_V, l_B, m_V, m_h, n_X, n_h, o_V, o_B, r_V, r_h, s_h) > 0$.

4.2.4.2. Equilibrium points of the observer equations. — When the observer have converged, Equations (126)–(128) of the observer write

$$\begin{aligned}
O_V E_V + O_B E_B &= 0 \\
R_V E_V + R_h E_h &= 0 \\
S_h E_h &= 0.
\end{aligned}$$

The choice of gain matrices above leads us to

$$I_a \times E_V = 0 \quad \text{and} \quad \langle I_a, E_V \rangle = 0.$$

So even if the model is wrong, for example if the Earth magnetic field is perturbed, the observer equations ensure $\hat{V} = V$ once it has converged. This important property led us to consider the fourth bias a_s in addition to the usual biases ω_b on the gyros. A similar conclusion is not possible with the Euler angles even if we consider additional biases: $E_B = 0$ does not ensure that the yaw angle, for example, is correctly estimated.

4.2.4.3. First-order approximation and coordinate change. — Considering the gain matrices described above, the linearized error equations around the equilibrium point

$(1,0,0,0,1,0)$ write

$$\begin{aligned}
\delta\dot{\eta} &= -\frac{1}{2}\delta\beta - l_V I_a \times \delta E_V + l_B\langle B \times \delta E_B, I_a\rangle I_a \\
\delta\dot{\nu} &= -2I_a \times \delta\eta - \delta\alpha I_a - m_V\delta E_V - m_h\delta E_h e_3 \\
\delta\dot{\chi} &= \delta\nu - n_X\delta E_X - n_h\delta E_h e_3 \\
\delta\dot{\beta} &= I_\omega \times \delta\beta + o_V I_a \times \delta E_V - o_B\langle B \times \delta E_B, I_a\rangle I_a \\
\delta\dot{\alpha} &= r_V\langle I_a, \delta E_V\rangle - r_h\delta E_h \\
\delta\dot{\lambda} &= s_h\delta E_h
\end{aligned}$$

with

$$\begin{aligned}
\delta E_V &= \delta\nu \\
\delta E_X &= \delta\chi \\
\delta E_B &= 2B \times \delta\eta \\
\delta E_h &= \langle\delta\chi, e_3\rangle - \delta\lambda.
\end{aligned}$$

We change the coordinates in order to have the estimated specific acceleration vector I_a vertical. Let η_0 be this frame rotation defined by

$$\eta_0^{-1} * I_a * \eta_0 = -kA, \quad \text{where} \quad k > 0 \tag{129}$$

$$\eta_0^{-1} * B * \eta_0 = \tilde{B} \quad \text{with} \quad \tilde{B} = (\tilde{B}_1\ 0\ \tilde{B}_3). \tag{130}$$

It follows that

$$\begin{aligned}
\tilde{\eta} &= \eta_0^{-1} * \eta * \eta_0 \qquad & \tilde{\nu} &= \eta_0^{-1} * \nu * \eta_0 \\
\tilde{\chi} &= \eta_0^{-1} * \chi * \eta_0 \qquad & \tilde{\beta} &= \eta_0^{-1} * \beta * \eta_0 \\
e_i^{'} &= \eta_0^{-1} * e_i * \eta_0.
\end{aligned}$$

The error system then becomes

$$\begin{aligned}
\delta\dot{\tilde{\eta}} &= 2\delta\tilde{\eta} \times (\eta_0^{-1} * \dot{\eta}_0) - \frac{1}{2}\delta\tilde{\beta} + kl_V A \times \delta\tilde{E}_V + k^2 l_B \langle \tilde{B} \times \delta\tilde{E}_B, A\rangle A \\
\delta\dot{\tilde{\nu}} &= 2\delta\tilde{\nu} \times (\eta_0^{-1} * \dot{\eta}_0) + 2kA \times \delta\eta + k\delta\alpha A - m_V \delta\tilde{E}_V - m_h \delta\tilde{E}_h e_3' \\
\delta\dot{\tilde{\chi}} &= 2\delta\tilde{\chi} \times (\eta_0^{-1} * \dot{\eta}_0) + \delta\tilde{\nu} - n_X \delta\tilde{E}_X - n_h \delta\tilde{E}_h e_3' \\
\delta\dot{\tilde{\beta}} &= 2\delta\tilde{\beta} \times (\eta_0^{-1} * \dot{\eta}_0) + \tilde{I}_\omega \times \delta\tilde{\omega} - ko_V A \times \delta\tilde{E}_V - k^2 o_B \langle \tilde{B} \times \delta\tilde{E}_B, A\rangle A \\
\delta\dot{\alpha} &= -r_V k \langle A, \delta\tilde{E}_V\rangle - r_h \delta\tilde{E}_h \\
\delta\dot{\lambda} &= s_h \delta\tilde{E}_h
\end{aligned}$$

with

$$\begin{aligned}
\delta\tilde{E}_V &= \delta\tilde{\nu} \\
\delta\tilde{E}_X &= \delta\tilde{\chi} \\
\delta\tilde{E}_B &= 2\tilde{B} \times \delta\tilde{\eta} \\
\delta\tilde{E}_h &= \langle \delta\tilde{\chi}, e_3' \rangle - \delta\lambda.
\end{aligned}$$

We suppose now that the system is moving along a "smooth" trajectory, i.e $\dot{\eta}_0$, $\dot{I}_a$ and I_ω are negligible (first order terms). All the terms of the form $\cdot \times (\eta_0^{-1} * \dot{\eta}_0)$ then disappear and k is now constant. The error system splits into three decoupled subsystems and one cascaded subsystem:

– the longitudinal subsystems

$$\begin{pmatrix} \delta\dot{\tilde{\eta}}_2 \\ \delta\dot{\tilde{\nu}}_1 \\ \delta\dot{\tilde{\beta}}_2 \end{pmatrix} = \begin{pmatrix} 0 & kl_V g & -\frac{1}{2} \\ -2kg & -m_V & 0 \\ 0 & -ko_V g & 0 \end{pmatrix} \begin{pmatrix} \delta\tilde{\eta}_2 \\ \delta\tilde{\nu}_1 \\ \delta\tilde{\beta}_2 \end{pmatrix}$$

$$\delta\tilde{\chi}_1 = \delta\tilde{\nu}_1 - n_X \delta\tilde{\chi}_1$$

– the lateral subsystems

$$\begin{pmatrix} \delta\dot{\tilde{\eta}}_1 \\ \delta\dot{\tilde{\nu}}_2 \\ \delta\dot{\tilde{\beta}}_1 \end{pmatrix} = \begin{pmatrix} 0 & -kl_V g & -\frac{1}{2} \\ 2kg & -m_V & 0 \\ 0 & ko_V g & 0 \end{pmatrix} \begin{pmatrix} \delta\tilde{\eta}_1 \\ \delta\tilde{\nu}_2 \\ \delta\tilde{\beta}_1 \end{pmatrix}$$

$$\delta\tilde{\chi}_2 = \delta\tilde{\nu}_2 - n_X \delta\tilde{\chi}_2$$

– the vertical subsystem

$$\begin{pmatrix} \delta\dot{\tilde{\nu}}_3 \\ \delta\dot{\alpha} \\ \delta\dot{\tilde{\chi}}_3 \\ \delta\dot{\lambda} \end{pmatrix} = \begin{pmatrix} -m_V & kg & -m_h & m_h \\ -kgr_V & 0 & -r_h & r_h \\ 1 & 0 & -(n_X + n_h) & n_h \\ 0 & 0 & s_h & -s_h \end{pmatrix} \begin{pmatrix} \delta\tilde{\nu}_3 \\ \delta\alpha \\ \delta\tilde{\chi}_3 \\ \delta\lambda \end{pmatrix}$$

– the heading subsystem

$$\begin{pmatrix} \delta\dot{\tilde{\eta}}_3 \\ \delta\dot{\tilde{\beta}}_3 \end{pmatrix} = \begin{pmatrix} -2k^2g^2l_B\tilde{B}_1^2 & -\frac{1}{2} \\ 2k^2g^2o_B\tilde{B}_1^2 & 0 \end{pmatrix} \begin{pmatrix} \delta\tilde{\eta}_3 \\ \delta\tilde{\beta}_3 \end{pmatrix} + \begin{pmatrix} 2k^2g^2l_B\tilde{B}_3\tilde{B}_1 \\ -2k^2g^2o_B\tilde{B}_3\tilde{B}_1 \end{pmatrix} \delta\tilde{\eta}_1.$$

Thanks to this decoupled structure, the convergence of each subsystem, and then the local convergence of the invariant observer, is straightforward, and leads to Theorem 3.

Theorem 3. — *Consider the physical system* (106)–(111) *with the measurements* (112). *Consider the nonlinear invariant observer defined by*

$$\begin{aligned} \dot{\hat{q}} &= \frac{1}{2}\hat{q} * (\omega_m - \omega_b) + (L_V E_V + L_B E_B) * \hat{q} \\ \dot{\hat{V}} &= A + \frac{1}{\hat{a}_s}\hat{q} * a_m * \hat{q}^{-1} + (M_V E_V + M_h E_h) \\ \dot{\hat{X}} &= \hat{V} + (N_X E_X + N_h E_h) \\ \dot{\hat{\omega}}_b &= \hat{q}^{-1} * (O_V E_V + O_B E_B) * \hat{q} \\ \dot{\hat{a}}_s &= \hat{a}_s(R_V E_V + R_h E_h) \\ \dot{\hat{h}}_b &= (S_h E_h), \end{aligned}$$

with the expression of the output errors given by Equations (119)–(122) *and the gain matrices given in Section 4.2.4.1. Then for any value* $(l_V, l_B, m_V, m_h, n_X, n_h, o_V, o_B, r_V, r_h, s_h) > 0$, *the solution* $(\hat{q}(t), \hat{V}(t), \hat{X}(t), \hat{\omega}_b(t), \hat{a}_s(t), \hat{h}_b(t))$ *locally asymptotically converges to* $(q(t), V(t), X(t), \omega_b, a_s, h_b)$ *around every "smooth" trajectory, i.e when* $\dot{\eta}_0$, $\dot{I}_a$, *and* I_ω *are first order terms.*

We insist that it is not usually obvious to come up with a similar convergence result for an EKF. The gains $l_V, l_B, m_V, m_h, n_X, n_h, o_V, o_B, r_V, r_h, s_h$ are also easy to tune, since the behaviors of each subsystem are independent. Moreover, the lateral, longitudinal and vertical subsystems do not depend on the magnetic measurements, so will not be affected if the magnetic field is perturbed.

4.2.4.4. Influence of magnetic disturbances on static behavior. — We now investigate how the equilibrium point $(1,0,0,0,1,0)$ is modified when the magnetic field is (statically) perturbed. We show that only the yaw angle ψ is affected while all the other variables, in particular the attitude angles ϕ, θ, remain unchanged. Here the Euler angles ϕ, θ, ψ correspond to the error quaternion $\tilde{\eta}$ in the new frame described by Equations (129)-(130).

The equilibrium points $(\overline{\tilde{\eta}}, \overline{\tilde{\nu}}, \overline{\tilde{\chi}}, \overline{\tilde{\omega}}, \overline{\tilde{\alpha}}, \overline{\tilde{\lambda}})$ are defined by

$$\begin{aligned}
(l_V kA \times \overline{\tilde{\nu}} + l_B \langle \tilde{B} \times \tilde{E}_B, kA \rangle kA) * \overline{\tilde{\eta}} - \frac{1}{2} \overline{\tilde{\eta}} * \overline{\tilde{\omega}} = 0 \\
-kA + \overline{\alpha} \overline{\tilde{\eta}}^{-1} * kA * \overline{\tilde{\eta}} - m_V \overline{\tilde{\nu}} - m_h (\langle \overline{\tilde{\chi}}, e_3' \rangle - \overline{\lambda}) e_3' = 0 \\
\overline{\tilde{\nu}} - n_X \overline{\tilde{\chi}} - n_h (\langle \overline{\tilde{\chi}}, e_3' \rangle - \overline{\lambda}) e_3' = 0 \\
\overline{\tilde{\eta}}^{-1} * (-o_V kA \times \overline{\tilde{\nu}} - o_B \langle \tilde{B} \times \tilde{E}_B, kA \rangle kA) * \overline{\tilde{\eta}} + (\overline{\tilde{\eta}}^{-1} * \overline{\tilde{I}}_\omega * \overline{\tilde{\eta}}) \times \overline{\tilde{\omega}} = 0 \\
r_V \langle kA, \overline{\tilde{\nu}} \rangle \overline{\alpha} - r_h (\langle \overline{\tilde{\chi}}, e_3' \rangle - \overline{\lambda}) = 0 \\
s_h (\langle \overline{\tilde{\chi}}, e_3' \rangle - \overline{\lambda}) = 0.
\end{aligned}$$

We ensure $\overline{\tilde{\omega}} = 0$ by choosing $L_V E_V + L_B E_B$ colinear with $O_V E_V + O_B E_B$, that is $\frac{o_V}{l_V} = \frac{o_B}{l_B} \triangleq \sigma$. This implies $\overline{\tilde{\nu}} = 0$, $\overline{\alpha} \overline{\tilde{\eta}} * A * \overline{\tilde{\eta}}^{-1} - A = 0$, $\langle \tilde{B} \times \tilde{E}_B, kA \rangle = 0$, $\langle \overline{\tilde{\chi}}, e_3' \rangle - \overline{\lambda} = 0$ and $\overline{\tilde{\chi}} = 0$.

Finally, the new equilibrium points is $(\overline{\tilde{\eta}}, \overline{\tilde{\nu}}, \overline{\tilde{\chi}}, \overline{\tilde{\omega}}, \overline{\alpha}, \overline{\lambda}) = (\overline{\tilde{\eta}}, 0, 0, 0, 1, 0)$; moreover $\overline{\phi} = \overline{\theta} = 0$ and $\overline{\psi}$ is determined by $\langle \tilde{B} \times \tilde{E}_B, kA \rangle = 0$, where the Euler angles $\overline{\phi}, \overline{\theta}, \overline{\psi}$ correspond to the error quaternion $\overline{\tilde{\eta}}$.

4.2.5. Simulation results. — We first illustrate on simulation the behavior of the invariant observer

$$\dot{\hat{q}} = \frac{1}{2} \hat{q} * (\omega_m - \omega_b) + (L_V E_V + L_X E_X + L_h E_h + L_B E_B) * \hat{q} + \varepsilon (1 - \|\hat{q}\|^2) \hat{q} \tag{131}$$

$$\dot{\hat{V}} = A + \frac{1}{\hat{a}_s} \hat{q} * a_m * \hat{q}^{-1} + (M_V E_V + M_X E_X + M_h E_h + M_B E_B) \tag{132}$$

$$\dot{\hat{X}} = \hat{V} + (N_V E_V + N_X E_X + N_h E_h + N_B E_B) \tag{133}$$

$$\dot{\hat{\omega}}_b = \hat{q}^{-1} * (O_V E_V + O_X E_X + O_h E_h + O_B E_B) * \hat{q} \tag{134}$$

$$\dot{\hat{a}}_s = \hat{a}_s (R_V E_V + R_X E_X + R_h E_h + R_B E_B) \tag{135}$$

$$\dot{\hat{h}}_b = (S_V E_V + S_X E_X + S_h E_h + S_B E_B). \tag{136}$$

with the choice of gain matrices described in §4.2.4.1.

We choose here time constants around 10s by taking $l_V = o_V = 4e-2$, $l_B = o_B = 1e-3$, $m_V = 5$, $m_h = 0.2$, $r_V = 1e-2$, $r_h = 8e-4$, $n_X = 0.8$, $n_h = 0.9$, $s_h = 0.4$ and $\varepsilon = 1$. The system follows the trajectory defined by

$$a_s = 1.1 \quad \text{and} \quad h_b = 1 \qquad\qquad \omega_b = \begin{pmatrix} 0.01 \\ -0.012 \\ 0.08 \end{pmatrix}$$

$$V = \begin{pmatrix} 3 - 4\cos(0.23t) \\ 3 - 5.6\cos(0.25t + \pi/4) \\ -1 - 3.4\sin(.02t) \end{pmatrix} \qquad \omega_m = \begin{pmatrix} \sin(0.5t + \pi/5) \\ \sin(0.3t + \pi/4) \\ -\sin(0.2t + \pi/3) \end{pmatrix},$$

in SI units, which is quite representative of a small UAV flight. The states are initialized far from their true values. At $t = 35s$, the magnetic field is changed from $B = (1\ 0\ 1)^T$ to $B = (0.7\ 0.7\ 0.8)^T$.

Though we have no proof of convergence but local, the domain of attraction seems to be large enough, see Figure 4.5. As expected, only the estimated yaw angle ψ is strongly affected by the magnetic disturbance. Because of the coupling terms $\tilde{I}_{\omega_m}$ and I_a, there is some dynamic influence on the other variables.

4.2.6. Experimental results. — We now compare the behavior of our observer with the commercial INS-GPS device MIDG II from Microbotics Inc. For each experiment we first save the raw measurements from the MIDG II gyroscopes, accelerometers and magnetic sensors (at a 50Hz refresh rate), the position and velocity provided by the navigation solutions of its GPS engine (at a 5 Hz refresh rate) and the raw measurements from a barometer module Intersema MS5534B (at a 12.5 Hz refresh rate). A microcontroller on a development kit communicates with these devices and sends the measurements to a computer via the serial port (see Figure 4.6). On Matlab Simulink we feed the observer with these data offline and then compare the estimations of the observer to the estimations given by the MIDG II. In order to have similar behaviors and considering the units of the raw measurements provided by the MIDG II, we have chosen $l_V = 2.8e-5$,$l_B = 1.4e-6$, $m_V = 9e-3$, $m_h = 5e-4$, $n_X = 1e-3$, $n_h = 5e-2$, $o_V = 4e-7$, $o_B = 2e-8$, $r_V = 9.4e-11$, $r_h = 1e-9$, $s_h = 5e-3$ and $\varepsilon = 1$.

4.2.6.1. Dynamic behavior (Figure 4.7). — We wait a few minutes until the biases reach constant values, then move the system in all directions. The observer and the MIDG II give very similar results (Figures 4.7(a)–4.7(d)). On Figure 4.7(d) it is in fact $h_b + 148m$ which is represented to plot a_s and h_b on the same axis. We can also notice on Figure 4.7(b)

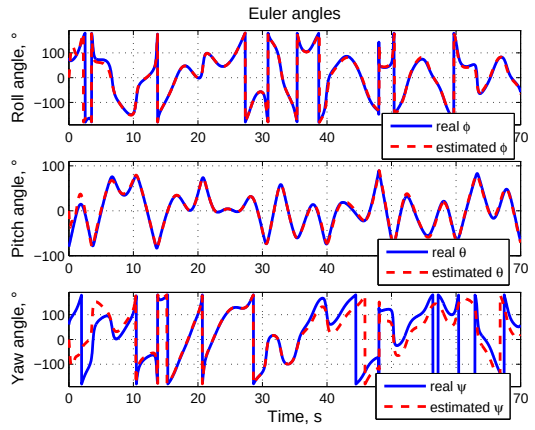

(a) Estimated Euler angles

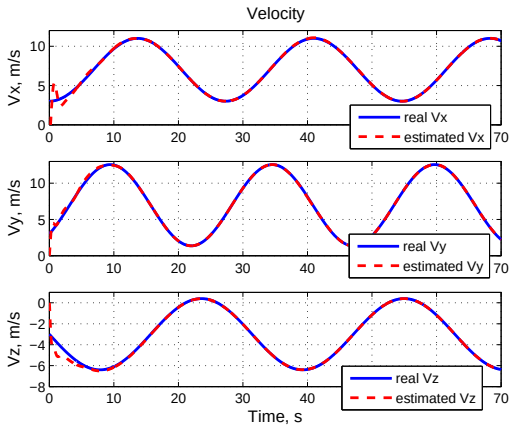

(b) Estimated velocity

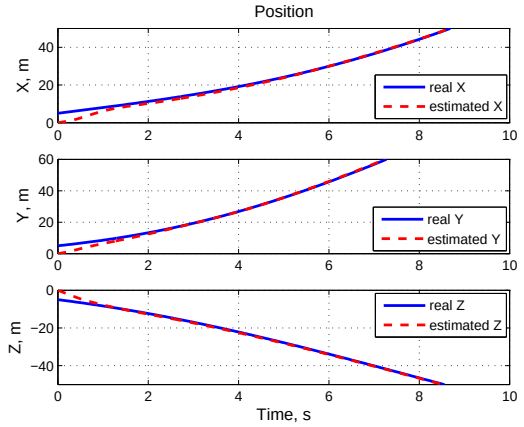

(c) Estimated position

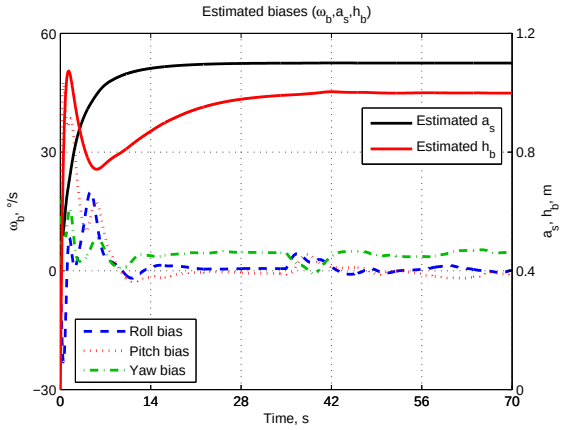

(d) Estimated biases

FIGURE 4.5. Observer validation (simulation)

that the estimation of V_Z given by our observer seems to be closer to the true value than the estimation provided by the MIDG II: we know that we leave the system motionless at $t = 42s$, which is coherent with our estimated V_Z.

4.2.6.2. Usefulness of the observer correction terms (Figure 4.8). — As explained in §4.2.4.1 we have chosen the correction terms so that:

– the magnetic measurements correct essentially the yaw angle and its corresponding bias, i.e. the heading subsystem

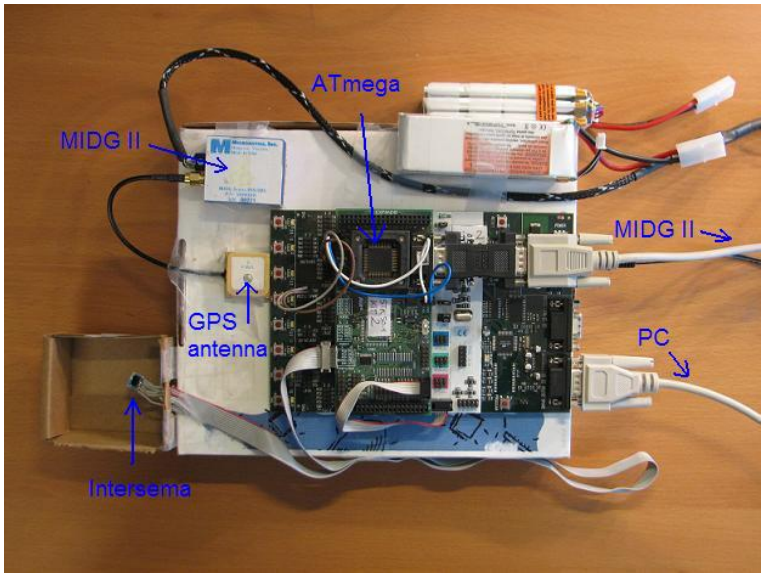

FIGURE 4.6. Experimental protocol

– the GPS measurements correct essentially the horizontal and vertical subsystems
– the barometric measurements correct essentially the vertical subsystem.

We highlight this property as well as the importance of correction terms with the following experiment. Once the biases have reached constant values, the system is left at rest during 50 minutes:

– for $t < 500s$ the results are very similar for the observer and the MIDG II (Figure 4.8).
– at $t = 500s$ the "magnetic correction terms" are switched off, i.e. the gains l_B and o_B are set to 0. The yaw angle estimated by the observer diverges because the corresponding bias is not perfectly estimated. Indeed, these variables are not observable without the magnetic measurements. The other variables are not affected (Figure 4.8).
– at $t = 1250s$ the "GPS correction terms" are also switched off, i.e. l_V,m_V,n_X,o_V and r_V are set to 0. We consider also that h_b is constant since there is no GPS measurements to correct its estimation. The estimated angles, velocities and positions of the attitude subsystem now diverge too. Zooming around $t = 1250s$, we see on Figure 4.8(d) that the estimated pitch angle diverges with a slope corresponding to the almost-constant difference between the estimated and actual pitch angular rate biases. This explains why the estimated velocity V_X diverges quadratically in time.

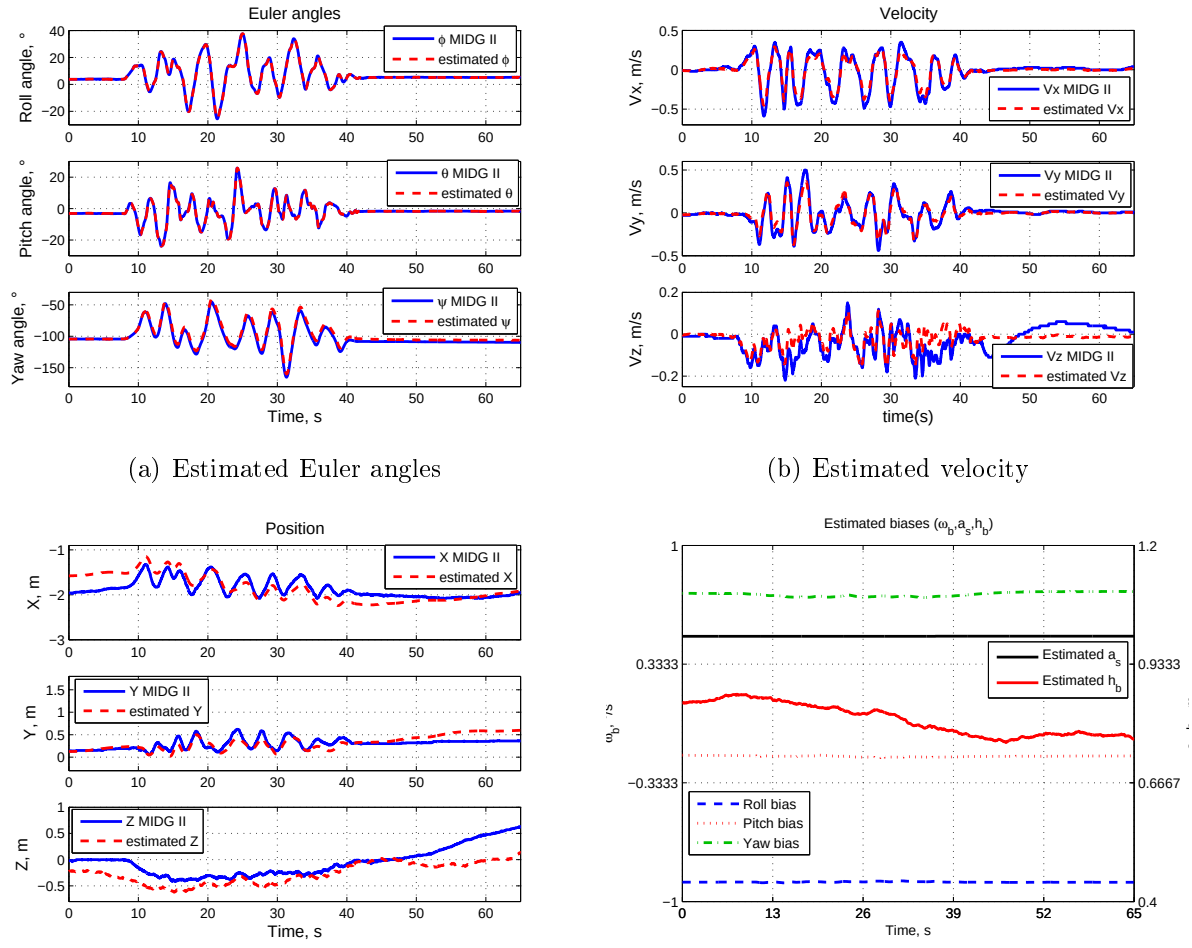

(a) Estimated Euler angles

(b) Estimated velocity

(c) Estimated position

(d) Estimated biases

FIGURE 4.7. Dynamic behavior (experiment)

– at $t = 2100s$ the "barometric correction terms" are also switched off, i.e. m_h,n_h,r_h and s_h are set to 0. All the estimated angles, velocities and positions now diverge (Figure 4.8).

4.2.6.3. Influence of magnetic disturbances (Figure 4.9). — Once the biases have reached constant values, the system is left motionless for $60s$. At $t = 16s$ a magnet is put close to the sensors for $10s$. As expected only the estimated yaw angle is affected by the magnetic disturbance (Figure 4.9); the MIDG II exhibits a similar behavior. For the experiments

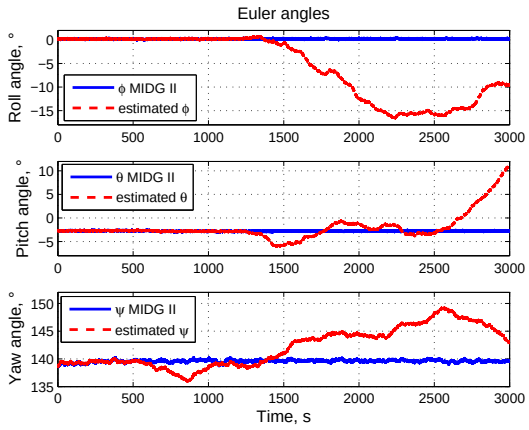

(a) Estimated Euler angles

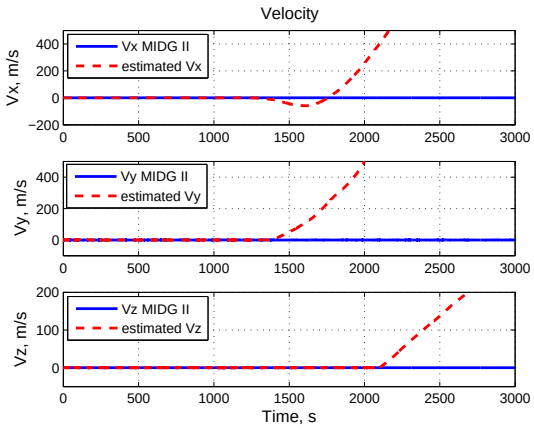

(b) Estimated velocity

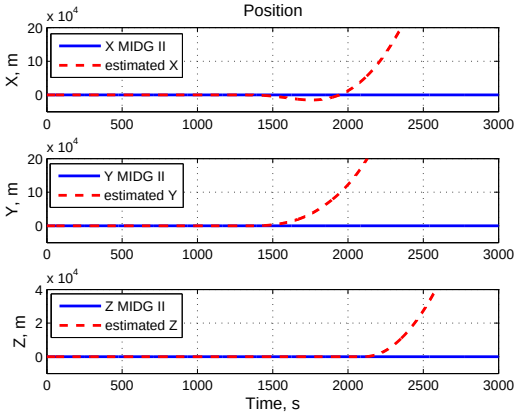

(c) Estimated position

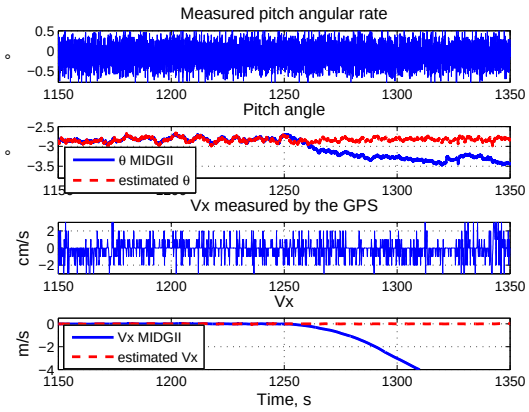

(d) Zoomed view at $t = 1250s$

FIGURE 4.8. Usefulness of correction terms (experiment)

related to Figures 4.9(a)–4.9(c) we used the constant gain values detailed above. We notice that the yaw angle estimated by our algorithm is more affected by the disturbance than the estimation provided by the MIDG II. Indeed the values of the observer gains are constant whatever the magnetic field is. If the norm of the magnetic measurements change, which means that there is some magnetic disturbance, we would like this to affect the gain values of the magnetic correction terms. A first possibility is to consider the gains l_B,o_B divided by $\|y_B\|^2$, supposing $\|y_B\|^2 \neq 0$. This gain scheduling scheme has

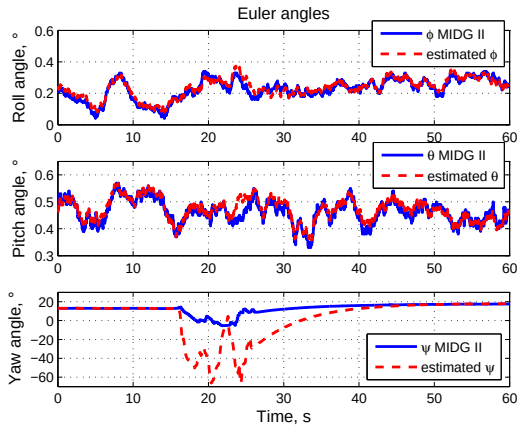

(a) Estimated Euler angles

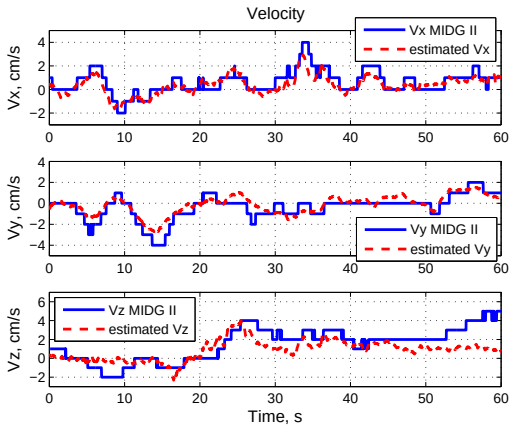

(b) Estimated velocity

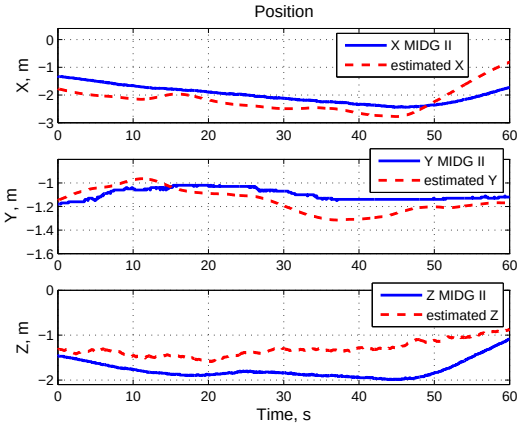

(c) Estimated position

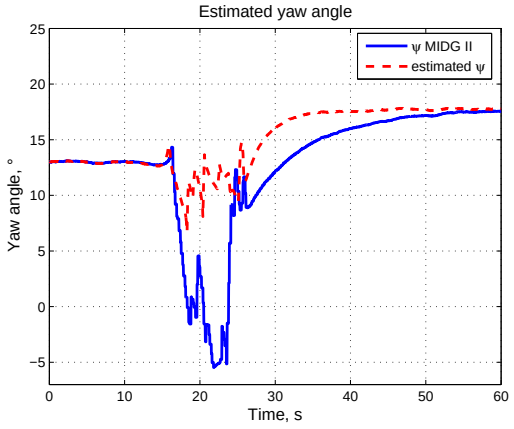

(d) Estimated yaw angle with adapted magnetic gains

FIGURE 4.9. Magnetic disturbances (experiment)

been implemented, and we see on Figure 4.9(d) that the estimated yaw angle is really less disturbed, and is now close to the estimation given by the MIDG II.

4.3. General invariant observer for aided AHRS

4.3.1. The considered system. — We now consider body-fixed and Earth-fixed velocity measurements (provided, for instance, by a GPS engine and an air-data system)

and altitude measurement (provided, for instance, by a barometric module). We therefore consider the following system, described in details in section 2.4

$$\dot{q} = \frac{1}{2} q * (\omega_m - \omega_b) \tag{137}$$

$$\dot{v} = v \times (\omega_m - \omega_b) + q^{-1} * A * q + a \tag{138}$$

$$\dot{h} = \langle q * v * q^{-1}, e_3 \rangle \tag{139}$$

$$\dot{\omega}_b = 0 \tag{140}$$

where ω_m and a are seen as known inputs, together with the output

$$\begin{pmatrix} y_v \\ y_V \\ y_B \\ y_h \end{pmatrix} = \begin{pmatrix} v \\ q * v * q^{-1} \\ q^{-1} * B * q \\ h \end{pmatrix}. \tag{141}$$

4.3.1.1. Invariance of the system equations. — We consider the following transformation group generated by constant rotations and translation in the body-fixed and Earth-fixed frames

$$\varphi_{(p_0,q_0,h_0,\omega_0)} \begin{pmatrix} q \\ v \\ h \\ \omega_b \end{pmatrix} = \begin{pmatrix} p_0 * q * q_0 \\ q_0^{-1} * v * q_0 \\ h + h_0 \\ q_0^{-1} * \omega_b * q_0 + \omega_0 \end{pmatrix} = \begin{pmatrix} \tilde{q} \\ \tilde{v} \\ \tilde{h} \\ \tilde{\omega}_b \end{pmatrix}$$

$$\psi_{(p_0,q_0,h_0,\omega_0)} \begin{pmatrix} \omega_m \\ a \\ A \\ B \end{pmatrix} = \begin{pmatrix} q_0^{-1} * \omega_m * q_0 + \omega_0 \\ q_0^{-1} * a * q_0 \\ p_0 * A * p_0^{-1} \\ p_0 * B * p_0^{-1} \end{pmatrix} = \begin{pmatrix} \tilde{\omega}_m \\ \tilde{a} \\ \tilde{A} \\ \tilde{B} \end{pmatrix}$$

$$\rho_{(p_0,q_0,h_0,\omega_0)} \begin{pmatrix} y_v \\ y_V \\ y_B \\ y_h \end{pmatrix} = \begin{pmatrix} q_0^{-1} * y_v * q_0 \\ p_0 * y_V * p_0^{-1} \\ q_0^{-1} * y_B * q_0 \\ y_h + h_0 \end{pmatrix} = \begin{pmatrix} \tilde{y}_v \\ \tilde{y}_V \\ \tilde{y}_B \\ \tilde{y}_h \end{pmatrix}.$$

There are $3+3+1+3=10$ parameters: the two unit quaternions p_0 and q_0, the scalar h_0 and the $\mathbb{R}^3$-vector ω_0. The group law $\diamond$ is given by

$$\begin{pmatrix} p_1 \\ q_1 \\ h_1 \\ \omega_1 \end{pmatrix} \diamond \begin{pmatrix} p_0 \\ q_0 \\ h_0 \\ \omega_0 \end{pmatrix} = \begin{pmatrix} p_1 * p_0 \\ q_0 * q_1 \\ h_1 + h_0 \\ q_1^{-1} * \omega_0 * q_1 + \omega_1 \end{pmatrix}.$$

The system (137)–(140) is of course invariant by the transformation group since

$$\begin{aligned}
\dot{\tilde{q}} &= p_0 * \dot{q} * q_0 = p_0 * (\frac{1}{2} q * \omega) * q_0 = \frac{1}{2}(p_0 * q * q_0) * (q_0^{-1} * \omega * q_0) = \frac{1}{2}\tilde{q} * \tilde{\omega} \\
\dot{\tilde{v}} &= q_0^{-1} * \dot{v} * q_0 \\
&= (q_0^{-1} * v * q_0) \times (q_0^{-1} * \omega * q_0) + q_0^{-1} * a * q_0 + (p_0 * q * q_0)^{-1} * (p_0 * A * p_0^{-1}) * (p_0 * q * q_0) \\
&= \tilde{v} \times \tilde{\omega} + \tilde{q}^{-1} * \tilde{A} * \tilde{q} + \tilde{a} \\
\dot{\tilde{h}} &= \dot{h} = \langle q * v * q^{-1}, e_3 \rangle = \langle \tilde{q} * \tilde{v} * \tilde{q}^{-1}, \tilde{e}_3 \rangle \\
\dot{\tilde{\omega}}_b &= q_0^{-1} * \dot{\omega}_b * q_0 = 0,
\end{aligned}$$

whereas the output (141) is equivariant since

$$\begin{pmatrix} \tilde{v} \\ \tilde{q} * \tilde{v} * \tilde{q}^{-1} \\ \tilde{q}^{-1} * \tilde{B} * \tilde{q} \\ \tilde{h} \end{pmatrix} = \rho_{(p_0,q_0,h_0,\omega_0)} \begin{pmatrix} v \\ q * v * q^{-1} \\ q^{-1} * B * q \\ h \end{pmatrix}.$$

4.3.2. Construction of the general invariant observer. — We solve for $(p_0, q_0, h_0, \omega_0)$ the normalization equations

$$\begin{aligned}
p_0 * q * q_0 &= 1 \\
p_0 * e_i * p_0^{-1} &= \tilde{e}_i \quad \text{with} \quad i = 1,2,3 \\
h + h_0 &= 0 \\
q_0^{-1} * \omega_b * q_0 + \omega_0 &= 0
\end{aligned} \tag{142}$$

where $(\tilde{e}_1, \tilde{e}_2, \tilde{e}_3)$ defines a new orthonormal frame. The moving frame $\gamma(q, h, \omega_b, e_1, e_2, e_3)$ is then defined by

$$\begin{aligned} q_0 &= q^{-1} * p_0^{-1} \\ h_0 &= -h \\ \omega_0 &= -p_0 * q * \omega_b * q^{-1} * p_0^{-1} \end{aligned}$$

where p_0 represents the rotation between the two frames (e_1, e_2, e_3) and $(\tilde{e}_1, \tilde{e}_2, \tilde{e}_3)$. We generalize the construction in [**12**] since we normalize not only with respect to φ but also with respect to ψ.

We can then find the 10 scalar invariant errors which correspond to the projections of the output error

$$\rho_{\gamma(\hat{q},\hat{h},\hat{\omega}_b,e_1,e_2,e_3)} \begin{pmatrix} \hat{y}_v \\ \hat{y}_V \\ \hat{y}_B \end{pmatrix} - \rho_{\gamma(\hat{q},\hat{h},\hat{\omega}_b,e_1,e_2,e_3)} \begin{pmatrix} y_v \\ y_V \\ y_B \end{pmatrix}$$

on the new frame $(\tilde{e}_1, \tilde{e}_2, \tilde{e}_3)$ and to the output error for y_h which is invariant. We get

$$\begin{aligned} E_{vi} &= \langle \hat{q} * (\hat{y}_v - y_v) * \hat{q}^{-1}, e_i \rangle \\ E_{Vi} &= \langle \hat{y}_V - y_V, e_i \rangle \\ E_{Bi} &= \langle B - \hat{q} * y_B * \hat{q}^{-1}, e_i \rangle \\ E_h &= \hat{h} - h, \end{aligned}$$

where $i = 1, 2, 3$. We detail how to get E_{vi}:

$$\begin{aligned} \langle \rho_{\gamma(\hat{q},\hat{h},\hat{\omega}_b,e_1,e_2,e_3)} \left(\hat{y}_v\right) - \rho_{\gamma(\hat{q},\hat{h},\hat{\omega}_b,e_1,e_2,e_3)} \left(y_v\right), \tilde{e}_i \rangle & \\ = \langle p_0 * \hat{q} * \hat{y}_v * \hat{q}^{-1} * p_0^{-1} - p_0 * \hat{q} * y_v * \hat{q}^{-1} * p_0^{-1}, \tilde{e}_i \rangle & \\ = \langle \hat{q} * \hat{y}_v * \hat{q}^{-1} - \hat{q} * y_v * \hat{q}^{-1}, p_0^{-1} * \tilde{e}_i * p_0 \rangle & \\ = \langle \hat{q} * (\hat{y}_v - y_v) * \hat{q}^{-1}, e_i \rangle. & \end{aligned}$$

We get also the 9 scalar complete invariants which correspond to the projections of

$$\phi_{\gamma(\hat{q},\hat{v},\hat{\omega}_b,e_1,e_2,e_3)} \left(\hat{v}\right) \quad \text{and} \quad \psi_{\gamma(\hat{q},\hat{v},\hat{\omega}_b,e_1,e_2,e_3)} \begin{pmatrix} \omega_m \\ a \end{pmatrix}$$

on the new frame $(\tilde{e}_1, \tilde{e}_2, \tilde{e}_3)$. We find

$$\begin{aligned} I_{\hat{v}i} &= \langle \hat{q} * \hat{v} * \hat{q}^{-1}, e_i \rangle \\ I_{\omega i} &= \langle \hat{q} * (\omega_m - \hat{\omega}_b) * \hat{q}^{-1}, e_i \rangle \\ I_{ai} &= \langle \hat{q} * a * \hat{q}^{-1}, e_i \rangle \qquad \text{where} \qquad i = 1, 2, 3. \end{aligned}$$

Notice that $I_{\hat{v}i}$, $I_{\omega i}$, I_{ai}, E_{vi}, E_{Vi}, E_{Bi}'s and E_h are functions of the estimates and the measurements. Hence they are known quantities which can be used in the construction of the observer. It is straightforward to check they are indeed invariant. For instance,

$$\begin{aligned} \langle \hat{q} * \hat{v} * \hat{q}^{-1}, e_i \rangle &= \langle p_0 * \hat{q} * \hat{v} * \hat{q}^{-1} * p_0^{-1}, p_0 * e_i * p_0^{-1} \rangle \\ &= \langle (p_0 * \hat{q} * q_0) * (q_0^{-1} * \hat{v} * q_0) * (p_0 * \hat{q} * q_0)^{-1}, \tilde{e}_i \rangle. \end{aligned}$$

To find invariant vector fields, we solve for $w(q, v, h, \omega_b)$ the 10 vector equations

$$\left[D\varphi_{\gamma(q,v,\omega_b,e_1,e_2,e_3)} \begin{pmatrix} q \\ v \\ h \\ \omega_b \end{pmatrix} \right] \cdot w(q, v, h, \omega_b) = \begin{pmatrix} \tilde{e}_i \\ 0 \\ 0 \\ 0 \end{pmatrix}, \begin{pmatrix} 0 \\ \tilde{e}_i \\ 0 \\ 0 \end{pmatrix}, \begin{pmatrix} 0 \\ 0 \\ e_7 \\ 0 \end{pmatrix}, \begin{pmatrix} 0 \\ 0 \\ 0 \\ \tilde{e}_i \end{pmatrix} \qquad i = 1, 2, 3.$$

Since

$$\left[D\varphi_{(p_0,q_0,h_0,\omega_0)} \begin{pmatrix} q \\ v \\ h \\ \omega_b \end{pmatrix} \right] \cdot \begin{pmatrix} \delta q \\ \delta v \\ \delta h \\ \delta \omega_b \end{pmatrix} = \begin{pmatrix} p_0 * \delta q * q_0 \\ q_0^{-1} * \delta v * q_0 \\ \delta h \\ q_0^{-1} * \delta \omega_b * q_0 \end{pmatrix},$$

this yields the 10 independent invariant vector fields $(i = 1, 2, 3)$

$$\begin{pmatrix} e_i * q \\ 0 \\ 0 \\ 0 \end{pmatrix}, \begin{pmatrix} 0 \\ q^{-1} * e_i * q \\ 0 \\ 0 \end{pmatrix}, \begin{pmatrix} 0 \\ 0 \\ e_7 \\ 0 \end{pmatrix}, \begin{pmatrix} 0 \\ 0 \\ 0 \\ q^{-1} * e_i * q \end{pmatrix}.$$

Indeed for instance the equations $p_0 * \delta q * q_0 = \tilde{e}_i$ gave us

$$\delta q = p_0^{-1} * \tilde{e}_i * q_0^{-1} = (p_0^{-1} * \tilde{e}_i * p_0) * (q_0 * p_0)^{-1} = e_i * q.$$

It is easy to check that these vector fields are invariant. The general invariant observer then reads

$$\begin{aligned}
\dot{\hat{q}} &= \frac{1}{2}\hat{q} * (\omega_m - \hat{\omega}_b) + \sum_{i=1}^{3}\Big(\sum_{j=1}^{3}(l_{vij}E_{vj} + l_{Vij}E_{Vj} + l_{Bij}E_{Bj}) + l_{hi}E_h\Big)e_i * \hat{q} \\
\dot{\hat{v}} &= \hat{v} \times (\omega_m - \hat{\omega}_b) + \hat{q}^{-1} * A * \hat{q} + a \\
&\quad + \hat{q}^{-1} * \Big(\sum_{i=1}^{3}\Big(\sum_{j=1}^{3}(m_{vij}E_{vj} + m_{Vij}E_{Vj} + m_{Bij}E_{Bj}) + m_{hi}E_h\Big)e_i\Big) * \hat{q} \\
\dot{\hat{h}} &= \langle \hat{q} * \hat{v} * \hat{q}^{-1}, e_3 \rangle + \sum_{j=1}^{3}(n_{vj}E_{vj} + n_{Vj}E_{Vj} + n_{Bj}E_{Bj}) + n_h E_h \\
\dot{\hat{\omega}}_b &= \hat{q}^{-1} * \Big(\sum_{i=1}^{3}\Big(\sum_{j=1}^{3}(o_{vij}E_{vj} + o_{Vij}E_{Vj} + o_{Bij}E_{Bj}) + o_{hi}E_h\Big)e_i\Big) * \hat{q},
\end{aligned}$$

where the l_{vij}, l_{Vij}, l_{Bij}, l_{hi}, m_{vij}, m_{Vij}, m_{Bij}, m_{hi}, n_{vj}, n_{Vj}, n_{Bj}, o_{vij}, o_{Vij}, o_{Bij}, o_{hi}'s and n_h are arbitrary scalars which possibly depend on E_{vi}, E_{Vi}, E_{Bi}, E_h, $I_{\hat{v}i}$, $I_{\omega i}$ and I_{ai}'s. Noticing

$$\sum_{i=1}^{3}\Big(\sum_{j=1}^{3}(l_{vij}E_{vj})\Big)e_i = L_v E_v$$

where $E_v = \hat{q} * (\hat{v} - v) * \hat{q}^{-1}$ and L_v is the 3×3 matrix whose coefficients are the l_{vij}'s, and defining E_V, E_B, L_V, L_B, L_h, M_v, M_V, M_B, M_h, N_v, N_V, N_B, N_h, O_v, O_V, O_B and O_h in the same way, the correction terms can be rewritten with the matrices E, L, M, N and O such as $E = (E_v \; E_V \; E_B \; E_h)^T$ and

$$L_v E_v + L_V E_V + L_B E_B + L_h E_h = LE,$$

and the same notation for M, N and O.

Then we can rewrite the observer as

$$\dot{\hat{q}} = \frac{1}{2}\hat{q} * (\omega_m - \omega_b) + (LE) * \hat{q} \tag{143}$$

$$\dot{\hat{v}} = \hat{v} \times (\omega_m - \omega_b) + \hat{q}^{-1} * A * \hat{q} + a + \hat{q}^{-1} * (ME) * \hat{q} \tag{144}$$

$$\dot{\hat{h}} = \langle \hat{q} * \hat{v} * \hat{q}^{-1}, e_3 \rangle + (NE) \tag{145}$$

$$\dot{\hat{\omega}}_b = \hat{q}^{-1} * (OE) * \hat{q}. \tag{146}$$

The observer is indeed invariant by considering the projection of the output errors E_v, E_V and E_B on the frame (e_1, e_2, e_3). As in section 4.1.3, the norm of $\hat{q}$ is left unchanged by Equation (143).

4.3.3. The invariant error system. — The state error is given by

$$\begin{aligned}\begin{pmatrix}\eta\\ \nu\\ \lambda\\ \beta\end{pmatrix} &= \varphi_{\gamma(q,v,\omega_b,e_1,e_2,e_3)}\begin{pmatrix}\hat{q}\\ \hat{v}\\ \hat{h}\\ \hat{\omega}_b\end{pmatrix} - \varphi_{\gamma(q,v,\omega_b,e_1,e_2,e_3)}\begin{pmatrix}q\\ v\\ h\\ \omega_b\end{pmatrix}\\ &= \begin{pmatrix}\hat{q}*q^{-1}-1\\ q*(\hat{v}-v)*q^{-1}\\ \hat{h}-h\\ q*(\hat{\omega}_b-\omega_b)*q^{-1}\end{pmatrix}.\end{aligned}$$

As in Section 4.1.3, we take $\eta = \hat{q} * q^{-1}$. As we did above, it can be easily checked that λ and the projections of η, ν and β on the frame (e_1, e_2, e_3) are invariant. Hence for $(i, j) = 1, 2, 3$,

$$\begin{aligned}\dot{\overbrace{\langle \eta * e_i * \eta^{-1}, e_j\rangle}} &= \langle \dot{\eta} * e_i * \eta^{-1} - \eta * e_i * \eta^{-1} * \dot{\eta} * \eta^{-1}, e_j\rangle\\ &= 2\langle(-\frac{1}{2}\eta * \beta * \eta^{-1}) \times (\eta * e_i * \eta^{-1}), e_j\rangle + 2\langle (LE) \times (\eta * e_i * \eta^{-1}), e_j\rangle\\ \langle \dot{\nu}, e_i\rangle &= \langle (\eta^{-1} * I_{\hat{v}} * \eta) \times \beta + \eta^{-1} * A * \eta - A, e_i\rangle + \langle \eta^{-1} * (ME) * \eta, e_i\rangle\\ \dot{\lambda} = \dot{\hat{h}} - \dot{h} &= \langle I_{\hat{v}} - \eta^{-1} * I_{\hat{v}} * \eta - \eta^{-1} * \nu * \eta, e_3\rangle + (NE)\\ \langle \dot{\beta}, e_i\rangle &= \langle (\eta^{-1} * I_\omega * \eta) \times \beta + \eta^{-1} * (OE) * \eta, e_i\rangle.\end{aligned}$$

Since we can write

$$\begin{aligned} E_v &= \eta * \nu * \eta^{-1} & E_V &= I_{\hat{v}} - \eta^{-1} * I_{\hat{v}} * \eta + \nu\\ E_B &= B - \eta * B * \eta^{-1} & E_h &= \lambda,\end{aligned}$$

we find as expected that the error system

$$\overdot{\eta * e_i * \eta^{-1}} = 2(-\frac{1}{2}\eta * \beta * \eta^{-1}) \times (\eta * e_i * \eta^{-1}) + 2(LE) \times (\eta * e_i * \eta^{-1}) \tag{147}$$

$$\dot{\nu} = (\eta^{-1} * I_{\hat{v}} * \eta) \times \beta + \eta^{-1} * A * \eta - A + \eta^{-1} * (ME) * \eta \tag{148}$$

$$\dot{\lambda} = \langle I_{\hat{v}} - \eta^{-1} * I_{\hat{v}} * \eta - \eta^{-1} * \nu * \eta, e_3 \rangle + (NE) \tag{149}$$

$$\dot{\beta} = (\eta^{-1} * I_{\omega} * \eta) \times \beta + \eta^{-1} * (OE) * \eta \tag{150}$$

depends only on the invariant state error $(\eta, \nu, \lambda, \beta)$ and the "free" known invariants $I_{\hat{v}}$ and I_{ω}, but not on the trajectory of the observed system (137)–(140). The error system (147)–(150) is invariant by considering the projection of the equations (147),(148) and (150) on the frame (e_1, e_2, e_3).

The linearized error system around $(\overline{\eta}, \overline{\nu}, \overline{\lambda}, \overline{\beta}) = (1, 0, 0, 0)$, i.e. the estimated state equals the actual state, is given by

$$\delta\dot{\eta} = -\frac{1}{2}\delta\beta + (L\delta E) \tag{151}$$

$$\delta\dot{\nu} = I_{\hat{v}} \times \delta\beta + 2A \times \delta\eta + (M\delta E) \tag{152}$$

$$\delta\dot{\lambda} = \langle -I_{\hat{v}} \times \delta\eta - \delta\nu, e_3 \rangle + (N\delta E) \tag{153}$$

$$\delta\dot{\beta} = I_{\omega} \times \beta + (O\delta E), \tag{154}$$

where

$$\delta E_v = \delta\nu \qquad \delta E_V = \delta\nu - 2I_{\hat{v}} \times \delta\nu$$
$$\delta E_B = 2B \times \delta\eta \qquad \delta E_h = \delta\lambda.$$

We notice that the normalization equation (142) led us to consider the velocity error ν in the Earth-fixed frame. Instead, choosing $q_0^{-1} * e_i * q_0 = \tilde{e}_i$ would lead us to a velocity error $\tilde{\nu} = \hat{v} - v$ in the body-fixed frame which seems more "natural" since Equation (138) is written in body-fixed coordinates. But in this case, the output error δE_B would become $\delta\tilde{E}_B = 2(\hat{q}^{-1} * B * \hat{q}) \times \delta\nu$; so the error system, and its convergence behavior, would depend on the trajectory $\hat{q}(t)$.

4.3.4. Design of the observer gain matrices. — Up to now, we have only investigated the structure of the observer. We now must choose the gain matrices L_v, L_V, L_B, L_h, M_v, M_V, M_B, M_h, N_v, N_V, N_B, N_h, O_v, O_V, O_B, O_h to meet the following requirements *locally around any trajectory*:

– at a low velocity “normal" flight, which is common for UAVs in an urban area, i.e. $I_{\hat{v}}$ and I_ω are first order terms: the error must converge to zero and its behavior should be easily tunable; the magnetic measurements should not affect the attitude, velocity and altitude estimations, but only the heading
– at a level flight, i.e. $I_{\hat{v}} = V_1 e_1 + V_2 e_2 + \delta V_3 e_3$ where V_1, V_2 are constant and $I_\omega, \delta V_3$ are first order terms, the behavior of the roll angle error towards the direction of $I_{\hat{v}}$, which is the most important estimation for a flight control, should not be affected by V_1,V_2,δV_3 and any magnetic disturbance.

Therefore we choose

$$\begin{aligned}
L_v E_v &= l_v A \times E_v & L_V E_V &= l_V A \times E_V \\
L_B E_B &= l_B \langle B \times E_B, A \rangle A & & \\
M_v E_v &= -m_v E_v & M_V E_V &= -m_V E_V \\
N_h E_h &= -n_h E_h & & \\
O_v E_v &= -o_v A \times E_v & O_V E_V &= -o_V A \times E_V \\
O_B E_B &= -o_B \langle B \times E_B, A \rangle A & &
\end{aligned}$$

with $(l_v, l_V, l_B, m_v, m_V, n_h, o_v, o_V, o_B) > 0$ and the other matrices equal to 0. At a low velocity “non-aggressive” flight, the error system (151)–(154) splits into three decoupled subsystems and two cascaded subsystems:

– the longitudinal subsystem

$$\begin{pmatrix} \delta\dot{\eta}_2 \\ \delta\dot{\nu}_1 \\ \delta\dot{\beta}_2 \end{pmatrix} = \begin{pmatrix} 0 & g*(l_v + l_V) & -\frac{1}{2} \\ -2g & -(m_v + m_V) & 0 \\ 0 & -(o_v + o_V) & 0 \end{pmatrix} \begin{pmatrix} \delta\eta_2 \\ \delta\nu_1 \\ \delta\beta_2 \end{pmatrix}$$

– the lateral subsystem

$$\begin{pmatrix} \delta\dot{\eta}_1 \\ \delta\dot{\nu}_2 \\ \delta\dot{\beta}_1 \end{pmatrix} = \begin{pmatrix} 0 & -g*(l_v + l_V) & -\frac{1}{2} \\ 2g & -(m_v + m_V) & 0 \\ 0 & o_v + o_V & 0 \end{pmatrix} \begin{pmatrix} \delta\eta_1 \\ \delta\nu_2 \\ \delta\beta_1 \end{pmatrix}$$

– the vertical subsystem

$$\delta\dot{\nu}_3 = -(m_v + m_V)\delta\nu_3$$

– the heading subsystem

$$\begin{pmatrix} \delta\dot{\eta}_3 \\ \delta\dot{\beta}_3 \end{pmatrix} = \begin{pmatrix} -2gB_1^2 l_B & -\frac{1}{2} \\ 2gB_1^2 o_B & 0 \end{pmatrix} \begin{pmatrix} \delta\eta_3 \\ \delta\beta_3 \end{pmatrix} + \begin{pmatrix} 2gB_1 B_3 l_B \\ -2gB_1 B_3 o_B \end{pmatrix} \delta\eta_1$$

– the altitude subsystem

$$\delta\dot{\lambda} = -n_h\delta\lambda - \delta\nu_3.$$

Thanks to this decoupled structure, the tuning of the gains $l_v, l_V, l_B, m_v, m_V, n_h, o_v, o_V, o_B$ and the local convergence of the invariant observer are straightforward. Obviously the lateral, longitudinal, vertical and altitude subsystems do not depend on the magnetic measurements, so will not be affected if the magnetic field is perturbed. As in Section 4.2.4.3, we can also prove that the choice of matrices meets the preceding requirements during a level flight, and leads to Theorem 4.

Theorem 4. — *Consider the physical system* (137)–(140) *with the measurements* (141). *Consider the nonlinear invariant observer defined by*

$$\begin{aligned}
\dot{\hat{q}} &= \frac{1}{2}\hat{q} * (\omega_m - \omega_b) + (LE) * \hat{q} \\
\dot{\hat{v}} &= \hat{v} \times (\omega_m - \omega_b) + \hat{q}^{-1} * A * \hat{q} + a + \hat{q}^{-1} * (ME) * \hat{q} \\
\dot{\hat{h}} &= \langle \hat{q} * \hat{v} * \hat{q}^{-1}, e_3 \rangle + (NE) \\
\dot{\hat{\omega}}_b &= \hat{q}^{-1} * (OE) * \hat{q},
\end{aligned}$$

with the expression of the output errors given in Section (4.3.2) *and the gain matrices given in Section 4.3.4. Then for any value* $(l_v, l_V, l_B, m_v, m_V, n_h, o_v, o_V, o_B) > 0$, *the solution* $(\hat{q}(t), \hat{v}(t), \hat{h}(t), \hat{\omega}_b(t))$ *locally asymptotically converges to* $(q(t), v(t), h(t), \omega_b)$ *around every trajectory during low velocity "normal" flight or during level flight, as previously defined.*

4.3.5. Simulation results. — We first illustrate the behavior of the invariant observer by means of a simulation

$$\begin{aligned}
\dot{\hat{q}} &= \frac{1}{2}\hat{q} * (\omega_m - \hat{\omega}_b) + (LE) * \hat{q} + \alpha(1 - \|\hat{q}\|^2)\hat{q} \\
\dot{\hat{v}} &= \hat{v} \times (\omega_m - \hat{\omega}_b) + \hat{q}^{-1} * A * \hat{q} + a + \hat{q}^{-1} * (ME) * \hat{q} \\
\dot{\hat{h}} &= \langle \hat{q} * \hat{v} * \hat{q}^{-1}, e_3 \rangle + (NE) \\
\dot{\hat{\omega}}_b &= \hat{q}^{-1} * (OE) * \hat{q}
\end{aligned}$$

with the choice of gain matrices described in section 4.3.4.

We choose here time constants around 20s by taking $l_v = l_V = 1e-2$, $l_B = 5.2e-3$, $m_v = m_V = 2.4$, $n_h = 1$, $o_v = o_V = 5.3e-3$, $o_B = 2.8e-3$ and $\alpha = 1$. The system follows

the trajectory defined by

$$a = \begin{pmatrix} .4g * \sin(t) \\ .4g * \sin(.5t + pi/4) \\ -g - .4g\cos(.5t) \end{pmatrix},\ \omega = \begin{pmatrix} .5\sin(.5t) \\ .9\sin(.3t) \\ -.5\sin(.25t) \end{pmatrix} \text{ and } \omega_b = \begin{pmatrix} .01 \\ .008 \\ -.01 \end{pmatrix},$$

which is representative of a small UAV flight. We see on Figure 4.10 the results of the following experiment:

- for $t < 40s$ the observer converges well. Though we have no proof of convergence but local, the domain of attraction seems to be large enough since the states are initialized far from their true values and the system moves quite fast
- at $t = 40s$ the "GPS correction terms" are switched off, i.e. the gains l_V, m_V and o_V are set to 0. The observer still behaves well
- at $t = 60s$ the magnetic field is changed from $B = (1\ 0\ 1)^T$ to $B = (0.5\ \ -0.8\ 0.7)^T$. As expected, only the estimated yaw angle ψ is strongly affected by the magnetic disturbance. Because of the coupling terms $I_{\hat{v}}$ and I_{ω_m}, there is some dynamic influence on the other variables as well.

4.3.6. Experimental results. — The experimental setup does not possess yet measurements from an air-data system, so we will use only Earth-fixed velocity, inertial and magnetic measurements provided by the commercial INS-GPS device MIDG II from Microbotics Inc and altitude measurements given by the barometer module Intersema MS5534B. We use the same experimental protocol as in section 4.2.5 (see Figure 4.6). Considering the units of the raw measurements provided by the MIDG II, we have chosen $l_V = 2.8e-5$, $l_B = 1.4e-6$, $m_V = 9e-3$, $n_h = 5e-2$, $o_V = 4e-7$, $o_B = 2e-8$ and $\alpha = 1$ and we have initialized the altitude measurement to 0 at the beginning of the experiment.

4.3.6.1. Dynamic behavior (Figure 4.11). — We wait a few minutes until the biases reach constant values, then move the system in all directions and orientations. The observer and the MIDG II give very similar results (Figure 4.11). To do comparison in the same frame we compare the Earth velocity provided by the MIDG II and $\hat{V} = \hat{q} * \hat{v} * \hat{q}^{-1}$ given by our observer. We can notice that the estimation of V_z given by our observer seems to be closer to the true value than the estimation provided by the MIDG II: we know that the system was motionless at $t = 42s$, which is coherent with our estimated $\hat{V}_z$.

4.3.6.2. Influence of magnetic disturbances (Figure 4.12). — Once the biases have reached constant values, the system is left motionless for $60s$. At $t = 72s$ a magnet is put close

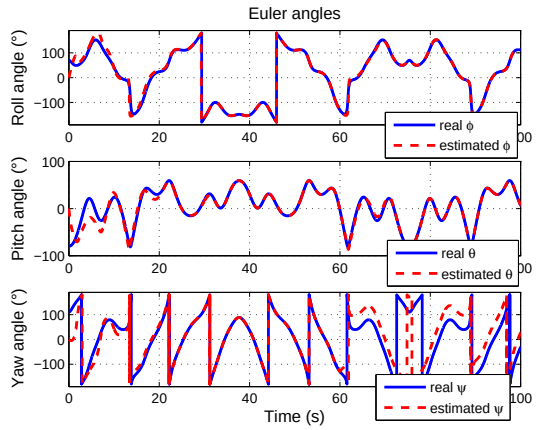

(a) Estimated Euler angles

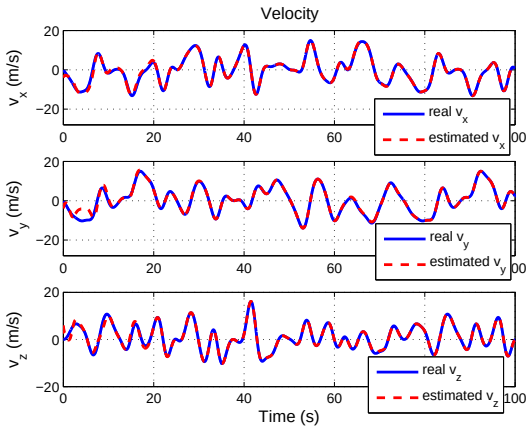

(b) Estimated velocity

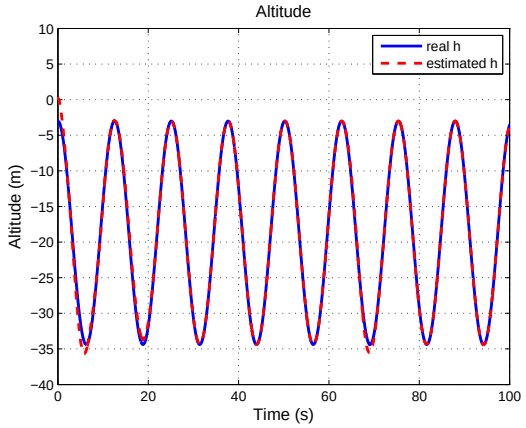

(c) Estimated altitude

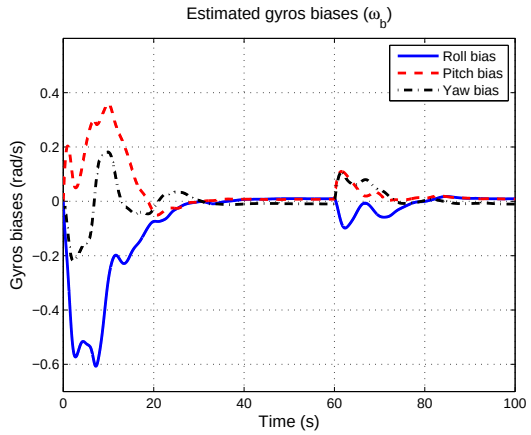

(d) Estimated biases

FIGURE 4.10. Observer validation (simulation)

to the sensors for 10s. As expected the estimated roll and pitch angles, longitudinal and lateral velocities are not affected by the magnetic disturbance (Figures 4.12(a)–4.12(b)); the MIDG II exhibits a similar behavior. However we notice that the yaw angle estimated by our algorithm is much more affected by the disturbance that the estimation provided by the MIDG II. And thus the estimated vertical velocity and altitude are also perturbed (Figures 4.12(a)–4.12(c)). Indeed for the experiments related to Figures 4.12(a)–4.12(c) we used the gain values detailed above, which are constant whatever the norm of the magnetic field is. Similarly to Section 4.2.6, we consider the gains l_B and o_B divided by $\|y_B\|^2$,

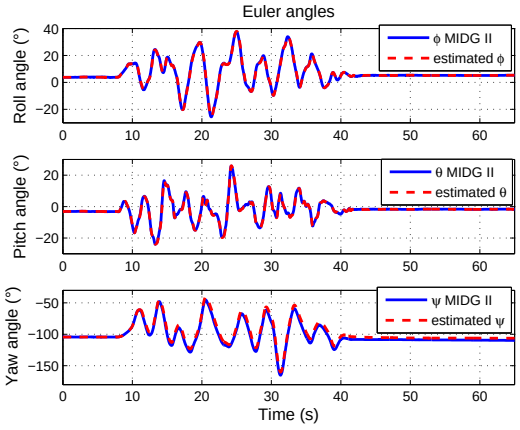

(a) Estimated Euler angles

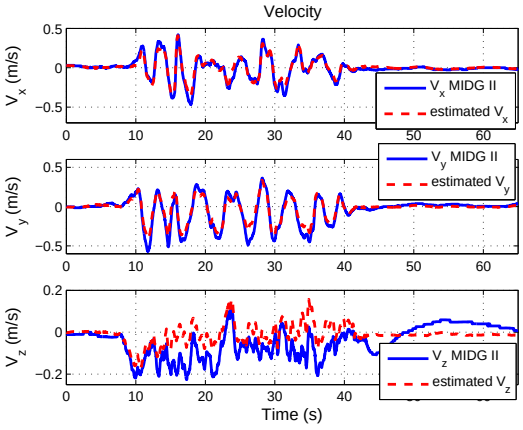

(b) Estimated velocity

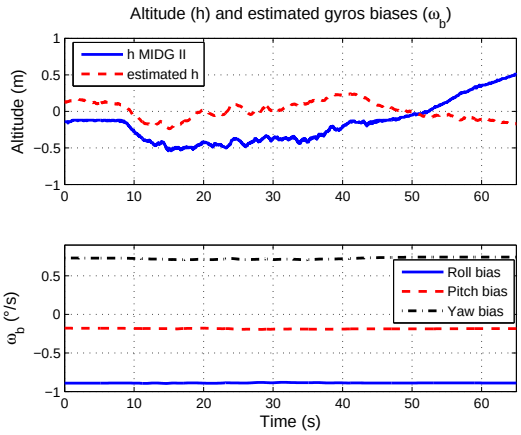

(c) Estimated altitude and biases

FIGURE 4.11. Dynamic behavior (experiment)

supposing $\|y_B\| \neq 0$, in order to bypass this limitation. This gain scheduling scheme has been implemented and we see on Figure 4.12(d) that the estimated vertical velocity, altitude and yaw angle are really less disturbed, and are now close to the estimations given by the MIDG II.

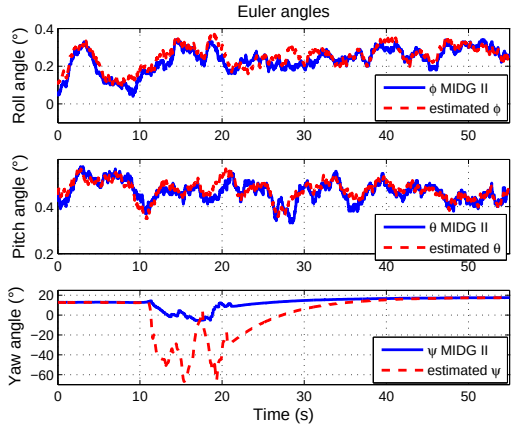

(a) Estimated Euler angles

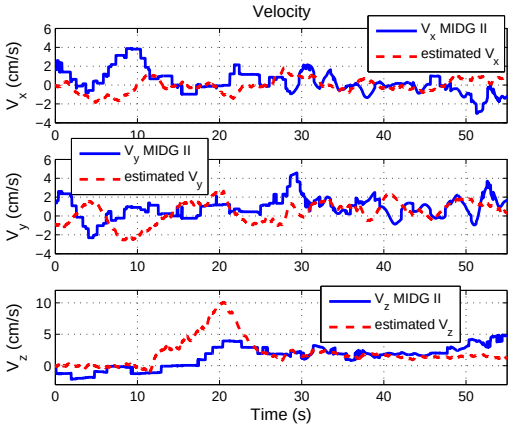

(b) Estimated velocity

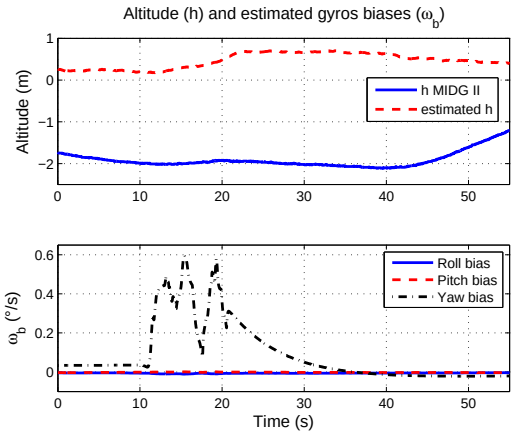

(c) Estimated altitude and biases

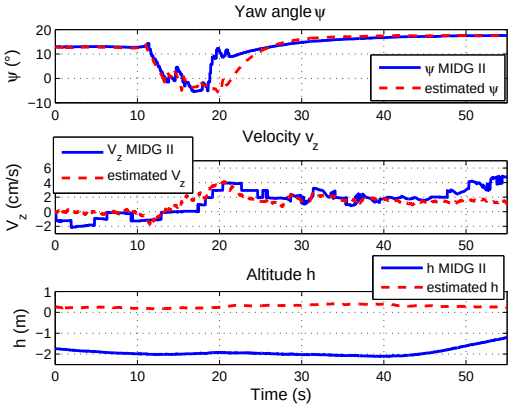

(d) Adapted gains

FIGURE 4.12. Influence of magnetic disturbances (experiment)

CHAPTER 5

INVARIANT KALMAN FILTER

Dans ce chapitre nous proposons une nouvelle version du filtre de Kalman étendu, l'"Invariant Extended Kalman Filter", qui tient compte des symétries naturelles du système dans la construction de ses termes de correction. Les matrices de gains et de covariance de ce filtre convergent vers des constantes pour un large éventail de trajectoires, permettant alors d'espérer une meilleure estimation de l'état qu'en utilisant un filtre de Kalman étendu. Nous illustrons l'intérêt de ce filtre en l'appliquant à un "aided Attitude and Heading Reference System".

5.1. Introduction

In the EKF, the system is seen as a stochastic differential equation,

$$\dot{x} = f(x,u) + Mw \tag{155}$$

$$y = h(x,u) + Nv, \tag{156}$$

where x, u, y belong to an open subset of $\mathbb{R}^n \times \mathbb{R}^m \times \mathbb{R}^p$; w, v are independent white gaussian noises of size n and p with unit power spectral density, and M, N are square

matrices. The input u and output y are known signals, and the state x must be estimated. An estimation $\hat{x}(t)$ of $x(t)$ is then computed by the EKF

$$\begin{aligned}\dot{\hat{x}} &= f(\hat{x},u) + K\big(y - h(\hat{x},u)\big)\\ \dot{P} &= AP + PA^T + MM^T - PC^T(NN^T)^{-1}CP,\end{aligned}$$

with $K = PC^T(NN^T)^{-1}$, $A = \partial_1 f(\hat{x},u)$ and $C = \partial_1 h(\hat{x},u)$ (∂_i means the partial derivative with respect to the i^{th} argument). The rationale is to compute the gain K as in a linear Kalman filter since the estimation error $\Delta x = \hat{x} - x$ satisfies the linear equation $\Delta\dot{x} = (A - KC)\Delta x$ up to first-order terms. Of course the convergence of the EKF is not guaranteed in general as in the linear case, see e.g. [**78**] for some (local) convergence results.

Another drawback of this "linear" approach is that it does not respect the geometry of the problem when (part of) the state space is a manifold. This situation frequently arises e.g. in the context of aerospace engineering, where the attitude of an aircraft is usually represented by a unit quaternion rather than Euler angles; ad hoc modifications of the EKF are then used, in particular the so-called Multiplicative EKF (MEKF) introduced in [**77, 49, 58**].

We propose a modification of the EKF for nonlinear systems that possess symmetries. Instead of using a linear correction term based on a linear output error, the proposed filter uses a geometrically adapted correction term based on an invariant output error; in the same way the gain matrix is not updated from of a linear state error, but from an invariant state error. For that to make sense from a stochastic point of view, we assume the driving and observation noise enter the system in an invariant way. As for the generic observers we developed in the preceding chapters, this "Invariant EKF" (IEKF) builds on the ideas developed in [**12, 13, 9**], see also [**56, 46, 52**] for related approaches. More generally it adds to the several attempts to introduce geometry in the problem of nonlinear filtering, see e.g. [**18, 57, 45**].

The main benefit of the IEKF is that the matrices A and C are constant on a much larger set of trajectories (so-called "permanent trajectories" [**13**]) than equilibrium points as is the case for the EKF. Near such trajectories, we are back to the "true", i.e. linear, Kalman filter where convergence is guaranteed. Informally, this means the IEKF should in general converge at least around any slowly-varying permanent trajectory, rather than just around any slowly-varying equilibrium point for the EKF.

We then apply the IEKF to the practically relevant problem of estimating the velocity and attitude of a moving rigid body, e.g. an aircraft, from velocity, inertial and magnetic

measurements. We design two different versions (Left and Right IEKF), which can be seen as extensions of the MEKF. Finally we present experimental and simulation results.

5.2. System with symmetries and Gaussian noises

Consider the system

$$\dot{x} = f(x,u) + M(x)w \tag{157}$$

$$y = h(x,u) + N(x)v \tag{158}$$

where $x \in \mathcal{X}$ an n-dimensional manifold, $u \in \mathcal{U} = \mathbb{R}^m$, $y \in \mathcal{Y} = \mathbb{R}^p$, and w, v are independent white gaussian noises.

The definitions recalled in Chapter 1.4 can be easily adapted to the system (157)–(158) by assuming the noise is turned off. Then, with the notations given in Section 1.4, the system (157)-(158) with noise turned off is left-invariant with equivariant output if for all $g \in G$ it is unaffected by the transformation that changes (u,x,y) into (U,X,Y): $\frac{d}{dt}X(t) = f(X,U), Y = h(X,U)$. We also want the driving noise w and observation noise v to preserve invariance and extend the definitions of recalled in Chapter 1.4.

Definition. — *Consider the change of variables* $X = \varphi_g(x)$, $U = \psi_g(u)$ *and* $Y = \rho_g(y)$.*The system with noise* (157)-(158) *is* invariant *with* equivariant *output and* invariant *noises if for all* g, x, u,

$$f\big(\varphi_g(x), \psi_g(u)\big) + M\big(\varphi_g(x)\big)w = D\varphi_g(x) \cdot \big(f(x,u) + M(x)w\big)$$
$$h\big(\varphi_g(x), \psi_g(u)\big) + N\big(\varphi_g(x)\big)v = \rho_g\big(h(x,u) + N(x)v\big),$$

i.e. if the system (157)-(158) *is unaffected by the considered transformation*

$$\dot{X} = f(X,U) + M(X)w$$
$$Y = h(X,U) + N(X)v.$$

Moreover, we assume ρ_g is linear for all g (which is the case in many examples), so that $\rho_g(y_1 + y_2) = \rho_g(y_1) + \rho_g(y_2)$ for all g, y_1, y_2.

5.3. Invariant Extended Kalman Filter

For simplicity we restrict to the case where the dimension of the group is $r = n$, and the action is free and effective, so that $\mathcal{X}$ can be identified with G (up to a discrete group action). Then $G = \mathcal{X}$ by left translation $L_g(x) = gx$, i.e. $\varphi_g(x) = L_g(x) = gx$.

An invariant driving noise then reads $DL_x\ M(e)w$, and an invariant output noise reads $D\rho_x\ N(e)v$. since $DL_g M(x) = M(L_g(x))$

5.3.1. A symmetry-preserving observer. — As recalled in Chapter 1.4, a symmetry-preserving observer reads (see **[12]** for details)

$$\dot{\hat{x}} = f(\hat{x}, u) + DL_{\hat{x}} K\big(\rho_{\hat{x}^{-1}}(y) - \rho_{\hat{x}^{-1}}(h(\hat{x}, u))\big),$$

where K is a gain which only depends on the invariant $\hat{I}(\hat{x}, u) = \psi_{\hat{x}^{-1}}(u)$.

5.3.1.1. Error equation. — Instead of the usual state error $\Delta x = \hat{x} - x$, we use the invariant error $\eta = x^{-1}\hat{x}$. We then have

$$\begin{aligned}\dot{\eta} = {} & DL_\eta f(e, \psi_{\eta^{-1}}(\hat{I})) - DR_\eta(f(e, \hat{I}) + M(e)w) \\ & + DL_\eta K[h(\eta^{-1}, \psi_{\eta^{-1}}(\hat{I})) - h(e, \psi_{\eta^{-1}}(\hat{I})) + N(\eta^{-1})v]\end{aligned}$$

where R_η denotes the right multiplication by η. A remarkable feature is this equation only depends on the trajectory via the invariant term $\hat{I}$.

This leads to define a new class of trajectories, so-called "permanent trajectories". They are characterized by the fact that $I(x, u)$ is constant over these trajectories. Thus, for a class of trajectories which can be large, the nonlinear error equation above becomes completely autonomous, which reminds the linear stationary case.

5.3.1.2. Linearized error equation. — For a small error, i.e. η close to e, the first order approximation of the error equation reads

$$\begin{aligned}\dot{\xi} = {} & [\xi, f(e, \psi_{x^{-1}}(u))] - \frac{\partial f}{\partial u}(e, \psi_{x^{-1}}(u))\frac{\partial \psi}{\partial g}(e, \psi_{x^{-1}}(u))\xi - M(e)w - r(\xi)M(e)w \\ & - K\frac{\partial h}{\partial x}(e, \psi_{x^{-1}}(u))\xi + l(\xi)KN(e)v + K\big(N(e)v - d(\xi)N(e)v\big),\end{aligned} \tag{159}$$

where $[\ ,\ ]$ is the Lie bracket of the Lie algebra of G,l, r and d are the derivative at e of DL, DR and $D\rho$: $l(\xi) = \frac{d}{ds}DL_{exp(s\xi)}$, $r(\xi) = \frac{d}{ds}DR_{exp(s\xi)}$ and $d(\xi) = \frac{d}{ds}D\rho_{exp(s\xi)}$, see **[13]** for details.

5.3.2. Equations of the Invariant Extended Kalman Filter. — The Invariant EKF then reads

$$\begin{aligned}\dot{\hat{x}} &= f(\hat{x}, u) + DL_{\hat{x}} K\big(\rho_{\hat{x}^{-1}}(y) - \rho_{\hat{x}^{-1}}(h(\hat{x}, u))\big) \\ K &= PC^T(NN^T)^{-1} \\ \dot{P} &= AP + PA^T + MM^T - PC^T(NN^T)^{-1}CP\end{aligned}$$

where

$$A(\hat{I}):\ \xi \mapsto [\xi, f(e,\hat{I})] - \frac{\partial f}{\partial u}(e,\hat{I})\frac{\partial \psi}{\partial g}(e,\hat{I})\xi$$
$$C = Dh(e,I), \qquad M = M(e), \qquad N = N(e).$$

It relies on the same ideas as the usual EKF, but instead of using a linear correction term based on a linear output error, it uses a geometrically adapted correction term based on an invariant output error; in the same way the gain matrix is not updated from of a linear state error, but from an invariant state error.

There is nevertheless a slight problem with the linearized invariant error equation (159), because of the quadratic terms of the type $r(\xi)M(e)w$ which do not appear in the usual linearized equation of the EKF

$$\frac{d}{dt}\xi = (A - KC)\xi - Mw + KNv. \tag{160}$$

Instead, here the linearized error equation is rather a multiplicative inhomogeneous equation of the form

$$\frac{d}{dt}\xi = A_0(t)\xi + \alpha W_1(t) + \alpha W_2(t)\xi \tag{161}$$

rather than of the form

$$\frac{d}{dt}\zeta = A_0(t)\zeta + \alpha W_1(t). \tag{162}$$

W_1 and W_2 are time-varying matrices, with entries being linear scalar functions of the white mutually independent noises w and v (thus $\langle W_1 \rangle = \langle W_2 \rangle = 0$), and α is a parameter measuring the magnitude of the noises. Linear multiplicative stochastic equations are standard in physics and chemistry, but unlike the linear inhomogeneous equations of the form (162) (as the Langevin equation) it can only be solved in special cases. Nevertheless, a rather general approach is based on approximations, since the true solution is written in the form of a series expansion in powers of α [**83**].

We are going to prove that the average and covariance matrix of the solution of (161) are solutions to order α^2 of the non-stochastic differential equations verified by the average and the covariance of the solution of Equation (162). Then: if the observer made for Equation (160) is robust, the expectation of ξ (verifying Equation (159)) will also tend to 0 when $t \to \infty$; and the covariance matrix of the solution of Equation (160) will be an approximation of the covariance of the solution of the true linearized equation (159). This argument is standard in mathematical physics, since multiplicative noise generally yields a shift of order α^2. For instance, the criterion for energy of the damped random frequency

oscillator with frequency $\omega_0^2(1+\alpha w(t))$ to tend to zero is that the damping coefficient, instead of being only strictly positive, is bounded from below by a linear function of α^2 (see [**83**]).

According to [**83**] (p403, rigourously proved a few pages later) we see we have for the solution of Equation (161)

$$\frac{d}{dt}\langle\xi(t)\rangle = [A_0(t) + \alpha\langle W_2(t)\rangle + \alpha^2\langle W_2(t)^2\rangle]\langle\xi(t)\rangle + \alpha^2\langle W_1(t)W_2(t)\rangle + O(\alpha^3)$$

and thus, as $\langle W_2(t)\rangle = 0$, the mean values $\langle\xi\rangle$ and $\langle\zeta\rangle$ obey to the same equation up to terms of order α^2. Still using [**83**] p404 we also see that the covariances obey the same differential equations up to terms of order α^2, once again because the $\alpha\langle W_2\rangle$ term vanishes.

5.4. Considered system

We now apply the IEKF to the aided AHRS problem, with velocity, inertial and magnetic measurements from low-cost sensors. We therefore consider the system presented in 4.1, i.e.

$$\dot{q} = \frac{1}{2}q * (\omega_m - \omega_b) \tag{163}$$

$$\dot{V} = A + \frac{1}{a_s}q * a_m * q^{-1} \tag{164}$$

$$\dot{\omega}_b = 0 \tag{165}$$

$$\dot{a}_s = 0, \tag{166}$$

where ω_m and a_m are seen as known inputs, together with the output

$$\begin{pmatrix} y_V \\ y_B \end{pmatrix} = \begin{pmatrix} V \\ q^{-1} * B * q \end{pmatrix}. \tag{167}$$

It is reasonable to assume each scalar sensor is corrupted by an additive gaussian white noise with identical variance for each of the three scalar sensors constituting a triaxial sensor, and all the noises are mutually independent (this is technologically motivated for the accelerometers, gyroscopes and magnetic sensors, though much more questionable for the GPS engine). Hence we can see each triaxial sensor as corrupted by a "coordinate-free vector noise" whose coordinates are gaussian in the body frame as well as the Earth frame (or any other smooth time-varying frame). Indeed, the mean and the auto-correlation time of such a noise is not affected by a (smoothly) time-varying rotation.

5.5. Multiplicative Extended Kalman Filter

We begin with the design of a Multiplicative EKF (MEKF) in the spirit of [**77, 49, 58**] (see also [**41, 8**]), in order to compare the structure and the properties of an IEKF with the "well-known" MEKF. The idea is to respect the geometry of the quaternion space, by using for the quaternion estimation a multiplicative correction term $\hat{q} * K_q E$ which preserves the unit norm, and by computing the error equation with the error $q^{-1} * \hat{q}$ (or equivalently $\hat{q}^{-1} * q = (q^{-1} * \hat{q})^{-1}$). Notice the standard linear correction term does not preserve the norm, hence some projection would be needed, whereas the standard linear error $\hat{q} - q$ does not really make sense for quaternions.

We assume the noise enters the system as

$$\dot{q} = \frac{1}{2} q * (\omega_m - \omega_b) + q * M_q w_q \tag{168}$$

$$\dot{V} = A + \frac{1}{a_s} q * a_m * q^{-1} + q * M_V w_V * q^{-1} \tag{169}$$

$$\dot{\omega}_b = M_\omega w_\omega \tag{170}$$

$$\dot{a}_s = M_a w_a, \tag{171}$$

and the output as

$$\begin{pmatrix} y_V \\ y_B \end{pmatrix} = \begin{pmatrix} V + N_V v_V \\ q^{-1} * B * q + N_B v_B \end{pmatrix}, \tag{172}$$

with $M_q, M_V, M_\omega, N_V, N_B$ diagonal matrices. The driving and observation noises are thus consistent with a scalar additive noise on each individual sensor. The term $q * M_q w_q$ preserves the norm of the quaternion.

The MEKF then takes the form

$$\dot{\hat{q}} = \frac{1}{2} \hat{q} * (\omega_m - \hat{\omega}_b) + \hat{q} * K_q E \tag{173}$$

$$\dot{\hat{V}} = A + \frac{1}{\hat{a}_s} \hat{q} * a_m * \hat{q}^{-1} + K_V E \tag{174}$$

$$\dot{\hat{\omega}}_b = K_\omega E \tag{175}$$

$$\dot{\hat{a}}_s = K_a E. \tag{176}$$

where the output error is given by

$$E = \begin{pmatrix} \hat{y}_V - y_V \\ \hat{y}_B - y_B \end{pmatrix} = \begin{pmatrix} \hat{V} - V - N_V v_V \\ \hat{q}^{-1} * B * \hat{q} - y_B - N_B v_B \end{pmatrix}.$$

We consider the state error $\mu = q^{-1} * \hat{q}$, $\nu = \hat{V} - V$, $\beta = \hat{\omega}_b - \omega_b$ and $\alpha = \hat{a}_s - a_s$. A tedious but simple computation yields the error system

$$\begin{aligned}
\dot{\mu} &= -\frac{1}{2}\beta * \mu + \mu \times \hat{J}_\omega - M_q w_q * \mu + \mu * K_q E \\
\dot{\nu} &= \hat{I}_a - \frac{1}{\hat{a}_s - \alpha}\hat{q}\mu * a_m * \mu^{-1} * \hat{q}^{-1} - \mu * \hat{q} * M_V w_V * \hat{q}^{-1} * \mu^{-1} + K_V E \\
\dot{\beta} &= K_\omega E - M_\omega w_\omega \\
\dot{\alpha} &= \alpha K_a E - \alpha M_a w_a,
\end{aligned}$$

where the output error is rewritten as

$$E = \begin{pmatrix} \nu - N_V v_V \\ \hat{J}_B - \mu^{-1} * \hat{J}_B * \mu - N_B v_B \end{pmatrix},$$

and $\hat{J}_\omega = \omega_m - \hat{\omega}_b$, $\hat{I}_a = \frac{1}{\hat{a}_s}\hat{q} * a_m * \hat{q}^{-1}$ and $\hat{J}_B = \hat{q}^{-1} * B * \hat{q}$.

We next linearize this error system around $(\overline{\mu}, \overline{\nu}, \overline{\beta}, \overline{\alpha}) = (1, 0, 0, 0)$, drop all the quadratic terms in noise and infinitesimal state error according to the approximation in section 5.3.2, and eventually find

$$\begin{pmatrix} \delta\dot{\mu} \\ \delta\dot{\nu} \\ \delta\dot{\beta} \\ \delta\dot{\alpha} \end{pmatrix} = (A - KC) \begin{pmatrix} \delta\mu \\ \delta\nu \\ \delta\beta \\ \delta\alpha \end{pmatrix} - M \begin{pmatrix} w_q \\ w_V \\ w_\omega \\ w_a \end{pmatrix} + KN \begin{pmatrix} v_V \\ v_B \end{pmatrix},$$

which has the desired form of Equation (160) with

$$A = \begin{pmatrix} -\hat{J}_{\omega\times} & 0_{33} & -\frac{1}{2}I_3 & 0_{31} \\ 2\hat{J}_{a\times}R(\hat{q}) & 0_{33} & \hat{J}_{\omega\times} & -\hat{J}_a \\ 0_{33} & 0_{33} & 0_{33} & 0_{31} \\ 0_{31} & 0_{31} & 0_{31} & 0_{31} \end{pmatrix} \qquad C = \begin{pmatrix} 0_{33} & I_3 & 0_{33} & 0_{31} \\ -2\hat{J}_{B_\times} & 0_{33} & 0_{33} & 0_{31} \end{pmatrix}$$

$$M = Diag(M_q, R(\hat{q})M_V, M_\omega, M_a) \qquad N = Diag(N_V, N_B)$$

$$K = -(K_q,\ K_V,\ K_\omega,\ K_a)^T.$$

We have used the matrices $I_\times$ and $R(q)$ defined by $I_\times u = I \times u$ and $R(q)u = q * u * q^{-1}$ for all for $u \in \mathbb{R}^3$.

Features of the MEKF

– Sound geometric structure for the quaternion estimation equation: by construction Equation (178) preserves the unit norm of the estimated quaternion.

– Possible convergence issues of the error equation (and then of the filter) in many situations: indeed, the matrices A and C used for computing the gain matrix K are constant only in level flight, i.e. $\hat{I}_\omega \simeq 0$ and $\hat{I}_a \simeq -A$, because of the trajectory-dependent terms $R(q)$ in A.

5.6. Left Invariant Extended Kalman Filter

We now design a first Invariant Extended Kalman Filter, which can be seen as a generalization and an improvement of the MEKF. It is a direct application of the method presented in section 5.3. It is termed "Left IEKF" (LIEKF) because in the transformation group defined below the quaternion q is multiplied on the left by a constant quaternion p_0.

5.6.1. Problem setting in terms of transformation groups. — We notice the state space is a group for the law given by

$$\begin{pmatrix} p_0 \\ V_0 \\ \omega_0 \\ a_0 \end{pmatrix} \diamond \begin{pmatrix} q \\ V \\ \omega_b \\ a_s \end{pmatrix} = \begin{pmatrix} p_0 * q \\ p_0 * (V + V_0) * p_0^{-1} \\ \omega_b + \omega_0 \\ a_s a_0 \end{pmatrix},$$

and hence acts on itself (the physical meaning is clear: rotation and translation in Earth axes, translation in body axes, and scaling). It also yields the transformation groups

$$\psi_{(p_0,V_0,\omega_0,a_0)} \begin{pmatrix} \omega_m \\ a_m \\ A \\ B \end{pmatrix} = \begin{pmatrix} \omega_m + \omega_0 \\ a_0 a_m \\ p_0 * A * p_0^{-1} \\ p_0 * B * p_0^{-1} \end{pmatrix}$$

$$\rho_{(p_0,V_0,\omega_0,a_0)} \begin{pmatrix} y_V \\ y_B \end{pmatrix} = \begin{pmatrix} p_0 * (y_V + V_0) * p_0^{-1} \\ y_B \end{pmatrix}.$$

The system (163)–(166) is clearly invariant, for instance

$$\dot{\overbrace{p_0 * q}} = p_0 * \dot{q} = \frac{1}{2}(p_0 * q) * \big((\omega_m + \omega_0) - (\omega_b + \omega_0)\big),$$

whereas the output (167) is equivariant since

$$\begin{pmatrix} p_0 * (V + V_0) * p_0^{-1} \\ (p_0 * q)^{-1} * (p_0 * B * p_0^{-1}) * (p_0 * q) \end{pmatrix} \rho_{(q_0,V_0,\omega_0,a_0)} \begin{pmatrix} V \\ q^{-1} * B * q \end{pmatrix}.$$

The complete set of invariants is given by $\psi_{\hat{x}^{-1}}(u)$, with $\hat{x}^{-1} = (\hat{q}^{-1}, -\hat{V}, -\hat{\omega}_b, \frac{1}{\hat{a}_s})$, hence reads

$$\begin{pmatrix} \hat{J}_\omega \\ \hat{J}_a \\ \hat{J}_A \\ \hat{J}_B \end{pmatrix} = \begin{pmatrix} \omega_m - \hat{\omega}_b \\ \frac{1}{\hat{a}_s} a_m \\ \hat{q}^{-1} * A * \hat{q} \\ \hat{q}^{-1} * B * \hat{q} \end{pmatrix}.$$

Moreover the driving noise as defined in Equations (168)–(171) for the MEKF is also invariant. We finally define an invariant observation noise by

$$\begin{pmatrix} y_V \\ y_B \end{pmatrix} = \begin{pmatrix} V + q * N_V v_V * q^{-1} \\ q^{-1} * B * q + N_B v_B \end{pmatrix}. \tag{177}$$

Notice the noise on y_V is different from the noise in Equation (172), which is not invariant: it is additive in body axes rather than in Earth axes, see section 5.4 for a tentative physical justification.

5.6.2. Left IEKF equations. — We directly follow section 5.3 to derive the structure of the LIEKF and the linearized error equation (160) used to compute the gains. The LIEKF takes the form

$$\dot{\hat{q}} = \frac{1}{2}\hat{q} * (\omega_m - \hat{\omega}_b) + \hat{q} * (K_q E) \tag{178}$$

$$\dot{\hat{V}} = A + \frac{1}{\hat{a}_s}\hat{q} * a_m * \hat{q}^{-1} + \hat{q} * (K_V E) * \hat{q}^{-1} \tag{179}$$

$$\dot{\hat{\omega}}_b = K_\omega E \tag{180}$$

$$\dot{\hat{a}}_s = \hat{a}_s K_a E, \tag{181}$$

where the invariant output error is given by

$$E = \rho_{\hat{x}^{-1}} \begin{pmatrix} \hat{y}_V \\ \hat{y}_B \end{pmatrix} - \rho_{\hat{x}^{-1}} \begin{pmatrix} y_V \\ y_B \end{pmatrix} = \begin{pmatrix} \hat{q}^{-1} * (\hat{V} - y_V) * \hat{q} \\ \hat{q}^{-1} * B * \hat{q} - y_B \end{pmatrix}.$$

Notice Equation (178) and Equation (180) are the same as Equation (173) and Equation (175) in the MEKF, while Equation (179) and Equation (181) are different from Equation (174) and Equation (176).

The invariant state error $x^{-1}\hat{x}$ reads

$$\begin{pmatrix} \mu \\ \nu \\ \beta \\ \alpha \end{pmatrix} = \begin{pmatrix} q^{-1} * \hat{q} \\ q^{-1} * (\hat{V} - V) * q \\ \hat{\omega}_b - \omega_b \\ \frac{\hat{a}_s}{a_s} \end{pmatrix},$$

hence we recover the quaternion error used in the MEKF.

The error system is

$$\begin{aligned} \dot{\mu} &= -\frac{1}{2}\beta * \mu + \mu \times \hat{J}_\omega - M_q w_q * \mu + \mu * K_q E \\ \dot{\nu} &= \mu * \hat{J}_a * \mu^{-1} - \alpha \hat{J}_a + \nu \times (\hat{J}_\omega + \beta) - M_V w_V + 2\nu \times M_q w_q + \mu * K_V E * \mu^{-1} \\ \dot{\beta} &= K_\omega E - M_\omega w_\omega \\ \dot{\alpha} &= \alpha K_a E - \alpha M_a w_a, \end{aligned}$$

where the invariant output error is rewritten as

$$E = \begin{pmatrix} \mu^{-1} * (\nu - N_V v_V) * \mu \\ \hat{J}_B - \mu * \hat{J}_B * \mu^{-1} - N_B v_B \end{pmatrix}.$$

We then linearize this error system around the group identity element $(\overline{\mu}, \overline{\nu}, \overline{\beta}, \overline{\alpha}) = (1, 0, 0, 1)$. We drop all the quadratic terms in noise and infinitesimal state error according to the approximation in section 5.3.2, and eventually find

$$\begin{pmatrix} \delta\dot{\mu} \\ \delta\dot{\nu} \\ \delta\dot{\beta} \\ \delta\dot{\alpha} \end{pmatrix} = (A - KC) \begin{pmatrix} \delta\mu \\ \delta\nu \\ \delta\beta \\ \delta\alpha \end{pmatrix} - M \begin{pmatrix} w_q \\ w_V \\ w_\omega \\ w_a \end{pmatrix} + KN \begin{pmatrix} v_V \\ v_B \end{pmatrix},$$

which has the desired form of Equation (160) with

$$A = \begin{pmatrix} -\hat{J}_{\omega\times} & 0_{33} & -\frac{1}{2}I_3 & 0_{31} \\ -2\hat{J}_{a\times} & 0_{33} & -\hat{J}_{\omega\times} & -\hat{J}_a \\ 0_{33} & 0_{33} & 0_{33} & 0_{31} \\ 0_{31} & 0_{31} & 0_{31} & 0_{31} \end{pmatrix} \qquad C = \begin{pmatrix} 0_{33} & I_3 & 0_{33} & 0_{31} \\ 2\hat{I}_{B\times} & 0_{33} & 0_{33} & 0_{31} \end{pmatrix}$$

$$M = Diag(M_q, M_V, M_\omega, M_a) \qquad N = Diag(N_V, N_B)$$

$$K = -(K_q,\ K_V,\ K_\omega,\ K_a)^T.$$

Features of the LIEKF

- Symmetry-preserving structure: rotations, translations and scaling in the appropriated frames leave the error system unchanged, which is meaningful from an engineering point of view.
- Sound geometric structure for the quaternion estimation equation: by construction Equation (178) preserves the unit norm of the estimated quaternion.
- Larger expected domain of convergence: the matrices A and C used for computing the gain matrix K are constant not only in level flight but also on every permanent trajectory defined by constant $\hat{J}_\omega, \hat{J}_a, \hat{J}_A, \hat{J}_B$. This is a much bigger set of trajectories than for the MEKF, especially if K_q is kept small by choosing a large N_B (little confidence in the magnetic measurements) so that $\hat{J}_B$ does not really matter.

5.7. Right Invariant Extended Kalman Filter

We now design a second Invariant Extended Kalman Filter, with a different transformation group. It is termed "Right IEKF" (RIEKF) because the quaternion q is now multiplied on the right by a constant quaternion q_0.

5.7.1. Problem setting in terms of transformation groups. — The state space is also a group for the law given by

$$\begin{pmatrix} q_0 \\ V_0 \\ \omega_0 \\ a_0 \end{pmatrix} \diamond \begin{pmatrix} q \\ V \\ \omega_b \\ a_s \end{pmatrix} = \begin{pmatrix} q * q_0 \\ V + V_0 \\ q_0^{-1} * \omega_b * q_0 + \omega_0 \\ a_s a_0 \end{pmatrix},$$

hence acts on itself (the physical meaning is now: translation in Earth axes, rotation and translation in body axes, and scaling). It also yields the transformation groups

$$\psi_{(q_0,V_0,\omega_0,a_0)} \begin{pmatrix} \omega_m \\ a_m \end{pmatrix} = \begin{pmatrix} q_0^{-1} * \omega_m * q_0 + \omega_0 \\ a_0 q_0^{-1} * a_m * q_0 \end{pmatrix}$$

$$\rho_{(q_0,V_0,\omega_0,a_0)} \begin{pmatrix} y_V \\ y_B \end{pmatrix} = \begin{pmatrix} y_V + V_0 \\ q_0^{-1} * y_B * q_0 \end{pmatrix}.$$

The system (163)–(166) is invariant and the output (167) is equivariant. The complete set of invariants, given by $\psi_{\hat{x}^{-1}}(u)$ with $\hat{x}^{-1} = (\hat{q}^{-1}, -\hat{V}, -\hat{q} * \hat{\omega}_b * \hat{q}^{-1}, \frac{1}{\hat{a}_s})$, reads

$$\begin{pmatrix} \hat{I}_\omega \\ \hat{I}_a \end{pmatrix} = \begin{pmatrix} \hat{q} * (\omega_m - \hat{\omega}_b) * \hat{q}^{-1} \\ \frac{1}{\hat{a}_s} \hat{q} * a_m * \hat{q}^{-1} \end{pmatrix}.$$

To be invariant the driving noise must enter the system as

$$\dot{q} = \frac{1}{2} q * (\omega_m - \omega_b) + M_q w_q * q \tag{182}$$

$$\dot{V} = A + \frac{1}{a_s} q * a_m * q^{-1} + M_V w_V \tag{183}$$

$$\dot{\omega}_b = q^{-1} * M_\omega w_\omega * q \tag{184}$$

$$\dot{a}_s = a_s M_a w_a, \tag{185}$$

and the observation noise as

$$\begin{pmatrix} y_V \\ y_B \end{pmatrix} = \begin{pmatrix} V + N_V v_V \\ q^{-1} * (B + N_B v_B) * q \end{pmatrix}. \tag{186}$$

The noise configuration used here is “dual" to the one used for the LIEKF, with Earth and body axes exchanged.

5.7.2. Right IEKF equations. — We follow section 5.3 again to derive the structure of the RIEKF and the linearized error equation (160) used to compute the gains. The RIEKF takes the form

$$\dot{\hat{q}} = \frac{1}{2} \hat{q} * (\omega_m - \hat{\omega}_b) + K_q E * \hat{q} \tag{187}$$

$$\dot{\hat{V}} = \frac{1}{\hat{a}_s} \hat{q} * a_m * \hat{q}^{-1} + A + K_V E \tag{188}$$

$$\dot{\hat{\omega}}_b = \hat{q}^{-1} * K_\omega E * \hat{q} \tag{189}$$

$$\dot{\hat{a}}_s = \hat{a}_s K_a E, \tag{190}$$

where the invariant output error is given by

$$E = \rho_{\hat{x}^{-1}} \begin{pmatrix} \hat{y}_V \\ \hat{y}_B \end{pmatrix} - \rho_{\hat{x}^{-1}} \begin{pmatrix} y_V \\ y_B \end{pmatrix} = \begin{pmatrix} \hat{y}_V - y_V \\ B - \hat{q} * y_B * \hat{q}^{-1} \end{pmatrix}.$$

The invariant state error $x^{-1}\hat{x}$ reads

$$\begin{pmatrix} \mu \\ \nu \\ \beta \\ \alpha \end{pmatrix} = \begin{pmatrix} \hat{q} * q^{-1} \\ \hat{V} - V \\ q * (\hat{\omega}_b - \omega_b) * q^{-1} \\ \frac{\hat{a}_s}{a_s} \end{pmatrix}.$$

The error system is

$$\begin{aligned}
\dot{\mu} &= -\frac{1}{2}\mu * \beta - \mu * M_q w_q + K_q E \\
\dot{\nu} &= \hat{I}_a - \alpha\mu^{-1} * \hat{I}_a * \mu - M_V w_V + K_V E \\
\dot{\beta} &= (\mu^{-1} * \hat{I}_\omega * \mu) \times \beta + \mu^{-1} * K_\omega E * \mu + M_q w_q \times \beta - M_\omega w_\omega \\
\dot{\alpha} &= -\alpha M_a w_a + \alpha K_a E.
\end{aligned}$$

where the invariant output error is rewritten as

$$E = \begin{pmatrix} \nu + N_V v_V \\ B - \mu * (B + N_B v_B) * \mu^{-1} \end{pmatrix}$$

We linearize this error system around the group identity element $(\overline{\mu}, \overline{\nu}, \overline{\beta}, \overline{\alpha}) = (1, 0, 0, 1)$. We drop all the quadratic terms in noise and infinitesimal state error according to the approximation in section 5.3.2, and eventually find

$$\begin{pmatrix} \delta\dot{\mu} \\ \delta\dot{\nu} \\ \delta\dot{\beta} \\ \delta\dot{\alpha} \end{pmatrix} = (A - KC) \begin{pmatrix} \delta\mu \\ \delta\nu \\ \delta\beta \\ \delta\alpha \end{pmatrix} - M \begin{pmatrix} w_q \\ w_V \\ w_\omega \\ w_a \end{pmatrix} + KN \begin{pmatrix} v_V \\ v_B \end{pmatrix},$$

which has the desired form of Equation (160) with

$$A = \begin{pmatrix} 0_{33} & 0_{33} & -\frac{1}{2}I_3 & 0_{31} \\ -2\hat{I}_{a\times} & 0_{33} & 0_{33} & -\hat{I}_a \\ 0_{33} & 0_{33} & \hat{I}_{\omega\times} & 0_{31} \\ 0_{31} & 0_{31} & 0_{31} & 0_{31} \end{pmatrix} \qquad C = \begin{pmatrix} 0_{33} & I_3 & 0_{33} & 0_{31} \\ 2B_\times & 0_{33} & 0_{33} & 0_{31} \end{pmatrix}$$

$$M = Diag(M_q, M_V, M_\omega, M_a) \qquad N = Diag(N_V, N_B)$$

$$K = -(K_q,\ K_V,\ K_\omega,\ K_a)^T.$$

Features of the RIEKF

- Symmetry-preserving structure: rotations, translations and scaling in the appropriated frames leave the error system unchanged, which is meaningful from an engineering point of view.
- Sound geometric structure for the quaternion estimation equation: by construction Equation (187) preserves the unit norm of the estimated quaternion.
- Larger expected domain of convergence: the matrices A and C used for computing the gain matrix K are constant not only in level flight but also on every permanent trajectory defined by constant $\hat{I}_\omega, \hat{I}_a$. Since there are less invariant quantities than

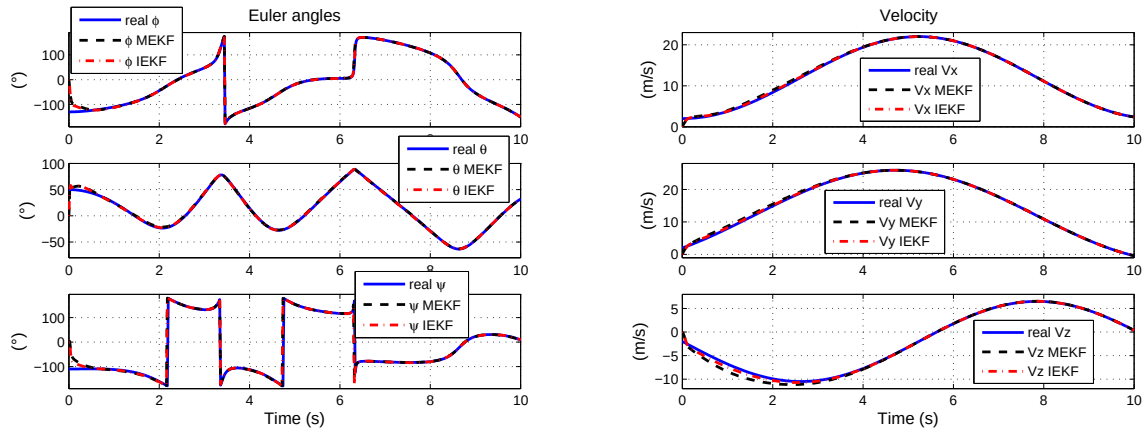

(a) Estimated Euler angles

(b) Estimated velocities

FIGURE 5.1. Comparison of the estimations (simulation)

in the LIEKF (in particular the gain matrices are independent of $\hat{J}_B$), there are in consequence more permanent trajectories.

5.8. Numerical results

We illustrate the behavior of the proposed filters on simulations and experimental data. The noises w_i, v_i (in the simulations) are independent normally distributed random 3-dimensional vectors with mean 0 and variance 1. The tuning of the EKF is made via the choice of covariance matrices $M_q = 0.5I_3$, $M_V = 0.01I_3$, $M_\omega = 0.001I_3$, $M_a = 0.1$, $N_V = 0.1I_3$, $N_B = 0.1I_3$. The (scaled) Earth magnetic field is taken as $B = (1\ 0\ 1)^T$ (roughly the value in France).

For instance for the right IEKF, we take

$$\dot{\hat{q}} = \frac{1}{2}\hat{q} * (\omega_m - \hat{\omega}_b) + K_q E * \hat{q} + \lambda(1 - \|\hat{q}\|^2)\hat{q}.$$

Notice the correction term $\lambda(1 - \|\hat{q}\|^2)\hat{q}$ is invariant under both left and right multiplication by a constant quaternion. We have used $\lambda = 1$.

Since the RIEKF behaves slightly better than the LIEKF, we do not show plots with the RIEKF.

5.8.1. Experimental results. — We first briefly compare the behavior of the RIEKF with the commercial INS-GPS device MIDG II from Microbotics. The IEKF is fed with

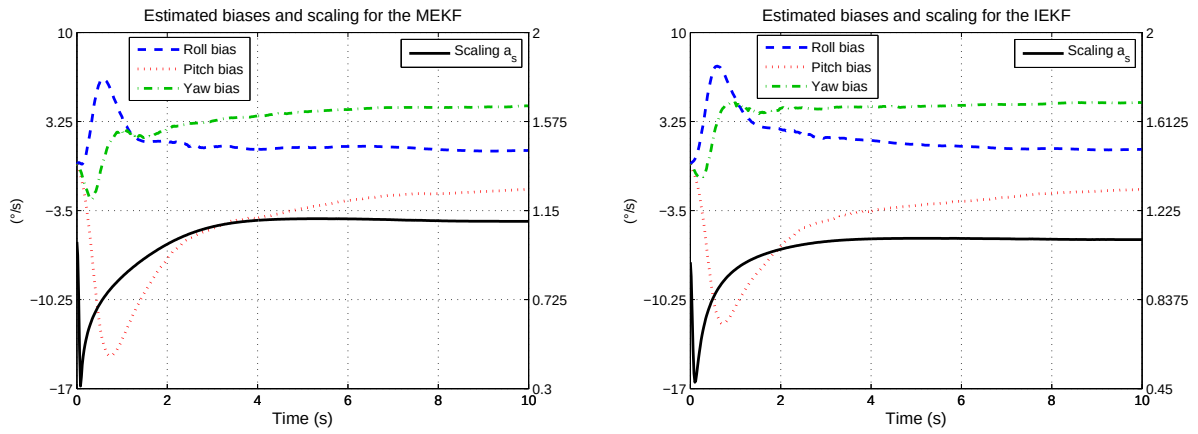

(a) MEKF (b) RIEKF

FIGURE 5.2. Comparison of the estimated biases and scaling (simulation)

the raw measurements from the MIDG II gyroscopes, accelerometers and magnetic sensors (update rate 50Hz), and the velocity provided by the navigation solutions of its GPS engine (update rate 4Hz). The IEKF estimations are compared with the MIDG II estimations produced from the same raw data (and computed according to the user manual by some kind of Kalman filter).

The experiment consists in keeping the system at rest for a few minutes (for the biases to converge), and then moving it for about $35s$. The IEKF and MIDG II results are very similar, see Figure 5.3 (only the Euler angles, converted from quaternions, are displayed).

5.8.2. Simulation results: comparison of MEKF and IEKF. — The system follows a (nearly) permanent trajectory $\mathcal{T}_0$, quite representative of a small UAV flight. The MEKF and RIEKF are initialized with the same values. Both filters give correct estimations after the initial transient, see Figures 5.1-5.2.

We now illustrate the invariance property of the IEKF: both IEKF are initialized with three different initial conditions having the same norms. The MEKF behavior depends on the initial conditions, while the RIEKF behavior does not, see Figure 5.4 (only the norm $E_V = \|\nu\|$ of the velocity error is displayed).

Finally we show the RIEKF gain matrix K becomes as expected constant on the permanent trajectory $\mathcal{T}_0$, while the MEKF gain does not, see Figure 5.5. This is remarkable since $\mathcal{T}_0$ is far from being an equilibrium point.

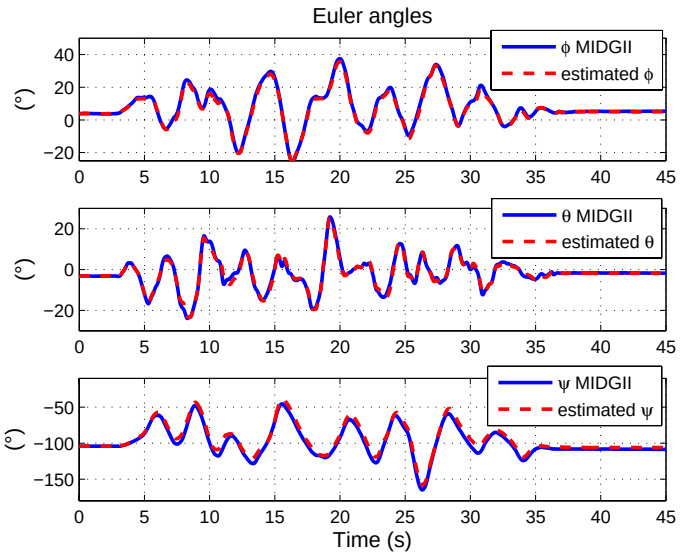

FIGURE 5.3. Estimated Euler angles (experiment)

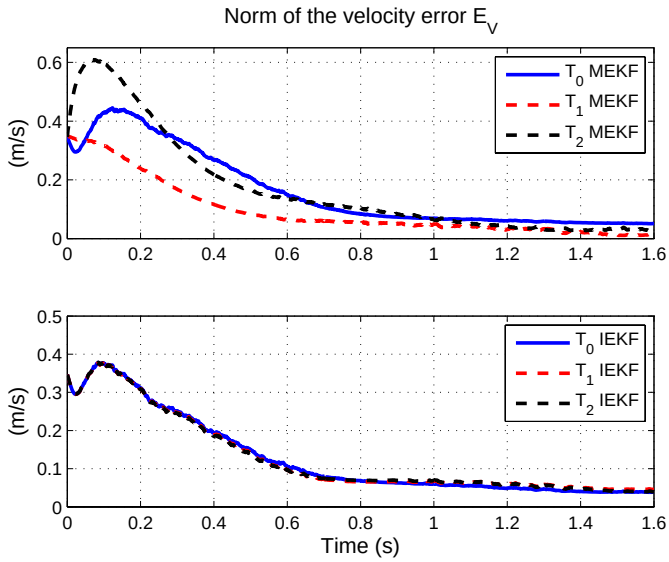

FIGURE 5.4. Evolution of $E_V = \|\nu\|$ for three initial conditions (simulation)

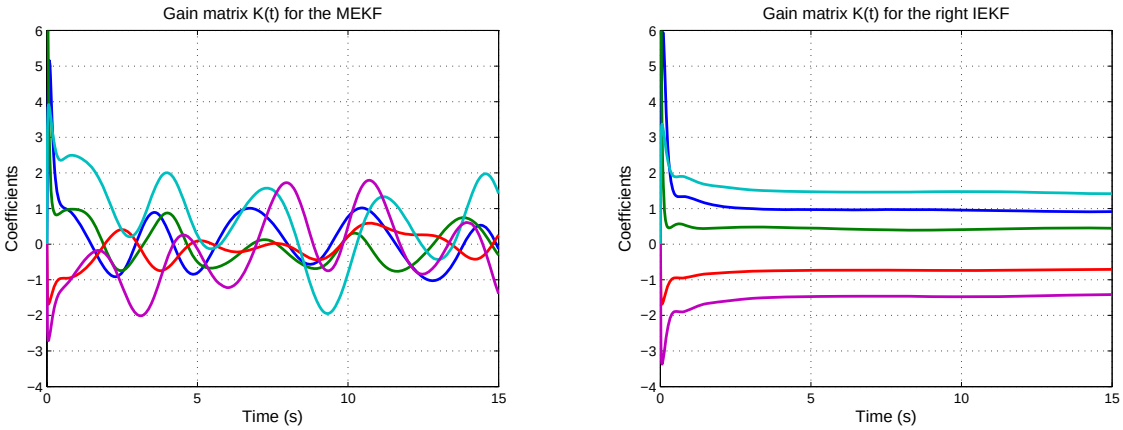

(a) MEKF (b) RIEKF

FIGURE 5.5. Evolution of K (simulation)

CHAPTER 6

SPECIFIC OBSERVER FOR MINI QUADROTOR

Nous nous interessons dans ce chapitre aux mini-drones de type quadrirotors. Nous en proposons un nouveau modèle prenant en compte des forces aérodynamiques jamais exploitées dans les travaux réalisés jusqu'à présent sur ce type de drone. Cette force permet d'estimer la vitesse à travers les mesures fournies par les accéléromètres. Nous construisons alors un observateur "spécifique" basé sur ce modèle, qui nous permets de contrôler le quadrotor en vitesse avec uniquement des capteurs inertiels. De plus, cette approche nous permets de voir d'un oeil neuf les algorithmes de filtrages et de contrôles habituellement utilisés sur les quadrotors (contrôle de l'assiette et estimation des angles d'attitude selon l'hypothèse d'une faible accélération linéaire), justifiant les résultats expérimentaux obtenus.

6.1. Introduction

Quadrotor control has been an active area of investigation for several years. On the one hand the quadrotor has several qualities, among them its very simple mechanical design, and qualifies as a viable concept of mini Unmanned Aerial Vehicle (UAV) for real-life missions; on the other hand it is perceived in the control community as a very

rich case study in theoretical and applied control. The first control objective is to ensure a stable flight at moderate velocities and in particular in hovering; this fundamental building block is then used to develop higher-level tasks (e.g. autonomous flight including waypoint following, obstacle avoidance, automatic take off and landing, etc.).

Putting aside purely control-theoretic works focused on the detailed analysis of control laws without real-world sensors in mind, as well as experiments designed to work only in the laboratory with an off-board measuring device (e.g. [**20**] use an electromagnetic motion tracking system, with very short range), real quadrotor designs all rely at the heart on strapdown MEMS inertial sensors (gyroscopes and accelerometers). Such sensors are also used in "preliminary" experiments where the quadrotor is tethered to a test rig and free only to rotate [**15, 80, 72**]. These inertial sensors may be used alone (as far as horizontal stabilization is concerned) [**34**], or supplemented by other sensors which provide usually some position-related information. Representative designs are: 3 ultrasonic rangers [**43**]; a (simple) GPS module when outdoors and 4 infrared rangers when indoors [**74**]; a carrier phase differential GPS [**40, 89, 39**]; a vision system [**16, 33, 36, 68**]; a laser scanner [**2, 1**]. Since these extra sensors have inherent drawbacks (low bandwidth, possible temporary unavailability, etc.), inertial sensors remain essential for basic stabilization.

Nearly all the above-mentioned works rely on essentially the same physical model: only aerodynamic forces and moments proportional to the square of the propellers angular velocities are explicitly taken into account. Other aerodynamics effects are omitted and considered as unmodeled disturbances to be rejected by the control law. The alleged reason is that these effects are proportional to the square of the quadrotor linear velocity [**7**], hence very small near hovering. Few authors explicitly consider other aerodynamic effects: [**72**] consider aerodynamic stability derivatives, but draw no clear-cut conclusion about their importance; [**27, 51**] consider without physical motivations aerodynamic effects linear w.r.t. the quadrotor linear and angular velocities, but propose negligible numerical values; [**40**] judge them negligible at low velocities, and focus on nonlinear aspects at moderate velocities; [**17**] physically motivates the presence of effects nearly linear w.r.t the quadrotor linear and angular velocities, but provide no experimental data and are concerned only with the open-loop system.

As for accelerometers, they are usually considered as giving approximately the components of gravity in body axes, under the assumption that the quadrotor linear acceleration is small (as explained in Section 2.3. Accordingly, the pitch and roll angles are estimated from gyroscope and accelerometer measurements thanks to some sensor fusion algorithm:

FIGURE 6.1. Our home-built quadrotor: the "Quadricopter".

Extended Kalman Filter (EKF) [**15**]; complementary filter, linear [**80, 74**] or nonlinear [**33**] and Chapter 3 ; unspecified algorithm [**34, 16**]. Commercial "attitude sensors" such as the 3DM-GX used in [**43**] run exactly on the same principles, with some sort of EKF. Recall that MEMS inertial sensors are not accurate enough for "true" Schuler-based inertial navigation, see e.g. [**32**, chap. 5] for details.

With so many theoretical and experimental works, one could think there is little more to say about such a basic issue as linear control around hovering with inertial sensors. We nevertheless support a different opinion: the traditional analysis is not quite correct, even at first order. Indeed aerodynamics effects proportional to the propeller angular velocity times the quadrotor linear or angular velocity do appear at first order. In particular the so-called rotor drag must be considered to correctly account for the accelerometer measurements.

According to Section 1.5, a generic observer is not able to estimate the velocity of the mini quadrotor using only inertial and magnetic sensors (see for instance the divergence of the estimated roll angle at $\dot{V} \neq 0$ in Section 3.4). Therefore we build specific observers for a mini quadrotor, based on the considered model, which estimate the linear velocity of the mini UAV, in order to stabilize it. This example highlights the major improvements

allowable by specific observers, which take into account the physical model of the vehicle (written from the dynamics laws).

6.2. Revisited quadrotor model

6.2.1. Model of a single propeller near hovering. — We first consider a single propeller rotating with angular velocity $\varepsilon_i\omega_i$ around its axis $\vec{k}_b$; ω_i is positive, with $\varepsilon_i = 1$ (resp. -1) for counterclockwise (resp. clockwise) rotation. The geometric center A_i of the propeller moves with a given velocity $\vec{V}_{A_i}$ while the rotor plane (by definition perpendicular to $\vec{k}_b$) undergoes angular velocity $\vec{\Omega}$; the total angular velocity of the propeller is thus $\vec{\Omega} + \varepsilon_i\omega_i\vec{k}_b$. Following e.g. [**42**], the aerodynamic efforts on the propeller resolve into the force $\vec{F}_i$ and moment $\vec{M}_i$ at A_i,

$$\vec{F}_i = -a\omega_i^2\vec{k}_b - \omega_i\left(\lambda_1\vec{V}_{A_i}^{\perp} - \lambda_2\vec{\Omega}\times\vec{k}_b\right) + \varepsilon_i\omega_i\left(\lambda_3\vec{V}_{A_i}\times\vec{k}_b - \lambda_4\vec{\Omega}^{\perp}\right) \tag{191}$$

$$\vec{M}_i = -b\varepsilon_i\omega_i^2\vec{k}_b - \omega_i\left(\mu_1\vec{V}_{A_i}^{\perp} + \mu_2\vec{\Omega}\times\vec{k}_b\right) - \varepsilon_i\omega_i\left(\mu_3\vec{V}_{A_i}\times\vec{k}_b + \mu_4\vec{\Omega}^{\perp}\right), \tag{192}$$

where a, b, the λ_i's and μ_i's are positive constants; the projection of a vector $\vec{u}$ on the rotor plane is

$$\vec{u}^{\perp} := \vec{k}_b\times\left(\vec{u}\times\vec{k}_b\right) = \vec{u} - \left(\vec{u}\cdot\vec{k}_b\right)\vec{k}_b.$$

The above relations rely on classical blade element theory, with two extra simplifications, and (approximately) apply to any propeller, rigid or not:

- higher-order terms in linear and angular velocities have been neglected. This is valid near hovering, i.e. for small $\vec{V}_{A_i}$ and $\vec{\Omega}$. Here $\vec{V}_{A_i}$ "small" means small with respect to the propeller tip speed (about $40m/s$ in our case), so that $5m/s$ can be considered small
- linear and angular accelerations have been neglected. Their contribution is small since the mass of the propeller is in our case very small with respect to the total mass of the quadrotor.

The velocities in the previous equations are of course velocities with respect to the air stream, not with respect to the ground. They coincide when there is no wind, which we assume in the sequel.

The term $\omega_i\lambda_1\vec{V}_{A_i}^{\perp}$ in (191) is often called *H-force* or *rotor drag* in the helicopter literature. Also notice the simplified expressions (191)-(192), though directly based on textbook aerodynamics, do not seem to appear in the literature under this compact form very handy for control purposes.

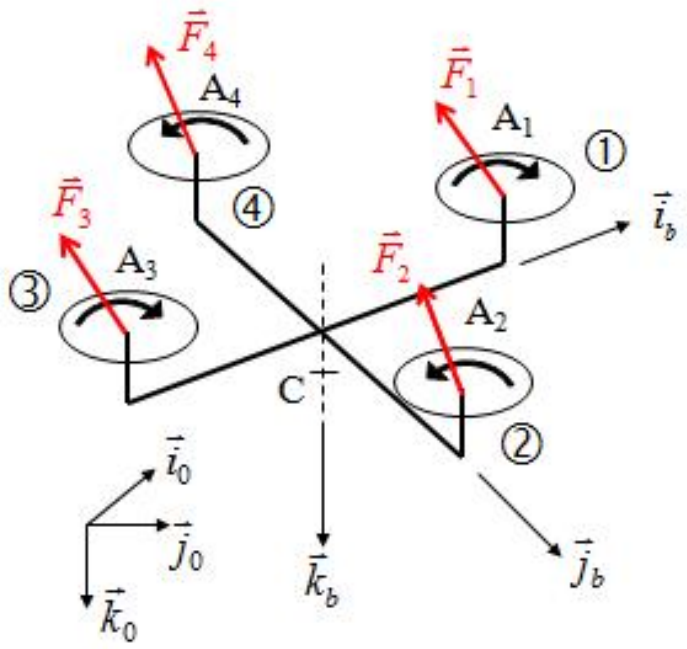

FIGURE 6.2. Sketch of the complete quadrotor.

6.2.2. Model of the complete quadrotor. — The quadrotor consists of a rigid frame with four propellers (directly) driven by electric motors, see Figure 6.2. The structure is symmetrically arranged, with one pair of facing propellers rotating clockwise and the other pair counterclockwise. The four propellers have the same axis $\vec{k}_b$; $\vec{\imath}_b := \frac{\vec{A_3A_1}}{\|\vec{A_3A_1}\|}$, $\vec{\jmath}_b := \frac{\vec{A_4A_2}}{\|\vec{A_4A_2}\|}$ and $\vec{k}_b$ then form a direct coordinate frame. Let A be the geometric center of the A_i's and $l := \frac{1}{2}\|\vec{A_3A_1}\| = \frac{1}{2}\|\vec{A_2A_4}\|$; clearly, $\sum_{i=1}^{4}\vec{AA_i} = 0$.

The whole system $\mathcal{B}$, with mass m and center of mass C, thus involves five rigid bodies: the frame/stators assembly $\mathcal{B}_0$ and the four propeller/motor assemblies $\mathcal{B}_i$; clearly, $\vec{CA} = h\vec{k}_b$ for some (signed) length h. Resolved in the $(\vec{\imath}_b, \vec{\jmath}_b, \vec{k}_b)$ frame, the velocity of C reads $\vec{V}_C = u\vec{\imath}_b + v\vec{\jmath}_b + w\vec{k}_b$ and the angular velocity of $\mathcal{B}_0$ reads $\vec{\Omega} = p\vec{\imath}_b + q\vec{\jmath}_b + r\vec{k}_b$.

We assume the only efforts acting on $\mathcal{B}$ are the weight and the aerodynamic efforts created by the propellers as described in the previous section. In particular we neglect the drag created by the frame, which is quadratic with respect to the velocity, hence small

at low velocities. Newton's laws for the whole system then read

$$m\dot{\vec{V}}_C = m\vec{g} + \sum_{i=1}^{4} \vec{F}_i \tag{193}$$

$$\dot{\vec{\sigma}}_C^{\mathcal{B}} = \sum_{i=1}^{4} \vec{CA}_i \times \vec{F}_i + \vec{M}_i, \tag{194}$$

where $\vec{\sigma}_C^{\mathcal{B}} = \int_{\mathcal{B}} \vec{CM} \times \dot{\vec{CM}} d\mu(M)$ is the kinetic momentum of $\mathcal{B}$.

In hovering $\vec{V}_C$ and $\vec{\Omega}$, hence $\vec{V}_{A_i}$ are zero; from (191)–(194), see also (196)-(197), this implies $a(\omega_1^2 + \omega_2^2 + \omega_3^2 + \omega_4^2) = g$ and $\omega_1^2 - \omega_2^2 + \omega_3^2 - \omega_4^2 = \omega_1^2 - \omega_3^2 = \omega_2^2 - \omega_4^2 = 0$, hence $\omega_i = \bar{\omega} := \sqrt{\frac{mg}{4a}}$.

For each $\mathcal{B}_i$, we can also write

$$\dot{\vec{\sigma}}_{A_i}^{\mathcal{B}_i} \cdot \vec{k}_b = \vec{M}_i \cdot \vec{k}_b + \varepsilon_i \Gamma_i, \tag{195}$$

where $\vec{\sigma}_{A_i}^{\mathcal{B}_i} = \int_{\mathcal{B}_i} \vec{A_iM} \times \dot{\vec{A_iM}} d\mu(M)$ is the kinetic momentum of $\mathcal{B}_i$, and Γ_i is the (positive) torque created by the motor. For simplicity we have considered A_i as the center of mass of $\mathcal{B}_i$ (in fact the two points are slightly apart). We also consider the Γ_i's as the control inputs (it is nevertheless easy to include the behavior of the electric motors both for modeling and control).

We now evaluate the right-hand sides of (193)-(194)-(195). Since

$$\vec{V}_{A_i} = \vec{V}_C + \dot{\vec{CA}} + \dot{\vec{AA}}_i = \vec{V}_C + h\vec{\Omega} \times \vec{k}_b + \vec{\Omega} \times \vec{AA}_i,$$

we find

$$\begin{aligned}
\lambda_1 \vec{V}_{A_i}^{\perp} - \lambda_2 \vec{\Omega} \times \vec{k}_b &= \lambda_1 \left(\vec{V}_C^{\perp} + \left(h\vec{\Omega} \times \vec{k}_b \right)^{\perp} + \left(\vec{\Omega} \times \vec{AA}_i \right)^{\perp} \right) - \lambda_2 \vec{\Omega} \times \vec{k}_b \\
&= \lambda_1 \vec{V}_C^{\perp} - \lambda_2' \vec{\Omega} \times \vec{k}_b - r\lambda_1 \vec{AA}_i \times \vec{k}_b \\
\lambda_3 \vec{V}_{A_i} \times \vec{k}_b - \lambda_4 \vec{\Omega}^{\perp} &= \lambda_3 \left(\vec{V}_C + h\vec{\Omega} \times \vec{k}_b + \vec{\Omega} \times \vec{AA}_i \right) \times \vec{k}_b - \lambda_4 \vec{\Omega}^{\perp} \\
&= \lambda_3 \vec{V}_C \times \vec{k}_b + \lambda_4' \vec{\Omega}^{\perp} + r\lambda_3 \vec{AA}_i.
\end{aligned}$$

We have used the fact that $\vec{AA}_i$ is colinear to either $\vec{\imath}_b$ or $\vec{\jmath}_b$, and set $\lambda_2' =: \lambda_2 - h\lambda_1$ and $\lambda_4' := \lambda_4 + h\lambda_3$. Therefore,

$$\begin{aligned}\sum_{i=1}^4 \vec{F}_i = -a\left(\sum_{i=1}^4 \omega_i^2\right)\vec{k}_b - \left(\sum_{i=1}^4 \omega_i\right)\left(\lambda_1 \vec{V}_C^{\perp} - \lambda_2' \vec{\Omega} \times \vec{k}_b\right) \\ + \left(\sum_{i=1}^4 \varepsilon_i \omega_i\right)\left(\lambda_3 \vec{V}_C \times \vec{k}_b - \lambda_4' \vec{\Omega}^{\perp}\right) \\ + r\lambda_1 \left(\sum_{i=1}^4 \omega_i \vec{AA}_i\right) \times \vec{k}_b + r\lambda_3 \left(\sum_{i=1}^4 \varepsilon_i \omega_i \vec{AA}_i\right).\end{aligned}$$

Notice the last two lines contain only second order terms: indeed, $\vec{\Omega}$, $\vec{V}_C$, $\sum_{i=1}^4 \varepsilon_i \omega_i$, $\sum_{i=1}^4 \omega_i \vec{AA}_i$ and $\sum_{i=1}^4 \varepsilon_i \omega_i \vec{AA}_i$ all vanish in hovering. Neglecting these terms, we have

$$\sum_{i=1}^4 \vec{F}_i \approx -a\left(\sum_{i=1}^4 \omega_i^2\right)\vec{k}_b - \left(\sum_{i=1}^4 \omega_i\right)\left(\lambda_1 \vec{V}_C^{\perp} - \lambda_2' \vec{\Omega} \times \vec{k}_b\right).$$

Likewise,

$$\begin{aligned}\sum_{i=1}^4 \vec{CA} \times \vec{F}_i + \vec{AA}_i \times \vec{F}_i + \vec{M}_i \approx -a\left(\sum_{i=1}^4 \omega_i^2 \vec{AA}_i\right) \times \vec{k}_b - b\left(\sum_{i=1}^4 \varepsilon_i \omega_i^2\right)\vec{k}_b \\ - r\lambda_1 l^2 \left(\sum_{i=1}^4 \omega_i\right)\vec{k}_b - \left(\sum_{i=1}^4 \omega_i\right)\left(\mu_1' \vec{V}_C \times \vec{k}_b + \mu_2'' \vec{\Omega}^{\perp}\right),\end{aligned}$$

where $\mu_1' := \mu_1 - h\lambda_1$, $\mu_2' := \mu_2 - h\mu_1$ and $\mu_2'' := \mu_2' - h\lambda_2$.

A further simplification, valid for a rather rigid propeller, is to consider that λ_2' is zero. Indeed h is by design small, and for a rather rigid propeller so is λ_2. This yields

$$\sum_{i=1}^4 \vec{F}_i \approx -a\left(\sum_{i=1}^4 \omega_i^2\right)\vec{k}_b - \lambda_1 \left(\sum_{i=1}^4 \omega_i\right)\vec{V}_C^{\perp}.$$

Gathering the previous computations, (193)-(194)-(195) now read

$$
\begin{aligned}
m\dot{\vec{V}}_C &= m\vec{g} - a\left(\omega_1^2+\omega_2^2+\omega_3^2+\omega_4^2\right)\vec{k}_b - \lambda_1(\omega_1+\omega_2+\omega_3+\omega_4)\vec{V}_C^{\perp} \qquad (196)\\
\dot{\vec{\sigma}}_C^{\mathcal{B}} &= -b\left(\omega_1^2-\omega_2^2+\omega_3^2-\omega_4^2\right)\vec{k}_b + al(\omega_1^2-\omega_3^2)\vec{\jmath}_b - al(\omega_2^2-\omega_4^2)\vec{\imath}_b\\
&\quad - (\omega_1+\omega_2+\omega_3+\omega_4)\left(\mu_1'\vec{V}_C\times\vec{k}_b + \mu_2''\vec{\Omega}^{\perp}\right)\\
&\quad - r\lambda_1 l^2(\omega_1+\omega_2+\omega_3+\omega_4)\vec{k}_b \qquad (197)\\
\dot{\vec{\sigma}}_{A_i}^{\mathcal{B}_i}\cdot\vec{k}_b &= \varepsilon_i(\Gamma_i - b\omega_i^2). \qquad (198)
\end{aligned}
$$

We then evaluate the left-hand sides of (193)-(194)-(195). The approach is fairly standard.

$$
\begin{aligned}
\vec{\sigma}_C^{\mathcal{B}} &= \int_{\mathcal{B}} C\vec{M}\times C\dot{\vec{M}}d\mu(M)\\
&= \int_{\mathcal{B}_0} C\vec{M}\times C\dot{\vec{M}}d\mu(M) + \sum_{i=1}^{4}\int_{\mathcal{B}_i} C\vec{M}\times\left(C\dot{\vec{A}}_i + A_i\dot{\vec{M}}\right)d\mu(M)\\
&= \int_{\mathcal{B}_0} C\vec{M}\times\left(\vec{\Omega}\times C\vec{M}\right)d\mu(M) + \sum_{i=1}^{4}\int_{\mathcal{B}_i} C\vec{M}\times\left(\vec{\Omega}\times C\vec{A}_i + \left(\vec{\Omega}+\varepsilon_i\omega_i\vec{k}_b\right)\times A_i\vec{M}\right)d\mu(M)\\
&= \int_{\mathcal{B}} C\vec{M}\times\left(\vec{\Omega}\times C\vec{M}\right)d\mu(M) + \sum_{i=1}^{4}\int_{\mathcal{B}_i} A_i\vec{M}\times\left(\varepsilon_i\omega_i\vec{k}_b\times A_i\vec{M}\right)d\mu(M)\\
&= \mathcal{I}_C^{\mathcal{B}}\cdot\vec{\Omega} + \sum_{i=1}^{4}\varepsilon_i\omega_i\left(\mathcal{I}_{A_i}^{\mathcal{B}_i}\cdot\vec{k}_b\right)\\
&= Ip\vec{\imath}_b + Iq\vec{\jmath}_b + \left(Jr + J_r\sum_{i=1}^{4}\varepsilon_i\omega_i\right)\vec{k}_b,
\end{aligned}
$$

where I, J, J_r are strictly positive constants. In the last equation we replaced in the computation of the inertia tensors $\mathcal{I}^{\mathcal{B}}, \mathcal{I}_{A_i}^{\mathcal{B}_i}$ the actual propellers by disks with the same masses and radii, and took advantage of the various symmetries; this "averaging" approximation is justified by the fact that the propeller angles vary much faster than all the other kinematic variables (besides this approximation is already heavily used in the blade element theory used to derive (191)-(192)).

Using the same approximation,

$$\begin{aligned}\vec{\sigma}_{A_i}^{\mathcal{B}_i} &= \int_{\mathcal{B}_i} A_i\vec{M} \times A_i\dot{\vec{M}} d\mu(M) \\ &= \int_{\mathcal{B}_i} A_i\vec{M} \times \left(\left(\vec{\Omega} + \varepsilon_i\omega_i\vec{k}_b\right) \times A_i\vec{M} \right) d\mu(M) \\ &= \mathcal{I}_{A_i}^{\mathcal{B}_i} \cdot \left(\vec{\Omega} + \varepsilon_i\omega_i\vec{k}_b\right) \\ &= I_r p\vec{\imath}_b + I_r q\vec{\jmath}_b + J_r(r + \varepsilon_i\omega_i)\vec{k}_b,\end{aligned}$$

where I_r is a strictly positive constant.

Eventually,

$$\begin{pmatrix} \dot{\vec{V}}_C \cdot \vec{\imath}_b \\ \dot{\vec{V}}_C \cdot \vec{\jmath}_b \\ \dot{\vec{V}}_C \cdot \vec{k}_b \end{pmatrix} = \begin{pmatrix} \dot{u} + qw - rv \\ \dot{v} + ru - pw \\ \dot{w} + pv - qu \end{pmatrix} \tag{199}$$

$$\begin{pmatrix} \dot{\vec{\sigma}}_C^{\mathcal{B}} \cdot \vec{\imath}_b \\ \dot{\vec{\sigma}}_C^{\mathcal{B}} \cdot \vec{\jmath}_b \\ \dot{\vec{\sigma}}_C^{\mathcal{B}} \cdot \vec{k}_b \end{pmatrix} = \begin{pmatrix} I\dot{p} + (J-I)qr + J_r q\sum_{i=1}^4 \varepsilon_i\omega_i \\ I\dot{q} - (J-I)pr - J_r p\sum_{i=1}^4 \varepsilon_i\omega_i \\ J\dot{r} + J_r\sum_{i=1}^4 \varepsilon_i\dot{\omega}_i \end{pmatrix} \tag{200}$$

$$\dot{\vec{\sigma}}_{A_i}^{\mathcal{B}_i} \cdot \vec{k}_b = J_r(\dot{r} + \varepsilon_i\dot{\omega}_i), \qquad i = 1, 2, 3, 4. \tag{201}$$

To describe the orientation of the quadrotor we use the classical ϕ, θ, ψ Euler angles (quaternions could of course be used). The direction cosine matrix $R_{\phi,\theta,\psi}$ to go from Earth coordinates to aircraft coordinates is then

$$\begin{pmatrix} C\theta C\psi & C\theta S\psi & -S\theta \\ S\phi S\theta C\psi - C\phi S\psi & S\phi S\theta S\psi + C\phi C\psi & S\phi C\theta \\ C\phi S\theta C\psi + S\phi S\psi & C\phi S\theta S\psi - S\phi S\psi & C\phi C\theta \end{pmatrix},$$

so that

$$\vec{g} = g(-\vec{\imath}_b \sin\theta + \vec{\jmath}_b \sin\phi\cos\theta + \vec{k}_b \cos\phi\cos\theta). \tag{202}$$

Finally the angles and angular velocities are linked by

$$\dot{\phi} = p + \tan\theta(q\sin\phi + r\cos\phi) \tag{203}$$

$$\dot{\theta} = q\cos\phi - r\sin\phi \tag{204}$$

$$\dot{\psi} = \frac{q\sin\phi + r\cos\phi}{\cos\theta}. \tag{205}$$

The thirteen equations (196)–(205) form the complete quadrotor model.

6.2.3. Model of the inertial sensors. — The quadrotor is equipped with strapdown triaxial gyroscope and accelerometer. Without restriction, we assume the sensing axes coincide with $\vec{\imath}_b, \vec{\jmath}_b, \vec{k}_b$. The gyroscope measures the angular velocity $\vec{\Omega}$, projected on its sensing axes, i.e. $(g_x, g_y, g_z) := (p, q, r)$; the accelerometer measures the specific acceleration $\vec{a} := \dot{\vec{V}}_P - \vec{g}$ of the point P where it is located, projected on its sensing axe; see e.g. Chapter 2 and [**32**, chap. 4] for details on inertial sensors. Hence by (193) if the accelerometer is located at the center of mass C, which is the case for most quadrotors, it measures $\vec{a} = \dot{\vec{V}}_C - \vec{g} = \frac{1}{m}\sum_{i=1}^{4} \vec{F}_i$; by (196) the accelerometer thus measures

$$a_x := \vec{a} \cdot \vec{\imath}_b \approx -\frac{\lambda_1}{m}(\omega_1 + \omega_2 + \omega_3 + \omega_4)u \tag{206}$$

$$a_y := \vec{a} \cdot \vec{\jmath}_b \approx -\frac{\lambda_1}{m}(\omega_1 + \omega_2 + \omega_3 + \omega_4)v \tag{207}$$

$$a_z := \vec{a} \cdot \vec{k}_b \approx -\frac{a}{m}\left(\omega_1^2 + \omega_2^2 + \omega_3^2 + \omega_4^2\right). \tag{208}$$

6.2.4. Linearized model. — To highlight the salient features of the revisited model (196)–(205), it is enough to consider its first-order approximation. Suitably putting together variables, this linearized model splits into four independent subsystems:

– longitudinal subsystem

$$\begin{aligned} m\dot{u} &\approx -mg\theta - 4\lambda_1\bar{\omega}u \\ \dot{\theta} &\approx q \\ I\dot{q} &\approx 4\mu_1'\bar{\omega}u - 4\mu_2''\bar{\omega}q + 2al\bar{\omega}(\omega_1 - \omega_3) \\ J_r(\dot{\omega}_1 - \dot{\omega}_3) &\approx \Gamma_1 - \Gamma_3 - 2b\bar{\omega}(\omega_1 - \omega_3), \end{aligned}$$

with measurements $a_x \approx -\frac{4\lambda_1\bar{\omega}}{m}u$ and $g_y = q$

– lateral subsystem

$$\begin{aligned} m\dot{v} &\approx mg\phi - 4\lambda_1\bar{\omega}v \\ \dot{\phi} &\approx p \\ I\dot{p} &\approx -4\mu_1'\bar{\omega}v - 4\mu_2''\bar{\omega}p + 2al\bar{\omega}(\omega_4 - \omega_2) \\ J_r(\dot{\omega}_4 - \dot{\omega}_2) &\approx \Gamma_4 - \Gamma_2 - 2b\bar{\omega}(\omega_4 - \omega_2), \end{aligned}$$

with measurements $a_y \approx -\frac{4\lambda_1\bar{\omega}}{m}v$ and $g_x = p$

– vertical subsystem

$$m\dot{w} \approx -2a\bar{\omega}\left(\left(\sum_{i=1}^{4}\omega_i\right) - 4\bar{\omega})\right)$$
$$J_r\left(\sum_{i=1}^{4}\dot{\omega}_i\right) \approx \left(\sum_{i=1}^{4}\Gamma_i\right) - 2b\bar{\omega}\left(\sum_{i=1}^{4}\omega_i\right),$$

with measurement $a_z \approx -g - \frac{2a\bar{\omega}}{m}\left(\sum_{i=1}^{4}\omega_i\right)$

– heading subsystem

$$\dot{\psi} \approx r$$
$$(J - 4J_r)\dot{r} \approx -\left(\sum_{i=1}^{4}\varepsilon_i\Gamma_i\right) - 4\bar{w}\lambda_1 l^2 r$$
$$\left(\sum_{i=1}^{4}\varepsilon_i\dot{\omega}_i\right) \approx \frac{J}{J_r(J-4J_r)}\left(\sum_{i=1}^{4}\varepsilon_i\Gamma_i\right) - \frac{2b\bar{\omega}}{J_r}\left(\sum_{i=1}^{4}\varepsilon_i\omega_i\right) + \frac{16\lambda_1\bar{\omega}l^2}{J-4J_r}r,$$

with measurement $g_z = r$.

In the sequel we concentrate on the longitudinal system, where accelerometer feedback is of paramount importance (the lateral subsystem is the same up to sign-reversing coordinate changes). Setting

$$(f_1, f_2, f_3, f_4, f_5) := \left(\frac{4\lambda_1\bar{\omega}}{m}, \frac{4\mu_1'\bar{\omega}}{I}, \frac{4\mu_2''\bar{\omega}}{I}, \frac{2al\bar{\omega}}{I}, \frac{2b\bar{\omega}}{J_r}\right)$$

and $\omega_q := \omega_1 - \omega_3$, $\Gamma_q := \frac{\Gamma_1 - \Gamma_3}{J_r}$, it reads

$$\dot{u} = -f_1 u - g\theta \tag{209}$$
$$\dot{\theta} = q \tag{210}$$
$$\dot{q} = f_2 u - f_3 q + f_4\omega_q \tag{211}$$
$$\dot{\omega}_q = \Gamma_q - f_5\omega_q, \tag{212}$$

with measurements $a_x = -f_1 u$ and $g_y = q$.

6.2.5. Departure from literature. — Most authors consider a propeller model with only the $\vec{k}_b$ terms in (191)-(192), i.e. with all λ_i's and μ_i's equal to zero. They thus end

up with the quadrotor model

$$m\dot{\vec{V}}_C = m\vec{g} - a\left(\omega_1^2 + \omega_2^2 + \omega_3^2 + \omega_4^2\right)\vec{k}_b \tag{213}$$

$$\dot{\vec{\sigma}}_C = -b\left(\omega_1^2 - \omega_2^2 + \omega_3^2 - \omega_4^2\right)\vec{k}_b + al(\omega_1^2 - \omega_3^2)\vec{\jmath}_b - al(\omega_2^2 - \omega_4^2)\vec{\imath}_b. \tag{214}$$

Now a big problem should arise with such a model: indeed $\vec{a} = \dot{\vec{V}}_C - \vec{g}$ is now colinear with $\vec{k}_b$, hence $a_x = a_y = 0$, which is certainly not true! Without clearly acknowledging this paradox, the approximation $\vec{a} \approx -\vec{g}$ is used instead, i.e.

$$(a_x, a_y, a_z) \approx (g\sin\theta, -g\sin\phi\cos\theta, -g\cos\phi\cos\theta). \tag{215}$$

The alleged motivation is that $\dot{\vec{V}}_C$ is small near hovering. This is indeed true if the aircraft were stabilized by some extraneous means, but a very questionable assumption to use in a closed-loop perspective. Nevertheless, successful flights with controllers relying on this approximation have been reported. We suggest in section 6.4.3 an explanation reconciling all those facts in the light of the revisited quadrotor model.

The longitudinal subsystem traditionally considered is then

$$\dot{u} = -g\theta \tag{216}$$

$$\dot{\theta} = q \tag{217}$$

$$\dot{q} = f_4\omega_q \tag{218}$$

$$\dot{\omega}_q = \Gamma_q - f_5\omega_q, \tag{219}$$

with measurements $a_x = g\theta$ and $g_y = q$, to be compared with (209)–(212) with measurements $a_x = -f_1 u$ and $g_y = q$.

6.3. Experimental validation

6.3.1. Experimental setup. — To validate our modeling assumptions, we recorded flight data with our home-built "Quadricopter", see Figure 6.1. Due to limitations of our experimental setup, we could collect data to validate only the force model (209), but not the moment model (211); this is nevertheless the most important part of the model since it accounts for the accelerometer measurements. The quadrotor was fitted with a MIDG II with its GPS engine and a radio data link towards the ground station. The raw measurements are "merged" on the onboard computer to provide estimates of the orientation and of the velocity vector in Earth axes. The MIDG II is an "independent" device with no knowledge of the specific system it is fitted on; it heavily relies on the GPS

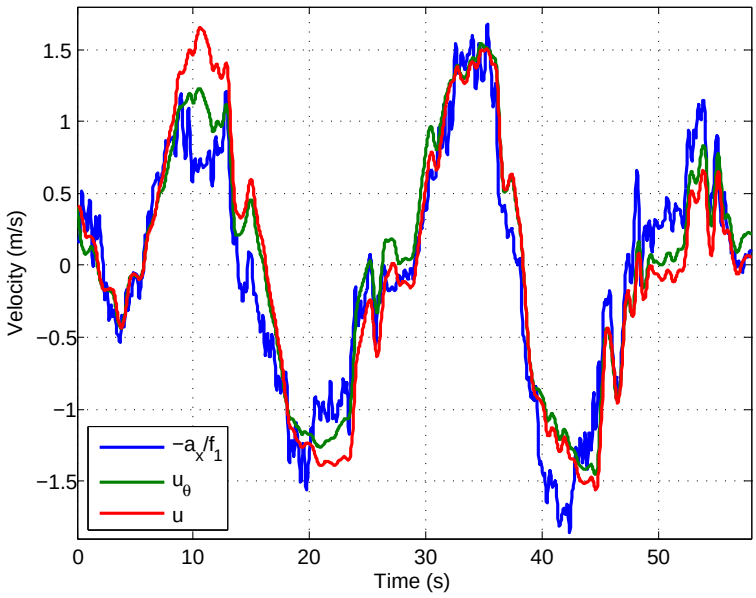

FIGURE 6.3. Comparison between $-\frac{a_x}{f_1}$, u_θ and u.

engine for good dynamic estimates, without using assumption (215). All the data can be issued at a pace up to 20ms. Due to the low throughput of the radio data link, only the accelerometer raw measurements a_{xm}, a_{ym} and the computed quantities ϕ_m, θ_m, ψ_m and V_x, V_y, V_z were transmitted to the ground station, at the reduced pace of 40ms.

We flew the quadrotor in repeated back and forth translations at a (nearly) constant altitude and recorded one minute of flight data. Since a GPS module is used the test was conducted outdoors, on a very calm day to respect the no-wind assumption.

6.3.2. Validation of the force model. — Due to an imperfect mechanical design of our quadrotor, the MIDG II case is not exactly aligned with the quadrotor frame, but tilted by the unknown (small) angles ϕ_0, θ_0, ψ_0. The acceleration and angle data must be rotated accordingly to be expressed in the quadrotor axes (the velocity data need not correction, since expressed in Earth axes), that is

$$(\phi, \theta, \psi) = (\phi_m - \phi_0, \theta_m - \theta_0, \psi_m - \psi_0)$$

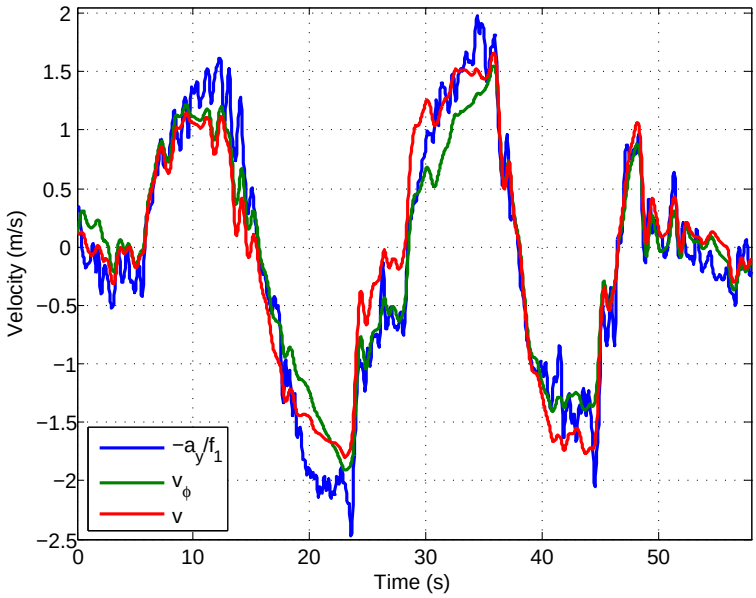

FIGURE 6.4. Comparison between $-\frac{a_y}{f_1}$, v_ϕ and v.

and

$$\begin{pmatrix} a_x \\ a_y \\ a_z \end{pmatrix} = R^T_{\phi_0,\theta_0,\psi_0} \begin{pmatrix} a_{xm} \\ a_{ym} \\ a_{zm} \end{pmatrix}.$$

Dropping higher-order terms, this yields

$$\begin{aligned} a_x &\approx a_{xm} - \psi_0 a_{ym} + \theta_0 a_{zm} && \approx a_{xm} - \theta_0 g \\ a_y &\approx \psi_0 a_{xm} + a_{ym} - \phi_0 a_{zm} && \approx a_{ym} + \phi_0 g. \end{aligned}$$

The velocity vector in quadrotor axes is then obtained by

$$\begin{pmatrix} u \\ v \\ w \end{pmatrix} = R_{\phi,\theta,\psi} \begin{pmatrix} V_x \\ V_y \\ V_z \end{pmatrix},$$

and is considered as the "true" reference velocity to validate our modeling assumptions.

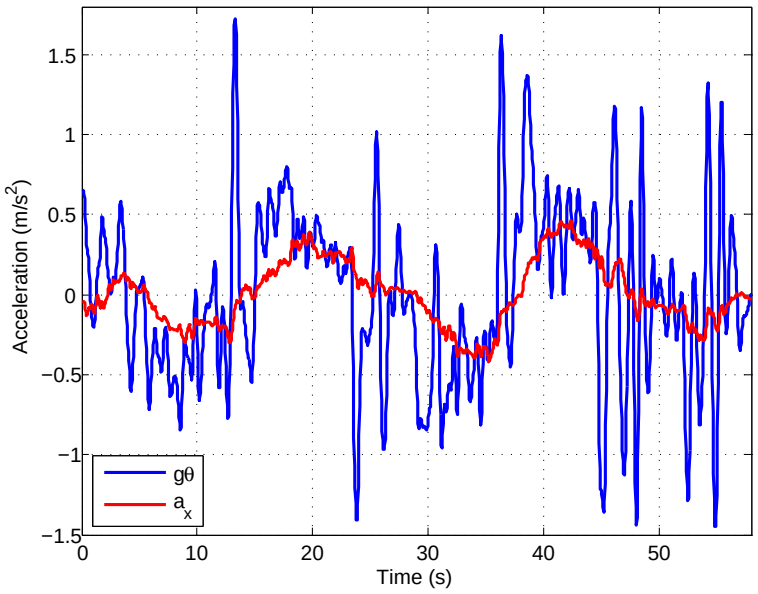

FIGURE 6.5. Comparison between a_x and $g\theta$.

We also want to compute the velocities u_θ and v_ϕ predicted by the integration of the linearized force model (209)

$$\dot{u}_\theta = -f_1 u_\theta - g\theta$$
$$\dot{v}_\phi = -f_1 v_\phi + g\phi,$$

with initial conditions $u_\theta(0) := u(0)$ and $v_\phi(0) := v(0)$.

The task was then to adjust $f_1, \phi_0, \theta_0, \psi_0$ to get a good fit between $-\frac{a_x}{f_1}$, u and u_θ on the one hand; and between $-\frac{a_y}{f_1}$, v and v_ϕ on the other hand. Since the accelerometer data are quite noisy and need some filtering, the same filter (5^{th}-order Bessel filter with 2Hz cutoff frequency) was applied to all the data to preserve the transfer functions among them.

With $(f_1, \phi_0, \theta_0, \psi_0) := (0.25\text{s}^{-1}, 1.2°, -2.4°, 2°)$ the agreement is good, see Figure 6.3 and 6.4, which reasonably validates our force model.

To test the traditional approximation (215) we also plotted $(a_x, g\theta)$ and $(a_y, -g\phi)$, see Figure 6.5 and 6.6. Though the trend is roughly correct, the fit is much worse.

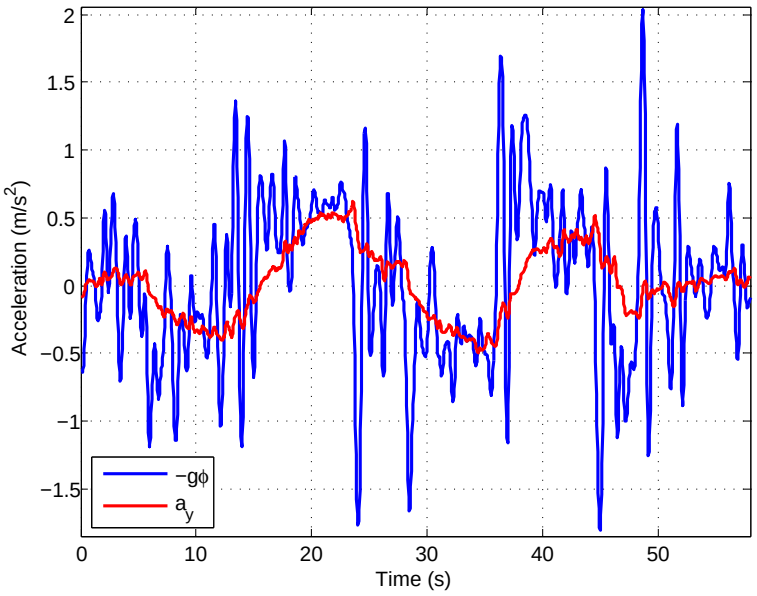

FIGURE 6.6. Comparison between a_y and $-g\phi$.

6.4. Implications on control schemes

In the sequel we use the numerical values

$$(f_1, f_2, f_3, f_4, f_5) = (0.25, 0.76, -9.8, 0.34, 12.74);$$

f_1 was determined from flight tests, and f_4, f_5 from static tests on the motor-propeller subsystems. The aerodynamic coefficients f_2, f_3 were analytically derived; their values are plausible but nevertheless questionable.

6.4.1. Two-time-scale "full-state" feedback. — We first assume the whole state is known, or which turns out to be equivalent, that u and q are measured without noise so that they can be used in ideal Proportional-Derivative (PD) controllers. It is customary to design a two-time-scale control law, with a fast inner loop to control q, ω_q and a slow outer loop to control u, θ.

The fast inner loop is the ideal PD controller

$$\Gamma_q = -\frac{k_p}{\varepsilon^2} q - \frac{k_d}{\varepsilon} \dot{q} + \frac{k_p}{\varepsilon^2} q_r,$$

where q_r is the desired pitch rate; k_p, k_d are the PD gains and $\varepsilon > 0$ is a "small" parameter. Applying this feedback to (209)-(212) yields

$$\begin{aligned}\dot{u} &= -f_1 u - g\theta \\ \dot{\theta} &= q \\ \varepsilon \dot{q} &= f_4 \tilde{\omega}_q + \mathcal{O}(\varepsilon) \\ \varepsilon \dot{\tilde{\omega}}_q &= -k_p q - f_4 k_d \tilde{\omega}_q + k_p q_r + \mathcal{O}(\varepsilon),\end{aligned}$$

where $\tilde{\omega}_q := \varepsilon \omega_q$. From standard arguments of singular perturbations theory [**44**], the convergence of the fast variables is up to order ε ruled by the well-known coefficient f_4 and the PD gains; and the behavior of the slow variables u, θ is up to order ε ruled by the slow approximation

$$\dot{u} = -f_1 u - g\theta \tag{220}$$

$$\dot{\theta} = q_r. \tag{221}$$

Hence the role of the aerodynamic coefficients f_2, f_3 is marginal is the inner loop is fast enough.

The slow outer loop is the ideal PD controller

$$q_r = k_1 u + k_2 \dot{u} - k_1 u_r,$$

where u_r is the desired velocity, and k_1, k_2 the PD gains. Applying this feedback to (220)-(221) yields

$$\begin{aligned}\dot{u} &= -f_1 u - g\theta \\ \dot{\theta} &= (k_1 - f_1 k_2) u - g k_2 \theta - k_1 u_r,\end{aligned}$$

with characteristic polynomial $s^2 + (f_1 + g k_2) s + g k_1$. A reasonable closed-loop settling time is about $1s$, which requires $g k_1 = 6^2$ and $f_1 + g k_2 = 6\sqrt{2}$. This means $f_1 = 0.25$ is negligible w.r.t to the effect of the controller.

We thus see that the revisited moment model (211) does not rely matter if the gyroscope measurements are good enough for a fast loop, which is usually the case in practice; nevertheless taking into account f_2 and especially f_3 may help to design a better inner loop. As for the force model (209), it does not really matter either, provided a velocity measurement is available. The importance of f_1 is nevertheless paramount to account for the accelerometer measurements, as will be seen in the following sections.

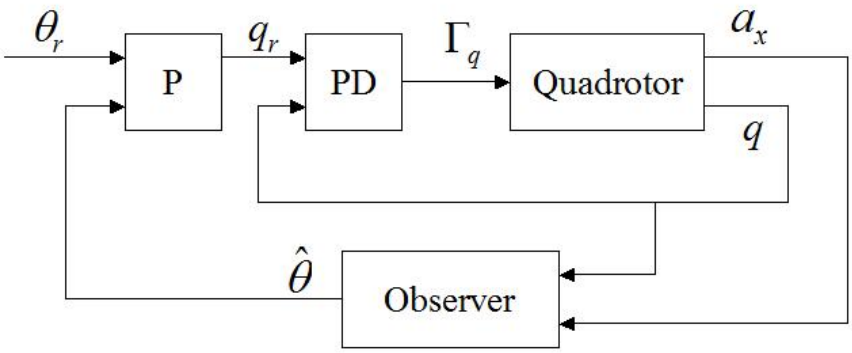

FIGURE 6.7. Traditional interpretation of accelerometer feedback

6.4.2. Traditional interpretation of accelerometer feedback. — Once the inner loop closed, the traditional slow model is

$$\dot{u} = -g\theta$$
$$\dot{\theta} = q_r,$$

with measurement $a_x = g\theta$. Since the velocity u is clearly not observable, the role of the outer loop is simply to control the measured angle θ. In theory the simple proportional feedback $q_r = k(\theta_r - \frac{a_x}{g})$ does the trick, but in practice the accelerometer measurements are too noisy to be directly used (not only because of the intrinsic sensor noise, but also because of mechanical vibrations). Instead an "angle estimator" is often used, based on the model $\dot{\theta} = q$ with measurements $a_x = g\theta$ and $g_y = q$ (see Figure 6.7). A more elaborate estimator, e.g. an EKF or a nonlinear observer, can also be used, see the references in the introduction; it is then based on the nonlinear kinematic equations (203)–(205), and relies on the approximation (215). Whatever the filter, the first-order approximation is essentially the linear observer $\dot{\hat{\theta}} = g_y + l(\frac{a_x}{g} - \hat{\theta})$. The outer loop thus is the controller-observer

$$q_r = k(\theta_r - \hat{\theta}) \tag{222}$$
$$\dot{\hat{\theta}} = q + l\Big(\frac{a_x}{g} - \hat{\theta}\Big). \tag{223}$$

Applied to the traditional model and defining the observation error $e_\theta := \hat{\theta} - \theta$, it yields the closed-loop system

$$\begin{aligned} \dot{u} &= -g\theta \\ \dot{\theta} &= k(\theta_r - \theta - e_\theta) \\ \dot{e}_\theta &= -le_\theta. \end{aligned}$$

For θ_r constant, the last two equations have the unique steady state $(\theta, e_\theta) = (\theta_r, 0)$. The characteristic polynomial is

$$\Delta_0 := (s+k)(s+l),$$

and the closed-loop transfer functions are

$$\theta = \frac{k}{s+k}\theta_r \tag{224}$$

$$u = \frac{-gk}{s(s+k)}\theta_r. \tag{225}$$

Provided $k, l > 0$ we have as desired $(\theta, e_\theta) \to (\theta_r, 0)$, while u grows linearly unbounded. A good tuning of (222)-(223) requires for robustness that the controller and observer act in distinct time scales (Loop Transfer Recovery), i.e. $k \gg l$ or $l \gg k$. We consider in the sequel a "slow" observer, which is representative of commercial "angle sensors" such as the 3DM-GX, and a "fast" controller; for a settling time of about $1s$, we choose e.g. $k := \frac{1}{0.3}$ and $l := \frac{1}{12}$.

We tested this control scheme experimentally, with a rather satisfying result: the angle θ reaches the desired θ_r, though the dynamics is somewhat more sluggish than expected. The traditional analysis could thus be considered as reasonably justified. Nevertheless it does not account for the following experimental observations already visible to the naked eye:

- when pushed away from hovering, the quadrotor returns to hovering (of course at a different position)
- when flying at a constant velocity u, the angle θ is not zero but approximately proportional to u
- in response to a constant θ_r, u does not grow unbounded but reaches a value approximately proportional to θ_r.

Though these experimental facts are well-known to people in the field, they do not seem to be reported in the literature. The discrepancy is usually attributed to the neglected second-order aerodynamical drag and the inevitably unperfect experimental conditions.

Another more subtle discrepancy is that the observer gain l must be smaller than predicted by the theory to avoid a badly damped transient (e.g. $l = 1/3$ does not work well in practice).

As will be seen in the following section, these experimental facts can be explained by the revisited model.

6.4.3. Revisited interpretation of accelerometer feedback. — We now apply the controller-observer (222)-(223) to the revisited longitudinal model. The closed-loop system is now

$$\begin{aligned}\dot{u} &= -f_1 u - g\theta \\ \dot{\theta} &= k(\theta_r - \theta - e_\theta) \\ \dot{e}_\theta &= -l\Big(\frac{f_1}{g}u + \theta + e_\theta\Big),\end{aligned}$$

with $e_\theta := \hat{\theta} - \theta$. For θ_r constant, the only steady state is $(u, \theta, e_\theta) = (-\frac{g}{f_1}\theta_r, \theta_r, 0)$; the characteristic polynomial is

$$\Delta = s^3 + (k + l + f_1)s^2 + f_1(k + l)s + f_1 kl.$$

If $k \gg l$, $\Delta \simeq (s + k)(s^2 + f_1 s + f_1 l)$, so that the closed-loop system is stable as soon as $k, l > 0$. Hence $\theta \to \theta_r$ as desired, and $e_\theta \to 0$ as expected from the observer; u now tends to the finite value $-\frac{g}{f_1}\theta_r$, which is more consistent with experimental tests. If moreover $l \ll f_1$,

$$\Delta \approx (s + f_1)(s + k)(s + l) = (s + f_1)\Delta_0.$$

As a consequence, the closed-loop transfer functions are

$$\begin{aligned}\theta &= \frac{k(s + f_1)(s + l)}{\Delta}\theta_r &&\approx \frac{k}{s + k}\theta_r \\ u &= \frac{-gk(s + l)}{\Delta}\theta_r &&\approx \frac{-gk}{(s + f_1)(s + k)}\theta_r,\end{aligned}$$

to be compared with (224)-(225): the angle dynamics is nearly the same as the one given by the traditional interpretation, while the velocity dynamics is dominated by the rotor drag time constant $\frac{1}{f_1}$. Defining the reference velocity $u_r := -\frac{g}{f_1}\theta_r$, we see the traditional control scheme, designed as an angle controller, is in fact a velocity controller!

The behavior experienced in practice is qualitatively and quantitatively well predicted by the revisited model, see Figure 6.8 ("traditional design") the time response to a $-1.5°$ step in θ_r (i.e. a $1m/s$ step in u_r).

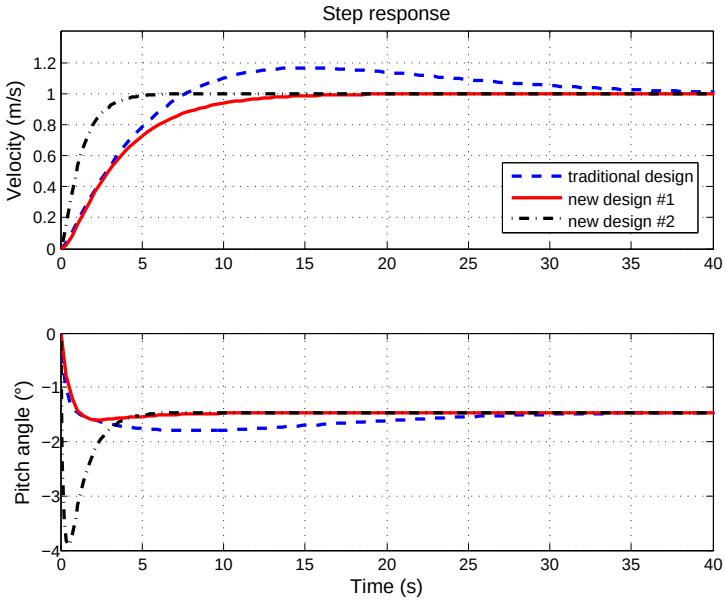

FIGURE 6.8. Comparison between control schemes (simulation).

From this analysis, we see the importance of the coefficient f_1 is paramount: the traditional scheme works reasonably well only because f_1 is positive and not too small.

6.4.4. A better control law. — The performance of the traditional control scheme is limited by the rotor drag time constant $\frac{1}{f_1}$. Better performance can be achieved by considering a controller-observer based on the revisited model (see Figure 6.9),

$$
\begin{aligned}
q_r &= -k_1\hat{u} - k_2\hat{\theta} + \left(k_1 - \frac{f_1 k_2}{g}\right)u_r \\
\dot{\hat{u}} &= -f_1\hat{u} - g\hat{\theta} + l_1(a_x + f_1\hat{u}) \\
\dot{\hat{\theta}} &= g_y + l_2(a_x + f_1\hat{u}),
\end{aligned}
$$

where u_r is the velocity reference; k_1, k_2 are the controller gains, l_1, l_2 the observer gains. Figure 6.8 shows simulation results for the same scenario as before ($1m/s$ reference step in velocity). Two different tunings were used: in the first case ("new design #1") the controller is tuned for a settling time of about $12s$ and the observer for about $48s$, so that the angle and velocity have initial transients similar to the tuning used previously for the traditional design (and with a similar control effort); in the second case ("new design #2")

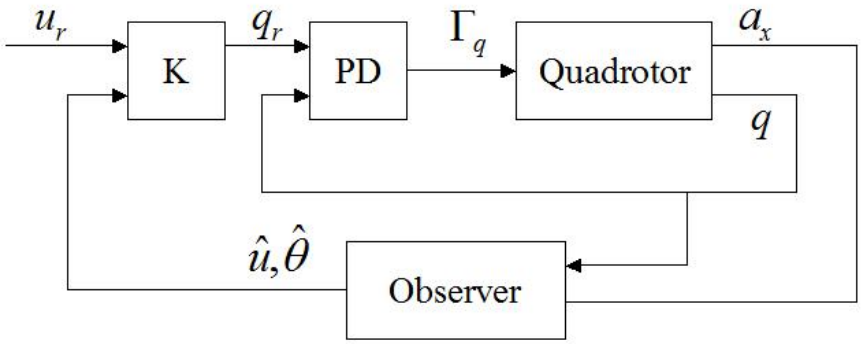

FIGURE 6.9. Controller-observer based on the revisited model

the controller is made four times faster. Both design were successfully implemented, resulting in a quadrotor much easier to fly than with the traditional scheme. In practice it was not really possible to further accelerate the time responses, probably mainly because of the accelerometer noise.

CHAPTER 7

REAL-TIME IMPLEMENTATION AND LOW-COST EMBEDDED PROTOTYPE SYSTEM

Dans ce chapitre nous validons l'implémentation des observateurs génériques invariants pour les "(aided) Attitude and Heading Reference Systems" en temps-réel sur un microcontrôleur bon marché, à savoir un ATmega128 de chez Atmel. Nous mettons ainsi en évidence une autre propriété très interessante de ces estimateurs par rapport aux techniques de filtrage habituelles: ils sont très économiques en temps de calcul, et donc tout-à-fait adaptés à la problématique des mini-drones. Dans ce chapitre, nous présentons et validons également notre propre système avionique bas-coûts, composé de capteurs "bruts" et du microcontrôleur sur lequel sont implantés les observateurs invariants. Nous donnons l'architecture du code permettant l'interface avec les différents capteurs, l'estimation des variables et l'envoi des estimées via un port série.

7.1. Real-time implementation on a cheap microcontroller

7.1.1. Real-time implementation of invariant observers for AHRS. — In Chapter 3 we developed an invariant nonlinear observer for AHRS. We validated it by using measurements from a commercial navigation system (MIDG II from Microstrain in Vertical Gyro mode) and by implementing the estimator algorithm (see Equations (82)–(85))

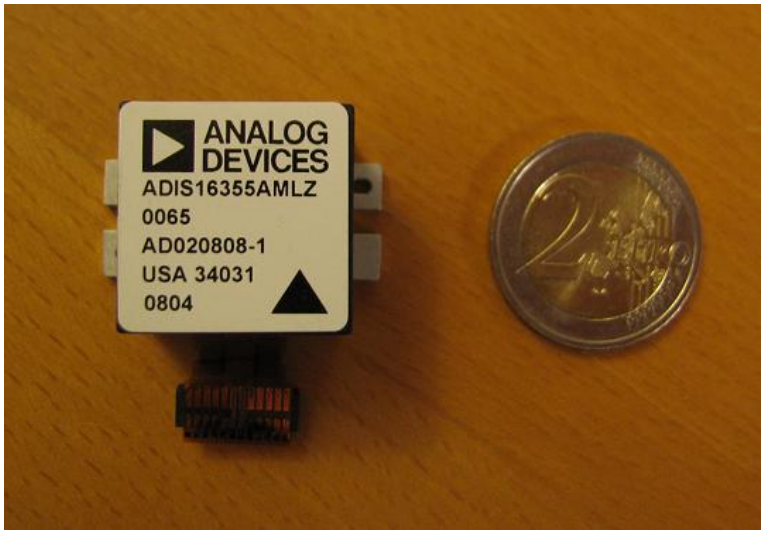

FIGURE 7.1. ATmega128 from Atmel

on Matlab. Then we compared our estimations and the estimations given by the MIDG II, which were very similar. Since the avionics system needs to meet the requirements described in Chapter 1.2, the observer needs to be implemented on a low-cost computational board.

Therefore, we have implemented the algorithm on a low-cost microcontroller Atmel ATmega128 (see Figure 7.1) with the following main characteristics (for further details, see [**4**]):

- 8-bit microcontroller
- a cost of 5€
- a clock frequency up to 16MHz
- computations done in integer (no floating point coprocessor)
- 128K bytes of reprogrammable flash
- 4K bytes of SRAM

It is important to notice that it is impossible to run an usual filtering algorithm (such as an extended Kalman filter) on such a microntroller while getting the estimates at a high update rate (greater than 50Hz). On the contrary, our observers are well adapted to it.

Since we want to validate only the algorithm itself, we use the ATmega128 on its development kit STK500/501 for simplicity in the "hardware" interfacing. Indeed, all the

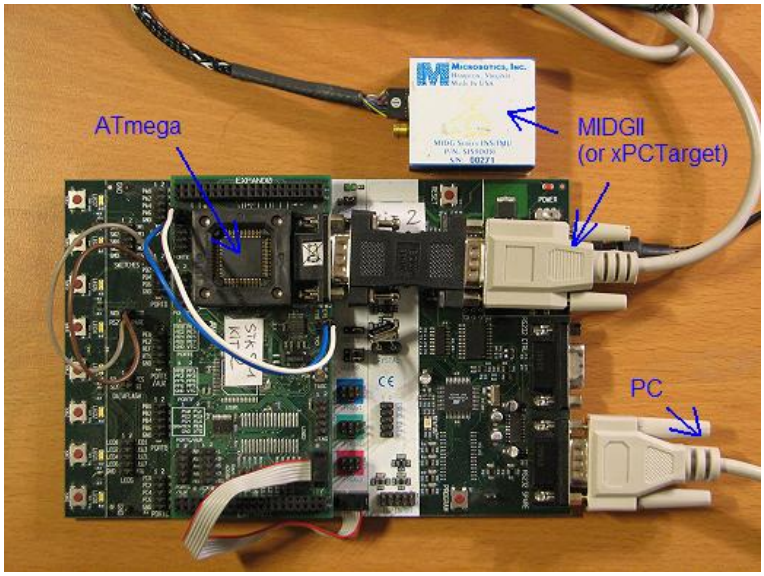

FIGURE 7.2. Experimental protocol

pins are easily accessible and a TTL/RS232 converter (i.e. microcontroller/PC serial port) is built-in. The computations of Equations (82)–(85) are done in C with the standard floating point emulation. We have used a simple Euler explicit approximation for the integration scheme.

The experimental protocol was the following:

1. move the sensors in all directions and save on a computer the MIDG II raw measurements and estimations at 50Hz.
2. use of xPCTarget to feed the ATmega with these data at 50Hz via a serial port and send to a computer at 50Hz the estimated variables given by the microcontroller.
3. save these estimates.
4. compare offline the estimations given by the microcontroller and those given by the observer written in the Matlab embedded function.

This protocol can be illustrated by the figure 7.2, where the computer with xPCTarget has been replaced by the MIDG II. We use xPCTarget instead of feeding directly the microcontroller with the MIDG II raw data because it allows us to run different algorithms on the microcontroller with the same set of data (e.g. in order to do some corrections in the C code).

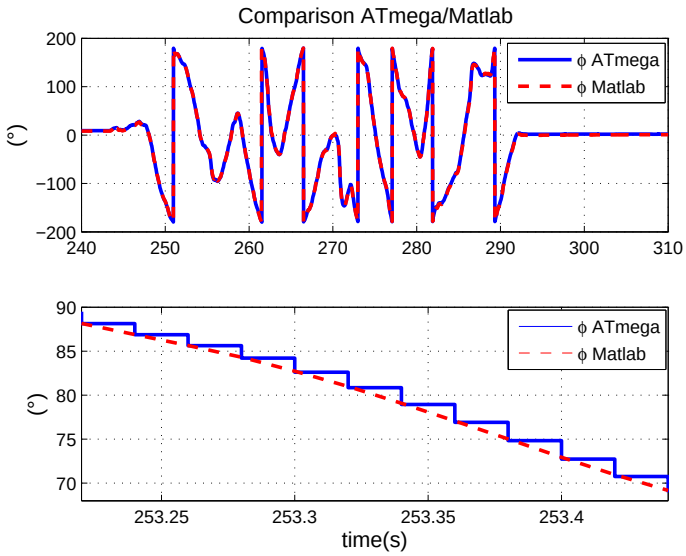

FIGURE 7.3. Comparison ATmega/Matlab

We obtain the results displayed on Figure 7.3. The two estimations are very similar, which validates the real-time implementation of the invariant observer. Notice that we see on the bottom plot of Figure 7.3 the discretization at 50Hz due to the microcontroller.

7.1.2. Real-time implementation of invariant observers for aided AHRS. — We want to validate the real-time implementation of the invariant observers for aided AHRS developed in Chapter 4 on a cheap microcontroller. Since the validation method is very similar for the three kinds of observers described in Chapter 4, we only detail the experimental protocol corresponding to the AHRS aided by Earth-fixed velocity and position measurements (see 4.2). We use the MIDG II to get the inertial, velocity and position measurements and the barometer module MS5534B from Intersema to get the altitude. We implement the equations of the invariant observer (131)–(136) on the ATmega128, as we did in section 7.1.1.

To validate the algorithm, the experimental protocol was the following:

1. move the sensors in all directions and save on a computer the MIDG II inertial raw measurements and estimations at 50Hz, the MIDG II velocity and position raw

measurements (from its GPS engine) at 4 Hz and the Intersema altitude measurement at 12.5 Hz

2. use of xPCTarget to feed the ATmega128 with these data via a serial port and send to a computer at 50Hz the estimated variables given by the microcontroller.
3. save these estimates.
4. compare offline the estimations given by the microcontroller and those given by the observer written in the Matlab embedded function.

This protocol can be illustrated by Figure 4.6. The results are the same as in section 7.1.1: the estimations given by our algorithm and those provided by the MIDG II are very similar, which validates the real-time implementation of the invariant observer.

7.2. Low-cost embedded avionics system

7.2.1. Creation of the sensors card. — In the preceding chapters, we validated the invariant observers using raw measurements provided by the commercial navigation system (MIDG II). Even if this commercial system is small enough to be embedded on a mini-UAV, using it only to get inertial, magnetic and GPS measurements is not the best way to develop our own low-cost avionics system. Indeed, this approach suffers several drawbacks

- most of the price of the commercial device is in the filtering algorithm itself, and we want to replace it by our own invariant observer
- the estimations rate provided by our algorithm is limited by the raw measurements rate of the commercial AHRS
- we do not know the specifications of the used sensors, and we cannot change them

The next step to build our low-cost avionics system is to use our own inertial and magnetic sensors. Therefore we create a "Sensors Card" (see Figure 14(a)), which contains a tri-axial inertial sensor (ADIS16355 from Analog Devices), and a tri-axial magnetometer (Micromag3 from PNI). We also added on the same card the barometric module (MS5534B from Intersema). The GPS module is still off this card, but it can be easily inserted on it. Each kind of sensors has his own specifications (communication protocol, dimensions, voltage...), as we detailed it in Chapter 1.3.

As illustrated by Figure 7.5, we use one single ATmega128 microcontroller

- to interface with all the sensors
- to run the invariant observer algorithm at a 65Hz rate

FIGURE 7.4. Sensors card

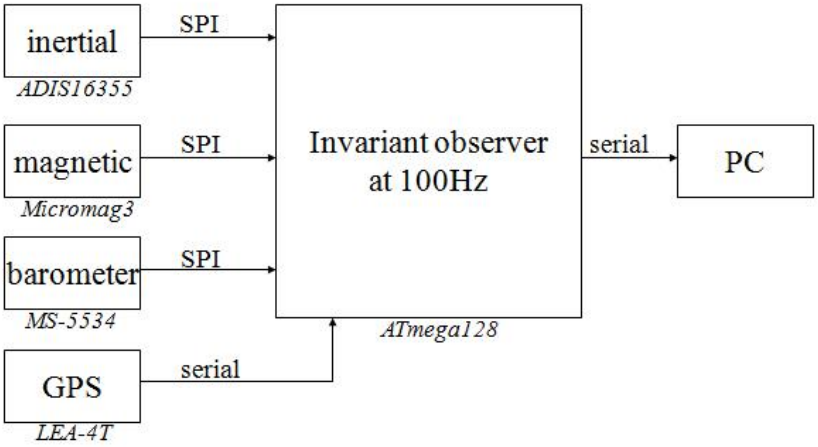

FIGURE 7.5. Several tasks of the central microcontroller

– to send the estimations at a 65Hz rate to a computer via a serial port

The Figures 7.6 and 7.7 summarize the code implemented on the microcontroller. It gives an overview of the structure of the code:

– *main loop*: contains the invariant observer algorithm, called every 65Hz

– *interruptions*: called when the corresponding external event arises (e.g. when the microcontroller receives data from the serial port for the GPS or the SPI port for the inertial sensor)
– *initializations*: called at the beginning of the program to set the configuration of the used registers (e.g. to set the baudrate of the serial port)

Since the microcontroller needs to interface with different peripherals with different protocol with a clock frequency of only 14.745MHz, it is really crucial that the filtering algorithm is computationally economic to get estimates at a high update rate (100 Hz). As we illustrated it in Section 7.1, it is the case for the invariant observers we propose in this thesis. It is in fact even one of the motivation of developing this kind of filters. For simplicity, we still use the microcontroller on its development kit STK500/501 (see Figure 7.8).

7.2.2. Validation of the invariant observer for AHRS. — In order to validate the invariant nonlinear observer for AHRS developed in Chapter 3 (see Equations (82)–(85)) with our own sensors, we feed the microcontroller with the raw measurement provided by the sensors card. Since this algorithm does not consider velocity and position measurements, we do not use the GPS and the barometric modules. As shown on Figure 7.9, we put the our system and the MIDG II very close, and we move them in all directions. We save the estimations given by our system and those given by the MIDG II on a computer to compare them. On Figure 7.10 we see that the two estimations are very similar, which validates our avionics system, i.e. the implemented invariant filter and the sensors card. On Figure 7.10(b), we notice the discretization at 100Hz.

The Figure 7.11 gives an idea of the time to run the observer equations. Indeed, we put a flag in the code that sets the corresponding output pin at a low level at the beginning of the observer code and sets it at a high level at the end. On Figure 7.11 we measure a 10ms period of the signal, which corresponds to the 100Hz update rate. Since the filtering algorithm only uses 28% of the allowed time (i.e. 2.8ms of the 10ms), it shows that the implemented invariant observer is computationally really efficient. It saves time and computational power to run the rest of the code: sending the estimates to a PC via a serial port or running the control algorithm.

7.2.3. Validation of the invariant observer for aided AHRS. — In order to validate the invariant nonlinear observer for aided AHRS developed in Chapter 4 (see Equations (131)–(136)) with our own sensors, we feed the microcontroller with the raw measurement provided by the sensors card and the GPS module. As in Section 7.2.2, we

```
// Include and definitions

#include <avr/interrupt.h>
#define LED0on (PORTC &= ~_BV(0))
#define CStri_is_on (!(PORTB & _BV(7)))
#define Do_Xgyro 0
#define X_axis_finished (!(refreshing & _BV(0)))
#define SPIF_bas (!(SPSR & _BV(SPIF)))

// Global variables

volatile uint8_t      tab_nboctet[]={21,3,3};
volatile uint8_t      tab_octet[]={0x05,0x0F,(1| _BV(5) |_BV(4))};
volatile uint8_t      tx_head,tx_tail,tx_buf[ TX_BUF_SIZE ];

// Fonctions Inline

inline float rotation0 (float Q[],float V0,float V1,float V2)
{ return ((float)((Q[0]*Q[0]+Q[1]*Q[1]-Q[2]*Q[2]-Q[3]*Q[3])*V0+2*(Q[1]*Q[2]-
Q[0]*Q[3])*V1+2*(Q[0]*Q[2]+Q[1]*Q[3])*V2));
}

// Fonctions for data transmission to the ground station

void USART1_Transmission_Init(void)
{
   UCSR1B |= _BV(TXEN);                    // Enables the USART1 interruption
         UBRR1L = 7;                                          // 115200 bauds at 14.7456MHz
}
ISR( SIG_UART1_DATA ) // Interruption when the register is empty
{
uint8_t    tmp_tail;
tmp_tail = tx_tail + 1;
UDR1 = tx_buf[tmp_tail];
}

// Fonctions to communicate with the sensors

void SPI_MasterInit(void) // Initialization for the SPI comm and the tri-axis
{
         DDRB |= _BV(5) | _BV(4) | _BV(2) | _BV(1) | _BV(0) | _BV(7);    // MOSI, SCLK and CS as Output
         DDRB &= ~_BV(3);        // MISO as Input
         SPCR &= ~_BV(CPOL);
}
void Domeasure_mag_init(void)  // Initialization for the magnetometers
{
         spi_buf[(uint8_t)(spi_head+1)]=Do_X_axis;
         spi_head++;
         measured_axis=Do_X_axis;
}
void Domeasure_word_intersema_init(void)   // Initialization for the barometer
{
         spi_buf[(uint8_t)(spi_head+1)]=Reset_inter;
}

ISR (SIG_SPI)  // Communication with the sensors via the SPI protocol
{
         SPCR |= _BV(CPOL) | _BV(CPHA);
         SPDR = (tab_octet[spi_buf[spi_tail]]&~_BV(6) & ~_BV(7));
}
```

```
ISR( SIG_UART0_RECV ) // Communication with the GPs module via the serial port
{
        volatile char                   c = UDR0;
        static uint8_t          bytecounter_ublox;
  bytecounter_ublox++;
        if (bytecounter_ublox==(rx_buf_ublox[2]+8))
                {rx_buf_ublox[bytecounter_ublox-3]=c;}
}

// Timer interruption at 65Hz

ISR( SIG_OUTPUT_COMPARE1A)
{
        spi_buf[(uint8_t)(spi_head+1)]=Do_Xgyro;
        spi_head++;
        do_algo=1;
}

// Main alogithm

int main(void)
{

// Functions and ports initialization
USART1_Transmission_Init();
SPI_MasterInit();
DDRC = 0xFF;  // Leds on PORTC
PORTC=255;  // Leds off at the beginning
OCR1A = 288;   // timer interruption at 65Hz

// Local variables
static float q[4];        // quaternion
q[0]=1,q[1]=0,q[2]=0,q[3]=0;
static float v[4];        // velocity
float lv=4e-2f,lb=1e-3f;   // gains

while(1) // main loop
        {
        if (do_algo==1) // Every 65Hz
        {
                // Error vectors
                Ev[0]=v[0]-1.0e-2f*(float)(tmp_int16[0]);
                Eb[0]=vecteur_b[0]-2.0e-
4f*(rotation0(q,(float)(tmp_int16[0]),(float)(tmp_int16[1]),(float)(tmp_int16[2])));
                Eh=p[2]-hb+0*(1e-2f*(float)(tmp_int16[2]));

                // Ia vector creation
                Ia[0]=9.81e-3f/as*rotation0(q,(float)(tmp_int16[0]),(float)(tmp_int16[1]),(float)(tmp_int16[2]));

                // State update
                q[0]=tmp_quat[0]+.02f*(.5f*(prod_pq0(tmp_quat,omega_quat))+(prod_pq0(lvpbh,tmp_quat))
                v[0]=tmp_v[0]+.02f*(vecteur_a[0]+Ia[0]+mvpbh[0]);

                // Send data to the ground station
                tx_buf[1] = 250; // Header 1
                tx_buf[2] = (uint8_t)(v[0]);
                UCSR1B |= _BV(UDRIE1);
        }
        }
}
```

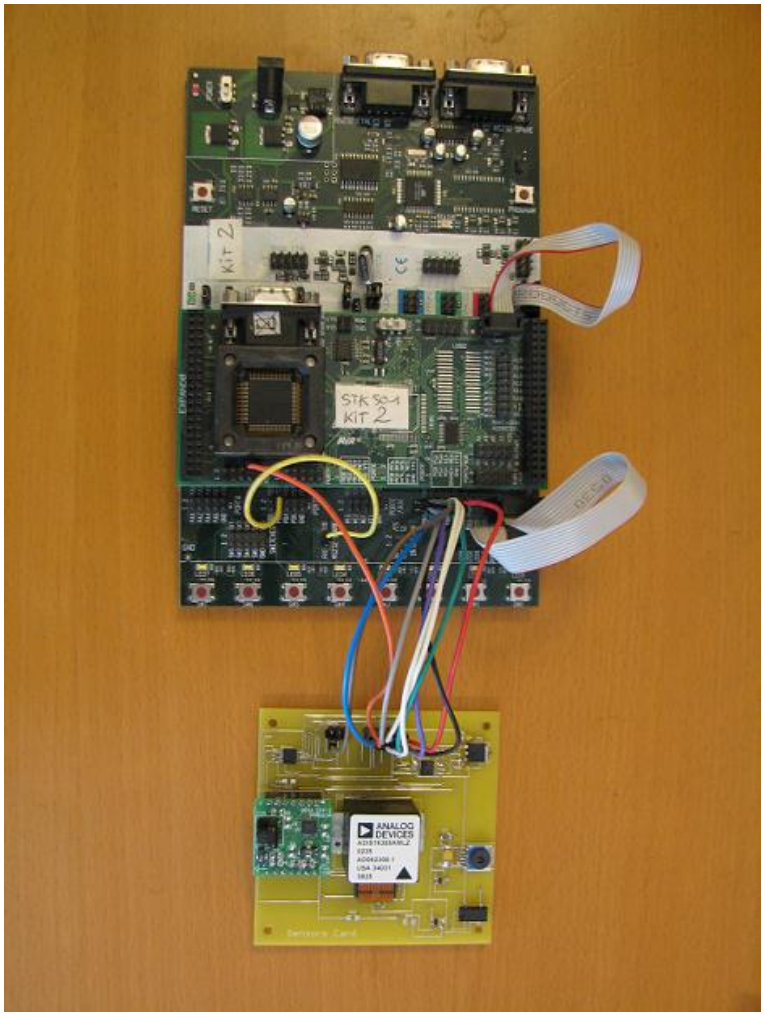

FIGURE 7.8. Interfacing the ATmega128 with the sensors card

put the our system and the MIDG II very close (see Figure 7.12), and we move them in all directions. We save the estimations given by our system and those given by the MIDG II on a computer to compare them. As in the preceding experiment, the two estimations are very similar, which validates our avionics systems with the invariant observer desribed by Equations (131)–(136). The Figure 7.13 gives an idea of the time to run the observer equations using the same method as in section 7.2.2. The filtering algorithm only uses around 53% of the allowed time (i.e. 5.3ms of the 10ms), which shows again that the implemented invariant observer is computationally really efficient.

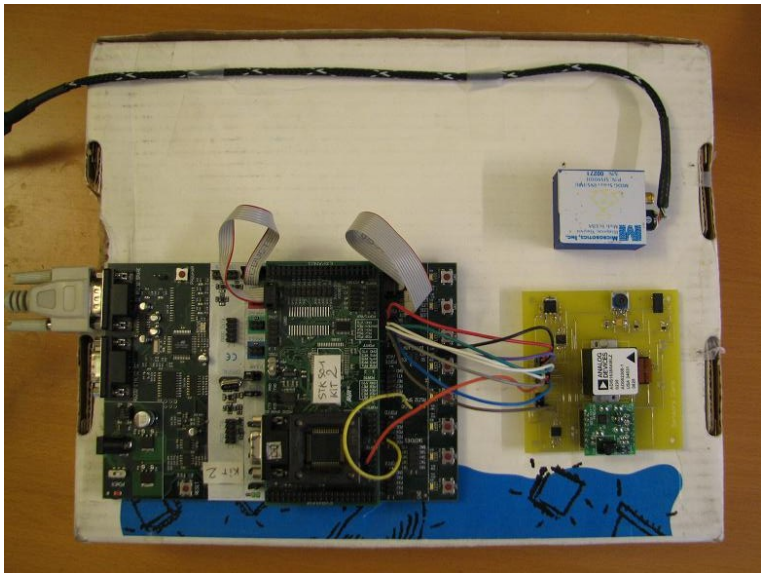

FIGURE 7.9. Experimental setup (AHRS)

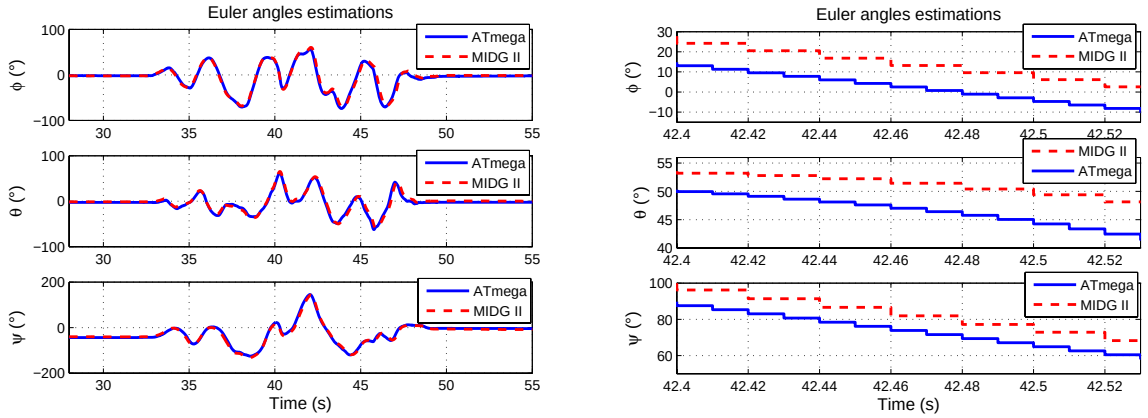

(a) Long experiment

(b) Zoomed view

FIGURE 7.10. Comparison of our avionics system and the MIDG II estimations (AHRS)

7.2.4. Low-cost embedded avionics system. — The last step before having a really embedded system is to replace the development kit STK500/501 of the microcontroller ATmega128 (see Figures 7.9 and 7.12). Indeed, this development kit is is big, heavy, ant most of the electronics on it are not used in our system. Therefore we replace it by

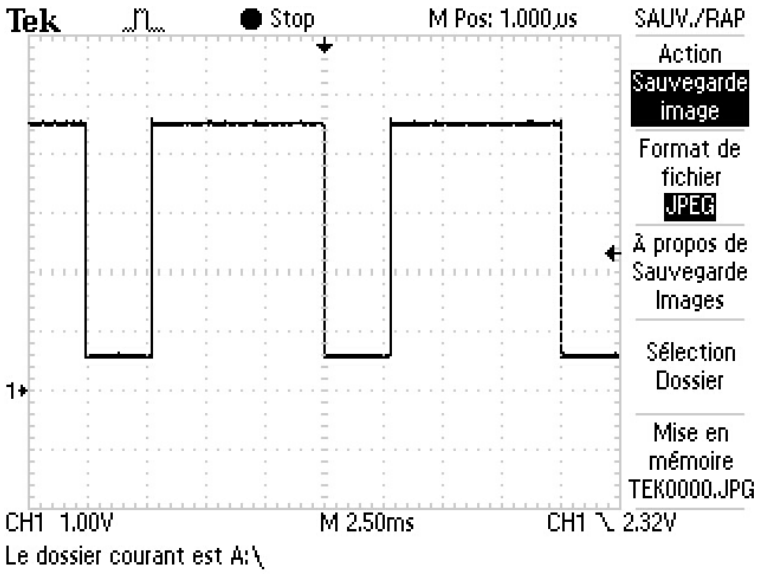

FIGURE 7.11. Time needed for the filtering algorithm (AHRS)

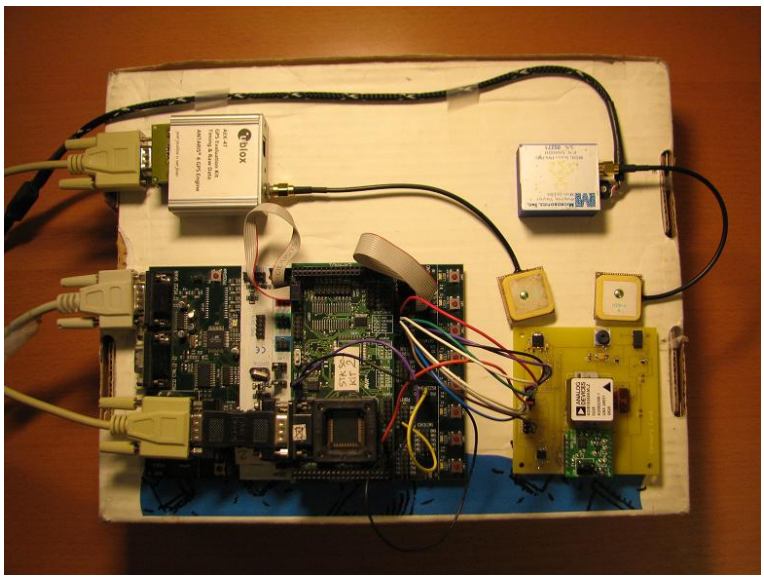

FIGURE 7.12. Experimental setup (aided AHRS)

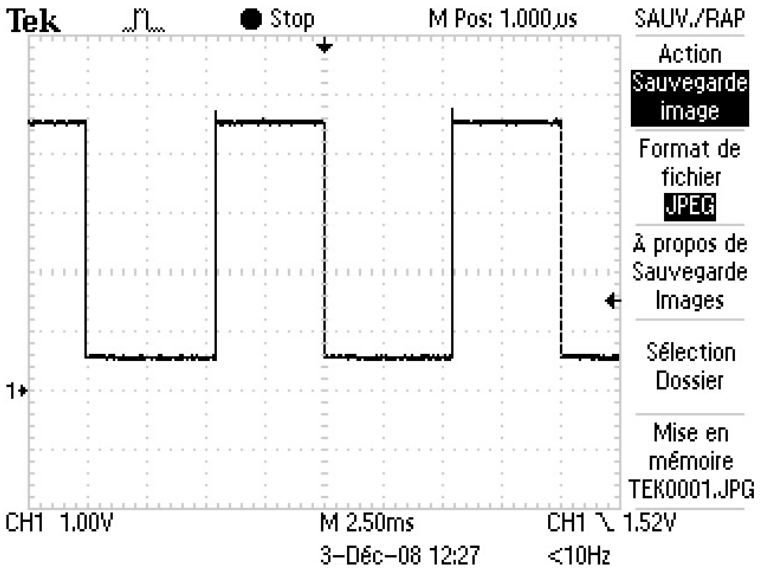

FIGURE 7.13. Time needed for the filtering algorithm (aided AHRS)

our own "microcontroller card", which contains the ATmega128 microcontroller and the necessary hardware for interfacing the other parts of the avionics system (the sensors and the communication devices. On Figure 7.14 we present the two main parts of our low-cost embedded avionics system:

- the "sensors card" with the accelerometers, the gyroscopes, the magnetometers and the barometer. A GPS module is also connected if needed (see Figure 7.14(a)).
- the "microcontroller card" with the ATmega128, which does the interface with the various sensors, runs the algorithm, and sends the estimates at a 100Hz update rate (see Figure 7.14(b)).

This avionics system can be easily embedded on most of the mini-UAVs.

(a) Sensors card

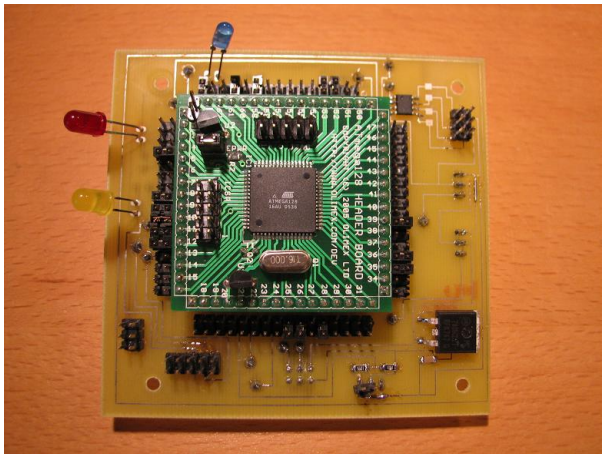

(b) Microcontroller card

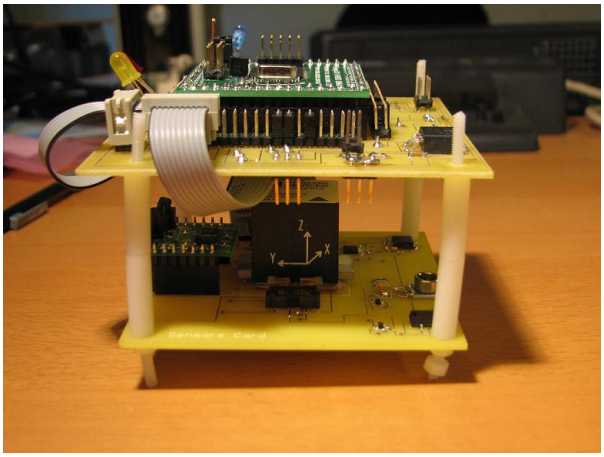

(c) Avionics system

FIGURE 7.14. Low-cost embedded avionics system

BIBLIOGRAPHY

[1] M. Achtelik, A. Bachrach, R. He, S. Prentice, and N. Roy, "Autonomous Navigation and Exploration of a Quadrotor Helicopter in GPS-denied Indoor Environments," in *Robotics: Science and Systems Conference*, 2008.

[2] ——, "Stereo vision and laser odometry for autonomous helicopters in GPS-denied indoor environments," in *Proc. of SPIE Conference on Unmanned Systems Technology*, 2009.

[3] A. Alcocer, P. Oliveira, A. Pascoal, R. Cunha, and C. Silvestre, "A dynamic estimator on SE (3) using Range-Only measurements," in *Proc. of the 47th IEEE Conf. on Decision and Control*, 2008, pp. 2302–2307.

[4] Atmel, "ATmega128(L) Datasheet," User manual, http://www.atmel.com/dyn/resources/prod_documents/doc2467.pdf.

[5] G. Baldwin, R. Mahony, J. Trumpf, T. Hamel, and T. Cheviron, "Complementary filter design on the special euclidean group SE(3)," in *Proc. of the 2007 European Control Conference*, 2007, pp. 3763–3770.

[6] I. Bar-Itzhack and N. Berman, "Control theoretic approach to inertial navigation systems," *Journal of Guidance, Control and Dynamics*, vol. 11, no. 3, pp. 237–245, 1988.

[7] A. Benallegue, A. Mokhtari, and L. Fridman, "High-order sliding-mode observer for a quadrotor UAV," *International Journal of Robust and Nonlinear Control*, vol. 18, pp. 427–440, 2008.

[8] J. Bijker and W. Steyn, "Kalman filter configurations for a low-cost loosely integrated inertial navigation system on an airship," *Control Engineering Practice*, vol. 16, no. 12, pp. 1509–1518, 2008.

[9] S. Bonnabel, "Left-invariant extended Kalman filter and attitude estimation," 2007, pp. 1027–1032.

[10] S. Bonnabel, P. Martin, and P. Rouchon, "A non-linear symmetry-preserving observer for velocity-aided inertial navigation," in *Proc. of the 2006 American Control Conference*, 2006, pp. 2910–2914.

[11] ——, "Non-linear observer on Lie group for left-invariant dynamics with right-left equivariant output," in *Proc. of the* 17*th IFAC World Congress*, 2008, pp. 8594–8598.

[12] ——, "Symmetry-preserving observers," *IEEE Trans. Automat. Control*, vol. 53, no. 11, pp. 2514–2526, 2008.

[13] ——, "Non-linear symmetry-preserving observers on Lie groups," *IEEE Trans. Automat. Control*, To appear in 2009, preliminary version http://arxiv.org/abs/0707.2286.

[14] S. Bonnabel, P. Martin, and E. Salaün, "Invariant Extended Kalman Filter: theory and application to a velocity-aided attitude estimation problem," in *Proc. of the* 48*th IEEE Conf. on Decision and Control*, 2009, pp. 1297–1304.

[15] S. Bouabdallah, A. Noth, and R. Siegwart, "Pid vs lq control techniques applied to an indoor micro quadrotor," in *Proc. of the 2004 IEEE/RSJ International Conference on Intelligent Robots and Systems*, vol. 3, 2004, pp. 2451–2456.

[16] S. Bouabdallah and R. Siegwart, "Full control of a quadrotor," in *Proc. of the 2007 IEEE/RSJ International Conference on Intelligent Robots and Systems*, 2007, pp. 153–158.

[17] P.-J. Bristeau, P. Martin, E. Salaün, and N. Petit, "The role of propeller aerodynamics in the model of a quadrotor UAV," in *Proc. of the 2009 European Control Conference*, 2009, pp. 683–688.

[18] R. Brockett, "Remarks on finite dimensional nonlinear estimation," *Astersique*, vol. 75-76, pp. 47–55, 1980.

[19] J. Carpenter and I. Bar-Itzhack, "On the commonality between Schuler-period in terrestrial INS and LEO satellites," in *Proc. of the 2004 AIAA/AAS Astrodynamics Specialist Conference and Exhibit*, 2004, pp. 4850–4858.

[20] P. Castillo, A. Dzul, and R. Lozano, "Real-time stabilization and tracking of a four-rotor mini rotorcraft," *IEEE Trans. Control Systems Technology*, vol. 12, no. 4, pp. 510–516, 2004.

[21] Y. Cheng and J. Crassidis, "Particle filtering for sequential spacecraft attitude estimation," in *Proc. of the 2004 AIAA Guidance, Navigation, and Control Conference*, 2004, pp. 5337–5354.

[22] D. Choukroun, "Adaptative optimal-REQUEST algorithm for attitude determination," in *Proc. of the 2007 AIAA Guidance, Navigation, and Control Conference*, 2007, pp. 6813–6837.

[23] R. Collinson, *Introduction to avionics systems*, 2nd ed. Kluwer Academic Publishers, 2003.

[24] J. Crassidis, "Sigma-point Kalman filtering for integrated GPS and inertial navigation," *IEEE Trans. on Aerospace and Electronic Systems*, vol. 42, no. 2, pp. 750–756, 2006.

[25] J. Crassidis and F. Markley, "Unscented filtering for spacecraft attitude estimation," *Journal of Guidance, Control and Dynamics*, vol. 26, no. 4, pp. 536–542, 2003.

[26] J. Crassidis, F. Markley, and Y. Cheng, "Survey of nonlinear attitude estimation methods," *Journal of Guidance, Control and Dynamics*, vol. 30, no. 1, pp. 12–28, 2007.

[27] L. Derafa, T. Madani, and A. Benallegue, "Dynamic modelling and experirnental identification of four rotors helicopter pararmeters," in *Proc. of the 2006 IEEE International Conference on Industrial Technology*, 2006, pp. 1834–1839.

[28] J. Farrell and M. Barth, *The global positioning system and inertial navigation.* McGraw-Hill, 1998.

[29] F. Faruqi and K. Turner, "Extended Kalman filter synthesis for integrated global positioning/inertial navigation systems," *Applied Mathematics and Computation*, vol. 115, no. 2-3, pp. 213–227, 2000.

[30] D. Gleason and A. Hanscom, "Critical role of gravity compensation in a stand-alone precision INS," in *Proc. of the 2003 DARPA Precision Inertial Navigation Systems Meeting*, 2003.

[31] M. Grewal, L. Weill, and A. Andrews, *Global positioning systems, inertial navigation, and integration*. Wiley, 2001.

[32] P. D. Groves, *Principles of GNSS, inertial, and multisensor integrated navigation systems*. Artech House, 2008.

[33] N. Guenard, T. Hamel, and R. Mahony, "A practical visual servo control for an unmanned aerial vehicle," *IEEE Trans. on Robotics*, vol. 24, no. 2, pp. 331–340, 2008.

[34] N. Guenard, T. Hamel, and V. Moreau, "Dynamic modeling and intuitive control strategy for an "X4-flyer"," in *Proc. of the 2005 International Conference on Control and Automation*, 2005, pp. 141–146.

[35] T. Hamel and R. Mahony, "Attitude estimation on $SO(3)$ based on direct inertial measurements," in *Proc. of the 2006 IEEE International Conference on Robotics and Automation*, 2006, pp. 2170–2175.

[36] B. Herisse, F. Russotto, T. Hamel, and R. Mahony, "Hovering flight and vertical landing control of a VTOL Unmanned Aerial Vehicle using Optical Flow," in *Proc. of the 2008 IEEE/RSJ International Conference on Intelligent Robots and Systems*, 2008, pp. 801–806.

[37] C. Hide, T. Moore, and M. Smith, "Adaptive Kalman filtering for low-cost INS/GPS," *The Journal of Navigation*, vol. 56, no. 01, pp. 143–152, 2003.

[38] ——, "Adaptive Kalman filtering algorithms for integrating GPS and low cost INS," in *Proc. of the Position Location and Navigation Symposium*, 2004, pp. 227–233.

[39] G. Hoffmann, D. Rajnarayan, S. Waslander, D. Dostal, J. Jang, and C. Tomlin, "The stanford testbed of autonomous rotorcraft for multi agent control (starmac)," in *Proc. of the 2004 Digital Avionics Systems Conference*, vol. 2, 2004.

[40] G. Hoffmann, H. Huang, S. Waslander, and C. Tomlin, "Quadrotor helicopter flight dynamics and control: Theory and experiment," in *Proc. of the 2007 AIAA Guidance, Navigation, and Control Conference*, 2007, pp. 6461–6480.

[41] Y. Huang, F. Chang, and L. Wang, "The attitude determination algorithm using integrated GPS/INS data," in *Proc. of the* 16*th IFAC World Congress*, 2005.

[42] W. Johnson, *Helicopter Theory.* Princeton University Press, 1980.

[43] F. Kendoul, D. Lara, I. Fantoni-Coichot, and R. Lozano, "Real-time nonlinear embedded control for an autonomous quadrotor helicopter," *Journal of Guidance, Control and Dynamics*, vol. 30, no. 4, pp. 1049–1061, 2007.

[44] P. Kokotovic, H. K. Khalil, and J. O'Reilly, *Singular Perturbation Methods in Control: Analysis and Design.* SIAM, 1999.

[45] A. Krener, *Algebraic and Geometric Methods in Nonlinear Control Theory.* D. Reidel Publishing Company, 1986, ch. The intrinsic geometry of dynamic observations, pp. 77–87.

[46] C. Lageman, R. Mahony, and J. Trumpf, "State observers for invariant dynamics on a Lie group," in *Proc. of the International Conference on the Mathematical Theory of Networks and Systems*, 2008.

[47] C. Lageman, J. Trumpf, and R. Mahony, "Gradient-like observers for invariant dynamics on a Lie group," *IEEE Trans. Automat. Control*, 2008.

[48] ——, "Observer design for invariant systems with homogeneous observations," *Arxiv preprint arXiv:0810.0748*, 2008.

[49] E. Lefferts, F. Markley, and M. Shuster, "Kalman filtering for spacecraft attitude," *Journal of Guidance, Control and Dynamics*, vol. 5, no. 5, pp. 417–429, 1982.

[50] Y. Li, J. Wang, C. Rizos, P. Mumford, and W. Ding, "Low-cost tightly coupled GPS/INS integration based on a nonlinear Kalman filtering design," in *Proc. of ION National Technical Meeting*, 2006, pp. 18–26.

[51] T. Madani and A. Benallegue, "Backstepping control with exact 2-sliding mode estimation for a quadrotor unmanned aerial vehicle," in *Proc. of the 2007 IEEE/RSJ International Conference on Intelligent Robots and Systems*, 2007, pp. 141–146.

[52] R. Mahony, T. Hamel, and J.-M. Pfimlin, "Nonlinear complementary filters on the special orthogonal group," *IEEE Trans. Automat. Control*, vol. 53, no. 5, pp. 1203–1218, 2008.

[53] R. Mahony, T. Hamel, and J. Pflimlin, "Complementary filter design on the special orthogonal group SO (3)," in *Proc. of the 2005 European Control Conference*, 2005, pp. 1477–1484.

[54] D. Maithripala, J. Berg, and W. Dayawansa, "An intrinsic observer for a class of simple mechanical systems on a lie group," in *Proc. of the 2004 American Control Conference*, vol. 2, 2004, pp. 1546–1551.

[55] ——, "Almost-global tracking of simple mechanical systems on a general class of lie groups," *IEEE Trans. Automat. Control*, vol. 51, no. 1, pp. 216–225, 2006.

[56] D. Maithripala, W. Dayawansa, and J. Berg, "Intrinsec observer-based stabilization for simple mechanical systems on Lie groups," *SIAM J. Control and Optim.*, vol. 44, pp. 1691–1711, 2005.

[57] S. Marcus, "Algebric and geometric methods in nonlinear filtering," *SIAM J. Control Optimization*, vol. 22, pp. 817–844, 1984.

[58] F. Markley, "Attitude error representations for kalman filtering," *Journal of Guidance, Control and Dynamics*, vol. 26, no. 2, pp. 311–317, 2003.

[59] P. Martin and E. Salaün, "The True Role of Accelerometer Feedback in Quadrotor Control," in *Proc. of the 2009 IEEE International Conference on Robotics and Automation*, pp. 1623–1629.

[60] ——, "Invariant observers for attitude and heading estimation from low-cost inertial and magnetic sensors," in *Proc. of the 46th IEEE Conf. on Decision and Control*, 2007, pp. 1039–1045.

[61] ——, "Design and implementation of a low-cost aided attitude and heading reference system," in *Proc. of the 2008 AIAA Guidance, Navigation, and Control Conference*, 2008, pp. 7169–7187.

[62] ——, "Design and implementation of a low-cost attitude and heading nonlinear estimator," in *Proc. of the 5th International Conference on Informatics in Control, Automation and Robotics*, 2008, pp. 53–61.

[63] ——, "A general symmetry-preserving observer for aided attitude heading reference systems," in *Proc. of the 47th IEEE Conf. on Decision and Control*, 2008, pp. 2294–2301.

[64] ——, "An invariant observer for Earth-velocity-aided attitude heading reference systems," in *Proc. of the 17th IFAC World Congress*, 2008, pp. 9857–9864.

[65] ——, "An embedded attitude and heading reference system based on a nonlinear filter," *Lecture Notes in Electrical Engineering*, vol. 37, pp. 267–281, 2009.

[66] ——, "Design and implementation of a low-cost observer-based attitude and heading reference system," *Control Engineering Practice*, vol. 18, no. 7, pp. 712–722, 2010.

[67] N. Metni, J.-M. Pflimlin, T. Hamel, and P. Souères, "Attitude and gyro bias estimation for a VTOL UAV," *Control Engineering Practice*, vol. 14, no. 12, pp. 1511–1520, 2006.

[68] A. Neff, D. Lee, V. Chitrakaran, D. Dawson, and T. Burg, "Velocity control for a quad-rotor uav fly-by-camera interface," in *Proc. of the IEEE SoutheastCon*, 2007, pp. 273–278.

[69] R. Nelson, *Flight stability and automatic control*. McGraw-Hill College, 1989.

[70] Y. Oshman and A. Carmi, "Attitude estimation from vector observations using genetic-algorithm-embedded quaternion particle filter," *Journal of Guidance Control and Dynamics*, vol. 29, no. 4, pp. 879–891, 2006.

[71] P. Pounds, T. Hamel, and R. Mahony, "Attitude control of rigid body dynamics from biased imu measurements," in *Proc. of the 46th IEEE Conf. on Decision and Control*, 2007, pp. 4620–4625.

[72] P. Pounds, R. Mahony, and P. Corke, "Modelling and control of a quad-rotor robot," in *Proc. of the 2006 Australasian Conference on Robotics and Automation*, 2006.

[73] H. Rehbinder and B. Ghosh, "Pose estimation using line-based dynamic vision and inertial sensors," *IEEE Trans. Automat. Control*, vol. 48, no. 2, pp. 186–199, 2003.

[74] S. Salazar-Cruz, J. Escareño, D. Lara, and R. Lozano, "Embedded control system for a four-rotor UAV," *International Journal of Adaptive Control and Signal Processing*, vol. 21, no. 2-3, pp. 189–204, 2007.

[75] J. Sasiadek, Q. Wang, and M. Zeremba, "Fuzzy adaptive Kalman filtering for INS/GPS data fusion," in *Proc. of the 2000 IEEE International Symposium on Intelligent Control*, 2000, pp. 181–186.

[76] Y. Shin, J. Park, and C. Kim, "Fast calibration technique for a gimballed inertial navigation system," in *Proc. of the 23rd International Congress of Aeronautical Sciences*, 2002, pp. 742.1–742.7.

[77] M. Shuster and S. Oh, "Three-axis attitude determination from vector observations," *Journal of Guidance, Control and Dynamics*, vol. 4, no. 1, pp. 70–77, 1981.

[78] Y. Song and J. Grizzle, "The extended Kalman filter as a local asymptotic observer," *Estimation and Control*, vol. 5, pp. 59–78, 1995.

[79] B. Stevens and F. Lewis, *Aircraft control and simulation*, 2nd ed. Wiley, 2003.

[80] A. Tayebi and S. McGilvray, "Attitude stabilization of a vtol quadrotor aircraft," *IEEE Trans. Control Systems Technology*, vol. 14, no. 3, pp. 562–571, 2006.

[81] A. Tayebi, S. McGilvray, A. Roberts, and M. Moallem, "Attitude estimation and stabilization of a rigid body using low-cost sensors," in *Proc. of the 46th IEEE Conf. on Decision and Control*, 2007, pp. 6424–6429.

[82] R. van der Merwe, E. Wan, and S. Julier, "Sigma-point Kalman filters for nonlinear estimation and sensor-fusion: Applications to integrated navigation," in *Proceedings of the AIAA Guidance, Navigation & Control Conference*, 2004, pp. 5120–5150.

[83] N. Van Kampen, *Stochastic process in physics and chemistry.* Elsevier, North Holland Personal Library, 1992.

[84] J. Vasconcelos, R. Cunha, C. Silvestre, and P. Oliveira, "Landmark based nonlinear observer for rigid body attitude and position estimation," in *Proc. of the* 46*th IEEE Conf. on Decision and Control*, 2007, pp. 1033–1038.

[85] J. Vasconcelos, P. Oliveira, and C. Silvestre, "Inertial navigation system aided by GPS and selective frequency contents of vector measurements," in *Proc. of the 2005 AIAA Guidance, Navigation, and Control Conference*, 2005, pp. 6057–6072.

[86] J. Vasconcelos, C. Silvestre, and P. Oliveira, "A Nonlinear GPS/IMU Based Observer for Rigid Body Attitude and Position Estimation," in *Proc. of the* 47*th IEEE Conf. on Decision and Control*, 2008, pp. 1255–1260.

[87] D. Vissière, P.-J. Bristeau, A. Martin, and N. Petit, "Experimental autonomous flight of a small-scaled helicopter using accurate dynamics model and low-cost sensors," in *Proc. of the* 17*th IFAC World Congress*, pp. 14643–14650.

[88] D. Vissière and N. Petit, "An embedded system for small-scaled autonomous vehicles," in *Proc. of the* 5*th International Conference on Informatics in Control, Automation and Robotics*, 2008.

[89] S. Waslander, G. Hoffmann, J. Jang, and C. Tomlin, "Multi-agent quadrotor testbed control design: Integral sliding mode vs. reinforcement learning," in *Proc. of the IEEE/RSJ International Conference on Intelligent Robotics and Systems*, 2005, pp. 468–473.